MONASH University

Polymeric Systems for Gasotransmitter Delivery

Sul Hwa YU

Bachelor of Science (Honours)

A thesis submitted for the degree of ***Doctor of Philosophy*** at

Monash University in 2018

Drug Delivery, Disposition and Dynamics
Monash Institute of Pharmaceutical Sciences
Monash University (Parkville Campus)
381 Royal Parade, Parkville
Victoria 3052, Australia

Copyright notice

Abstract

Nitric oxide (NO) and hydrogen sulphide (H_2S) are gaseous molecules synthesized in the body which have a critical role in many cellular signalling processes. Through their roles in cellular signalling these molecules are involved in various important physiological functions. Thus, the use of NO or H_2S for therapeutic applications has been the subject of increasing interest. For controlled and targeted NO and H_2S delivery/release, NO and H_2S-releasing nanoparticle systems have been developed. The use of polymeric nanoparticles has proven to be a versatile technique for NO and H_2S delivery system.

The overall objective of this dissertation was to develop novel methods and chemistries to synthesize polymer-based nanoparticles for sustained, controlled and stimulated delivery of NO or H_2S by manipulating their physical/chemical properties. Furthermore, these unique delivery materials were exploited in a number of exemplar biomedical applications, demonstrating the potential benefits in various therapeutic studies.

Firstly, in chapter 1, the background of NO and H_2S is discussed with their releasing delivery nanoparticle systems and also therapeutical applications.

In chapter 2, Polymers with a terminal S-nitrosothiol moiety were prepared with a new synthetic method, enabling simple synthesis of biochemically active nanostructure. The results demonstrated that the release of NO from such materials can be tailored by altering the copolymer structure. Furthermore, the reactivity of the S-nitrosothiol moiety was strongly affected by the local chemical environment.

In chapter 3, H_2S-releasing polymers with an acyl-protected perthiol chain terminus were developed. In particular, pH-responsive H_2S-releasing micelles had a significant impact on thiol-triggered H_2S release kinetics by controlling the self-assembly of micelles at different pH conditions. Finally, these materials were capable of releasing H_2S to live cells upon exposure to thiol even at endogenous levels.

In chapter 4, a shape-controlled H_2S delivery polymeric system was exploited. Both spherical and worm-like nano-particulate H_2S donors were shown to successfully release H_2S in the presence of the model thiol, L-cysteine and even inside the cells

upon exposure to thiol even at intracellular levels. Finally, the co-administration of H_2S donor nanoparticles with doxorubicin (DOX) was found to enhance DOX cytotoxicity in osteosarcoma (U2OS) cells.

In chapter 5, NO-releasing core cross linked star polymers were developed containing S-nitrosoglutathione (GSNO), NO donor. These GSNO-conjugated star polymers showed a substantially slower NO release profile, compared to GSNO. Cytotoxic effects of co-delivery of GSNO or GSNO-conjugated star polymer in combination with and without DOX were investigated on human breast cancer (MCF7) cells and resistance cells (MCF7/VP16) cells. The results indicated that NO delivered from GSNO or GSNO-conjugated star polymers increased susceptibility of MCF7/VP16 cells to DOX cytotoxicity in comparison with MCF7 cells.

Declaration

This declaration is to be included in a standard thesis. Students should reproduce this section in their thesis verbatim.

This thesis contains no material which has been accepted for the award of any other degree or diploma at any university or equivalent institution and that, to the best of my knowledge and belief, this thesis contains no material previously published or written by another person, except where due reference is made in the text of the thesis.

Signature: …  …

Print Name: …SUL HWA YU.

Date: ……19/03/2018…….

Publications during enrolment

Hu, J., Whittaker, M.R., Yu, S.H., Quinn, J.F. and Davis, T.P., 2015. Nitric Oxide (NO) Cleavable Biomimetic Thermoresponsive Double Hydrophilic Diblock Copolymer with Tunable LCST. Macromolecules, 48(12), pp.3817-3824.

Yu, S.H., Hu, J., Ercole, F., Truong, N.P., Davis, T.P., Whittaker, M.R. and Quinn, J.F., 2015. Transformation of RAFT Polymer End Groups into Nitric Oxide Donor Moieties: En Route to Biochemically Active Nanostructures. ACS Macro Letters, 4(11), pp.1278-1282.

Yu, S.H., Ercole, F., Veldhuis, N.A., Whittaker, M.R., Davis, T.P. and Quinn, J.F., 2017. Polymers with acyl-protected perthiol chain termini as convenient building blocks for doubly responsive H_2S-donating nanoparticles. Polymer Chemistry, 8(41), pp.6362-6367.

Yu, S.H., Esser. L., Khor, S.Y., Senyschyn, D., Whittaker, M.R., Ercole, F., Davis, T.P. and Quinn, J.F., 2017. Development of a shape-controlled H_2S delivery system using epoxide-functional nanoparticles for improving chemosensitive in osteosarcoma cells. 2017. Biomacromolecules, in preparation.

Thesis including published works declaration

I hereby declare that this thesis contains no material which has been accepted for the award of any other degree or diploma at any university or equivalent institution and that, to the best of my knowledge and belief, this thesis contains no material previously published or written by another person, except where due reference is made in the text of the thesis.

This thesis includes 2 original papers published in peer reviewed journals and 2 submitted publications. The core theme of the thesis is the development of nanoparticles for gasotransmitter delivery. The ideas, development and writing up of all the papers in the thesis were the principal responsibility of myself, the student, working within the Drug Delivery, Disposition and Dynamics, Monash Institute of Pharmaceutical Sciences under the supervision of Prof Thomas Davis and Dr Michael Whittaker.

The inclusion of co-authors reflects the fact that the work came from active collaboration between researchers and acknowledges input into team-based research.

In the case of Chapter 2, 3, 4, and 5, my contribution to the work involved the following:

(If this is a laboratory-based discipline, a paragraph outlining the assistance given during the experiments, the nature of the experiments and an attribution to the contributors could follow.)

Thesis Chapter	Publication Title	Status *(published, in press, accepted or returned for revision, submitted)*	Nature and % of student contribution	Co-author name(s) Nature and % of Co-author's contribution*	Co-author(s), Monash student Y/N*
2	Transformation of RAFT Polymer End Groups into Nitric Oxide Donor Moieties: En Route to Biochemically Active Nanostructures	Published	80% Research design, performance of data collection and analysis, manuscript preparation	1) Jinming Hu helped synthesise the polymers, and provided expertise in fluorometric sensing of NO. 2) Francesca Ercole provided expertise on amperometric sensing of NO. 3) Nghia P. Truong provided expertise on the synthesis of pH-responsive polymers. 4) Thomas P. Davis, Michael R. Whittaker and John F. Quinn formulated the idea of the project, provided supervision, and had input into manuscript preparation	No
3	Polymers with acyl-protected perthiol chain termini as convenient building blocks for doubly responsive H_2S-donating nanoparticles	Published	75% Research design, performance of data collection and analysis, manuscript preparation	1) Francesca Ercole provided expertise on amperometric sensing of H_2S, and revised the manuscript. 2) Nicholas A. Veldhuis assisted with the cell imaging experiment. 3) Thomas P. Davis, Michael R. Whittaker and John F. Quinn, formulated the idea of the project, provided supervision, and had input into manuscript preparation	No

4	Development of a shape-controlled H_2S delivery system using epoxide-functional nanoparticles for improving chemosensitive in osteosarcoma cells.	Preparation	70% Concept and collecting data and writing first draft	1) Lars Esser provided expertise on the synthesis of different morphology nanoparticles 2) Song Yang Khor recorded the TEM images. 3) Danielle Senyschyn conducted the cell cytotoxicity assay. 4) Nicholas A. Veldhuis consulted on the design of cell imaging experiments. 5) Francesca Ercole had input into manuscript preparation 6) Thomas P. Davis, Michael R. Whittaker and John F. Quinn, formulated the idea of the project, provided supervision, and had input into manuscript preparation	1)No 2)Yes 3)No 4)No 5)No 6)No

**If no co-authors, leave fields blank*

I have / have not renumbered sections of submitted or published papers in order to generate a consistent presentation within the thesis.

Student signature: [redacted] **Date:** 19/03/2018

The undersigned hereby certify that the above declaration correctly reflects the nature and extent of the student's and co-authors' contributions to this work. In instances where I am not the responsible author I have consulted with the responsible author to agree on the respective contributions of the authors.

Main Supervisor signature: [redacted] **Date:** 19/03/2018

Acknowledgements

This thesis, and the 4 years of hard work that it represents could not have been completed with the support and encouragement of many people.

I would like to express the deepest appreciation to my supervisors, Prof Tom Davis and Dr Michael Whittaker for showing their trusts in me by first accepting me as a PhD candidate at Monash University and providing me the full scholarship and support during 4 years. I am very thanks for their excellent supervision, guidance and inspiration. Without their support and persistent help, this dissertation would not have been possible.

I would also like to extend my gratitude to Dr John Quinn. Even though you are not official my supervisor, you are also my co-supervisor during my whole PhD journey for giving me a lot of valuable advice, support, guidance and inspiration. Thank you very much for all your help.

I would particularly like to thank to Dr Fran Ercole and Dr Jinming Hu for their support and guidance in the laboratory, and their wonderful, patient help during my PhD.

I would like to thanks to Prof Maria Kavallaris and Dr Friederike Mansfeld for the collaboration with UNSW, Children's Cancer Institute. I am thankful for their guidance and support for carrying out my biology experiments over the years.

At CBNS, Centre of Excellence in Convergent Bio-Nano Science and Technology, I had many opportunities for interacting with different research groups, learning and experiencing different skills, and also financial support. I am very grateful for their all support and providing me great opportunities. Specially thanks Natalie, Anne, Charlotte and former member, Katrina for their hard works and kindness.

I thank MIPS for a great place to work. I thank the technical staff of the MIPS for their dedication and expertise. I would like to thank my PhD panel members for their critical advice and suggestions: Jonathan Baell and Georgina Such. Furthermore I would like to thank Karen M and Karen D for their help and support with my enrolment.

I would also like to thank everyone in our group for the great working environment, including Pu-chun, Kristian, Nighia, Ximo, Fran, Adrian, Lars, Yuhuan, Ruirui, Alex,

Joanne, James, Song, Qiuming, Emily, Cheng, Paulina, Jeffri, May, Marvin, Mai, Ayaaat, Ava, Nam, Alexander, Stefan, Aadarash, Ibrahim, Carlos and all other students. It was really great to work and hang out with you guys. Thanks for all the fun times and support. Specially thanks Lars, Qiuming, Emily, Joanne, Song and Clara for the great friendship. I really enjoyed talking with you guys and spending time together over the years.

Many thanks are owed to my family in Korea and my new family for all of their help, support and care over the many years. I am very fortunate to have you guys all in my life.

Finally, to my best colleague, friend and husband, Song Yang Khor. During my PhD, we had so many good memories each other. The greatest thing that I had during my PhD in our group is that I met you and have you in my life. I am sincerely grateful for your unconditional support, love, care and kindness during my PhD. I could not imagine how I could go through all the struggling and hard works without you during my PhD. I am looking forward to our journey together in next chapter of our life.

Sul Hwa YU

Abbreviations

NO	Nitric oxide
H_2S	Hydrogen sulfide
CO	Carbon monoxide
NOS	Nitric oxide synthase
nNOS	Neuronal nitric oxide synthase
NOS3	Endothelial nitric oxide synthase
eNOS	Endothelial nitric oxide synthase
iNOS	Inducible nitric oxide synthase
NOS2	Inducible nitric oxide synthase
NADPH	Nicotinamide adenine dinucleotide phosphate
EDRF	Endothelium-derived relaxing factor
sGC	Guanylate cyclase
GTS	Guanosine triphosphate
cGMP	Cyclic guanosine monophosphate
SiNP	Silica nanoparticle
TMOS	Tetramethoxysilane
TEOS	Tetraethoxysilane
AEMP3	(Aminoethylamino-methyl)phenethyltrimethoxysilane
AEAP3	N-(2-aminoethyl)-3-aminopropyltrimethoxysilane
AHAP3	N-(6-aminohexyl)aminopropyltrimethoxysilane
PEG	Polyethylene glycol
Au	Gold
DETA	Diethylenetriamine

MPCs	Tiopronin-monolayer-protected clusters
NHS	N-hydroxy-succinimide
EDC	N-(3-dimethylaminopropyl)-N’-ethylcarbodiimide
TEPA	Tetraethylenepentamine
PEHA	Pentaetheylenehexamine
MSA	Mercaptosuccinic acid
$FeCl_3 \cdot 6H_2O$	Iron(III) chloride hexahydrate
$FeCl_2 \cdot 4H_2O$	Iron(II) chloride tetrahydrate
MTT	3-(4-5-dimethylthiazolyl-2)-2,5-diphenyltetrazolium bromide
RAFT	Reversible addition fragmentation chain transfer
$AgNO_3$	Silver nitrate
GSNO	S-nitrosoglutathione
OEG-MA	Oligoethylene glycol-methacrylate
VDM	2-vinyl-4,4-dimethyl-5-oxazolone monomer
DAF-FM DA	4-amino-5-methylamino-2’,7’-difluorofluorescein diacetate
HSCs	Hepatic stellate cells
HNO	Nitroxyl
PAMAM	Polyamidoamine
NACys	N-acetyl-L-cysteine
NAP	N-acetyl-D,L-penicillamine
GSH	Glutathione
VDM	2-vinyl-4,4-dimethyl-5-oxazolone
SNAP	S-nitroso-N-acetylpenicillamine
DMPC	1,2-dimyristoyl-sn-glycero-3-phosphocholine
DETA NONOate	Diethylenetriamine

Hb	Haemoglobin
PBH	Polymerised bovine haemoglobin
NAC-SNO	S-nitroso-N-acetyl cysteine
MRC5	Lung fibroblasts cells
BE(2)-C	Neuroblastoma cells
PYRRO/NO	Sodium 1-(pyrrolidin-1-yl)diazen-1-ium-1,2-diolate
RNOS	Reactive nitrogen intermediates
TMOS	Tetramethylorthosilicate
CSE	Cystathionine-γ-lyase
CBS	Cystathionine β-synthase
3-MST	3-mercaptopyruvate sulfur transferase
CAT	Cysteine aminotransferase
3MP	3-mercaptopyruvate
ATP	Adenosine triphosphate
MAPK	Mitogen-activated protein kinases
ER	endoplasmic reticulum
CRT	Calreticulin
NSAIDs	Non-steroidal anti-inflammatory drugs
DOX	Doxorubicin
U2OS	osteosarcoma
ADT	Dithiol-3-thione
ADT-OH	Desmethyl form of dithiolethiones
PEG	Poly(ethylene glycol)
GDQ	Gardiquimod
TLR	Toll-like receptor

TNF-α	Tumour necrosis factor-α
NF-kB	Nuclear factor-κB
SATHA	S-aroylthiohydroxylamine
SATO	S-aroylthiooximes
MEO_2MA	2-(2-methoxyethoxy)ethyl methacrylate
FBEMA	2-(4-formylbenzoyloxy)ethyl methacrylate
TFA	Trifluoroacetic acid
ERK	Extracellular signal-regulated kinase
PKC	Protein kinase C
EKAR	Extracellular signal regulated kinase activity reporter
AUC	Area under the curve
SEM	Standard error of the mean
CKAR	C kinase activity reporter
MSN	Mesoporous silica nanoparticles
DATS	Diallyl trisulfide
UTMD	Ultrasound targeted microbubble destruction
C_3F_8	Octafluoropropane
hs-MB	Microbubble loaded with H_2S.
HO-SSS-CHOL	Cholesterol conjugated trisulfide bridge
MeO-PEG-SSS-CHOL	Trisulfide linked PEG-cholesterol conjugate
CH_2Cl_2	Dichloromethane
$CHCl_3$	Chloroform
SF4	H_2S-responsive fluorescent probe
HEK293	Human embryonic kidney
OEGMA	Oligo(ethylene glycol) methyl ether methacrylate

POEGMA	Poly(oligo(ethylene glycol) methyl ether methacrylate
PEG-SH	Poly(ethylene glycol) methyl ether thiol
SNO	S-nitrosothiol
P[OEGMA]-S-C(=S)Ph	Poly(oligoethylene glycol methyl ether) methacrylate
GPC	Gel permeation chromatography
^{1}H NMR	^{1}H nuclear magnetic resonance
SH	thiol
DIPMA	2-[N,N-(diisopropylamino)ethyl methacrylate
DMAEMA	N,N-(dimethylamino)ethyl methacrylate
HNO_2	Nitrous acid
H_2SO_4	Sulfuric acid
$NaNO_2$	Sodium nitrite
$NH_2NH_2 \cdot H_2O$	Hydrazine monohydrate
UV-vis	Ultraviolet-visible spectroscopy
MWD	Molecular weight distribution
DLS	Dynamic light scattering
PBS	Phosphate buffered saline
DAF	5,6-diaminofluorescein
HCl	Hydrogen chloride
AIBN	Azobisisobutyronitrile
CPADB	4-Cyano-4-(phenylcarbonothioylthio)pentanoic acid
$CDCl_3$	Deuterated chloroform
$(CD_3)_2SO$, C_2D_6OS, d_6-DMSO	Dimethyl sulfoxide-d6
DMSO	Dimethyl sulfoxide
DMF	Dimethylformamide

THF	Tetrahydrofuran
D_2O	Deuterium oxide
PSD	Particle size distribution
PDI	Polydispersity index
Na2S	Sodium sulfide
BMA	Butyl methacrylate
CPBD	2-cyanoprop-2-yl benzodithioate
DMEM	Dulbecco's modified eagle medium
P[OEGMA]-S(C=S)Ph	Poly(oligoethylene glycol methyl ether methacrylate)
P[OEGMA-*b*-BMA]-S(C=S)Ph	Poly(oligoethylene glycol methyl ether methacrylate-block-butyl methacrylate)
P[OEGMA-co-DMAEMA-*b*-DIPMA]-S(C=S)Ph	Poly(oligoethylene glycol methyl ether methacrylate-co-N,N-(dimethylamino)ethyl methacrylate-block- N,N (diisopropylamino)ethyl methacrylate)
Py-S-S-Py	Dipyridyl disulfide (aldrithiol™-2)
MPS	Measured at peaking concentration
-S-S-Py	Pyridyl disulfide group
-S-S-(C=O)Ph	Acyl(benzoyl)-protected perthiol moiety
-S-SH	Perthiol
GMA	Glycidyl methacrylate
HBSS	Hank's salt
PGMA	Poly(glycidyl methacrylate)
St	Styrene
TEA	Triethylamine
DMAc	N,N-Dimethylacetamide
TEM	Transmission electron microscopy
PDHMA	3-(pyridyldisulfanyl)-2-hydroxypropyl methacrylate

BTHMA	3-(benzoylthio)-2-hydroxypropyl methacrylate
BDTHMA	3-(benzoyldisulfanyl)-2-hydroxypropyl methacrylate
Macro-CTA	Macro-chain transfer agents
P[OEGMA-*co*-GMA]-S(C=S)Ph	Benzodithioate-terminated poly((oligoethylene glycol methyl ether) methacrylate-co-glycidyl methacrylate
P[GMA-*b*-POEGMA-*b*-PSt],	Poly(glycidyl methacrylate)-block-poly(oligo(ethylene glycol) methyl ether methacrylate)-block-poly(styrene)
-S(C=O)Ph)	Benzothioate moieties
PISA	Polymerization-induced self-assembly
RT	Room temperature
MDR	Multidrug resistance
DNA	Deoxyribonucleic acid
ABC	ATP binding cassette
Pgp	P-glycoprotein
MRPs	MDR–associated proteins
HT29-dx cells	Human epithelial colon doxorubicin-resistant cancer cells
HT29 cells	Human epithelial colon doxorubicin-sensitive cancer cells
SNP	Sodium nitroprusside
DETA NONOate	Diethylenetriamine diazeniumdiolate
MCF7/ADR cells	Multidrug resistant human breast cancer cell lines
MCF7/VP16 cells	Drug (etoposide)-resistant human breast cancer cells
MCF7 cells	Breast cancer cells
SKOV3 cells	Human ovarian carcinoma cells
SKOVCR cells	Drug (doxorubicin)-resistant ovarian carcinoma cells
SNAP	S-nitroso penicillamine
OEGA	Oligo(ethylene glycol) methyl ether acrylate
MBAA	N,N’-methylenebis(acrylamide)

TFE	2,2,2-trifluoroethanol
BSPA	3-(benzyl sulfanyl thiocarbonyl sulfanyl)-propanoic acid
PFPA	Pentafluorophenyl acrylate
^{19}F NMR	^{19}F nuclear magnetic resonance
FBS	Fetal bovine serum
RIPA	Radioimmunoprecipitation assay
SDS	Sodium dodecyl sulfate
Tris•HCl	Tris hydrochloride
NaCl	Sodium chloride
TBST	Tris-buffered saline
SDS-PAGE	Sodium dodecyl sulfate polyacrylamide gel electrophoresis
GAPDH	Glyceraldehyde-3-phosphate dehydrogenase
IgG	Immunoglobulin G
MRI	Magnetic resonance imaging
POEGA	Poly(ethylene glycol) methyl ether acrylate
PFP	Pentafluorophenol

CHAPTER 1: An introduction into macromolecular gasotransmitter (nitric oxide and hydrogen sulphide) delivery systems

1.1 The Gasotransmitters

The gasotransmitters are a family of endogenously-generated gaseous molecules that are present in many organs and intracellular organelles, and which have an important role in intra-and extra-cellular signalling.[1] The terminology 'gasotransmitter' was first introduced in 2001.[2] To date, nitric oxide (NO), hydrogen sulfide (H_2S) and carbon monoxide (CO) have been identified as physiologically relevant gasotransmitters.[3] These molecules are membrane permeable, enabling fast intracellular and intercellular migration without the requirement for any cognate membrane receptor or vesicle-derived transportation machineries.[2]

1.1.1 Introduction and biological roles of NO

As the first gasotransmitter to be identified, NO has been the subject of considerable investigation, and has been shown to play an important role in many different physiological processes.[4] NO was proclaimed "Molecule of the Year" in 1992 by the journal Science.[5] The use of L-arginine and various isoforms of NO synthase led to the discovery that NO was produced endogenously by mammalian cells. The role of NO in mammalian cells was extensively investigated and it was proven that NO plays an important role in signalling and regulating cellular functions.[6–10]

NO is bio-synthesized by three isoforms of nitric oxide synthase (NOS).[11] Neuronal NOS (nNOS) and endothelial NOS (NOS3, eNOS) are continuously expressed in neurons and endothelial cells respectively.[11] NOS2, also referred to as iNOS, is an inducible isoform.[12] Both nNOS and NOS3 (eNOS) are precisely regulated by intracellular calcium concentration through the binding to calmodulin.[11] In contrast inducible iNOS/NOS2 is a calcium-independent isoform, instead being triggered by immunological stimuli in many mammalian cell lines.[12,13]

Nitric oxide synthases convert L-arginine to L-citrulline and NO under oxygenated conditions, using nicotinamide adenine dinucleotide phosphate (NADPH) as a co-substrate.[11,14,15] With a 2 : 1.5 molar stoichiometry ratio of O_2 and NADPH, one mole of NO can be generated from NOS.[14,15] NO is then rapidly converted into nitrite and nitrate.[16]

NO was first identified as an important mediator of blood-vessel relaxation processes and macrophage activation processes.[17–20] Many studies in the late 1980s had recognised NO as the endothelium-derived relaxing factor (EDRF).[7,21,22] It was discovered that acetylcholine triggers the release of NO in the blood vessel wall, which only occurred when the endothelium was intact. NO then diffuses into the vascular smooth muscle, and activates guanylate cyclase (sGC).[21,23,24] sGC transforms guanosine triphosphate (GTS) into cyclic guanosine monophosphate (cGMP), which results in vasorelaxation by decreasing intracellular calcium concentration.[25,26] The elucidation of the mechanism of action of NO has allowed the identification of a large range of physiological functions that are regulated by NO. For example, NO is involved in controlling basal vascular tone and systolic blood pressure.[27,28] Platelet aggregation can be prevented by NO, which protects against thrombosis.[29] NO is involved in wound healing and angiogenesis.[30,31] NO has been associated with neuronal activities including learning, memory or long-term potentiation by acting as a neurotransmitter in the nervous system.[32]

The misregulation of NO leads to a number of pathological conditions. For example, excess NO production has been tied to many illness ranging from autoimmune disease to cancer.[33,34] Its overproduction has also been associated with transplant rejection or infection.[35] In addition, NO deficiency is related to a number of other pathologies, such as Prinzmetal's angina and erectile dysfunction.[36]

Due to its broad biological effects and very low concentrations, NO has been explored as a potential therapeutic agent. For instance, the tumoricidal properties of NO have been investigated for applications in cancer treatment and prevention.[34] Additionally, exogenous delivery of NO has also been shown to have potential clinical benefit in antibiotic treatment by a number of researchers.[37,38]

1.1.2 NO Delivery

As a gaseous radical species, NO is difficult to handle due to its high chemical reactivity. Nevertheless, the therapeutic potential for controlled delivery or generation of NO has received an increasing amount of attention. NO itself can be delivered to the lungs via inhalation, and thus therapeutically used for pulmonary hypertension.[39] With the exception of this specific NO clinical use, many therapeutic applications have

been reliant on NO carrier compounds capable of stabilizing the radical and generating NO when/where its release is required.

Many different classes of NO donor have been investigated and used in biological research, and these are summarised in Table 1.1.[40] NO donors decompose to release NO, which is then oxidised or reduced to other reactive nitrogen species. The pathway of NO generation through non-enzymatic or enzymatic processes differs greatly between individual NO donors, which leads to unique NO release kinetics and biological properties (Table 1.1).[40–42] A number of NO donors can spontaneously decompose to release NO under stimuli such as heat, pH, and light conditions (Table 1.1).[40] These include direct NO-donors, NO-donors requiring metabolism and bifunctional NO-donors.[42–45] However, there are limitations to the use of NO donors in therapeutic applications, including lack of selectivity and stability, and limited bioavailability. Therefore, there has been increasing attention given to developing NO delivery systems that can improve the selectivity and stability of NO-donor drugs.[44,46]

Table 1.1: Major small molecule nitric oxide donor compounds. Adapted with permission from Wang et al.[40] Copyright 2002 American Chemical Society.

Index	Name	Representative compounds	Pathway of NO Generation	
			Non-enzymatic	Enzymatic
A.	Organic nitrates	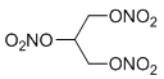	thiols	Cyt-P450, GST and a membrane-bound enzyme
B.	Organic nitrites	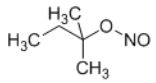	hydrolysis and trans-nitrosation; thiols; light; heat	cytosolic and microsomal enzymes; xanthine oxidase
C.	Metal-NO complexes	$Na_2[Fe(CN)_5(NO)]\,2H_2O$	light; thiols; reductants; nucleophiles	a membrane-bound enzyme
D.	*N*-Nitrosamines	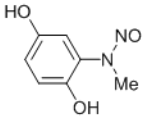	OH; light	Cyt-P450 related enzymes
E.	*N*-Hydroxyl nitrosamines	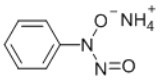	light; heat	peroxidases
F.	Nitrosimines	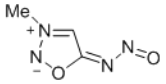	thiols; light	?
G.	Nitrosothiols	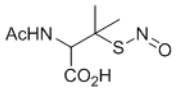	spontaneous; enhanced by thiols, light and metal ions	Unknown enzymes
H.	*C*-nitroso compounds	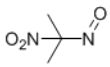	Light; heat	?
I.	Diazetine dioxides	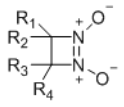	spontaneous; thiols	?
J.	Furoxans and benzofuroxans	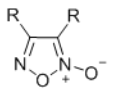	thiols	unknown enzymes
K.	Oxatriazole-5-imines	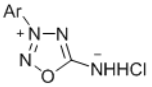	thiols	?
L.	Sydnonimines	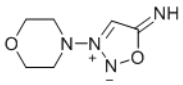	spontaneous, enhanced by light, oxidants and pH>5	prodrugs require enzymatic hydrolysis
M.	Oximes	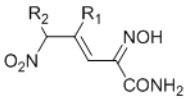	spontaneous; O_2/Fe^{III}-porphyrin	?
N.	Hydroxylamines		autoxidation enhanced by metal ions	catalase/H_2O_2
O.	*N*-Hydroxyguanidines	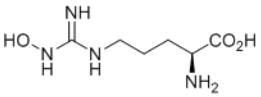	oxidants	NOSs, Cyt-P450
P.	Hydroxyureas	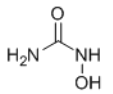	H_2O_2/CuZn-SOD or ceruloplasimin; H_2O^2/Cu^{2+}; heme-containing proteins	peroxidase

1.1.3 NO-releasing nanoparticle delivery systems

In order to overcome the limitations of these small molecule donors for delivering NO a range of NO-delivering nanomaterials have been investigated. Freidman and co-workers have previously noted that NO-releasing materials should be designed to

improve their stability, solubility and specificity to targets.[47–49] The incorporation of NO donors into nanoparticle systems represents a very promising strategy for enhancing the biodistribution and improving the pharmacokinetic properties of NO donors, thereby enabling new therapeutic applications for these materials.

Recent studies aimed at developing different types of NO-releasing/generating materials, include materials based on silica nanoparticles; metallic nanoparticles; polymeric vehicles; and lipid-based nanocarriers.

Silica nanoparticles

Sol-gel based materials have diverse biomedical applications. Many drug delivery vehicles and other bio nano-delivery systems have been investigated using sol-gel processed materials. These materials can safely encapsulate agents such as antibodies, enzymes or other therapeutic agents and protect their bioactivities for delivery into target areas.[50–52]Silica nanoparticles (SiNP) are commonly produced by the sol-gel method; the method of obtaining ceramic and glassy materials via the settling of nanoparticles from a colloidal suspension onto a pre-conditioned surface.[49,53,54] Silica nanoparticles are widely considered as non-toxic, possessing stable particle size and morphology, and biocompatible for delivering bioactive agents.[38,55] The most commonly used materials for the preparation of SiNP are alkoxysilanes, which develop a porous structure that can be used to simply load bioactive molecules into the pores.[46] Derivatives of silanes with different functional groups have been employed for various applications.

In recent years, SiNP have been applied for the delivery of NO. The synthesis of NO-releasing SiNP has been reported by the groups of Schoenfisch and Friedman. Schoenfisch and co-workers prepared NO releasing sol-gel based silica nanoparticles, based on the previous works of Meyerhoff and coworkers.[56,57] They investigated amine-functionalised SiNP having either primary or secondary amine functionality (or both) on the surface, which were converted to the common NO donor *N*-diazeniumdiolate via exposure to high pressure of NO gas under basic conditions.[58] The secondary amines were observed to be the best precursor for stable *N*-diazeniumdiolate formation. By using this chemistry, Schoenfisch and co-workers have reported secondary amine functionalised sol-gel SiNP, which was synthesised via condensation of tetramethoxysilane (TMOS) or tetraethoxysilane (TEOS) with

(aminoethylamino-methyl)phenethyltrimethoxysilane (AEMP3), *N*-(2-aminoethyl)-3-aminopropyltrimethoxysilane (AEAP3), or *N*-(6-aminohexyl)aminopropyltrimethoxysilane (AHAP3).[57] The secondary amine functionalised SiNP was then exposed to high NO pressure (5 atm) to form *N*-diazeniumdiolate moieties, which were capable of releasing NO in aqueous conditions. The total amount of secondary amine functional groups conjugated per particle dictated the total amount of NO release from each particle. However, there was a limit to the amount of secondary amine groups which could be incorporated into the SiNP based on TEOS. The authors indicated that higher proportions of amino functional monomers led to significant particle aggregation due to hydrogen bonding formation between the amino groups and silanols.[37,57] The same group has developed a procedure in which *N*-diazeniumdiolate-modified aminoalkoxysilanes were synthesized prior to SiNP formation. In this procedure, less particle aggregation was observed due to decreased hydrogen bond formation, and this resulted in 99 % *N*-diazeniumdiolate conversion generating higher NO release from each particle. (Figure 1.1).[37]

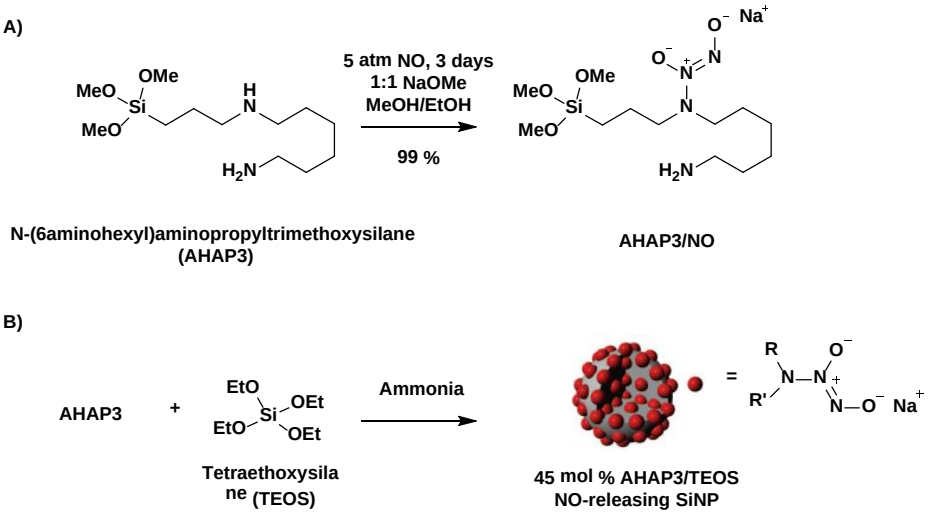

Scheme 1.1: (A) The synthesis of AHAP3 NO donor and (B) co-condensation with AHAP3 and TEOS to form NO-donor SiNP: R= -$(CH_2)_3Si\equiv$ and R'=-$H_2N(CH_2)_6$-. Adapted from with permission from Schoenfisch et al.[37] Copyright 2008 American Chemical Society.

In a further development, electrospun polyurethane fibers doped with NO-releasing SiNP have been recently presented from the same group. This study demonstrated that the NO release kinetics from each SiNP type was strongly affected by the local chemical environment as well as the particle size.[58]

Friedman et al. have also reported a new platform of NO-releasing SiNP.[49] Sol-gel processed silane was initially prepared from TMOS, which was then combined with sugars including glucose and tagatose to generate a hydrogen bonded network of glass forming sol-gel matrix. These properties influenced not only NO release through thermal reduction of nitrite ions by reducing sugars but also NO release from inside dry particles. Different molecular weights of polyethylene glycol (PEG)s were then incorporated into the hydrogel lattice of the particles, which have a substantial effect on NO formation, NO retention, and the kinetics of NO release. Samples incorporating PEG 3000 g mol^{-1} exhibited a rapid release of NO from the matrix, compared to the samples derived from PEG 200 g mol^{-1} or 400 g mol^{-1} respectively. This indicates that the smaller molecular weight of PEGs can decrease the pore size inside hydrogel lattice of the particles. In contrast, larger molecular weight PEGs facilitate more rapid water infiltration, either via dissolution of the hydrated particles or larger water filled channels within the particles once hydrated. More importantly, the authors indicated that the NO containing dry powder remained relatively stable for months, and that sustained release of the trapped NO was possible over an extended time frame when exposed to a moist environment. Therefore, the SiNP allowed for the controlled and tuneable delivery of NO through variations in hydrogel/glass composites as well as the nitrite concentration inside the SiNP. The authors noted that the particles have potential as a new class of therapeutically useful, sustained release NO products.

Metallic nanoparticles

Metallic nanoparticles have been employed as a platform for a variety of hybrid organic/inorganic NO-delivery vehicles. The preparation of NO-releasing gold nanoparticles was first reported by Rothrock and coworkers.[59] Gold nanoparticles were initially synthesized by the reaction of hydrogen tetrachloroaurate salt with hexanethiol in the presence of the reducing agent sodium borohydride. The gold nanoparticles were then ligand-exchanged by bromo-terminated alkanethiols through the place-exchange method. The purified bromo-functionalised gold nanoparticles were reacted with butylamine, hexanediamine, ethylenediamine or diethylenetramine to produce secondary amine-functional nanoparticles. To introduce NO donor moieties the secondary amine functional groups were converted to *N*-diazeniumdiolate functionalised gold nanoparticles via exposure to NO pressurised to 5 atm. The total NO loading capacity and NO release kinetics from *N*-diazeniumdiolate-modified gold

nanoparticles were shown to depend on the number or chemical structure of the functionalised amine precursor. Hexanediamine-modified particles showed the highest total NO loading of all the amine-functionalised particles, while NO-releasing gold nanoparticles functionalised with ethylene diamine exhibited the longest NO release half-life. Both thermal and proton-driven dissociation occurred in *N*-diazeniumdiolate-functionalised nanoparticles to release NO. In particular, the level of NO release was greater when the particles were exposed to aqueous solution.

Based on previous studies, water-soluble NO-releasing Tiopronin-monolayer-protected gold nanoparticles were developed to improve the aqueous solubility and NO payload of gold nanoparticles.[60]

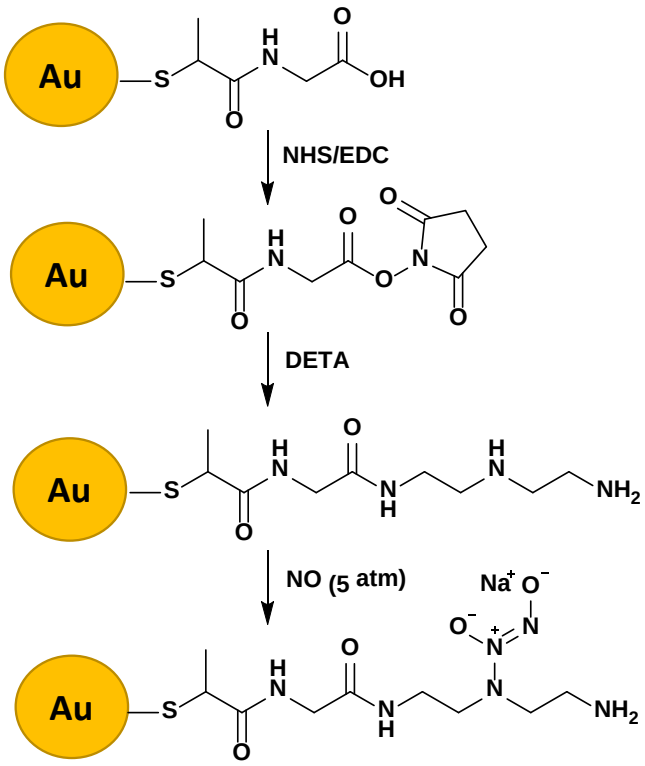

Figure 1.2: The strategy of diethylenetriamine (DETA) modified Tiopronin-monolayer-protected clusters (MPCs) gold nanoparticles via amide coupling, followed by *N*-diazeniumdiolate functionalization. Adapted from with permission from Polizzi et al.[60] Copyright 2007 American Chemical Society.

Specifically, tiopronin protected MPCs were reacted with *N*-hydroxy-succinimide (NHS) and *N*-(3-dimethylaminopropyl)-N-ethylcarbodiimide (EDC) to activate the terminal –COOH groups, which were then modified with amine groups, such as diethylentriamine (DETA), tetraethylenepentamine (TEPA) or pentaetheylenehexamine (PEHA). Secondary amine funtionalised MPCs were then

exposed to NO gas (5 atm) to form NO-donor gold nanoparticles. Unfortunately, these particles were not efficiently converted into *N*-diazeniumdiolate functional nanoparticles due to destabilisation of the nanoparticle dispersion. Nevertheless, pentaethylenehexamine (PEHA)-stabilized gold nanoparticles exhibited higher NO loading, resulting in enhanced NO-release from the particles.

In addition to work on gold nanoparticles, research has also been conducted into NO delivery using superparamagnetic iron oxide nanoparticles, as reported by Haddad and co-workers.[61] Water-soluble magnetic nanoparticles were first prepared by co-precipitation of $FeCl_3 \cdot 6H_2O$ and $FeCl_2 \cdot 4H_2O$ with a precipitator, NH_4OH. The particles were treated with oleic acid for initial stabilisation. Oleic acid coated nanoparticles were then exchanged with mercaptosuccinic acid (MSA) to yield thiolated nanoparticles. The free thiol groups on the magnetic nanoparticle surface were subsequently nitrosated by acidic aqueous sodium nitrite (i.e., nitrous acid), leading to the formation of S-nitrosothiol functionalised superparamagnetic iron oxide nanoparticles. The NO release profile over a period of hours was obtained by chemiluminescence measurements. The biological properties of these S-nitrosated iron-oxide magnetic nanoparticles were then examined in *in vitro* experiments and reported by the same group.[62] A MTT (3-(4-5-dimethylthiazolyl-2)-2,5-diphenyltetrazolium bromide) assay was carried out to examine the cytotoxicity of thiolated and S-nitrosated iron-oxide nanoparticles in acute T cell leukemia and Lewis lung carcinoma cells. The authors indicated that at low treatment concentrations both particles showed low cytotoxicity to both cell lines, while only the S-nitrosated nanoparticles promoted cell proliferation at higher concentrations.

Barone and co-workers have prepared NO photocaging platinum nanoparticles.[63] Ultra-small (ca. 1 nm), water soluble and stable platinum nanoparticles were synthesized,[64] and then protected with a monolayer of thioglycolic acid. The carboxyl-terminated, monolayer protected clusters were used as a suitable scaffold for conjugating with tailored NO photodonors with self-assembling characteristics, using a place exchange approach. The NO releasing platinum nanoparticles remained stable in the absence of light. However, irradiation with visible light triggered NO release through a nitro-to-nitrite photo-rearrangement, followed by cleavage of the O-NO bond to produce NO and a phenoxy radical.

Polymeric vehicles

Biocompatible polymeric nanoparticles have been widely used as drug or other bioactive agent delivery systems due to their stability, low toxicity, bioavailability, high drug loading and controlled delivery/release properties.[65] By harnessing these properties, polymeric systems for NO delivery have been developed to deliver and release NO at specific target sites.

Micelles

Polymeric micelles are generally larger in size than dendrimers and smaller than liposomes, and usually comprise amphiphilic block polymers termed unimers. Micelles are inherently dynamic in nature, existing in equilibrium with unimers. Significantly, depending on the structure of the polymeric unimer, micelles can be designed to assemble or disassemble using a range different triggering conditions, including temperature and pH. Jo and co-workers have designed block copolymer of *N*-acryloylmorpholine and *N*-acryloyl-2,5-dimethylpiperazine.[66] Poly(*N*-acryloyl-2,5-dimethylpiperazine) was used as a scaffold to provide secondary amines for reaction with NO gas, yielding *N*-diazeniumdiolate moieties. The formation of *N*-diazeniumdiolate converts the hydrophilic poly(*N*-acryloyl-2,5-dimethylpiperazine) segments into hydrophobic chains and serves as a chemical trigger to drive micellization. They demonstrated that the encapsulation of NO donors within the hydrophobic microenvironment of a micelle core could protect NO donors from proton catalysed burst NO release in an aqueous solution. As a result the NO release reaction exhibited a 7 day half-life under aqueous conditions.

Kanayama and co-workers have prepared photodriven NO-generating PEGylated polymer micelles, containing 4-nitro-3-trifluoro-methylphenyl units as NO donors confined within the micelle core.[67] The resulting particles were shown to exogenously deliver NO into target cells using light as a triggering stimulus. Further, these authors also demonstrated NO-mediated antitumor effects in this work.

Nitrate-containing micelles have also been reported by Duong et al.[68] In this work an amphiphilic block copolymer was synthesized via reversible addition fragmentation chain transfer polymerization (RAFT). Specifically, poly[oligo(ethylene glycol methyl ether methacrylate) macro-RAFT agent was chain extended in bulk with the co-

monomers vinylbenzyl chloride and styrene to form block copolymers. The ratio of chloromethyl-pendant group to styrene was easily manipulated by adjusting the feed ratio of the two monomers, and determined the number of sites available for subsequent nitrate functionalisation. The hydrophobic chloro-pendant groups in the block copolymer were converted into nitrate groups using silver nitrate ($AgNO_3$). The authors showed that in the presence of glutathione, only 36 % of total NO was observed at 37℃ over a period of 21 h, while 99 % release was measured at 60℃ for the same period.

The same group has also combined the incorporation of a small molecule NO donor, S-nitrosoglutathione (GSNO), into designed polymeric micelles.[69] Diblock copolymers were first prepared using RAFT polymerization. Specifically, oligoethylene glycol-methacrylate (OEG-MA) was initially polymerized, and then chain extended with 2-vinyl-4,4-dimethyl-5-oxazolone monomer (VDM) yielding diblock copolymers. The azlactone groups of the hydrophobic VDM domains were modified by reaction with GSNO under basic conditions (Figure 1.3). The release profiles of NO from free GSNO and GSNO-functionalised polymeric micelles were subsequently compared. The authors demonstrated that GSNO conjugated polymeric nanoparticles substantially improved NO stability in aqueous solutions when compared to the free GSNO under the same conditions. Intracellular NO release from GSNO polymeric nanoparticles was observed using 4-amino-5-methylamino-2',7'-difluorofluorescein diacetate (DAF-FM DA), which emits a green fluorescence signal when treated with GSNO-conjugated polymeric micelles inside the cells. Cytotoxicity assays of GSNO functionalised polymers with cisplatin were evaluated in different cell lines. The authors indicated that the cytotoxicity effect of NO-releasing micelles in combination with cisplatin on neuroblastoma cells was 5 times higher than non-NO treated cells. This synergistic effect was not observed in non-cancerous fibroblast cell controls.

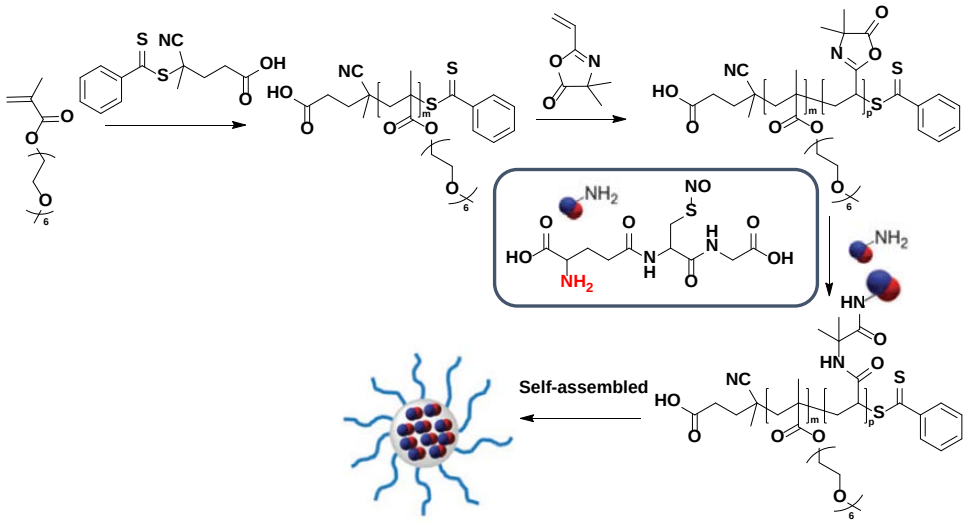

Figure 1.3: The synthesis of GSNO-functionalised polymeric micelles. Adapted from with permission from Duong et al.[69] Copyright 2013 Royal Society of Chemistry.

The same group has recently reported that GSNO modified polymeric micelles can be applied as a potential treatment for liver fibrosis and portal hypertension.[70] Using a similar strategy outlined above, GSNO-functionalised polymeric micelles were prepared and decorated with vitamin A, which allows the specific targeting of hepatic stellate cells (HSCs). These vitamin A decorated NO donor nanoparticles were shown to release NO in liver cells, which inhibited collagen I and α-smooth muscle actin fibrogenic genes associated with activated HSCs expression in primary rat and human livers without any cytotoxic effects.

Dendrimers

Dendrimers are highly monodisperse macromolecules with well-defined hyper-branched nanostructures. The synthesis of dendrimers is complex and easily manipulated to control the size of nanoparticles and the number of peripheral functional groups. These unique properties have provided an attractive scaffold for storing NO by increasing the payload of NO per dendrimer. Stasko and Schoenfisch have prepared NO releasing polypropylenimine dendrimers by generating *N*-diazeniumdiolate moieties under exposure to NO gas.[71] Large polyamines were grown in a divergent fashion, and terminated by primary amines based on the polypropylenimine dendrimer generation. The authors demonstrated that some primary amine- terminated dendrimers were able to store NO via *N*-diazeniumdiolate NO donors, however the conversion efficiency of the NO donor-modified dendrimers

was low, and failed to provide lengthy NO release duration. In addition, further studies indicated that the primary amine NO donors were predicted to generate nitroxyl (HNO) at a physiological pH (pH7.4), while only acidic pH (pH 3) conditions were able to trigger NO release from primary amine NO donors. To form more stable NO donor adducts, secondary amines were introduced into the dendrimers via the modification of primary amine-terminated dendrimers. Specifically, the primary amine in the polyamine backbone was acylated with heptanoyl chloride to form amide groups, which were then reduced using lithium aluminium hydride to produce secondary amines. The authors observed that secondary amine functionalised dendrimers showed higher NO loading capacity compared to the primary amine- terminated dendrimers. NO release duration and kinetics from secondary amine-containing precursor dendrimers exceeded those from equivalent small molecules as well as primary amine dendrimers, thereby providing a so-called “dendritic effect” on NO release kinetics.

The same authors further prepared two generation-4 polyamidoamine (PAMAM) dendrimers with S-nitrosothiol moieties.[72] Surface primary amines of PAMAM dendrimers were reacted with either N-acetyl-L-cysteine (NACys) or N-acetyl-D,L-penicillamine (NAP) to yield thiol-functionalised PAMAM dendrimers. The sulfhydryl groups of each dendrimer were then treated with different nitrite solutions (nitrous acid or isopentyl nitrite) to produce the corresponding *S*-nitrosothiol functionalised dendrimers. Copper and photoinitiated NO release were observed from these *S*-nitrosothiol modified dendrimers by triggering nitrosothiol decomposition processes, in which the kinetics of NO release was highly influenced by the structure of the *S*-nitrosothiol. S-nitroso-N-acetyl-D,L-penicillamine functionalised dendrimers were investigated for antiplatelet activity, and prevented platelet aggregation. A 62% inhibition in platelet aggregation was observed when exposed to *S*-nitrosothiol modified dendrimers, compared to only a 17 % reduction for small molecule donors.

Recently, the same group has developed a non-cancer related use of the glutathione (GSH) triggered NO release from *S*-nitroso-*N*-acetyl-D,L-penicillamine-derivatized PAMAM dendrimers.[73] In the presence of physiologically relevant concentrations of GSH, enhanced NO release was detected from the NO donor dendrimers. This combination represented a novel strategy for successfully reducing reperfusion /

ischemia injury in a perfused rat heart by obtaining a GSH-initiated therapeutic dose of NO from the dendritic NO donors.

Core cross-linked star polymers

Core cross-linked star polymers are considerably more straightforward to synthesize than dendrimers, and have more compact structure than micelles. Duong et al. reported the first use of core cross-linked star polymers for the encapsulation of NO donors.[74] The star polymers were prepared using an "arm-first" approach method, in which RAFT polymerisation was employed to synthesize poly ethylene glycol methyl ether acrylate, followed by chain extension with 2-vinyl-4,4-dimethyl-5-oxazolone (VDM) and the cross linker, *N,N*-methylenebisacrylamide. Spermine was then reacted with the VDM-functional star polymer through an azlactone ring-opening amidation, which in turn provided the secondary amine for modification to yield *N*-diazeniumdiolate in the presence of NO gas at 5 atm (Figure 1.4). NO-core cross-linked star polymers were found to release NO sustainably and were applied in the dispersal of bacterial biofilm by confining bacterial growth to the suspended liquid.

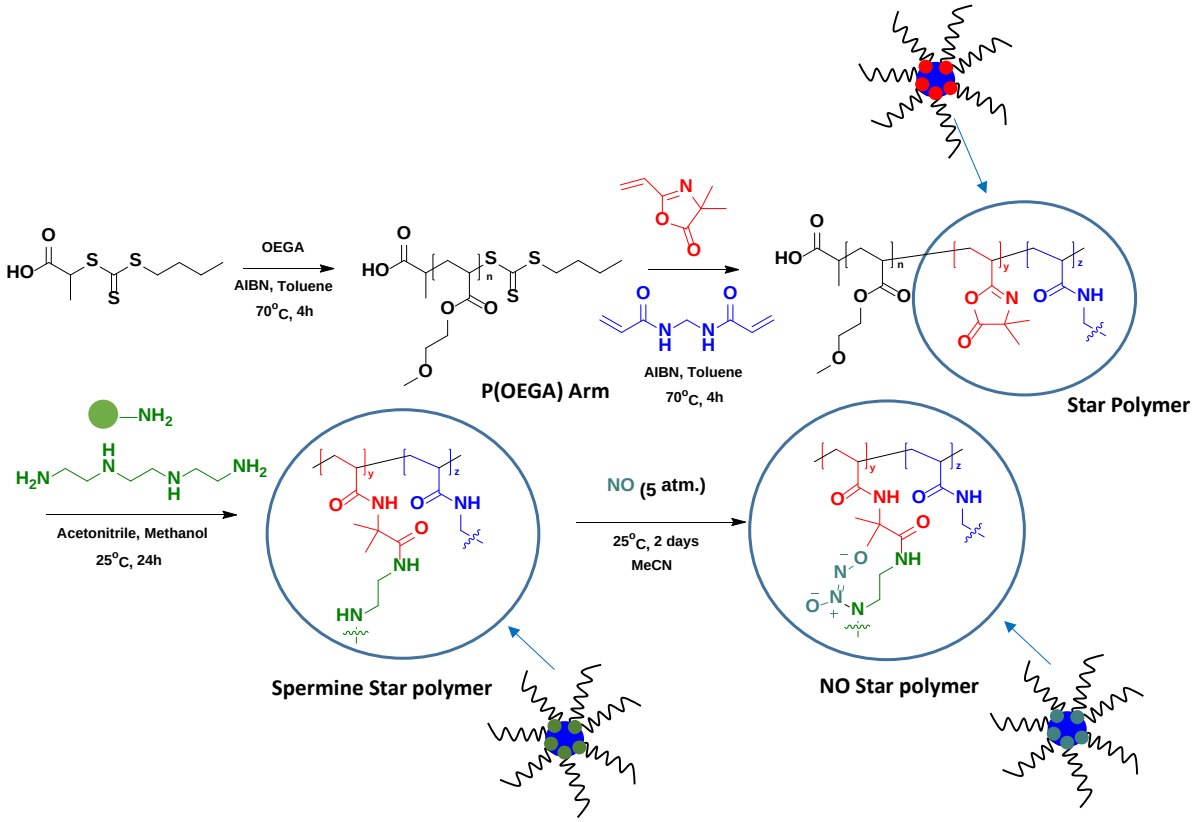

Figure 1.4: The synthesis of NO-releasing core cross-linked star polymers. Adapted from with permission from Duong et al.[74] Copyright 2014 American Chemical Society.

Multiarm polymeric nanocarriers for NO have been reported by Duan et al.[75] The synthesis of poly(1,2,3,4-di-O-isopropylidene-6-O-methacryloyl-*α*-*D*-galactopyranose) was conducted with a pentaerythritol based RAFT agent. Deprotection of isopropylidene groups was then performed to yield poly(6-O-acryloyl-*D*-galactose). The modification of the sugar polymers with succinic anhydride resulted in multi-arm polymers with increasing degrees of terminal carboxylic acid groups on the polymer arms. The acid functional groups of the glycopolymers were then conjugated to hydroxyl functional groups of N-diazeniumdiolate NO donors. The *in vitro* NO release data indicated that multi-arm polymer based nanoconjugates exhibited longer release half-life than the NO-releasing prodrugs. Furthermore, subcutaneously injected NO-conjugated multi-arm polymers improved the tumour inhibition and survival time of the tumour-bearing nude mice, when compared to intravenous therapy with NO prodrugs.

Lipid-based nanocarriers

Liposomes are spherical vesicles with an aqueous core surrounded by at least one lipid bilayer. Hydrophilic or lipophilic drugs, or genes incorporated into the aqueous core or within bilayers may be delivered into target areas. Recently liposomes have been used as NO carriers. For example, Huang and coworkers have developed echogenic liposomes as NO carriers.[76] The cationic liposome contained phospholipids and cholesterol, which were prepared by freezing under pressure. The authors observed that the NO-releasing liposomes showed an initial rapid NO release profile followed by a slower release phase lasting several hours. In addition, inhibition of intimal hyperplasia development and reduced arterial wall thickening were observed when NO-releasing lipid carriers were locally delivered into balloon-injured carotid arteries.

Koehler and coworkers have encapsulated a photosensitive NO donor, S-nitroso-N-acetylpenicillamine (SNAP), within 1,2-dimyristoyl-sn-glycero-3-phosphocholine (DMPC), cholesterol and dihexadecyl hydrogen phosphate lipid vesicles.[77] These vesicles were then doped into a sol-gel silica environment matrix, which has biological compatibility and capability as a growth surface for mammalian cells (Figure 1.5). Stimulation by a light source triggered rapid NO release from the nanocomposite material within seconds. The NO flux decreased with distance perpendicular to the surface, due to diffusion from a surface though an aqueous environment.

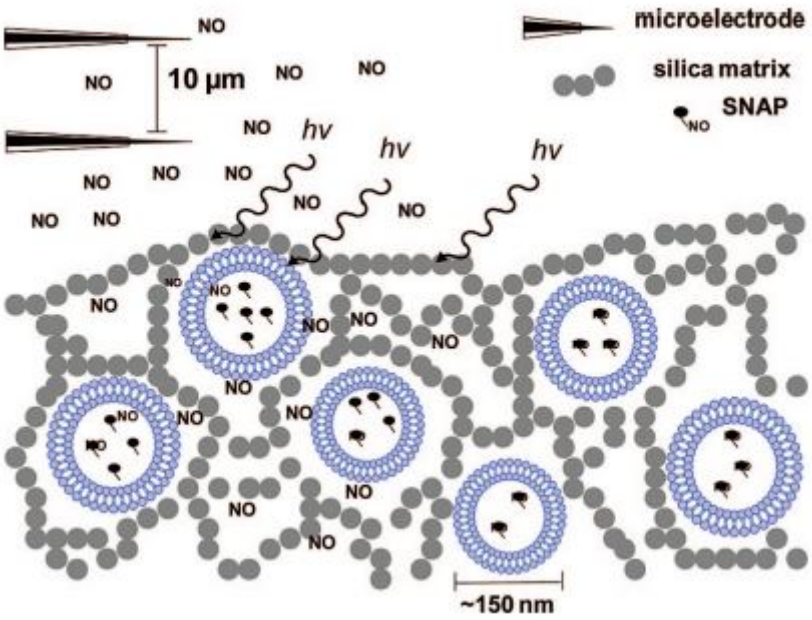

Figure 1.5: Compartmentalized nanocomposite liposome materials for light triggered NO release. In the dark condition, NO is bound to SNAP, which is unable to diffuse through the liposome compartment membrane. The liposome is trapped within pores of the silica cell culture substrate. In the presence of light, SNAP can release NO, which can diffuse to the surface of the materials. Reprinted with permission from Koehler et al.[77] Copyright 2008 American Chemical Society.

Recently, Perera et al. have reported using liposomes as nitric oxide synthase (NOS) enzyme carriers.[78] As noted above, NOS enzymes catalyse L-arginine to produce NO. The authors encapsulated recombinant NOS enzymes within 1,2-distearoyl-glycero-3-phosphocholine liposomes, having a loading capacity of 25-40 %. The NOS-carrying liposomes were observed to assess their stability by measuring NO production upon NOS stimulation. The authors demonstrated that the NOS-loaded liposomes remained stable for at least 15 days, during which native NOS structure and functions were also well preserved.

1.1.4 Therapeutic applications of NO-releasing nanoparticles

NO-releasing materials have been exploited in many biomedical applications, and offer potential benefits in various therapeutic situations. The potential clinical applications for NO-releasing nanoparticles have been explored and categorised into five different areas: wound healing, cardiovascular therapy, anticancer agents, erectile dysfunction therapy and antimicrobial applications.

Wound healing

Would healing is a complex process and is divided into three different phases: inflammation, proliferation and remodelling.[79] NO plays a critical role in all these phases. Specifically, during the early stage, NO mediates vasodilation, inhibits platelet aggregation, and protects against invading pathogens. In the proliferation phase, NO stimulates fibroblasts, keratinocytes and endothelial cells. During the final remodelling process, NO is involved in fibroblast production and deposition of collagen.[79–81] Blecher and coworkers have investigated NO-releasing nanoparticle platforms, and compared them to small-molecule NO donors (diethylenetriamine, DETA NONOate) in wound healing processes.[82] The authors prepared silane-based sol-gel derived NO generating nanoparticles that can generate and deliver NO in a controlled and sustained manner. In this study, non-obese, diabetic, severe combined immunodeficiency (NOD-SCID) mice were used. These mice were divided into four treatment groups, 1) no treatment, 2) treatment with empty nanoparticles without NO loading, 3) treatment with NO generating nanoparticles and 4) treatment with only NO donors (DETA NONOate). The authors found that treatment with NO generating nanoparticles resulted in accelerated wound closure on the wounded areas. Even though DETA NONOate is an effective NO-donor, there was no significant difference in wound closure observed between DETA NONOate-treated mice and controls. However, histological analysis revealed that wounds treated with NO generating nanoparticles showed less inflammation, more collagen deposition, and more blood vessel formation as compared to the other groups.

Han et al. have also examined the effects of NO releasing nanoparticles on the wound healing process.[83] The nanoparticles were prepared based on the work by Friedman and co-workers.[49] In this study, human dermal fibroblasts were observed with treatment of NO-releasing nanoparticles, control nanoparticles or untreated conditions. The authors demonstrated that NO generating nanoparticles increased fibroblast migration and collagen (type I and type II) deposition in wounded tissue, compared to control nanoparticles or untreated experiments. These processes are critical in the formation of new tissue in wounded areas, providing a foundation for subsequent keratinocyte migration and ultimately resolution of the wound.

Cardiovascular therapy

NO initiates and mediates vasodilation through a cascade of biological events. Specifically, NO diffuses across the endothelial cell layer and into the adjacent smooth muscle cell layer, where it leads to an increase in cyclic guanosine monophosphate monophosphate (cGMP) and thus relaxation of the smooth muscle by decreasing intracellular calcium concentration.[23–26] As such, NO may have some therapeutic potential in the treatment of cardiovascular diseases.

Cabrales et al. have reported the reversal of vasoconstriction using NO releasing nanoparticles.[84] These authors developed sol-gel NO generating nanoparticles for sustained delivery and release of NO from a long-circulating particle. These particles were then infused into Golden Syrian Hamsters[55] and found to slowly release physiologically relevant concentrations of NO. Systemic hypotension and increased exhaled NO concentration also supported the exogenous NO release from the NO generating nanoparticles with an infusion of 20 mg/kg. This sustained NO release resulted in both decreased blood pressure and increased vascular relaxation, which was limited by the dose and the time course of hydration. In particular, the authors observed that circulating NO generating nanoparticles induced vasodilation and increased microvascular perfusion over several hours' circulation, compared to the absence of any vascular response after the infusion of the control nanoparticles.

Encouraged by these results this group extended the application of NO releasing nanoparticles to the reversal of haemoglobin (Hb)-induced vasoconstriction.[84] Polymerised bovine haemoglobin (PBH) was used to induce vasoconstriction in Golden Syrian hamsters via a NO scavenging mechanism. NO scavenging by PBH occurs via three reactions: an oxidative reaction of NO with NO dioxygenase, NO binding to deoxyhemoglobin and NO binding to the β-chain cysteine amino acid at position 93 in Hb. These reactions result in observable vasoconstriction though a cascade of signalling pathways. Initially, PBH was infused to increase blood pressure and induce vasoconstriction. NO releasing nanoparticles were then introduced at doses of either 10 or 20 mg/kg. The authors observed that treatment with NO generating nanoparticles reduced blood pressure and vasoconstriction. The sustained NO release from nanoparticles was reflected by the continued reversal of the hypertension and vasoconstriction compared to the control nanoparticles. This result

was also supported by the evidence that NO releasing nanoparticles were effective in reducing mean arterial blood pressure of PBH treated hamsters with increasing heart rates. The effectiveness was more pronounced with a higher dose NO releasing nanoparticle concentration. Moreover, treatment with NO generating nanoparticles increased methemoglobin levels, functional capillary density, and plasma nitrite and nitrate concentrations.

Cabrales et al. have also examined the application of NO releasing nanoparticles for the treatment of hemorrhagic shock[85] induced cardiovascular collapse. The authors found that exogenous delivery of NO can prevent the risks of profound haemorrhage. Moreover, the continuous NO release from NO generating nanoparticles supported systemic and microvascular functions during hemorrhagic shock. Furthermore, NO releasing nanoparticles reverted arteriolar and venular vasoconstriction, thereby increasing blood flow (Figure 1.6). Both capillary density and microvascular blood flows were partially recovered with the treatment of NO-relasing nanoparticles. In addition, the authors observed that exogenous NO delivery prevented cardiac decompensation and improved intravascular pressure redistribution and blood flow, and therefore maintained heart rate with cardiac stability.

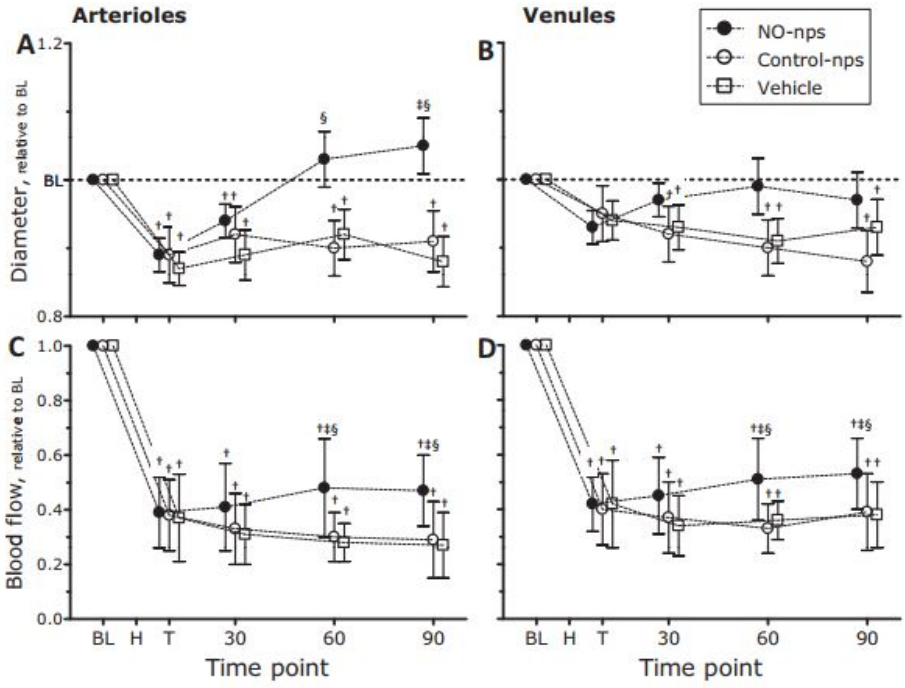

Figure 1.6: NO releasing nanoparticle effects on changes in arteriolar and venular diameter (A and B) and blood flow (C and D) during hemorrhagic shock. The broken line represents the baseline. Time points: BL, baseline; H, after haemorrhage; T, after treatment; 30, 60 and 90 min after treatment. †P < 0.05 compared with baseline; ‡ P < 0.05 compared with vehicle; § P < 0.05

compared with control-nps. Diameters (μm, mean ± SD) in A (arterioles) and B (venules) for each animal group were as follows: baseline: vehicle (arterioles (A): 62.7 ± 8.2, n=26; venules (V): 64.5 ± 6.8, n=24); Control-nps (A: 60.5 ± 6.8, n=24; V: 65.7 ± 8.7, n=27); NO-nps (A: 62.0 ± 7.4, n=25, V: 64.5 ± 8.2, n=26). n=number of vessels studied. RBC velocities (mm/s), mean ± SD for each animal group were as follows: baseline: vehicle (A: 4.3 ± 1.0, V: 2.3 ± 0.9); Control-nps (A: 4.5 ± 0.8; V: 2.4 ± 1.0); NO-nps (A: 4.3 ± 1.0, V: 2.6 ± 0.7). Flows (nl/s, mean ± SD) in C (arteriolar) and D (venular) for each animal group were as follows: baseline: Vehicle (A: 11.7 ± 3.4; V: 6.9 ± 2.2); Control-nps (A: 12.1 ± 3.2; V: 7.1 ± 2.3); NO-nps (A: 12.0 ± 2.8; V: 6.8 ± 2.3). Reprinted from Resuscitation, 82, P. Nachuraju, A. J. Friedman, J. M. Friedman, P. Cabrales, Exogenous nitric oxide prevents cardiovascular collapse during hemorrhagic shock, 607-613., Copyright (2011), with permission from Elsevier.

Recently, Nacharaju and coworkers have developed two hydrogel based *S*-nitrosothiol (SNO) containing nanoparticle platforms; i) SNO groups are covalently conjugated to the particles (SNO-np); (ii) S-nitroso-N-acetyl cysteine groups are encapsulated within the particles (NAC-SNO-np).[86] Both nanoparticles can release NO, and thus serve as trans-S-nitrosating agents. In particular, NAC-SNO-np was the most effective at generating S-nitrosoglutathione (GSNO) with a sustained high level of NO concentration for longer period of time. In *in vivo* studies, NAC-SNO-np and NO releasing nanoparticles were intravenously infused to Golden Syrian hamsters. Both nanoparticles resulted in decreased mean arterial pressure, and increased heart rate and vessel diameters. Specifically, longer vasodilatory effects were induced by NAC-SNO-np, compared to the other NO releasing nanoparticles. Furthermore, dose dependent vasodilatory effects of NAC-SNO-np were observed. 20 mg/kg of NAC-SNO-np showed more pronounced effects in reduced arterial pressure and heart rate, and increased vessel diameter as compared to infusing 10 mg/kg of NAC-SNO-np in hamsters.

Anticancer agents

NO has emerged as a potential anticancer agent, showing tumoricidal effects. Expression of nitric oxide synthase (NOS) has been detected in various cancers, and found to modulate different cancer-related events including angiogenesis, apoptosis, cell cycle, tissue invasion and metastasis.[34]

Kuppusamy and co-workers have demonstrated that the delivery of NO followed by cisplatin showed significantly greater cytotoxicity in drug resistant ovarian cancer cells when compared with those treated with cisplatin alone.[87] Stevens and coworkers investigated the first potential use of NO releasing nanoparticles in cancer therapy.[88] NO releasing nanoparticles were prepared by co-condensation of tetraethyoxysilane

(TEOS) with various ratios of an *N*-diazeniumdiolate-modified aminosilane. Different sizes of particles were prepared by varying the solvent or the amount of aminoalkoxysilane added. The cytotoxicity of the NO releasing silica nanoparticles was investigated using an MTT assay. NO-releasing nanoparticles showed greater antitumor activity when compared to the small molecule NO donor PYRRO/NO. The dose of NO required for cancer cell growth inhibition was significantly reduced when provided by an NO generating nanoparticle system, compared to a small molecule NO donor. This observation was attributed to the short half-life of the small molecule donors. In addition, the authors observed that increasing the size of nanoparticles (90 - 350nm) was more effective in inhibiting ovarian cancer cell growth compared to non-tumour ovarian cells. Confocal microscopy was used to examine cellular localisation of NO-releasing silica nanoparticles. The analysis revealed that the nanoparticles entered the cytosol of the cells and localised to late endosomes and lysosomes.

As aforementioned, Duong and coworkers have reported S-nitrosoglutathione (GSNO) conjugated polymeric micelles.[69] The cytotoxicity effects of GSNO-functionalised polymeric nanoparticles in combination of cisplatin were observed in normal lung fibroblasts (MRC5 cells) and neuroblastoma cells (BE(2)-C) using the Alamar Blue Assay. Prior to exposing the cells to cisplatin, the cells were pre-incubated with NO-releasing micelles. The authors observed that BE(2)-C cells pre-treated with GSNO-functionalised polymers showed a greater cytotoxic effect of cisplatin when compared with non NO pre-treated cells. The IC_{50} of cisplatin in GSNO conjugated nanoparticles pre-treated BE(2)-C cells was approximately 5 times lower than non pre-treated cells. Interestingly, there was no enhanced cytotoxic effect of GSNO conjugated nanoparticles with cisplatin in non-cancerous MRC5 cells.

Erectile dysfunction therapy

NO is widely known to be involved in the onset of erection. As such, Han and coworkers hypothesised that transdermal delivery of NO could trigger an erection.[89] Nanoparticles encapsulating NO were synthesized via sol-gel preparation with tetramethylorthosilicate (TMOS), sodium nitrite, glucose, polyethylene glycol and chitosan. These NO delivery nanoparticles were then applied to the glans and shaft of the penis of retired breeder male rats. Visible erections were observed in the animals approximately 4.5 mins following nanoparticle administration. These observations

were coupled with changes in intracorporal pressure and systemic blood pressure. Subsequently, the authors applied nanoparticles loaded with sialorphin (a neutral endopeptidase inhibitor). Administration of sialorphin-loaded nanoparticles resulted in longer-lasting erections when compared to rats administered with NO nanoparticles. Longer lasting erections were also observed after tadalafil (a phosphodiesterase type 5 inhibitor)-loaded nanoparticle administration, albeit when combined with cavernous nerve stimulation. Nonetheless, the authors demonstrated that NO releasing nanoparticles have some scope in treating erectile dysfunction. However, considerable further optimisation would be needed to increase the efficacy of NO-delivery nanoparticles for erectile dysfunction therapy.

Antimicrobial applications

Pelgrift and Friedman have reviewed the potential applications of nanoparticles to combat microbial resistance.[90] NO-releasing nanoparticles possess multiple antimicrobial mechanisms, which decreases the probability of microbes developing resistance to NO-releasing nanoparticles. NO primarily exerts its antimicrobial action via three different mechanisms. Firstly, NO causes direct nitrosative damage to DNA and reacts with several amino acid residues of bacterial proteins through the formation of reactive nitrogen intermediates (RNOS). RNOS also triggers increased generation of hydrogen peroxide and alkylating agents, which induces scission or modification of the DNA strands. Secondly, elevated NO concentrations can cause increased generation of RNOS including peroxynitrite and nitrogen dioxide, which can facilitate lipid peroxidation. Finally, NO may react with thiols to produce S-nitrosothiols (RSNO), which could nitrosylate the thiol groups on the cysteine residues of DNA repair enzymes. All these combined effects can overcome microbial drug resistance when NO is delivered either alone or with other antibiotic drugs. Previous work described above has demonstrated the application of NO-releasing polymeric nanoparticles in inhibiting the formation of biofilm.[74] NO-releasing star polymers were applied to *Pseudomonas. aeruginosa* biofilm, showing 90 % and 95 % reduction in film biomass compared to the untreated biofilm, including a nontoxic effect of planktonic growth. Furthermore, the authors tested NO releasing star polymers against biofilms of mutant strains lacking the phosphodiesterases *dipA* and *rdbA* that induce the reduction of intracellular levels of second messenger cyclic di-GMP in response to NO. Ultimately, dipA mutant biofilms were not affected, while *rbdA* mutant biofilms showed a 50 %

reduction compared to 99 % with wild type. These results indicated that NO releasing star polymers can continuously stimulate phosphodiesterase activity by maintaining low intracellular level of cyclic di-GMP, thereby inhibiting biofilm growth.

1.2 Hydrogen Sulfide (H_2S)

1.2.1 Introduction and Biological roles of H_2S

For centuries hydrogen sulfide (H_2S) was primarily known as a poisonous gas due to its toxicity and strong obnoxious and overpowering odour.[91,92] However, in 1996 H_2S was found to have a physiological function in the brain, acting as a neuromodulator.[93] Since this initial research, many studies have demonstrated the role of H_2S as an endogenous gasotransmitter, along with nitric oxide (NO) and carbon monoxide (CO).[2,94] The endogenous production of H_2S is implicated in numerous physiological functions, which led to its investigation as a potential therapeutic agent in much the same way as NO and CO.[95–99]

In mammals, H_2S is endogenously produced in many tissues including the brain, heart, vasculature and liver through three main enzymatic pathways, which are all part of cysteine metabolism (Figure 2.1).[91] Cystathionine-γ-lyase (CSE), cystathionine β-synthase (CBS), and 3-mercaptopyruvate sulfur transferase (3-MST) are the key enzymes involved in these pathways. CBS is responsible for catalysing a β-substitution reaction of serine to form cystathionine, which is then eliminated by CSE to produce cysteine, ketobutyrate and ammonia. The production of H_2S from cysteine or homocysteine is catalysed by CBS and CSE. Cysteine aminotransferase (CAT) is also involved in transferring the amino group from cysteine to a keto acid, forming 3-mercaptopyruvate (3MP). 3-MST then catalyses the process to generate H_2S from 3MP.

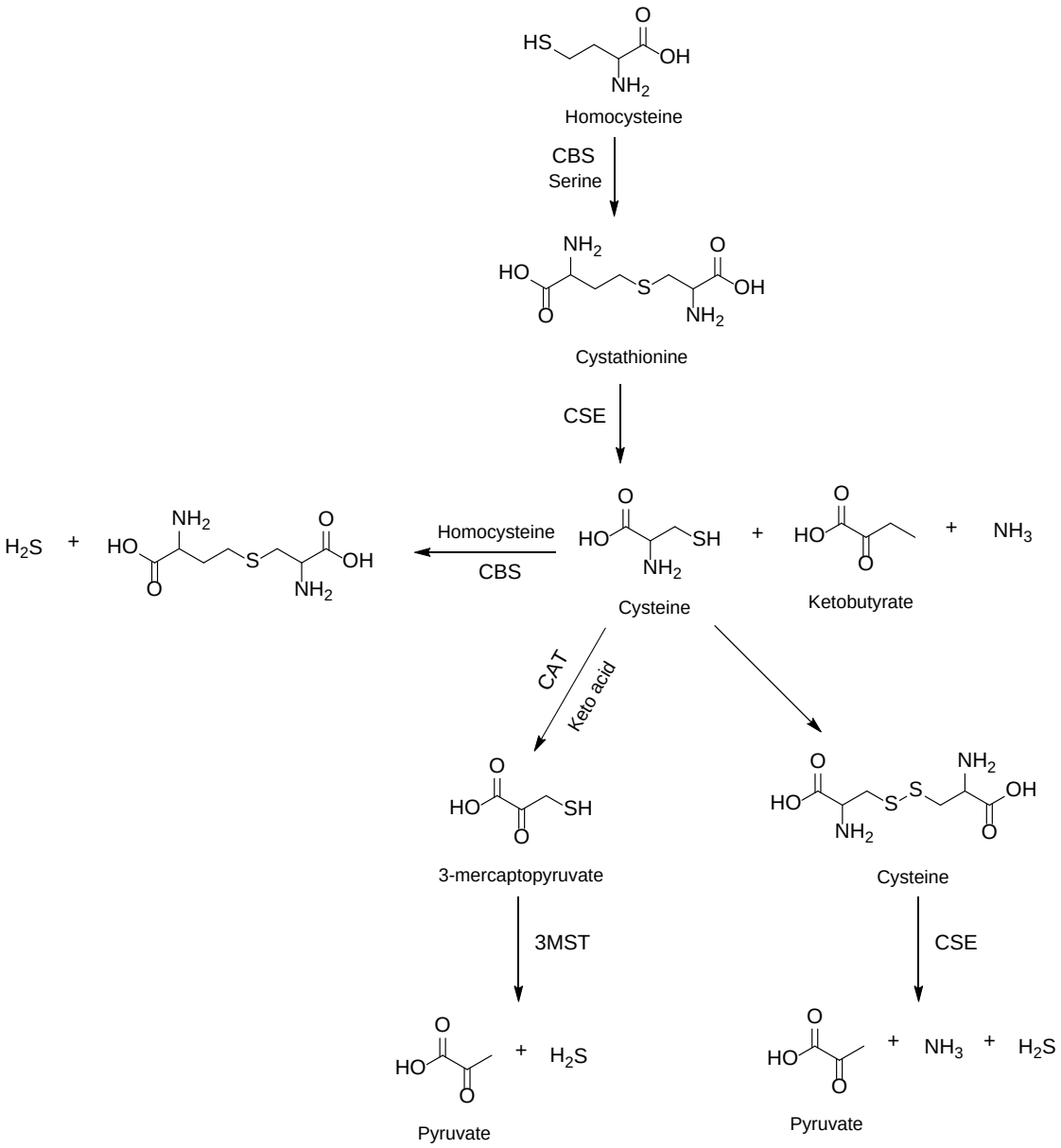

Figure 2.1: Enzymatic endogenous H_2S production in mammalian cells. Adapted from with permission from Zheng et al.[91] Copyright 2017 Wiley Periodicals, Inc.

H_2S can also be generated or stored in *vivo* through non-enzymatic processes. It can be stored in proteins by forming persulfide moieties through S-sulfhydration or generated from sources such as organic and inorganic polysulfides including, interestingly, garlic.[100–102]

Like NO, H_2S has been considered as an important and independent regulator of various physiological systems including mammalian cardiovascular, gastrointestinal, nervous and immune system. Both have paracrine modes of signalling as well as identical or shared signalling transduction pathways.[103,104] One of the well-known physiological roles of H_2S is the regulation of vascular contractility. Relaxation of

vascular smooth muscle cells can be mediated through H_2S-dependent adenosine triphosphate (ATP)-sensitive potassium channel opening.[105] H_2S acts as a major endothelium-derived relaxing factor by chemically modifying sulfhydryl groups of the proteins associated with the potassium channel.[106] Furthermore, H_2S has been found to provide some protective effects in various disease pathologies. It has been implicated in cardioprotective,[107,108] gastroprotective[109] and neuroprotective mechanisms.[110,111] H_2S also exhibits strong cytoprotective effects through a combination of antiapoptotic and antioxidant signals.[112–114] Improved wound healing and regulation of insulin release are controlled by H_2S.[115,116] During vascular inflammation, leukocyte adherence can be inhibited by H_2S in the microcirculation.[117,118] Deficiency of H_2S production has been also associated with hypertension, gastric mucosal injury and Alzheimer's disease.[119]

Various cellular signalling pathways involving intracellular mitogen-activated protein kinases (MAPK) have been found to be affected by H_2S. As an example, endogenous and exogenous H_2S were found to inhibit the proliferation of rat aortic vascular smooth muscle cells via through H_2S-dose dependent MAPK pathway.[120] In addition, the survival of human granulocytes was improved by exogenously delivered H_2S treatment, associated with the inhibition of p38 MAPK phosphorylation and attenuation of lipopolysaccharide-triggered p38 MAPK phosphorylation in keratinocytes and microglial cells.[121,122]

Several studies have shown the relationship between H_2S and antineoplastic antibiotics including doxorubicin (DOX) in various cell lines. For instance, treatment of DOX to H9c2 embryonic rat cardiac cells significantly reduced the activity of CSE, an H_2S synthetase, resulting in the decreased cell viability.[123] Exogenous H_2S was shown to protect H9c2 cells against DOX induced cardiotoxicity by inhibiting endoplasmic reticulum (ER) stress. Furthermore, H_2S pre-treated H9c2 cells were found to attenuate DOX-induced cardiotoxicity by decreasing calreticulin (CRT) expression in the cardiac cell lines.[124] However, in a different cell line (U2OS osteosarcoma cells), higher cytotoxicity was observed after co-treatment of DOX and H_2S.[125] H_2S was shown to improve intracellular DOX accumulation and cytotoxicity effects in these cancer cell lines.

1.2.2 H_2S Donors

To date, a range of donor compounds have been applied for delivering H_2S in biological investigations, with the inorganic sulfide salts (e.g., Na_2S/NaSH) commonly employed. While sulfide salts produce HS^- and H_2S under typical buffer conditions they unfortunately exhibit an uncontrolled release profile. Indeed, the instantaneous H_2S release profile from this small molecule donor may not reproduce the effects of continuous biosynthesis, nor allow H_2S to interact with particular intracellular targets in a reproducible or practical manner.[126–130] In consideration of this issue, a range of organic H_2S donors with superior and slower release profiles have been developed. These have been found to produce protective and beneficial effects: for example, non-steroidal anti-inflammatory drugs (NSAIDs) were incorporated with H_2S releasing molecules, resulting in improved gastrointestinal safety and more potent anti-inflammatory effects than the parent drugs.[129] A series of H_2S-releasing DOX moieties were prepared by conjugating DOX with different H_2S donor substructures (Scheme 2.1).[125]

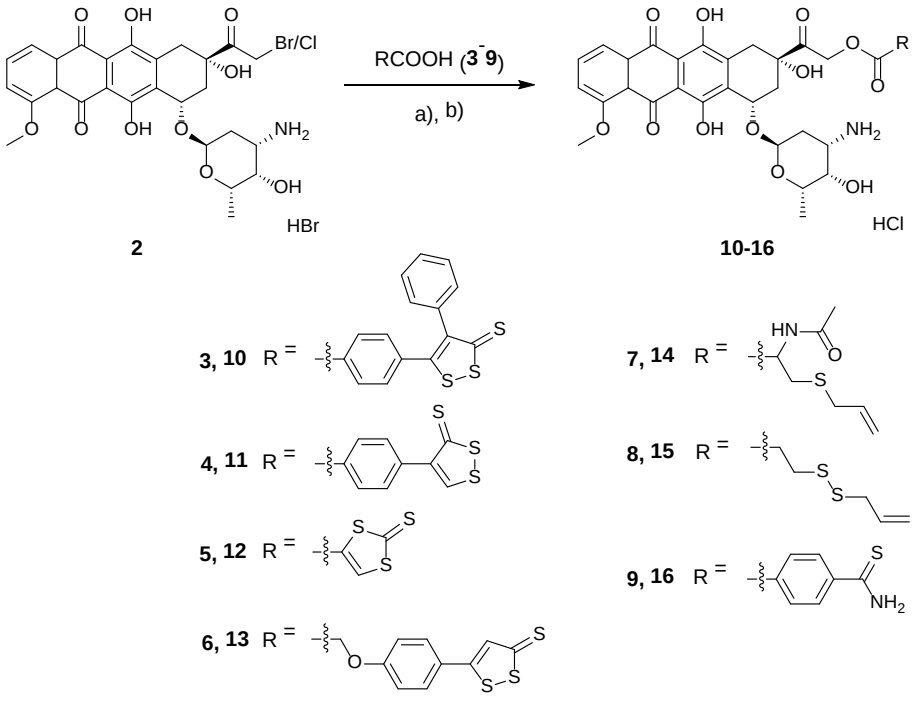

Scheme 2.1: A number of DOX-linked H_2S donors obtained by combining DOX with H_2S donors through an ester bond linkage. Adapted from with permission from Chegaev et al.[125] Copyright 2016 American Chemical Society.

These H_2S-DOX conjugate drugs were hydrolysed to release H_2S. Donor **11**, a derivative of benzoic acid bearing in *para*-position, showed the highest amount of

controlled H_2S release within 24 h. These conjugate drugs were then tested on U2OS osteosarcoma cells and shown to significantly increase intracellular DOX retention and cytotoxic effects in U2OS cells, compared to native DOX treatment.[125] In addition, several other H_2S donating small molecules have been synthesized based on aryl dithiole-3-thione (ADT),[126] acyl-protected perthiols,[131] dithioperoxyanhydrides,[132] 1,2-dithiole-3-thiones[133] and phosphonamidothioates.[134]

1.2.3 H_2S-releasing delivery nanoparticle systems

Nanoparticle-based H_2S delivery systems have shown improved stabilities and subsequently more controlled H_2S release profiles compared with small molecule H_2S donors.[135–137] Moreover, tightly controlled H_2S release profiles may enable investigation of how H_2S interacts with particular intracellular biomolecules or organelles, and thus help probe, understand and therefore reproduce the effects of the biosynthesis of H_2S. For example, a number of H_2S donor compounds based on aryl dithiole-3-thione have been incorporated into nanoparticles, and these undergo a slow hydrolytic H_2S release.[135,136] Initially, the conjugation of the desmethyl form of dithiolethiones (ADT-OH) with poly(ethylene glycol) (PEG) was reported to show its H_2S releasing properties and minimised the toxic side effects of ADT-OH in murine macrophages.[135] The result of the PEG-ADT conjugate led to the further development of H_2S releasing polymeric micelles, which have ADT in the core.[136] Block copolymer consisting of a hydrophilic PEG block and a hydrophobic dithiolethione-containing H_2S releasing block (PADT) was able to self-assemble into ADT micelles. These micelles showed a slow hydrolytic H_2S release in cell lysate. The H_2S releasing micelles were then studied for cytotoxic and proinflammatory effects. These micelles showed less cytotoxicity compared to the small H_2S donors (ADT-OH or Na_2S), and improved the gardiquimod (GDQ)-induced proinflammatory responses in murine macrophages. GDQ, an imidazoquinoline compound, can stimulate the toll-like receptor (TLR) 7 to induce the proinflammatory responses. H_2S-releasing micelles could enhance both tumour necrosis factor-α (TNF-α) production and nuclear factor-κB (NF-κB) activation under GDQ-induced inflammation to improve innate immunity.[136]

Another approach to deliver H_2S via a nanoparticle system is by using polymeric carriers in which side chains have been functionalised via post-polymerisation modification with different moieties such as S-benzoylthiohydroxylamines or

dithioperoxyanhydrides. These compounds give rise to H_2S release under thiol-triggered conditions (e.g., upon exposure to L-cysteine/glutathione).[138–141,92] One example is derivatizing side-chain with *S*-aroylthiohydroxylamine (SATHA) to develop H_2S releasing *S*-aroylthiooxime-functionalised polymeric systems.[139] *S*-aroylthiooximes (SATO) can be formed via the reaction between an aromatic aldehyde/ketone and a SATHA. To this end polymers bearing pendant aldehyde functionalities were first prepared via the polymerization of aromatic aldehyde containing monomers. In this system, 2-(2-methoxyethoxy)ethyl methacrylate (MEO_2MA) was introduced into the co-polymerization with 2-(4-formylbenzoyloxy)ethyl methacrylate (FBEMA) to improve the solubility in water (Scheme 2.2, P5).

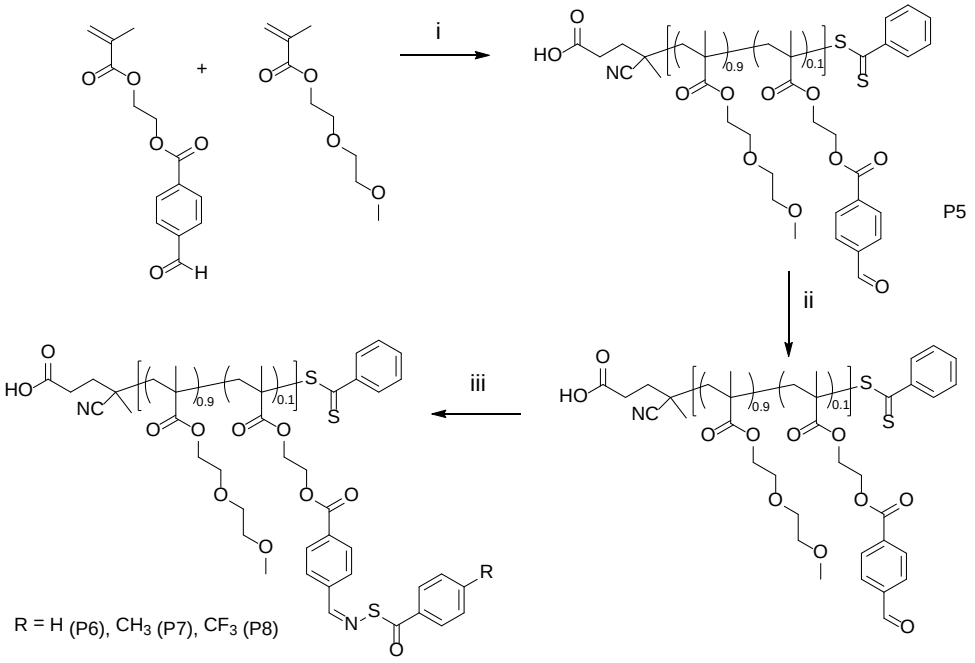

Scheme 2.2: The synthesis of Poly(FBEMA-co-MEO_2MA) copolymers via RAFT polymerization, followed by the removal of end group with AIBN and reaction with different SATHAs. Note: (i) chain-transfer agent 4-cyano-4-(phenylcarbonothioylthio)pentanoic acid (CTA1), 2,2'-azobis(2-methylpropionitrile) (AIBN), DMF, 75 °C; (ii) AIBN, 1,4-diozane, 80 °C; (iii) SATHA, CH_2Cl_2, trifluoroacetic acid (TFA, cat), rt. Adapted from with permission from Foster et al.[139] Copyright 2014 American Chemical Society.

In order to prevent an undesired side-reaction between the thiocarbonylthio end-groups of poly(FBEMA-co-MEO_2MA) copolymers and thiols, the endgroup moieties were removed using an excess of cyano-isopropyl radicals. The endgroup-removed copolymers were then reacted with SATHAs containing different functional groups in the presence of TFA to produce thiooxime-functionalised copolymers (P6-P8). The

thiooxime-functionalised copolymers were able to release H_2S in the presence of the thiol-containing triggers cysteine and glutathione. In addition, the relative H_2S releasing rates from thiooxime-functionalised copolymers (P6-P8) were greatly affected by the electronics of the substituent at the *para* position of the SATHA-derived ring structure.[139]

4-Hydroxythiobenzamide functionalised lactide monomers have been prepared based on the addition of a propanedithiol linker to an α,β-unsaturated lactide in the presence of catalytic I_2.[142] 4-Hydroxythiobenzamide has been known to release H_2S in *in vivo* studies and have synergistic effects with other drugs such as naproxen.[143,144] The lactide monomer covalently bonded to 4-hydroxythiobenzamide was then copolymerized with lactide to produce a series of polymers functionalised with different loadings of thiobenzamide, resulting in functionalized macromolecular H_2S donors (Scheme 2.3).

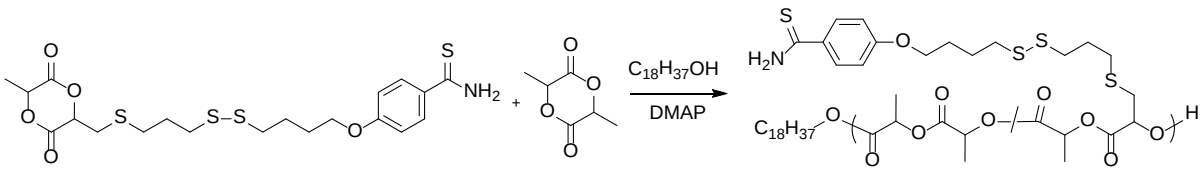

Scheme 2.3: The copolymerization of two monomers to yield poly(lactic acid) functionalized with different loadings of thiobenzamide. Adapted from with permission from Long et al.[142] Copyright 2015 Royal Society of Chemistry.

These polymeric particles were observed to release thiobenzamide over days to weeks. While the release of H_2S from the particles was not successfully measured, the release of thiobenzamide, precursor to H_2S, was observed from the particles depending on different loadings of thiobenzamide along the backbone of the poly(lactic acid).

Moreover, thiobenzamide (aryl thioamide)-functionalized block copolymers have also been prepared via thionation of benzonitrile-functionalized polymers.[92] These thioamide-functionalized polymers were found to effectively release H_2S under thiol-triggered conditions as well as hydrolytically. These H_2S release profiles were further enhanced when the thiobenzamides were incorporated into the micelle corona, rather than the core.

Previous studies have reported that H_2S can affect ERK (extracellular signal-regulated kinase) activity in HEK293, human embryonic kidney cells as a result of overexpression of cystathionine-γ-lyase.[145] In this study, HEK293 cells were subsequently treated with the H_2S macromolecular donors to monitor the effects on cytosolic/nuclear ERK and cytosolic/plasma membrane PKC (protein kinase C) activities in the cells. The macromolecular H_2S donors were shown to elicit a slow and sustained increase in cytosolic ERK signalling, and also induce a small, fast and sustained increase in plasma membrane-localized PKC signalling activity in the cells (Figure 2.2 and 2.3). No effects were observed for PBS alone and control polymers (i.e., with no thiobenzamides conjugated) on ERK and PKC signalling activities.

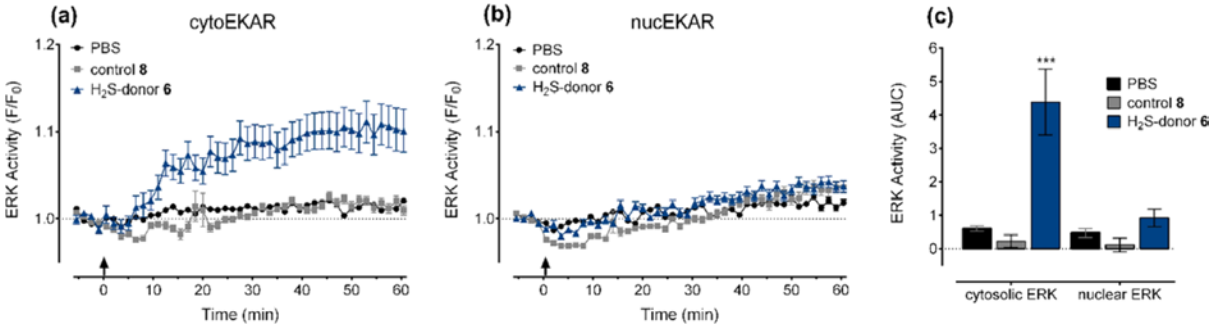

Figure 2.2: Time course of cytosolic ERK activation (a) and nuclear ERK activation (b) in HEK293 cells treated with PBS, H_2S macromolecular donors (6) and control (8), measured by EKAR (extracellular signal regulated kinase activity reporter) sensor. (C): Area under the curve (AUC) derived from time course. Symbols/bars represent means, and error bars SEM of 174-270 cells. Reprinted with permission from Ercole et al.[92] Copyright 2016 American Chemical Society.

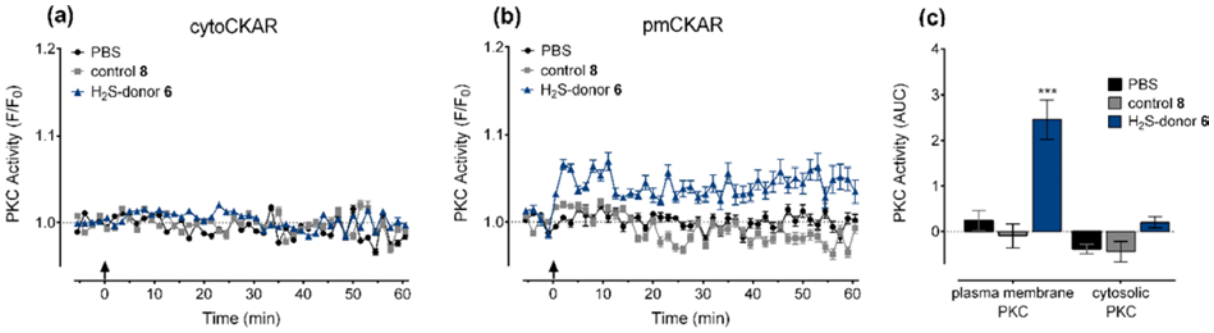

Figure 2.3: Time course of cytosolic PKC activation (a) and plasma membrane-localized PKC activation (b) in HEK293 cells treated with PBS, H_2S macromolecular donors (6) and control (8), measured by CKAR (C kinase activity reporter) sensor. (C): Area under the curve (AUC) derived from time course. Symbols/bars represent means, and error bars SEM of 73-145 cells. Reprinted with permission from Ercole et al.[92] Copyright 2016 American Chemical Society.

Mesoporous silica nanoparticles (MSN) have also been employed for the delivery of H_2S.[137] In this case the sol-gel technique was used to synthesize MSNs having a

narrow size distribution and high specific surface area. Diallyl trisulfide (DATS), an H_2S-releasing agent, was then loaded into the particle to form DATS-MSNs. H_2S release profiles were measured by using the H_2S-selective microelectrode, which showed that immediate release of H_2S was observed within 1 h, after which the release remained stable for an additional period of 3 hours. These results suggested that the use of DATS-MSNs could elicit biological effects by achieving the controlled delivery of H_2S. In *in vitro* experiments, DATS-MSNs improved the ability of endothelial cells to proliferate and form vascular structures by generating H_2S in a sustained and steady fashion. Since mitochondrial damage is a key factor in causing increased cellular inflammatory response, H_2S released from DATS-MSNs was shown to alleviate inflammatory response by preserving mitochondrial potential. These results indicated that these H_2S-releasing nanoparticles could effectively attenuate hypoxia-induced mitochondrial damage in endothelial cells. Further investigation of DATS-MSNs was performed on the endothelium of transplanted aortas. Transplanted aortas treated with DATS-MSNs during the preservation period clearly showed no evidence of endothelial cell apoptosis, demonstrating that H_2S released from DATS-MSNs could be used to effectively prevent ischemia-reperfusion-induced allograft injuries. This result implies an improved allograft function, and increased transport distance and available organ donors by prolonging the organ preservation time.

Ultrasound targeted microbubble destruction (UTMD) has become a promising tool for delivery of bioactive substances to desired areas, in which microbubbles oscillate and finally collapse to release the target compounds when exposed to ultrasound with high acoustic pressures.[146] The delivery of H_2S using ultrasound targeted microbubbles has been developed with different amounts of octafluoropropane (C_3F_8) and H_2S.[147] The most stable microbubbles were prepared using a 1:1ratio of H_2S:C_3F_8 with the highest H_2S loading capability. In an *in vitro* flow system, the H_2S level was significantly increased during H_2S-microbubble infusion (microbubbles loaded with H_2S) under low intensity ultrasound irradiation, compared to the H_2S level in the absence of ultrasound triggers (Figure 2.4). These results indicate that H_2S was successfully encapsulated in the bubbles and that its release could be triggered by ultrasonic irradiation.

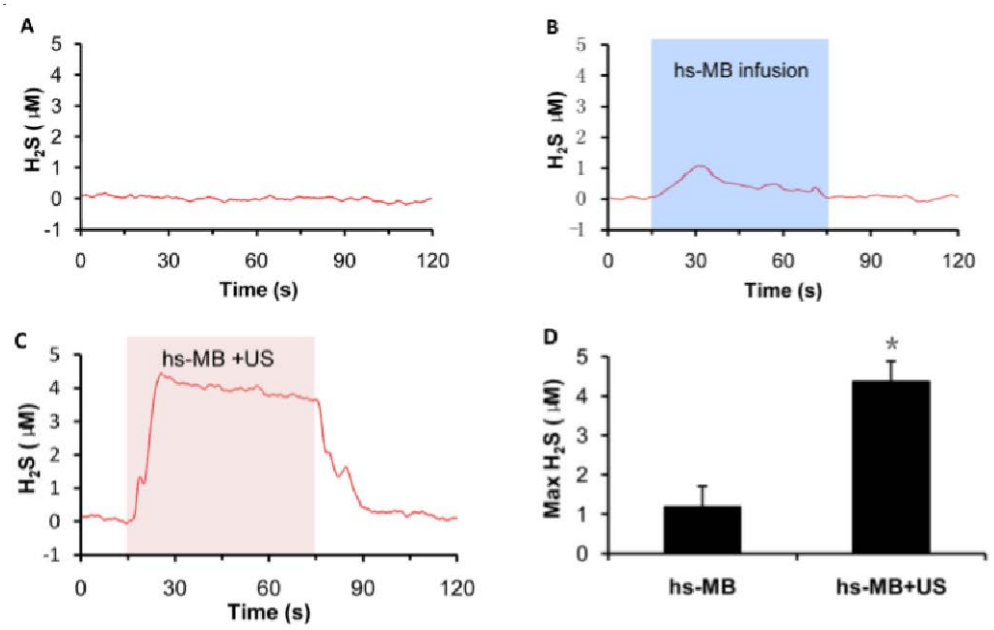

Figure 2.4: Ultrasound irradiation triggered H_2S release from H_2S-microbubbles (microbubbles loaded with H_2S) *in vitro*. (A) Baseline levels of H_2S measurement. (B) H_2S measurement during H_2S-microbubbles infusion. (C) Significantly increased H_2S level during H_2S-microbubbles infusion under ultrasound irradiation. (D) Comparison of maximum H_2S levels during H_2S-microbubbles infusion with/without ultrasound irradiation. *P < 0.05, vs hs-MB. US indicated ultrasound; hs-MB, microbubble loaded with H_2S. Reprinted with permission from Chen et al.[147] Copyright 2016, Springer Nature.

In vivo studies have demonstrated that microbubbles carrying H_2S were able to travel and reach the myocardium after intravenous infusion in rats. Under low intensity ultrasound irritation, the H_2S concentration in myocardium treated with H_2S-microbubbles was increased, demonstrating that H_2S can be successfully delivered to the target area. Apoptosis and oxidative stress were alleviated in rats treated with H_2S-microbubbles under ultrasound irritation, resulting in reduced myocardial injury and improved cardiac function. Furthermore delivery of H_2S to myocardium by UTMD could attenuate myocardial ischemia-reperfusion without causing unwanted side effects.[147]

Most recently, a self-assembling PEG–cholesterol conjugate incorporating a garlic-inspired trisulfide linkage between the two segments was developed (Scheme 2.4).[148] Firstly 3-(2-hydroxyethyl)trisulfane group (2) was developed via nucleophilic reaction of 2-mercaptoethanol with (methoxycarbonyl)disulfanyl chloride. A cholesterol conjugated trisulfide bridge (HO-SSS-CHOL) was then formed via a thiol-exchange fragmentation reaction. In order to form the final trisulfide linked PEG-cholesterol

conjugate (MeO-PEG-SSS-CHOL), the nitrophenyl carbonate of HO-SSS-CHOL was synthesized and then coupled with PEG-NH_2 through formation of a carbamate bond.

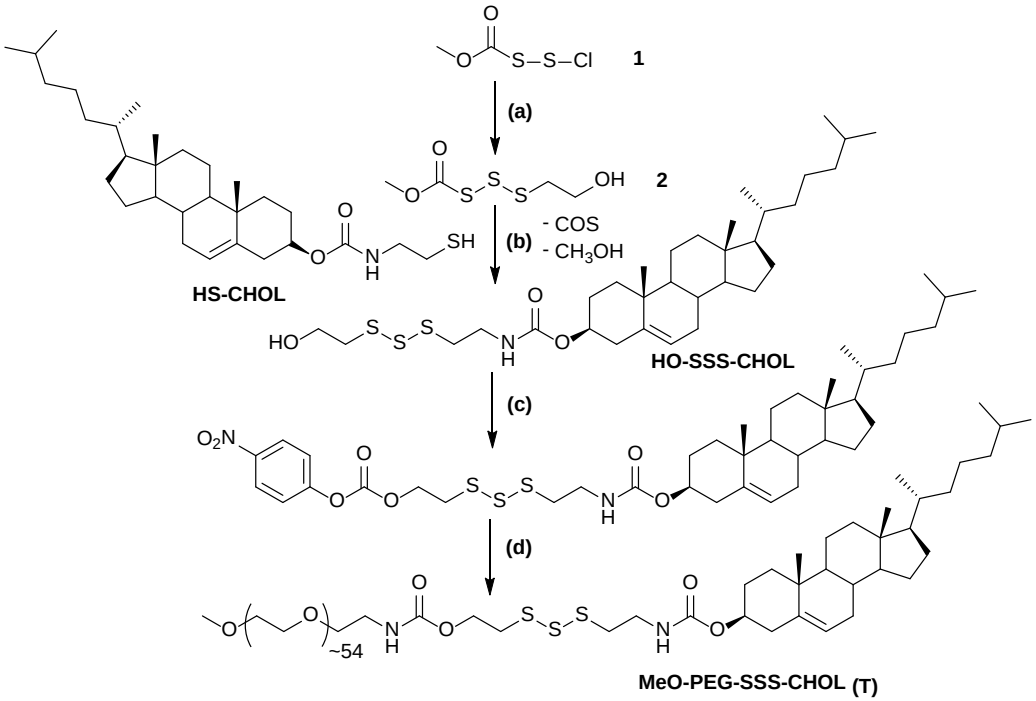

Scheme 2.4: Synthesis of a trisufide-bridged PEG–cholesterol conjugate, MeO-PEG-SSS-CHOL, via the thiol mediated fragmentation reaction of 2 (a) mercaptoethanol, CH_2Cl_2 (b) $CHCl_3$, N-methylmorpholine (c) 4-nitrophenyl chloroformate, triethylamine, CH_2Cl_2 (d) PEG(2k)-NH_2, N,N-diisopropylethylamine,4-dimethylaminopyridine, CH_2Cl_2. Adapted from with permission from Ercole et al.[148] Copyright 2017 Royal Society of Chemistry.

Finally, MeO-PEG-SSS-CHOL, trisulfide donors were then tested and found to produce H_2S by the addition of the thiol. Even in a cellular environment, the materials were able to release H_2S without the addition of exogenous thiol (Figure 2.5).[148]

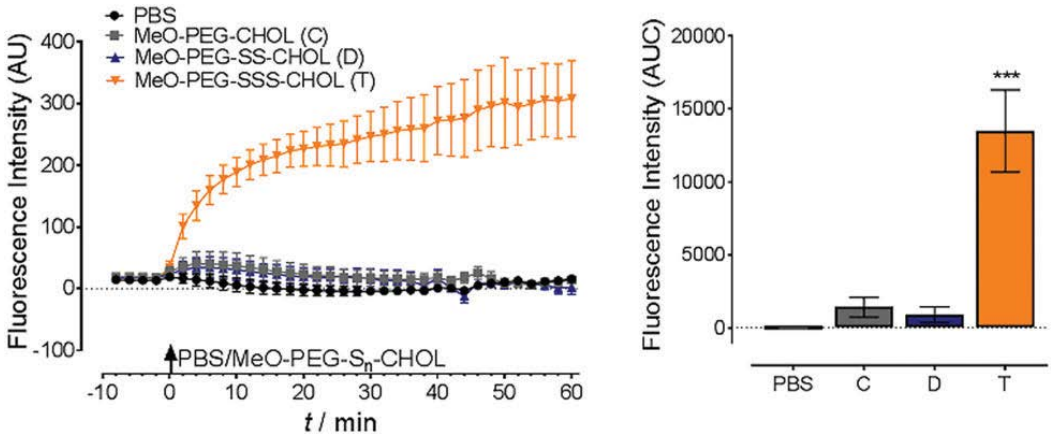

Figure 2.5: Left: Fluorescence intensity of SF4 probe for H_2S detection over time in HEK293 cells in response to the addition of PBS, MeO-PEG-CHOL, MeO-PEG-SS-CHOL and MeO-PEG-SSS-CHOL. Right: Area under the curve (AUC) derived from the time course SF4 probe test.). Note: Symbols/bars represent means and error bars SEM from three independent

experiments conducted in triplicate. ***p < 0.01 vs PBS, one-way ANOVA with Dunnett's multiple comparison test. Reprinted with permission from Ercole et al.[148] Copyright 2017 Royal Society of Chemistry.

HEK293 cells were treated with the trisulfide conjugate, and increasing H_2S over time was measured by employing an H_2S specific fluorescent probe (SF4). Specifically, the chemoselective H_2S-responsive fluorescent probe SF4 becomes fluorescent (λ=520 nm) in the presence of H_2S due to the H_2S-mediated reduction of azide groups to amines.[149,150] Only the trisulfide-containing donor was able to give an increase in fluorescence over time, indicating that H_2S was only released from these donors, compared to non-trisulfide functional controls. For these cell based studies, no exogenous thiols were added. As such the nano-assemblies incorporating the trisulfide conjugate were clearly capable of releasing H_2S to live cells upon exposure to thiol even at intracellular levels.

1.3 Aims

In summary, NO and H_2S, two of the three so-called gasotransmitters, are gaseous molecules synthesized in many organs and intracellular organelles with important roles in intra/extra-cellular signalling and biological processes. The use of NO and H_2S for therapeutic applications has been the subject of increasing interest. However the direct use of NO and H_2S has many limitations largely related to their high reactivity, poor stability and lack of site specificity. To meet the challenge of controlled and targeted NO and H_2S delivery/release, NO and H_2S-releasing polymeric nanoparticle systems are currently been developed. The use of nanoparticles for NO and H_2S delivery has the potential to significantly control both their biodistribution and pharmacokinetic properties.

The overall objective of this dissertation was to develop novel methods and chemistries to synthesize polymer-based nanoparticles for sustained, controlled and stimulated delivery of NO or H_2S by manipulating their physical/chemical properties. Furthermore, these unique delivery materials were exploited in a number of exemplar biomedical applications, demonstrating the potential benefits in various therapeutic studies.

First in chapter 2, a new approach for NO delivery was investigated by developing a directly modified NO releasing polymeric system, enabling simple synthesis of biochemically active nanostructures. The efficacy of NO release from such materials was then examined by using several techniques in different chemical environments.

In chapter 3, an H_2S delivery system was developed via a high-yielding end-group modification approach for incorporating H_2S donor moieties into polymers. H_2S-releasing polymers with an acyl-protected perthiol chain terminus were prepared, and assembled into nanoparticles. Such nanoparticles were then investigated for thiol-triggered H_2S release test by subtle changes in environmental pH, and even in a cellular environment.

In chapter 4, the synthesis of shape-controlled H_2S delivery systems was performed using epoxide-functional nanoparticles. Polymeric nano-particulate donors with different morphologies were developed by dovetailing with polymerization-induced

self-assembly. The H_2S releasing properties of the particles were studied in aqueous and cellular environment. Furthermore, the effect of combining delivery of H_2S with anticancer agents was investigated using these H_2S donating nanoparticles.

Finally, in chapter 5, a novel NO releasing polymeric carrier was designed containing the NO donor, S-nitrosoglutathione (GSNO). The NO releasing capacity from the polymeric carrier was then examined. In the second part of the chapter, the relationship between NO from GSNO or NO-releasing polymers and an anticancer agent, doxorubicin, was studied in a doxorubicin-resistance cancer cell line. Highly expressed membrane transporters were identified on the cells, which would contribute to the drug resistance by effluxing the drugs. It was then observed that the resistance of the cells to DOX could be reversed by the treatment of NO using GSNO or NO-delivery polymers through the nitration of tyrosine residues in the transporters.

1.4 References

1 R. Wang, Gasotransmitters: growing pains and joys, *Trends Biochem. Sci.*, 2014, **39**, 227–232.

2 R. Wang, Two's company, three's a crowd: can H2S be the third endogenous gaseous transmitter?, *FASEB J.*, 2002, **16**, 1792–1798.

3 R. Wang, Toxic Gas, Lifesaver, *Sci. Am.*, 2010, **302**, 66–71.

4 J. S. Stamler, D. J. Singel and J. Loscalzo, Biochemistry of nitric oxide and its redox-activated forms., *Science.*, 1992, **258**, 1898–902.

5 A. Burnett, C. Lowenstein, D. Bredt, T. Chang and S. Snyder, Nitric oxide: a physiologic mediator of penile erection, *Science.*, 1992, **257**, 401–403.

6 R. F. Furchgott, The Discovery of Endothelium-Derived Relaxing Factor and Its Importance in the Identification of Nitric Oxide, *JAMA.*, 1996, **276**, 1186–1188.

7 L. J. Ignarro, G. M. Buga, K. S. Wood, R. E. Byrns and G. Chaudhuri, Endothelium-derived relaxing factor produced and released from artery and vein is nitric oxide., *Proc. Natl. Acad. Sci. U.S.A.*, 1987, **84**, 9265–9269.

8 L. J. Ignarro, Nitric oxide: a unique endogenous signaling molecule in vascular biology., *Biosci. Rep.*, 1999, **19**, 51–71.

9 D. A. Riccio and M. H. Schoenfisch, Nitric oxide release: Part I. Macromolecular scaffolds, *Chem. Soc. Rev.*, 2012, **41**, 3731.

10 N. Tuteja, M. Chandra, R. Tuteja and M. K. Misra, Nitric Oxide as a Unique Bioactive Signaling Messenger in Physiology and Pathophysiology., *J. Biomed. Biotechnol.*, 2004, **2004**, 227–237.

11 U. Forstermann and W. C. Sessa, Nitric oxide synthases: regulation and function, *Eur. Heart J.*, 2012, **33**, 829–837.

12 S. Moncada, R. M. Palmer and E. A. Higgs, Nitric oxide: physiology, pathophysiology, and pharmacology., *Pharmacol. Rev.*, 1991, **43**, 109–142.

13 S. Ambs, W. G. Merriam, M. O. Ogunfusika, W. P. Bennett, N. Ishibe, S. P. Hussain, E. E. Tzeng, D. A. Geller, T. R. Billiar and C. C. Harris, p53 and

vascular endothelial growth factor regulate tumor growth of NOS2-expressing human carcinoma cells, *Nat. Med.*, 1998, **4**, 1371–1376.

14 R. G. Knowles and S. Moncada, Nitric oxide synthases in mammals, *Biochem. J.*, 1994, **298**, 249–258.

15 C. Nathan and Q. W. Xie, Regulation of biosynthesis of nitric oxide., *J. Biol. Chem.*, 1994, **269**, 13725–13728.

16 D. A. Wink and J. B. Mitchell, Chemical biology of nitric oxide: insights into regulatory, cytotoxic, and cytoprotective mechanisms of nitric oxide, *Free Radic. Biol. Med.*, 1998, **25**, 434–456.

17 F. Murad, Nitric Oxide and Cyclic GMP in Cell Signaling and Drug Development, *N. Engl. J. Med.*, 2006, **355**, 2003–2011.

18 C. Bogdan, Nitric oxide and the immune response., *Nat. Immunol.*, 2001, **2**, 907–916.

19 J. B. Hibbs, Z. Vavrin and R. R. Taintor, L-arginine is required for expression of the activated macrophage effector mechanism causing selective metabolic inhibition in target cells., *J. Immunol.*, 1987, **138**, 550–565.

20 D. J. Stuehr, S. S. Gross, I. Sakuma, R. Levi and C. F. Nathan, Activated murine macrophages secrete a metabolite of arginine with the bioactivity of endothelium-derived relaxing factor and the chemical reactivity of nitric oxide., *J. Exp. Med.*, 1989, **169**, 1011–1020.

21 R. F. Furchgott and J. V. Zawadzki, The obligatory role of endothelial cells in the relaxation of arterial smooth muscle by acetylcholine., *Nature*, 1980, **288**, 373–376.

22 S. Moncada and E. A. Higgs, The discovery of nitric oxide and its role in vascular biology., *Br. J. Pharmacol.*, 2006, **147**, S193-201.

23 R. F. Furchgott, P. D. Cherry, J. V Zawadzki and D. Jothianandan, Endothelial Cells as Mediators of Vasodilation of Arteries, *J. Cardiovasc. Pharmacol.*, 1984, **6**, S336–S343.

24 R. J. Gryglewski, R. M. J. Palmer and S. Moncada, Superoxide anion is

involved in the breakdown of endothelium-derived vascular relaxing factor, *Nature*, 1986, **320**, 454–456.

25 J. W. Denninger and M. A. Marletta, Guanylate cyclase and the ·NO/cGMP signaling pathway, *Biochim. Biophys. Acta - Bioenerg.*, 1999, **1411**, 334–350.

26 A. Martínez-Ruiz, S. Cadenas and S. Lamas, Nitric oxide signaling: Classical, less classical, and nonclassical mechanisms, *Free Radic. Biol. Med.*, 2011, **51**, 17–29.

27 D. D. Rees, R. M. Palmer and S. Moncada, Role of endothelium-derived nitric oxide in the regulation of blood pressure., *Proc. Natl. Acad. Sci.*, 1989, **86**, 3375–3378.

28 J. Loscalzo and G. Welch, Nitric oxide and its role in the cardiovascular system, *Prog. Cardiovasc. Dis.*, 1995, **38**, 87–104.

29 M. W. Radomski, R. M. J. Palmer and S. Moncada, The anti-aggregating properties of vascular endothelium: interactions between prostacyclin and nitric oxide, *Br. J. Pharmacol.*, 1987, **92**, 639–646.

30 T. Murohara, T. Asahara, M. Silver, C. Bauters, H. Masuda, C. Kalka, M. Kearney, D. Chen, J. F. Symes, M. C. Fishman, P. L. Huang and J. M. Isner, Nitric oxide synthase modulates angiogenesis in response to tissue ischemia., *J. Clin. Invest.*, 1998, **101**, 2567–2578.

31 M. Rizk, M. B. Witte and A. Barbul, Nitric Oxide and Wound Healing, *World J. Surg.*, 2004, **28**, 301–306.

32 G. A. Böhme, C. Bon, M. Lemaire, M. Reibaud, O. Piot, J. M. Stutzmann, A. Doble and J. C. Blanchard, Altered synaptic plasticity and memory formation in nitric oxide synthase inhibitor-treated rats., *Proc. Natl. Acad. Sci. U. S. A.*, 1993, **90**, 9191–9194.

33 Y. Ueki, S. Miyake, Y. Tominaga and K. Eguchi, Increased nitric oxide levels in patients with rheumatoid arthritis., *J. Rheumatol.*, 1996, **23**, 230–6.

34 S. Korde Choudhari, M. Chaudhary, S. Bagde, A. R. Gadbail and V. Joshi, Nitric oxide and cancer: a review, *World J. Surg. Oncol.*, 2013, **11**, 118.

35 S. D. Smith, M. A. Wheeler, R. Zhang, E. D. Weiss, M. I. Lorber, W. C. Sessa and R. M. Weiss, Nitric oxide synthase induction with renal transplant rejection or infection., *Kidney Int.*, 1996, **50**, 2088–2093.

36 K. Kugiyama, H. Yasue, K. Okumura, H. Ogawa, K. Fujimoto, K. Nakao, M. Yoshimura, T. Motoyama, Y. Inobe and H. Kawano, Nitric Oxide Activity Is Deficient in Spasm Arteries of Patients With Coronary Spastic Angina, *Circulation*, 1996, **94**, 266–272.

37 E. M. Hetrick, J. H. Shin, N. A. Stasko, C. B. Johnson, D. A. Wespe, E. Holmuhamedov and M. H. Schoenfisch, Bactericidal Efficacy of Nitric Oxide-Releasing Silica Nanoparticles, *ACS Nano*, 2008, **2**, 235–246.

38 A. W. Carpenter, D. L. Slomberg, K. S. Rao and M. H. Schoenfisch, Influence of Scaffold Size on Bactericidal Activity of Nitric Oxide-Releasing Silica Nanoparticles, *ACS Nano*, 2011, **5**, 7235–7244.

39 M. J. D. Griffiths and T. W. Evans, Inhaled Nitric Oxide Therapy in Adults, *N. Engl. J. Med.*, 2005, **353**, 2683–2695.

40 P. G. Wang, M. Xian, X. Tang, X. Wu, Z. Wen, T. Cai and A. J. Janczuk, Nitric Oxide Donors: Chemical Activities and Biological Applications, *Chem. Rev.*, 2002, **102**, 1091–1134.

41 T. Yamamoto and R. J. Bing, Nitric Oxide Donors, *Proc. Soc. Exp. Biol. Med.*, 2000, **225**, 200–206.

42 C. Napoli and L. J. Ignarro, Nitric oxide-releasing drugs., *Annu. Rev. Pharmacol. Toxicol.*, 2003, **43**, 97–123.

43 L. J. Ignarro, Nitric Oxide Donors and Cardiovascular Agents Modulating the Bioactivity of Nitric Oxide: An Overview, *Circ. Res.*, 2002, **90**, 21–28.

44 M. R. Miller and I. L. Megson, Recent developments in nitric oxide donor drugs, *Br. J. Pharmacol.*, 2009, **151**, 305–321.

45 A. (Andrew L. . Lewis, *Drug-device combination products : delivery technologies and applications*, CRC Press, 2010.

46 H. Liang, P. Nacharaju, A. Friedman and J. M. Friedman, Nitric oxide

generating/releasing materials, *Futur. Sci. OA*, 2015, **1**, fso.15.54.

47 P. D. Marcato and N. Durán, New Aspects of Nanopharmaceutical Delivery Systems, *J. Nanosci. Nanotechnol.*, 2008, **8**, 2216–2229.

48 N. Duran, P. Marcato, Z. Teixeira, M. Duran, F. Costa and M. Brocchi, State of the Art of Nanobiotechnology Applications in Neglected Diseases, *Curr. Nanosci.*, 2009, **5**, 396–408.

49 A. J. Friedman, G. Han, M. S. Navati, M. Chacko, L. Gunther, A. Alfieri and J. M. Friedman, Sustained release nitric oxide releasing nanoparticles: characterization of a novel delivery platform based on nitrite containing hydrogel/glass composites., *Nitric oxide Biol. Chem.*, 2008, **19**, 12–20.

50 R. Gupta and A. Kumar, Bioactive materials for biomedical applications using sol–gel technology, *Biomed. Mater.*, 2008, **3**, 34005.

51 D. J. Dickson and R. L. Ely, Silica sol-gel encapsulation of cyanobacteria: lessons for academic and applied research, *Appl. Microbiol. Biotechnol.*, 2013, **97**, 1809–1819.

52 D. Avnir, T. Coradin, O. Lev and J. Livage, Recent bio-applications of sol–gel materials, *J. Mater. Chem.*, 2006, **16**, 1013–1030.

53 C. Gonzalez-Arellano, R. Luque and D. J. Macquarrie, Nanotubular self-assembly of n-dodecylamine–TEOS–water–acetonitrile mixtures, *Chem. Commun.*, 2009, **0**, 4581.

54 Z. Bian, J. Zhu, F. Cao, Y. Lu and H. Li, In situ encapsulation of Au nanoparticles in mesoporous core–shell TiO2 microspheres with enhanced activity and durability, *Chem. Commun.*, 2009, **0**, 3789.

55 P. Cabrales, G. Han, C. Roche, P. Nacharaju, A. J. Friedman and J. M. Friedman, Sustained release nitric oxide from long-lived circulating nanoparticles, *Free Radic. Biol. Med.*, 2010, **49**, 530–538.

56 H. Zhang, G. M. Annich, J. Miskulin, K. Stankiewicz, K. Osterholzer, S. I. Merz, R. H. Bartlett and M. E. Meyerhoff, Nitric Oxide-Releasing Fumed Silica Particles: Synthesis, Characterization, and Biomedical Application, *J. Am. Chem. Soc.*, 2003, **125**, 5015–5024.

57 J. H. Shin, S. K. Metzger and M. H. Schoenfisch, Synthesis of Nitric Oxide-Releasing Silica Nanoparticles, *J. Am. Chem. Soc.*, 2007, **129**, 4612–4619.

58 A. Koh, A. W. Carpenter, D. L. Slomberg and M. H. Schoenfisch, Nitric Oxide-Releasing Silica Nanoparticle-Doped Polyurethane Electrospun Fibers, *ACS Appl. Mater. Interfaces*, 2013, **5**, 7956–7964.

59 A. R. Rothrock, R. L. Donkers and M. H. Schoenfisch, Synthesis of Nitric Oxide-Releasing Gold Nanoparticles, *J. Am. Chem. Soc.*, 2005, **127**, 9362–9363.

60 M. A. Polizzi, N. A. Stasko and M. H. Schoenfisch, Water-Soluble Nitric Oxide-Releasing Gold Nanoparticles, *Langmuir*, 2007, **23**, 4938–4943.

61 M. M. Molina, A. B. Seabra, M. G. de Oliveira, R. Itri and P. S. Haddad, Nitric oxide donor superparamagnetic iron oxide nanoparticles, *Mater. Sci. Eng. C*, 2013, **33**, 746–751.

62 P. S. Haddad, T. N. Britos, M. C. Santos, A. B. Seabra, M. V Palladino and G. Z. Justo, Synthesis, Characterization and Cytotoxicity Evaluation of Nitric Oxide-Iron Oxide magnetic Nanoparticles, *J. Phys. Conf. Ser.*, 2015, **617**, 12022.

63 M. Barone, M. T. Sciortino, D. Zaccaria, A. Mazzaglia and S. Sortino, Nitric oxide photocaging platinum nanoparticles with anticancer potential, *J. Mater. Chem.*, 2008, **18**, 5531.

64 S. Giuffrida, G. Ventimiglia, F. L. Callari and S. Sortino, Straightforward light-driven synthesis of ultrasmall, water-soluble monolayer-protected platinum nanoparticles, *Eur. J. Inorg. Chem.*, 2006, **2006**, 4022–4025.

65 O. Pillai and R. Panchagnula, Polymers in drug delivery, *Curr. Opin. Chem. Biol.*, 2001, **5**, 447–451.

66 Y. S. Jo, A. J. van der Vlies, J. Gantz, T. N. Thacher, S. Antonijevic, S. Cavadini, D. Demurtas, N. Stergiopulos and J. A. Hubbell, Micelles for Delivery of Nitric Oxide, *J. Am. Chem. Soc.*, 2009, **131**, 14413–14418.

67 N. Kanayama, K. Yamaguchi and Y. Nagasaki, PEGylated Polymer Micelle-based Nitric Oxide (NO) Photodonor with NO-mediated Antitumor Activity,

Chem. Lett., 2010, **39**, 1008–1009.

68 H. T. T. Duong, A. Ho, T. P. Davis and C. Boyer, Organic nitrate functional nanoparticles for the glutathione-triggered slow-release of nitric oxide, *J. Polym. Sci. Part A Polym. Chem.*, 2014, **52**, 2099–2103.

69 H. T. T. Duong, Z. M. Kamarudin, R. B. Erlich, Y. Li, M. W. Jones, M. Kavallaris, C. Boyer and T. P. Davis, Intracellular nitric oxide delivery from stable NO-polymeric nanoparticle carriers, *Chem. Commun.*, 2013, **49**, 4190–4192.

70 H. T. T. Duong, Z. Dong, L. Su, C. Boyer, J. George, T. P. Davis and J. Wang, The Use of Nanoparticles to Deliver Nitric Oxide to Hepatic Stellate Cells for Treating Liver Fibrosis and Portal Hypertension, *Small*, 2015, **11**, 2291–2304.

71 N. A. Stasko and M. H. Schoenfisch, Dendrimers as a Scaffold for Nitric Oxide Release, *J. Am. Chem. Soc.*, 2006, **128**, 8265–8271.

72 N. A. Stasko, T. H. Fischer and M. H. Schoenfisch, S -Nitrosothiol-Modified Dendrimers as Nitric Oxide Delivery Vehicles, *Biomacromolecules*, 2008, **9**, 834–841.

73 T. A. Johnson, N. A. Stasko, J. L. Matthews, W. E. Cascio, E. L. Holmuhamedov, C. B. Johnson and M. H. Schoenfisch, Reduced ischemia/reperfusion injury via glutathione-initiated nitric oxide-releasing dendrimers, *Nitric Oxide*, 2010, **22**, 30–36.

74 H. T. T. Duong, K. Jung, S. K. Kutty, S. Agustina, N. N. M. Adnan, J. S. Basuki, N. Kumar, T. P. Davis, N. Barraud and C. Boyer, Nanoparticle (Star Polymer) Delivery of Nitric Oxide Effectively Negates Pseudomonas aeruginosa Biofilm Formation, *Biomacromolecules*, 2014, **15**, 2583–2589.

75 S. Duan, S. Cai, Q. Yang and M. L. Forrest, Multi-arm polymeric nanocarrier as a nitric oxide delivery platform for chemotherapy of head and neck squamous cell carcinoma, *Biomaterials*, 2012, **33**, 3243–3253.

76 S.-L. Huang, P. H. Kee, H. Kim, M. R. Moody, S. M. Chrzanowski, R. C. MacDonald and D. D. McPherson, Nitric Oxide-Loaded Echogenic Liposomes for Nitric Oxide Delivery and Inhibition of Intimal Hyperplasia, *J. Am. Coll.*

Cardiol., 2009, **54**, 652–659.

77 J. J. Koehler, J. Zhao, S. S. Jedlicka, D. M. Porterfield and J. L. Rickus, Compartmentalized Nanocomposite for Dynamic Nitric Oxide Release, *J. Phys. Chem. B*, 2008, **112**, 15086–15093.

78 R. H. Perera, P. M. Peiris, S. F. Peteu and M. Bayachou, Nitric Oxide Synthase Encapsulation in Liposomes: a Potential Delivery Platform to (Nitric Oxide)-Deficient Targets, *Electroanalysis*, 2012, **24**, 37–41.

79 G. Broughton, J. E. Janis and C. E. Attinger, The Basic Science of Wound Healing, *Plast. Reconstr. Surg.*, 2006, **117**, 12S–34S.

80 M. R. Schäffer, Udaya Tantry, Inhibition of Nitric Oxide Synthesis in Wounds: Pharmacology and Effect on Accumulation of Collagen in Wounds in Mice, *Eur. J. Surg.*, 1999, **165**, 262–267.

81 A. Shukla, A. M. Rasik and R. Shankar, Nitric oxide inhibits wounds collagen synthesis., *Mol. Cell. Biochem.*, 1999, **200**, 27–33.

82 K. Blecher, L. R. Martinez, C. Tuckman-Vernon, P. Nacharaju, D. Schairer, J. Chouake, J. M. Friedman, A. Alfieri, C. Guha, J. D. Nosanchuk and A. J. Friedman, Nitric oxide-releasing nanoparticles accelerate wound healing in NOD-SCID mice, *Nanomedicine Nanotechnology, Biol. Med.*, 2012, **8**, 1364–1371.

83 G. Han, L. N. Nguyen, C. Macherla, Y. Chi, J. M. Friedman, J. D. Nosanchuk and L. R. Martinez, Nitric Oxide–Releasing Nanoparticles Accelerate Wound Healing by Promoting Fibroblast Migration and Collagen Deposition, *Am. J. Pathol.*, 2012, **180**, 1465–1473.

84 P. Cabrales, G. Han, P. Nacharaju, A. J. Friedman and J. M. Friedman, Reversal of hemoglobin-induced vasoconstriction with sustained release of nitric oxide, *Am. J. Physiol. Circ. Physiol.*, 2011, **300**, H49–H56.

85 P. Nachuraju, A. J. Friedman, J. M. Friedman and P. Cabrales, Exogenous nitric oxide prevents cardiovascular collapse during hemorrhagic shock, *Resuscitation*, 2011, **82**, 607–613.

86 P. Nacharaju, C. Tuckman-Vernon, K. E. Maier, J. Chouake, A. Friedman, P.

Cabrales and J. M. Friedman, A nanoparticle delivery vehicle for S-nitroso-N-acetyl cysteine: Sustained vascular response, *Nitric Oxide*, 2012, **27**, 150–160.

87 A. Bratasz, N. M. Weir, N. L. Parinandi, J. L. Zweier, R. Sridhar, L. J. Ignarro and P. Kuppusamy, Reversal to cisplatin sensitivity in recurrent human ovarian cancer cells by NCX-4016, a nitro derivative of aspirin, *Proc. Natl. Acad. Sci.*, 2006, **103**, 3914–3919.

88 E. V. Stevens, A. W. Carpenter, J. H. Shin, J. Liu, C. J. Der and M. H. Schoenfisch, Nitric Oxide-Releasing Silica Nanoparticle Inhibition of Ovarian Cancer Cell Growth, *Mol. Pharm.*, 2010, **7**, 775–785.

89 G. Han, M. Tar, D. S. R. Kuppam, A. Friedman, A. Melman, J. Friedman and K. P. Davies, Nanoparticles as a Novel Delivery Vehicle for Therapeutics Targeting Erectile Dysfunction, *J. Sex. Med.*, 2010, **7**, 224–233.

90 R. Y. Pelgrift and A. J. Friedman, Nanotechnology as a therapeutic tool to combat microbial resistance, *Adv. Drug Deliv. Rev.*, 2013, **65**, 1803–1815.

91 Y. Zheng, B. Yu, L. K. De La Cruz, M. Roy Choudhury, A. Anifowose and B. Wang, Toward Hydrogen Sulfide Based Therapeutics: Critical Drug Delivery and Developability Issues, *Med. Res. Rev.*, 2018, **38**, 57–100.

92 F. Ercole, F. M. Mansfeld, M. Kavallaris, M. R. Whittaker, J. F. Quinn, M. L. Halls and T. P. Davis, Macromolecular Hydrogen Sulfide Donors Trigger Spatiotemporally Confined Changes in Cell Signaling, *Biomacromolecules*, 2016, **17**, 371–383.

93 K. Abe and H. Kimura, The possible role of hydrogen sulfide as an endogenous neuromodulator., *J. Neurosci.*, 1996, **16**, 1066–1071.

94 M. M. Gadalla and S. H. Snyder, Hydrogen sulfide as a gasotransmitter, *J. Neurochem.*, 2010, **113**, 14–26.

95 R. Wang, C. Szabo, F. Ichinose, A. Ahmed, M. Whiteman and A. Papapetropoulos, The role of H2S bioavailability in endothelial dysfunction, *Trends Pharmacol. Sci.*, 2015, **36**, 568–578.

96 R. Wang, Physiological Implications of Hydrogen Sulfide: A Whiff Exploration That Blossomed, *Physiol. Rev.*, 2012, **92**, 791–896.

97 K. R. Olson, The therapeutic potential of hydrogen sulfide: separating hype from hope, *Am. J. Physiol. Integr. Comp. Physiol.*, 2011, **301**, R297–R312.

98 M. Soma, T. Nakayama and K. Kanmatsuse, Nitric oxide synthase gene polymorphism and its influence on cardiovascular disease., *Curr. Opin. Nephrol. Hypertens.*, 1999, **8**, 83–87.

99 X. Ji, K. Damera, Y. Zheng, B. Yu, L. E. Otterbein and B. Wang, Toward Carbon Monoxide–Based Therapeutics: Critical Drug Delivery and Developability Issues, *J. Pharm. Sci.*, 2016, **105**, 406–416.

100 T. V Mishanina, M. Libiad and R. Banerjee, Biogenesis of reactive sulfur species for signaling by hydrogen sulfide oxidation pathways, *Nat. Chem. Biol.*, 2015, **11**, 457–464.

101 B. D. Paul and S. H. Snyder, H 2 S: A Novel Gasotransmitter that Signals by Sulfhydration, *Trends Biochem. Sci.*, 2015, **40**, 687–700.

102 U. Münchberg, A. Anwar, S. Mecklenburg and C. Jacob, Polysulfides as biologically active ingredients of garlic, *Org. Biomol. Chem.*, 2007, **5**, 1505–1518.

103 B. V. Nagpure and J.-S. Bian, Interaction of hydrogen sulfide with nitric oxide in the cardiovascular system, *Oxid. Med. Cell. Longev.*, 2016, **2016**, 1–16.

104 C. Coletta, A. Papapetropoulos, K. Erdelyi, G. Olah, K. Modis, P. Panopoulos, A. Asimakopoulou, D. Gero, I. Sharina, E. Martin and C. Szabo, Hydrogen sulfide and nitric oxide are mutually dependent in the regulation of angiogenesis and endothelium-dependent vasorelaxation, *Proc. Natl. Acad. Sci.*, 2012, **109**, 9161–9166.

105 W. Zhao, The vasorelaxant effect of H2S as a novel endogenous gaseous KATP channel opener, *EMBO J.*, 2001, **20**, 6008–6016.

106 A. K. Mustafa, G. Sikka, S. K. Gazi, J. Steppan, S. M. Jung, A. K. Bhunia, V. M. Barodka, F. K. Gazi, R. K. Barrow, R. Wang, L. M. Amzel, D. E. Berkowitz and S. H. Snyder, Hydrogen Sulfide as Endothelium-Derived Hyperpolarizing Factor Sulfhydrates Potassium Channels, *Circ. Res.*, 2011, **109**, 1259–1268.

107 G. Yang, L. Wu, B. Jiang, W. Yang, J. Qi, K. Cao, Q. Meng, A. K. Mustafa, W.

Mu, S. Zhang, S. H. Snyder and R. Wang, H2S as a physiologic vasorelaxant: Hypertension in mice with deletion of cystathionine γ-lyase, *Science (80-.).*, 2008, **322**, 587–590.

108 X. Wang, Q. Wang, W. Guo and Y. Z. Zhu, Hydrogen sulfide attenuates cardiac dysfunction in a rat model of heart failure: a mechanism through cardiac mitochondrial protection, *Biosci. Rep.*, 2011, **31**, 87–98.

109 J. V. R. Medeiros, V. H. Bezerra, A. S. Gomes, A. L. R. Barbosa, R. C. P. Lima-Junior, P. M. G. Soares, G. A. C. Brito, R. A. Ribeiro, F. Q. Cunha and M. H. L. P. Souza, Hydrogen Sulfide Prevents Ethanol-Induced Gastric Damage in Mice: Role of ATP-Sensitive Potassium Channels and Capsaicin-Sensitive Primary Afferent Neurons, *J. Pharmacol. Exp. Ther.*, 2009, **330**, 764–770.

110 L.-F. Hu, M. Lu, C. X. Tiong, G. S. Dawe, G. Hu and J.-S. Bian, Neuroprotective effects of hydrogen sulfide on Parkinson's disease rat models, *Aging Cell*, 2010, **9**, 135–146.

111 M. Lee, C. Schwab, S. Yu, E. McGeer and P. L. McGeer, Astrocytes produce the antiinflammatory and neuroprotective agent hydrogen sulfide, *Neurobiol. Aging*, 2009, **30**, 1523–1534.

112 W. Guo, J. Kan, Z. Cheng, J. Chen, Y. Shen, J. Xu, D. Wu and Y. Zhu, Hydrogen Sulfide as an Endogenous Modulator in Mitochondria and Mitochondria Dysfunction, *Oxid. Med. Cell. Longev.*, 2012, **2012**, 1–9.

113 J. W. Calvert, S. Jha, S. Gundewar, J. W. Elrod, A. Ramachandran, C. B. Pattillo, C. G. Kevil and D. J. Lefer, Hydrogen Sulfide Mediates Cardioprotection Through Nrf2 Signaling, *Circ. Res.*, 2009, **105**, 365–374.

114 E. Łowicka and J. Bełtowski, Hydrogen sulfide (H2S) - the third gas of interest for pharmacologists., *Pharmacol. Rep.*, 2007, **59**, 4–24.

115 L. Wu, W. Yang, X. Jia, G. Yang, D. Duridanova, K. Cao and R. Wang, Pancreatic islet overproduction of H2S and suppressed insulin release in Zucker diabetic rats, *Lab. Investig.*, 2009, **89**, 59–67.

116 J. L. Wallace, M. Dicay, W. McKnight and G. R. Martin, Hydrogen sulfide enhances ulcer healing in rats, *FASEB J.*, 2007, **21**, 4070–4076.

117 R. C. O. Zanardo, Hydrogen sulfide is an endogenous modulator of leukocyte-mediated inflammation, *FASEB J.*, 2006, **20**, 2118–2120.

118 B. Gemici and J. L. Wallace, in *Methods in enzymology*, 2015, vol. 555, pp. 169–193.

119 B. L. Predmore, D. J. Lefer and G. Gojon, Hydrogen Sulfide in Biochemistry and Medicine, *Antioxid. Redox Signal.*, 2012, **17**, 119–140.

120 J. Du, Y. Hui, Y. Cheung, G. Bin, H. Jiang, X. Chen and C. Tang, The possible role of hydrogen sulfide as a smooth muscle cell proliferation inhibitor in rat cultured cells, *Heart Vessels*, 2004, **19**, 75–80.

121 G. Gobbi, F. Ricci, C. Malinverno, C. Carubbi, M. Pambianco, G. de Panfilis, M. Vitale and P. Mirandola, Hydrogen sulfide impairs keratinocyte cell growth and adhesion inhibiting mitogen-activated protein kinase signaling, *Lab. Investig.*, 2009, **89**, 994–1006.

122 L.-F. Hu, P. T.-H. Wong, P. K. Moore and J.-S. Bian, Hydrogen sulfide attenuates lipopolysaccharide-induced inflammation by inhibition of p38 mitogen-activated protein kinase in microglia, *J. Neurochem.*, 2007, **100**, 1121–1128.

123 X.-Y. Wang, C.-T. Yang, D.-D. Zheng, L.-Q. Mo, A.-P. Lan, Z.-L. Yang, F. Hu, P.-X. Chen, X.-X. Liao and J.-Q. Feng, Hydrogen sulfide protects H9c2 cells against doxorubicin-induced cardiotoxicity through inhibition of endoplasmic reticulum stress, *Mol. Cell. Biochem.*, 2012, **363**, 419–426.

124 M.-H. LIU, Y. ZHANG, X.-L. LIN, J. HE, T.-P. TAN, S.-J. WU, S. YU, L. CHEN, Y.-D. CHEN, H.-Y. FU, C. YUAN and J. LI, Hydrogen sulfide attenuates doxorubicin-induced cardiotoxicity by inhibiting calreticulin expression in H9c2 cells, *Mol. Med. Rep.*, 2015, **12**, 5197–5202.

125 K. Chegaev, B. Rolando, D. Cortese, E. Gazzano, I. Buondonno, L. Lazzarato, M. Fanelli, C. M. Hattinger, M. Serra, C. Riganti, R. Fruttero, D. Ghigo and A. Gasco, H 2 S-Donating Doxorubicins May Overcome Cardiotoxicity and Multidrug Resistance, *J. Med. Chem.*, 2016, **59**, 4881–4889.

126 G. Caliendo, G. Cirino, V. Santagada and J. L. Wallace, Synthesis and

Biological Effects of Hydrogen Sulfide (H 2 S): Development of H 2 S-Releasing Drugs as Pharmaceuticals, *J. Med. Chem.*, 2010, **53**, 6275–6286.

127 A. Sparatore, G. Santus, D. Giustarini, R. Rossi and P. Del Soldato, Therapeutic potential of new hydrogen sulfide-releasing hybrids, *Expert Rev. Clin. Pharmacol.*, 2011, **4**, 109–121.

128 X. Gu and Y. Z. Zhu, Therapeutic applications of organosulfur compounds as novel hydrogen sulfide donors and/or mediators, *Expert Rev. Clin. Pharmacol.*, 2011, **4**, 123–133.

129 J. L. Wallace, Hydrogen sulfide-releasing anti-inflammatory drugs, *Trends Pharmacol. Sci.*, 2007, **28**, 501–505.

130 L. Li, M. Whiteman, Y. Y. Guan, K. L. Neo, Y. Cheng, S. W. Lee, Y. Zhao, R. Baskar, C.-H. Tan and P. K. Moore, Characterization of a Novel, Water-Soluble Hydrogen Sulfide-Releasing Molecule (GYY4137): New Insights Into the Biology of Hydrogen Sulfide, *Circulation*, 2008, **117**, 2351–2360.

131 Y. Zhao, S. Bhushan, C. Yang, H. Otsuka, J. D. Stein, A. Pacheco, B. Peng, N. O. Devarie-Baez, H. C. Aguilar, D. J. Lefer and M. Xian, Controllable Hydrogen Sulfide Donors and Their Activity against Myocardial Ischemia-Reperfusion Injury, *ACS Chem. Biol.*, 2013, **8**, 1283–1290.

132 T. Roger, F. Raynaud, F. Bouillaud, C. Ransy, S. Simonet, C. Crespo, M.-P. Bourguignon, N. Villeneuve, J.-P. Vilaine, I. Artaud and E. Galardon, New Biologically Active Hydrogen Sulfide Donors, *ChemBioChem*, 2013, **14**, 2268–2271.

133 J. L. Wallace, G. Caliendo, V. Santagada, G. Cirino and S. Fiorucci, Gastrointestinal Safety and Anti-Inflammatory Effects of a Hydrogen Sulfide–Releasing Diclofenac Derivative in the Rat, *Gastroenterology*, 2007, **132**, 261–271.

134 J. Kang, Z. Li, C. L. Organ, C.-M. Park, C. Yang, A. Pacheco, D. Wang, D. J. Lefer and M. Xian, pH-Controlled Hydrogen Sulfide Release for Myocardial Ischemia-Reperfusion Injury, *J. Am. Chem. Soc.*, 2016, **138**, 6336–6339.

135 U. Hasegawa and A. J. van der Vlies, Design and Synthesis of Polymeric

Hydrogen Sulfide Donors, *Bioconjug. Chem.*, 2014, **25**, 1290–1300.

136 U. Hasegawa and A. J. van der Vlies, Polymeric micelles for hydrogen sulfide delivery, *Medchemcomm*, 2015, **6**, 273–276.

137 W. Wang, X. Sun, H. Zhang, C. Yang, Y. Liu, W. Yang, C. Guo and C. Wang, Controlled release hydrogen sulfide delivery system based on mesoporous silica nanoparticles protects graft endothelium from ischemia–reperfusion injury, *Int. J. Nanomedicine*, 2016, **Volume 11**, 3255–3263.

138 K. Kashfi and K. R. Olson, Biology and therapeutic potential of hydrogen sulfide and hydrogen sulfide-releasing chimeras, *Biochem. Pharmacol.*, 2013, **85**, 689–703.

139 J. C. Foster and J. B. Matson, Functionalization of Methacrylate Polymers with Thiooximes: A Robust Postpolymerization Modification Reaction and a Method for the Preparation of H 2 S-Releasing Polymers, *Macromolecules*, 2014, **47**, 5089–5095.

140 Y. Zhao, J. Kang, C.-M. Park, P. E. Bagdon, B. Peng and M. Xian, Thiol-Activated gem -Dithiols: A New Class of Controllable Hydrogen Sulfide Donors, *Org. Lett.*, 2014, **16**, 4536–4539.

141 Y. Zhao, H. Wang and M. Xian, Cysteine-Activated Hydrogen Sulfide (H 2 S) Donors, *J. Am. Chem. Soc.*, 2011, **133**, 15–17.

142 T. R. Long, A. Wongrakpanich, A.-V. Do, A. K. Salem and N. B. Bowden, Long-term release of a thiobenzamide from a backbone functionalized poly(lactic acid), *Polym. Chem.*, 2015, **6**, 7188–7195.

143 J. L. Wallace, G. Caliendo, V. Santagada and G. Cirino, Markedly reduced toxicity of a hydrogen sulphide-releasing derivative of naproxen (ATB-346), *Br. J. Pharmacol.*, 2010, **159**, 1236–1246.

144 A. Martelli, L. Testai, V. Citi, A. Marino, I. Pugliesi, E. Barresi, G. Nesi, S. Rapposelli, S. Taliani, F. Da Settimo, M. C. Breschi and V. Calderone, Arylthioamides as H 2 S Donors: l -Cysteine-Activated Releasing Properties and Vascular Effects in Vitro and in Vivo, *ACS Med. Chem. Lett.*, 2013, **4**,

904–908.

145 G. Yang, K. Cao, L. Wu and R. Wang, Cystathionine γ-Lyase Overexpression Inhibits Cell Proliferation via a H 2 S-dependent Modulation of ERK1/2 Phosphorylation and p21 Cip/WAK-1, *J. Biol. Chem.*, 2004, **279**, 49199–49205.

146 E. Unger, T. Porter, J. Lindner and P. Grayburn, Cardiovascular drug delivery with ultrasound and microbubbles, *Adv. Drug Deliv. Rev.*, 2014, **72**, 110–126.

147 G. Chen, L. Yang, L. Zhong, S. Kutty, Y. Wang, K. Cui, J. Xiu, S. Cao, Q. Huang, W. Liao, Y. Liao, J. Wu, W. Zhang and J. Bin, Delivery of Hydrogen Sulfide by Ultrasound Targeted Microbubble Destruction Attenuates Myocardial Ischemia-reperfusion Injury, *Sci. Rep.*, 2016, **6**, 30643–30656.

148 F. Ercole, M. R. Whittaker, M. L. Halls, B. J. Boyd, T. P. Davis and J. F. Quinn, Garlic-inspired trisulfide linkers for thiol-stimulated H 2 S release, *Chem. Commun.*, 2017, **53**, 8030–8033.

149 P. K. Sasmal, S. Carregal-Romero, A. A. Han, C. N. Streu, Z. Lin, K. Namikawa, S. L. Elliott, R. W. Köster, W. J. Parak and E. Meggers, Catalytic azide reduction in biological environments., *Chembiochem*, 2012, **13**, 1116–1120.

150 V. S. Lin, A. R. Lippert and C. J. Chang, Cell-trappable fluorescent probes for endogenous hydrogen sulfide signaling and imaging H2O2-dependent H2S production, *Proc. Natl. Acad. Sci.*, 2013, **110**, 7131–7135.

CHAPTER 2: Transformation of RAFT polymer end groups into nitric oxide donor moieties: En route to biochemically active nanostructures

ACS Macro Letters

Letter

pubs.acs.org/macroletters

Transformation of RAFT Polymer End Groups into Nitric Oxide Donor Moieties: En Route to Biochemically Active Nanostructures

Sul Hwa Yu,[†] Jinming Hu,[†] Francesca Ercole,[†] Nghia P. Truong,[†] Thomas P. Davis,*[,†,‡] Michael R. Whittaker,*[,†] and John F. Quinn*[,†]

[†]ARC Centre of Excellence in Convergent Bio-Nano Science and Technology, Monash Institute of Pharmaceutical Sciences, Monash University, Parkville, VIC 3052, Australia

[‡]Department of Chemistry, University of Warwick, Coventry, ULCV4 7AL, United Kingdom

Supporting Information

ABSTRACT: Polymers with a terminal *S*-nitrosothiol moiety were synthesized by modifying the thiocarbonylthio end group formed by reversible addition−fragmentation chain transfer polymerization. Specifically, benzodithioate-terminated poly[oligo(ethylene glycol) methyl ether methacrylate] (POEGMA) was first synthesized by polymerizing OEGMA in the presence of 4-cyano-4-(phenylcarbonothioylthio)pentanoic acid. Sequential treatment with hydrazine hydrate and a stoichiometric amount of nitrous acid resulted in the formation of *S*-nitrosothiol-terminated polymers. A similar approach was applied to block copolymers of POEGMA incorporating a domain of poly[(*N*,*N*-diisopropylamino)ethyl methacrylate], thus, enabling the preparation of pH responsive nitric oxide (NO)-releasing micelles. The micelles possessed substantially modified *S*-nitrosothiol loss kinetics compared to the hydrophilic homopolymer analogue. Moreover, thiol-triggered degradation of the *S*-nitrosothiol was significantly slower when the *S*-nitrosothiol was embedded in a micellar structure. These results demonstrate that it is possible to incorporate nitric oxide donor moieties directly onto a polymer chain end, enabling simple synthesis of biochemically active nanostructures.

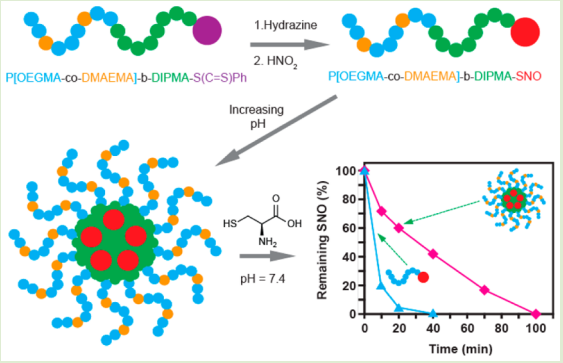

Nitric oxide (NO) is a lipophilic radical species with numerous functions in human physiology.[1] In addition to its role in intra- and extracellular signaling, nitric oxide also has utility in antimicrobial applications such as in the dispersal of biofilms.[2,3] As such, controlled delivery of nitric oxide using nanoparticle-based delivery systems is receiving an increasing amount of attention.[4−7] Nitric oxide-releasing nanoparticles have been investigated for possible application in fields as diverse as cardiology,[8] microbiology,[9] and sexual health.[10] Facile approaches for the incorporation of nitric oxide donors into polymer or particle systems are therefore of considerable interest.

Since its introduction in the late 1990s, reversible addition−fragmentation chain transfer (RAFT) polymerization has been recognized as a powerful methodology for the preparation of polymers with well-defined molecular weight and functional end groups.[11,12] A considerable amount of investigation has occurred into modification of the RAFT end group,[13−21] which is often seen as undesirable due to its reactivity, color, and odor. In other cases, the end group has been manipulated so as to provide reactive handles for Diels−Alder coupling,[16] copper-catalyzed azide−alkyne click reactions,[17] thiol−disulfide exchange,[18] or thiol−ene click reactions.[19−21] Clearly, the major emphasis to date has been on modifying the end group for either removal or subsequent conjugation to another chemical entity, such as a polymer, biomolecule, or particle surface. To our knowledge, there have been no reports of converting polymer end groups into nitric oxide donor moieties.

Herein we report the conversion of thiocarbonylthio end groups formed by RAFT polymerization into *S*-nitrosothiol moieties. The *S*-nitrosothiols are an important class of nitric oxide donor molecules and include substances such as *S*-nitroso-glutathione (GSNO) and *S*-nitroso-*N*-acetylpenicillamine.[22,23] By using the RAFT end group to provide the substrate for *S*-nitrosation, it was possible to incorporate the *S*-nitroso group directly into the polymer chain. In contrast, previous reports describing the attachment of nitric oxide donors to polymers synthesized by RAFT polymerization have required the conjugation of a presynthesized donor or the incorporation of some other molecular host for subsequent conversion to a NO donor. For instance, the reactive monomer 2-vinyl-4,4-dimethyl-5-oxazolone has been used to provide a locus for conjugation of (i) a small molecule donor (GSNO)[7] or (ii) a 2° amine-containing molecule (spermine),[9] which in turn provides a site for formation of a *N*-diazeniumdiolate NO donor (by exposure to elevated pressures of NO gas). While

Received: October 15, 2015
Accepted: October 28, 2015
Published: November 3, 2015

DOI: 10.1021/acsmacrolett.5b00733
ACS Macro Lett. 2015, 4, 1278−1282

these approaches are effective for incorporating NO donors, they necessitate the use of reactive monomers and result in more complicated synthesis. The results reported herein provide a more straightforward approach than has previously been applied.

Thiol-containing small molecules (such as glutathione) can be readily modified into the corresponding *S*-nitrosothiol (e.g., GSNO) by reaction with nitrous acid (i.e., H_2SO_4 and $NaNO_2$ in a stoichiometric ratio of 1:2). However, effective nitrosation of a sulfhydryl group at the terminus of a polymer requires careful optimization. Before attempting modification of a polymer generated by RAFT polymerization, we conducted a model reaction using commercially available poly(ethylene glycol) methyl ether thiol (PEG-SH) with M_n = 2000 g mol^{-1}. First, in order to determine whether there was any disulfide formation in the PEG-SH (i.e., loss of free thiol), we calculated the amount of free thiol using Ellman's reagent (SI, Figure S1). This assay indicated that there was approximately 0.45 mM free thiol in a 0.5 mM sample of polymer, and so subsequent reactions were conducted with a suitably adjusted molar ratio of reagents. Specifically, H_2SO_4, $NaNO_2$, and PEG-SH were combined in a molar ratio of 0.45:0.9:1 at 0 °C to facilitate reaction of nitrous acid with the thiol moiety. Successful formation of the *S*-nitrosothiol was confirmed by the emergence of two characteristic UV−vis bands between 330 and 350 nm and 550−600 nm (Figure 1).[23] Moreover, these

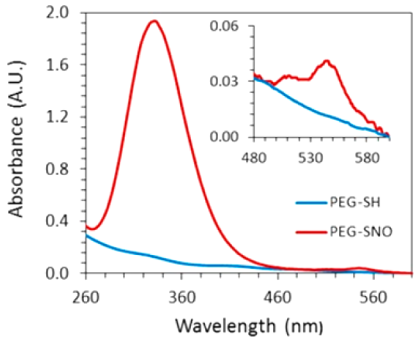

Figure 1. UV−visible spectra for PEG-SH (M_n = 2000 g mol^{-1}) and PEG-SNO. The blue line corresponds to PEG-SH, while the red line represents PEG-SNO. In each case, the polymer concentration = 5.67 mg mL^{-1}.

peaks were accompanied by a change in the solution color from clear to red. These results confirm that the formation of PEG-SNO (Chart 1, compound 1) was successfully achieved. Importantly, we found that precise control over the reaction stoichiometry was essential to the formation of a stable *S*-nitrosothiol. When a 2:1 excess of nitrous acid was used, we observed diminished yields of *S*-nitrosothiol, while a nitrous acid excess of 4:1 or 8:1 appeared to yield no *S*-nitrosothiol at all (as characterized by the absence of the characteristic UV−vis bands between 330 and 350 nm and 550−600 nm, Figure S2−S3). We postulated that excess nitrous acid (or degradation products thereof) facilitated the destruction of the *S*-nitrosothiol and that, for larger excesses of nitrous acid, this was sufficiently rapid as to make measurement of the *S*-nitrosothiol spectrum impossible (see Supporting Information). To verify that destruction of the *S*-nitrosothiol could be attributed to excess nitrous acid, we conducted an additional experiment wherein a stable *S*-nitrosothiol was first formed by adding a stoichiometric amount of nitrous acid. After the resulting *S*-

Chart 1. *S*-Nitrosothiol-Terminated Polymers

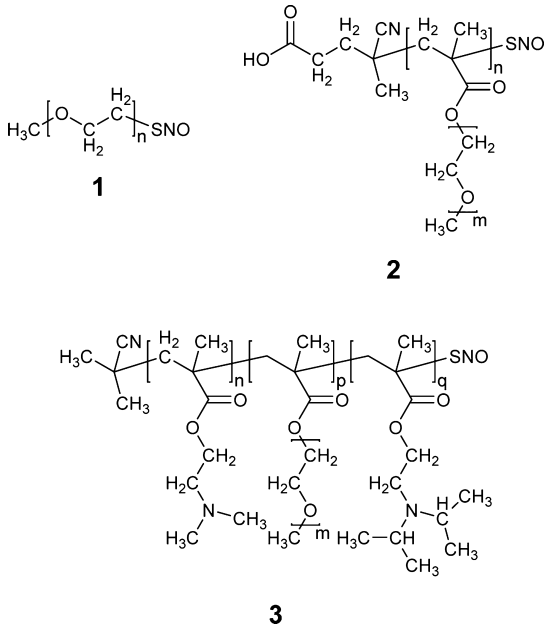

nitrosothiol was confirmed to be stable, an additional equivalent of either nitrous acid or sulfuric acid was added. Addition of nitrous acid resulted in a progressive destruction of the *S*-nitrosothiol over the ensuing 24 h (Figure S4), while the additional equivalent of sulfuric acid had only a slight impact on the *S*-nitrosothiol signal (Figure S5). Taken together, these results demonstrate that the terminal *S*-nitrosothiol moieties are susceptible to degradation by excess nitrous acid but are otherwise relatively stable in acidic conditions. As such, the reaction stoichiometry should be precisely controlled in order to achieve an optimal yield of *S*-nitrosothiol on the polymer end group.

Having demonstrated the effective formation of the *S*-nitrosothiol moiety on the chain terminus of linear PEG, a further suite of *S*-nitrosothiol-terminated polymers were synthesized by modifying the thiocarbonylthio end group formed by RAFT polymerization. First, benzodithioate-terminated poly(oligoethylene glycol methyl ether) methacrylate (P[OEGMA]-S-C(=S)Ph) was prepared by polymerizing oligo(ethylene glycol methyl ether) methacrylate (MW = 300 g mol^{-1}) in the presence of the RAFT agent 4-cyano-4-(phenylcarbonothioylthio)pentanoic acid.

The resulting polymer (Table 1, entry 1) was purified by repeated precipitations into an appropriate nonsolvent (see SI for detailed procedure), and characterized using gel permeation chromatography (GPC) and ^{1}H nuclear magnetic resonance

Table 1. Molecular Weight of Polymers Synthesized

entry	M_n[a] (g mol^{-1})	M_n[b] (g mol^{-1})	PDI
1	5100	6700	1.09
2		7000	1.08
3		7000	1.09
4	22200	18800	1.11
5		20400	1.10
6		19600	1.21

[a]Molecular weight determined by ^{1}H NMR spectroscopy. [b]Molecular weight determined by gel permeation chromatography.

DOI: 10.1021/acsmacrolett.5b00733
ACS Macro Lett. 2015, 4, 1278−1282

(^{1}H NMR) spectroscopy (Figures 2A and S6). The benzodithioate end group of the P[OEGMA]−S-C(=S)Ph

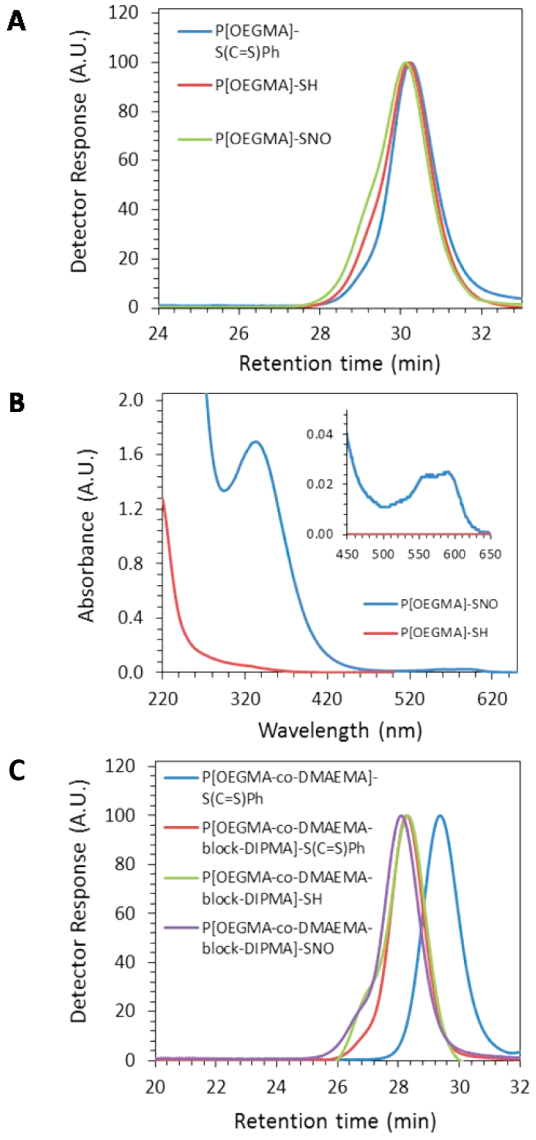

Figure 2. (A) GPC chromatograms for P[OEGMA]-S(C=S)Ph, P[OEGMA]-SH, and P[OEGMA]-SNO (Table 1, entries 1−3). (B) UV−visible spectra for P[OEGMA]-SH and P[OEGMA]-SNO, recorded at a polymer concentration = 2.28 mM. (C) GPC chromatograms for P[OEGMA-*co*-DMAEMA]-S(C=S)Ph, P-[OEGMA-*co*-DMAEMA-*block*-DIPMA]-S(C=S)Ph, P[OEGMA-*co*-DMAEMA-*block*-DIPMA]-SH, and P[OEGMA-*co*-DMAEMA-*block*-DIPMA]-SNO (Table 1, entries 4−6).

was then converted to thiol by treating with hydrazine monohydrate for 1 min in dry deoxygenated DMF, yielding thiol-terminated polymer (P[OEGMA]-SH) (Table 1, entry 2).[24] P[OEGMA]-SH was purified by dialysis against dilute HCl (pH 3.3) to ensure removal of the dithioester end group residue and minimize the formation of disulfide bonds,[24] and analyzed using GPC and ^{1}H NMR (Figures 2A and S7). GPC analysis indicated that the formation of disulfide coupled polymer during this process was minimized, as reflected by the emergence of only a small high molecular weight shoulder, accounting for about 15−20% of the total polymer. Effective removal of the benzodithioate moiety was also observed using UV−visible spectrophotometry (Figure S8). After drying, the P[OEGMA]-SH was redissolved in distilled water and reacted with a stoichiometric amount of nitrous acid (H_2SO_4 with $NaNO_2$ in a molar ratio of 1:2). Importantly, the molar amount of nitrous acid was adjusted down by 20% to account for the estimated loss of the thiol moiety due to disulfide formation during hydrazine treatment and purification. Formation of P[OEGMA]-SNO (Chart 1, compound 2 and Table 1, entry 3) was confirmed by UV−visible spectrophotometry (Figure 2B). Again, the appearance of characteristic peaks in the ranges 330−350 nm and 550−600 nm indicated successful formation of the *S*-nitrosothiol groups. Further, GPC analysis indicated that nitrous acid treatment had a slight impact on the molecular weight distribution, with the emergence of a small high molecular weight shoulder, likely due to bimolecular coupling from disulfide formation (Figure 2A). ^{1}H NMR spectroscopy confirmed that there were no other deleterious impacts on the polymer structure (Figure S9).

Having confirmed the formation of *S*-nitrosothiol groups in the terminal position of a homopolymer (P[OEGMA]-SNO), the same approach was then applied to a pH responsive block copolymer. Using this approach we hypothesized that it would be possible to prepare pH responsive micelles with tunable nitric oxide release capability (see Scheme 1).

Scheme 1. Synthesis of a Biochemically Active Nanostructure Incorporating an *S*-Nitrosothiol Moiety

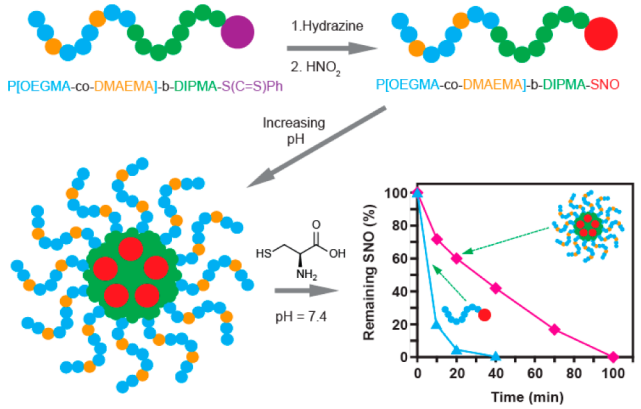

The block copolymer was prepared by first synthesizing a copolymer of OEGMA (MW = 500 g mol^{-1}) with *N*,*N*-(dimethylamino)ethyl methacrylate (89:11) in the presence of 2-cyanoprop-2-yl benzodithioate (Figures 2C and S10), and then chain extending with 2-[*N*,*N*-(diisopropylamino)ethyl methacrylate (DIPMA) to form P[OEGMA-*co*-DMAEMA-*block*-DIPMA]-S(C=S)Ph. The resulting polymer (Table 1, entry 4) was purified and characterized using GPC and ^{1}H NMR spectroscopy (Figures 2C and S11). P[OEGMA-*co*-DMAEMA-*block*-DIPMA]-S(C=S)Ph was converted to the *S*-nitrosothiol-terminated analogue using the same approach outlined above. First, the dithioester end group was converted to a thiol by treatment with hydrazine monohydrate, thereby yielding P[OEGMA-*co*-DMAEMA-*block*-DIPMA]-SH (Table 1, entry 5). Removal of the benzodithioate was readily confirmed by ^{1}H NMR spectroscopy and UV−visible spectrophotometry (Figures S12 and S13). Again, treatment with hydrazine hydrate was shown to have only a small impact on the molecular weight distribution (Figure 2C). The thiol-terminated polymer was then nitrosated using a stoichiometric

DOI: 10.1021/acsmacrolett.5b00733
ACS Macro Lett. 2015, 4, 1278−1282

amount of nitrous acid to form P[OEGMA-*co*-DMAEMA-*block*-DIPMA]-SNO (Chart 1, compound 3, and Table 1, entry 6). As with the homopolymer, the required amount of nitrous acid was adjusted down by 20% to account for loss of thiol to disulfide during hydrazine treatment. Formation of the *S*-nitrosothiol end group was confirmed by UV−visible spectrophotometry. Again ^{1}H NMR spectroscopy demonstrated that there were no significant impacts on the other chemical moieties in the polymer (Figure S14), while GPC demonstrated the emergence of a small high molecular weight shoulder in the MWD (Figure 2C). The incorporation of the pH-sensitive hydrophobic DIPMA domain enabled the formation of micelles when P[OEGMA-*co*-DMAEMA-*block*-DIPMA]-SNO was dispersed in phosphate buffered saline. Dynamic light scattering measurements were employed to examine particle size of the micelles, with a number-average particle size of 17 nm recorded at pH 7.4 and 20 nm at pH 6.0. (Figure S15).

In order to examine whether the *S*-nitrosothiol end groups formed were efficacious for the release of NO a sample of P[OEGMA]-SNO was dissolved in phosphate buffered saline (PBS) solution incorporating 5,6-diaminofluorescein (DAF). DAF is commonly used as a test agent for NO as it is ordinarily nonfluorescent but undergoes a reaction in the presence of NO to form a fluorescent species, thereby providing evidence for NO release.[6,25] Importantly, DAF is not reactive to nitrite, nitrate, hydrogen peroxide or peroxynitrite alone,[25] and as such a fluorescent turn-on is highly suggestive of nitric oxide release. While DAF may become fluorescent in the presence of ascorbic acid or dehydroascorbic acid,[26] these compounds are unlikely to be present in the system under study here. An increase in fluorescence was observed with time when P[OEGMA]-SNO was dissolved in water, indicating that NO is indeed released (Figure S16). Additionally, we also examined the release of NO from both the PEG-SNO and P[OEGMA]-SNO using an electrochemical probe (Figures S17−19). These results demonstrated that there was a relatively constant level of NO evolved from the polymers at 37 °C and pH 7.4. The NO flux generated by PEG-SNO (0.58 mM) was equivalent to that which was obtained from *S*-nitrosoglutathione at 0.2 mM, indicating a slower release from the polymeric donor compared to the small molecule. However, in the case of P[OEGMA]-SNO at 0.58 mM, the flux generated was similar to that from ∼2 mM GSNO, indicating faster release from the P[OEGMA]-SNO than from the small molecule. These differences can be attributed not only to variations in the molecular weight, but also to structural differences around the *S*-nitrosothiol moiety. In subsequent experiments we followed the decrease in the UV signal corresponding to the *S*-nitrosothiol as indicative of NO release. This approach has recently been validated by Reynolds and co-workers,[27] who correlated the decrease in the UV signal from *S*-nitrosothiol functionalized poly(lactic-*co*-glycolic acid) at pH 7.4 and 37 °C with nitric oxide concentrations determined using chemiluminescence.

Release of NO from P[OEGMA]-SNO dissolved in dilute HCl (pH 3−4) was observed at room temperature (Figures 3A, S20, and S21). The NO release kinetics were slow and relatively constant over several days. As expected, the decrease in the *S*-nitrosothiol concentration was evident in both the peaks at 330−350 nm (Figure S21) and 550−600 nm (Figure 3A).

When P[OEGMA]-SNO was dissolved in PBS solution at pH 7.4 and the temperature elevated to 37 °C, substantially

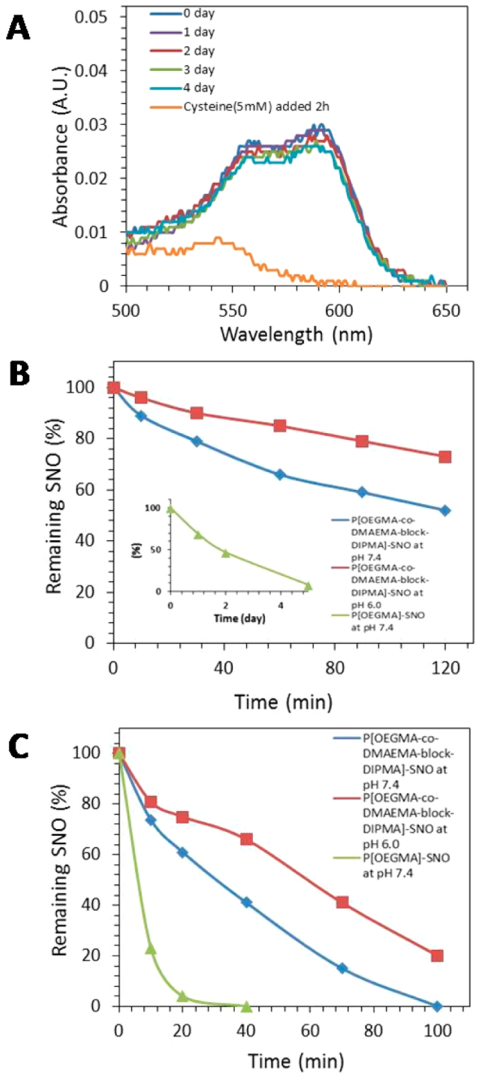

Figure 3. (A) UV−visible spectra corresponding to P[OEGMA]-SNO (2.28 mM) at room temperature with time or addition of cysteine. (B) % SNO remaining for P[OEGMA-*co*-DMAEMA-*block*-DIPMA]-SNO (1.98 mM) at 37 °C and pH 6.0 or pH 7.4. Inset shows % SNO remaining for P[OEGMA]-SNO (0.68 mM) at 37 °C and pH 7.4. (C) % SNO remaining in the presence of cysteine (5 mM) at 37 °C: P[OEGMA]-SNO (2.28 mM) at pH 7.4 and P[OEGMA-*co*-DMAEMA-*block*-DIPMA]-SNO (1.90 mM) at pH 6.0 or 7.4.

different release kinetics were observed. Specifically, the release of NO was significantly faster than that observed at room temperature and lower pH (2−3). Further, the release was relatively constant over several days (Figures 3B (inset) and S22).

Examination of *S*-nitrosothiol loss from P[OEGMA-*co*-DMAEMA-*block*-DIPMA]-SNO micelles at 37 °C in PBS (pH 6.0 and 7.4) revealed remarkably different behavior to the homopolymer. Specifically, the rate of *S*-nitrosothiol loss from the block copolymer was substantially increased when compared to that for the homopolymer at all measured conditions. Moreover, the block copolymer lost the *S*-nitrosothiol substantially faster at 37 °C and pH 7.4 or 6.0 than it did at room temperature and low pH (2−3) (see Figures S23−S24). Interestingly, Figure 3B shows that *S*-nitrosothiol loss from P[OEGMA-*co*-DMAEMA-*block*-DIPMA]-SNO at pH 7.4 is faster than at pH 6.0. This is in

DOI: 10.1021/acsmacrolett.5b00733
ACS Macro Lett. 2015, 4, 1278−1282

contrast to what might ordinarily be expected in a micellar structure, with the DIPMA moieties imparting greater hydrophobicity at pH 7.4 than 6.0. However, variation of pH from 7.4 to 6.0 also has a substantial impact on the degree of protonation of the tertiary amine groups. Previous studies have shown that tertiary amines (including the hindered tertiary amine quinuclidine) can react with *S*-nitrosothiols resulting in loss of *S*-nitrosothiol.[28] As such, exposing P[OEGMA-*co*-DMAEMA-*block*-DIPMA]-SNO to a pH that will provide more nonprotonated tertiary amine groups is likely to accelerate the loss of *S*-nitrosothiol. Moreover, these results provide clear evidence that the reactivity of the *S*-nitrosothiol moiety is strongly affected by the local chemical environment.

Degradation of *S*-nitrosothiols has also been observed upon exposure to thiol-containing compounds.[29,30] As such, we examined the effect of exposing *S*-nitrosothiol-terminated polymers to the amino acid cysteine as a means to elucidate the impact of embedding the *S*-nitrosothiol in a micelle core (Figure 3C). While degradation of the *S*-nitrosothiol on the chain end of the hydrophilic homopolymer was near instantaneous (with 95% of the *S*-nitrosothiol being destroyed within 20 min upon exposure to 5 mM cysteine), in contrast, degradation of the *S*-nitrosothiol in the micelles when exposed to 5 mM cysteine was much slower. We attribute this reduced rate of degradation compared to the homopolymer to reduced accessibility of the thiol to the *S*-nitrosothiol moiety. These results demonstrate the potential for using nanostructures to tailor the reactivity of *S*-nitrosothiol functionalized materials.

In conclusion, we present a new approach for incorporating *S*-nitrosothiol moieties into thiocarbonylthio-terminated polymers prepared using RAFT polymerization. We demonstrate that the release of NO from such materials can be tailored by altering the copolymer structure. In particular, we show that incorporating the *S*-nitrosothiol into a micelle can significantly reduce thiol triggered degradation of *S*-nitrosothiol when compared to a hydrophilic homopolymer at the same pH. These results illustrate a convenient and versatile method for delivering nitric oxide which may have ultimate application in therapeutic situations, including (but not limited to) antibacterial and cardiovascular interventions.[31]

■ ASSOCIATED CONTENT

Supporting Information

The Supporting Information is available free of charge on the ACS Publications website at DOI: 10.1021/acsmacrolett.5b00733.

Experimental procedures for the preparation and characterization of all polymers, ^{1}H NMR spectra, additional release profiles, UV−visible and fluorescence spectra, and DLS size distribution of micelles (PDF).

■ AUTHOR INFORMATION

Corresponding Authors

*E-mail: thomas.p.davis@monash.edu.
*E-mail: michael.whittaker@monash.edu.
*E-mail: john.f.quinn@monash.edu.

Notes

The authors declare no competing financial interest.

■ ACKNOWLEDGMENTS

This work was carried out within the Australian Research Council (ARC) Centre of Excellence in Convergent Bio-Nano Science and Technology (Project No. CE140100036). T.P.D. acknowledges the award of an Australian Laureate Fellowship from the ARC.

■ REFERENCES

(1) Stamler, J. S.; Singel, D. J.; Loscalzo, J. *Science* **1992**, *258*, 1898.
(2) Barraud, N.; Hassett, D. J.; Hwang, S. H.; Rice, S. A.; Kjelleberg, S.; Webb, J. S. *J. Bacteriol.* **2006**, *188*, 7344.
(3) McDougald, D.; Rice, S. A.; Barraud, N.; Steinberg, P. D.; Kjelleberg, S. *Nat. Rev. Microbiol.* **2011**, *10*, 39.
(4) Rothrock, A. R.; Donkers, R. L.; Schoenfisch, M. H. *J. Am. Chem. Soc.* **2005**, *127*, 9362.
(5) Shin, J. H.; Metzger, S. K.; Schoenfisch, M. H. *J. Am. Chem. Soc.* **2007**, *129*, 4612.
(6) Friedman, A. J.; Han, G.; Navati, M. S.; Chacko, M.; Gunther, L.; Alfieri, A.; Friedman, J. M. *Nitric Oxide* **2008**, *19*, 12.
(7) Duong, H. T. T.; Kamarudin, Z. M.; Erlich, R. B.; Li, Y.; Jones, M. W.; Kavallaris, M.; Boyer, C.; Davis, T. P. *Chem. Commun.* **2013**, *49*, 4190.
(8) Cabrales, P.; Han, G.; Nacharaju, P.; Friedman, A. J.; Friedman, J. M. *Am. J. Physiol. Heart Circ. Physiol.* **2011**, *300*, H49.
(9) Duong, H. T. T.; Jung, K.; Kutty, S. K.; Agustina, S.; Adnan, N. N. M.; Basuki, J. S.; Kumar, N.; Davis, T. P.; Barraud, N.; Boyer, C. *Biomacromolecules* **2014**, *15*, 2583.
(10) Han, G.; Tar, M.; Kuppam, D. S. R.; Friedman, A.; Melman, A.; Friedman, J.; Davies, K. P. *J. Sex. Med.* **2010**, *7*, 224.
(11) Chiefari, J.; Chong, Y. K.; Ercole, F.; Krstina, J.; Jeffery, J.; Le, T. P. T.; Mayadunne, R. T. A.; Meijs, G. F.; Moad, C. L.; Moad, G.; Rizzardo, E.; Thang, S. H. *Macromolecules* **1998**, *31*, 5559.
(12) Perrier, S.; Takolpuckdee, P. *J. Polym. Sci., Part A: Polym. Chem.* **2005**, *43*, 5347.
(13) Willcock, H.; O'Reilly, R. K. *Polym. Chem.* **2010**, *1*, 149.
(14) Roth, P. J.; Boyer, C.; Lowe, A. B.; Davis, T. P. *Macromol. Rapid Commun.* **2011**, *32*, 1123.
(15) Postma, A.; Moad, G.; O'Shea, M. S.; Davis, T. P. *Macromolecules* **2005**, *38*, 5371.
(16) Sinnwell, S.; Inglis, A. J.; Davis, T. P.; Stenzel, M. H.; Barner-Kowollik, C. *Chem. Commun.* **2008**, *17*, 2052.
(17) Quemener, D.; Davis, T. P.; Barner-Kowollik, C.; Stenzel, M. H. *Chem. Commun.* **2006**, *48*, 5051.
(18) Boyer, C.; Bulmus, V.; Davis, T. P. *Aust. J. Chem.* **2009**, *62*, 830.
(19) Lima, V.; Jiang, X. L.; Brokken-Zijp, J.; Schoenmakers, P. J.; Klumperman, B.; Van Der Linde, R. *J. Polym. Sci., Part A: Polym. Chem.* **2005**, *43*, 959.
(20) Boyer, C.; Granville, A.; Bulmus, V.; Davis, T. P. *J. Polym. Sci., Part A: Polym. Chem.* **2009**, *47*, 3773.
(21) Boyer, C.; Davis, T. P. *Chem. Commun.* **2009**, *47*, 6029.
(22) Miller, M. R.; Megson, I. L. *Br. J. Pharmacol.* **2007**, *151*, 305.
(23) Wang, P. G.; Xian, M.; Tang, X. P.; Wu, X. J.; Wen, Z.; Cai, T. W.; Janczuk, A. *Chem. Rev.* **2002**, *102*, 1091.
(24) Shen, W.; Qiu, Q.; Wang, Y.; Miao, M.; Li, B.; Zhang, T.; Cao, A.; An, Z. *Macromol. Rapid Commun.* **2010**, *31*, 1444.
(25) Kojima, H.; Nakatsubo, N.; Kikuchi, K.; Kawahara, S.; Kirino, Y.; Nagaoshi, H.; Hirata, Y.; Nagano, T. *Anal. Chem.* **1998**, *70*, 2446.
(26) Zhang, X.; Kim, W. S.; Hatcher, N.; Potgieter, K.; Moroz, L. L.; Gillette, R.; Sweedler, J. V. J. *J. Biol. Chem.* **2002**, *277*, 48472.
(27) Joslin, J. M.; Neufeld, B. H.; Reynolds, M. M. *RSC Adv.* **2014**, *4*, 42039.
(28) Munro, A. P.; Williams, D. L. H. *J. Chem. Soc., Perkin Trans. 2* **1999**, 1989.
(29) Wong, P. S. Y.; Hyun, J.; Fukuto, J. M.; Shirota, F. N.; DeMaster, E. G.; Shoeman, D. W.; Nagasawa, H. T. *Biochemistry* **1998**, *37*, 5362.
(30) Arnelle, D. R.; Stamler, J. S. *Arch. Biochem. Biophys.* **1995**, *318*, 279.
(31) Quinn, J. F.; Whittaker, M. R.; Davis, T. P. *J. Controlled Release* **2015**, *205*, 190−205.

DOI: 10.1021/acsmacrolett.5b00733
ACS Macro Lett. 2015, 4, 1278−1282

Supporting Information

Transformation of RAFT Polymer End Groups into Nitric Oxide Donor Moieties: En Route to Biochemically Active Nanostructures

Sul Hwa Yu,[†] *Jinming Hu,*[†] *Francesca Ercole,*[†] *Nghia P. Truong,*[†] *Thomas P. Davis,*[†‡*] *Michael R. Whittaker*[†*] *and John F. Quinn*[†*]

[†] *ARC Centre of Excellence in Convergent Bio-Nano Science and Technology, Monash Institute of Pharmaceutical Sciences, Monash University, Parkville, VIC 3052, Australia;*

[‡] *Chemistry Department, University of Warwick, Coventry, ULCV4 7AL, UK*

Synthesis and Characterization Methods

A. Materials

Oligo(ethylene glycol) methyl ether methacrylate (OEGMA) with M_n = 300 g mol^{-1} or 500 g mol^{-1} (denoted as $OEGMA_{300}$ or $OEGMA_{500}$ where relevant) were purchased from Sigma-Aldrich and deinhibited by percolating over a column of basic alumina. 2-(dimethylamino)ethyl methacrylate (DMAEMA) and 2-(diisopropylamino)ethyl methacrylate (DIPMA) were purchased from Sigma-Aldrich and passed through a column of basic alumina in order to remove inhibitor. Azobisisobutyronitrile (AIBN) was purified by recrystallization from methanol before use. 4-Cyano-4-(phenylcarbonothioylthio)pentanoic acid (CPADB), hydrazine monohydrate, poly(ethylene glycol) methyl ether thiol (PEG-SH) (M_n = 2000 g mol^{-1}), and 5,5'-dithio-bis(2-nitrobenzoic acid) were purchased from Sigma-Aldrich at the highest purity available and were used as received. Sodium nitrite ($NaNO_2$) and sulphuric acid (98%) were purchased from Ajax Finechem and RCI Labscan, respectively, and used as received. Petroleum ether (b.p. 40 - 60 °C), diethyl ether, toluene, dimethylformamide and dioxane were purchased from Merck Millipore and used as received. 5,6-diaminofluorescein (D0084, Chemodex Customized Molecules) was obtained from Sapphire Biosciences (Sydney, Australia).

B. Synthetic Methods

B.1 Synthesis of P[OEGMA]-S(C=S)Ph (Precursor for P[OEGMA]-SNO)

The synthesis of P[OEGMA]-S(C=S)Ph was carried out using the following stoichiometry: $[CPADB]_0$:$[OEGMA_{300}]_0$:$[AIBN]_0$=1:20:0.1. Briefly, $OEGMA_{300}$ (6.00 g, 2×10^{-2} mol), CPADB RAFT agent (0.28 g, 1.0×10^{-3} mol), AIBN (1.64×10^{-2} g, 9.98×10^{-5} mol) and toluene (12 mL) were placed in a glass vial equipped with a magnetic stirrer bar and capped with a rubber septum. The reaction mixture was deoxygenated for 25 min at 0 °C by sparging with N_2. The deoxygenated and sealed reaction vessel was placed into a pre-heated oil bath at 70 °C and the polymerization was run with stirring for 6.5 h. The resulting mixture was then allowed to cool to 0 °C for about 15 min to terminate polymerization. The monomer conversion was determined by ^{1}H NMR. The polymer was purified of unreacted monomer by first precipitating into a 50/50 (v/v) mixture of diethyl ether and petroleum ether (bp 40-60 °C), followed by two subsequent precipitations into petroleum ether (bp 40-60 °C). The product was then placed in a vacuum oven overnight to remove remaining solvent. The final product was analysed by ^{1}H NMR and GPC. The molecular weight and average monomer

chain length calculated from ^{1}H NMR were determined to be 5100 g mol^{-1} and 16 units, respectively. The polydispersity index (determined by GPC) was 1.09.

B.2 Synthesis of P[OEGMA-co-DMAEMA]-S(C=S)Ph (Precursor for block polymer)

The synthesis of P[OEGMA-co-DMAEMA]-S(C=S)Ph was carried out using the following stoichiometry: $[CPADB]_0$:$[OEGMA_{500}]_0$:$[DMAEMA]_0$:$[AIBN]_0$=1:50:6:0.08. Briefly, $OEGMA_{500}$ (10.00 g, 2×10^{-2} mol), DMAEMA (0.38 g, 2.40×10^{-3} mol), CPADB RAFT agent (0.09 g, 4.00×10^{-4} mol), AIBN (0.52×10^{-2} g, 3.20×10^{-5} mol) and toluene (20 mL) were placed in a glass vial equipped with a magnetic stirrer bar and capped with a rubber septum. The reaction mixture was deoxygenated for 1 h by sparging with N_2. The deoxygenated and sealed reaction vessel was placed into a pre-heated oil bath at 70 °C and the polymerisation was run with stirring for 6.15 h. The resulting mixture was then allowed to cool to 0 °C for about 15 min to halt polymerisation. The monomer conversion was determined by ^{1}H NMR. The polymer was purified via three precipitation and centrifugation steps (using a 50/50 (v/v) mixture of petroleum ether (bp 40-60 °C) and diethyl ether as the precipitant) to remove any traces of unreacted monomer. The product was then placed in a vacuum oven overnight to remove remaining solvent. The final product was analysed by ^{1}H NMR and GPC. The molecular weight and average monomer chain length calculated from ^{1}H NMR were determined to be 14,200 g mol^{-1} and 27 units, respectively. The polydispersity index determined by GPC was 1.12.

B.3 Synthesis of P[OEGMA-co-DMAEMA-block-DIPMA]-S(C=S)Ph

P[OEGMA-co-DMAEMA-block-DIPMA]-S(C=S)Ph was prepared using the following stoichiometry: $[P[OEGMA\text{-}co\text{-}DMAEMA]\text{-}S(C=S)Ph]_0$:$[DIPMA]_0$:$[AIBN]_0$=1:100:0.08. P[OEGMA-co-DMAEMA]-S(C=S)Ph (1.31 g, 9.38×10^{-5} mol), DIPMA (2.00 g, 9.38×10^{-3} mol), and AIBN (0.12×10^{-2} g, 7.50×10^{-6} mol) were added to a glass vial equipped with a magnetic stirrer bar and capped with a rubber septum. The reaction mixture was deoxygenated by sparging with nitrogen for 1 h. The deoxygenated solution was placed into a pre-heated oil bath at 70 °C and the polymerisation was allowed to proceed with stirring for 12 h. The polymerisation was stopped by placing the sample in an ice bath for 15 min. The product was recovered by dialysis with acetone. The purified block polymer was then dried in vacuo. P[OEGMA-co-DMAEMA-block-DIPMA]-S(C=S)Ph was analysed by ^{1}H NMR and GPC.

B.4 Hydrazinolysis of the thiocarbonylthio end group from P[OEGMA]-S(C=S)Ph to form P[OEGMA]-SH

A solution of P[OEGMA]-S(C=S)Ph (0.20 g, 3.78×10^{-5} mol) in dimethylformamide (3 mL) was deoxygenated with nitrogen for 15 min. Hydrazine monohydrate (aq, 64 - 65%) was added to the deoxygenated solution (2.75 µL, 2.84×10^{-3} g, 5.67×10^{-5} mol). The deoxygenated reaction mixture was then stirred for 1 min at room temperature to convert the P[OEGMA]-S(C=S)Ph to P[OEGMA]-SH (i.e. convert the dithioester endgroup to sulfhydryl). The polymer obtained was then purified by dialysis with dilute HCl (pH 3.3) to minimise the formation of disulfide bonds. The purification process was conducted overnight to ensure removal of the benzothiohydrazide side product, and the resulting polymer was dried under N_2 and analysed by UV-Vis, ^{1}H NMR spectroscopy and Ellman's test to confirm the removal of the dithioester end group and the formation of thiol end group. Three distinct signals in the ^{1}H NMR spectrum (δ 7.3, 7.5 and 7.8 ppm, representing the aromatic benzodithioate) were lost upon hydrazinolysis. UV-Vis spectrophotometry also confirmed the disappearance of the absorbance at 320 nm which confirmed loss of the dithioester moiety.

B.5 Synthesis of PEG-SNO

PEG-SH (0.012 g, 0.62×10^{-5} mol) was dissolved in distilled water (2 mL). A stock solution of sodium nitrite (0.012 g, 1.74×10^{-4} mol) was prepared in distilled water (3.0 mL) at 0 °C and a second stock solution of sulphuric acid (0.9 µL, 0.84×10^{-5} mol) was also prepared in distilled water (600 µL) at 0 °C. 97.5 µL of sodium nitrite stock solution and 100 µL of sulphuric acid stock solution were combined at 0 °C to form a solution of nitrous acid. The resulting solution was then added to the PEG-SH solution with stirring for at least 1 min in an ice bath at 0 °C. The reaction vessel was covered with aluminium foil to exclude light. The formation of the SNO group was confirmed by UV-Vis spectrophotometry. Specifically, the emergence of an intense absorbance in the region 330-350 nm and a weak absorbance in the region 550-600 nm was noted, which is consistent with the formation of S-nitrosothiol moieties.[23] Synthesis of PEG-SNO was repeated with varying stoichiometric ratios of PEG-SH to nitrous acid.

B.6 Synthesis of P[OEGMA]-SNO

P[OEGMA]-SH prepared as above (B.4) (0.19 g, 3.73×10^{-5} mol) was dissolved in distilled water (2 mL). Sodium nitrite (0.21×10^{-2} g, 2.98×10^{-5} mol) was dissolved in distilled water

(100 µL), chilled to 0 °C and combined with sulphuric acid at 0 °C (0.8 µL, 1.49×10^{-5} mol) to form nitrous acid. The nitrous acid solution was then added to the P[OEGMA]-SH solution with stirring and allowed to react for at least 1 min at 0 °C prior to analysis. The reaction vessel was covered with aluminium foil to exclude light. The crude product was analysed by ^{1}H NMR, UV-Vis, and GPC. The formation of the S-nitrosothiol was confirmed by UV-Visible spectrophotometry. Specifically, the emergence of a strong absorbance in the region 330-350 and a weaker absorbance in the region 550-600 nm confirmed formation of the SNO group, which is in agreement with data reported in the literature.[23]

B.7 Hydrazinolysis of the thiocarbonylthio end group from P[OEGMA-co-DMAEMA-block-DIPMA]-S(C=S)Ph to form P[OEGMA-co-DMAEMA--block-DIPMA]-SH

A solution of P[OEGMA-co-DMAEMA-block-DIPMA]-S(C=S)Ph (0.60 g, 2.70×10^{-5} mol) in dimethylformamide (3 mL) was deoxygenated by sparging with with nitrogen for 15 min. To the deoxygenated solution hydrazine monohydrate was added (2.00 µL, 2.03×10^{-3} g, 4.06×10^{-5} mol). The deoxygenated reaction mixture was then stirred for 1 min at room temperature to convert the P[OEGMA-co-DMAEMA-block-DIPMA]-S(C=S)Ph to P[OEGMA-co-DMAEMA-block-DIPMA]-SH (i.e. to convert the dithioester end group to sulfhydryl). The polymer obtained was then purified by dialysis with dilute HCl (pH 3.3) to minimise the formation of disulfide bonds. The dialysis was conducted overnight to ensure complete removal of the expected benzothiohydrazide side product, and the resulting block copolymer was dried under N_2 and analysed by UV-Vis spectrophotometry, ^{1}H NMR spectroscopy and the Ellman's test to confirm removal of the dithioester end group and formation of the thiol end group. Three distinct signals in the ^{1}H NMR spectrum (δ 7.3, 7.5 and 7.8 ppm, representing the aromatic benzodithioate) were lost upon hydrazinolysis. UV-Visible spectrophotometry also confirmed the disappearance of the absorbance at 320 nm corresponding to the dithioester end group.

B.8 Synthesis of P[OEGMA-co-DMAEMA-block-DIPMA]-SNO

P[OEGMA-co-DMAEMA-block-DIPMA]-SH (0.60 g, 2.71×10^{-5} mol) prepared as above (B.7) was dissolved in distilled water (5 mL). Sodium nitrite (0.15×10^{-2} g, 2.17×10^{-5} mol) was dissolved in distilled water (100 µL), chilled to 0 °C and combined with sulphuric acid at 0 °C (0.58 µL, 1.09×10^{-5} mol) to form nitrous acid. The nitrous acid solution was then added to the P[OEGMA-co-DMAEMA-block-DIPMA]-SH prepared above with stirring and allowed to react for at least for 1 min at 0 °C. Hydrochloric acid (0.5 mL, 1 M) was added to

the reaction mixture to ensure that the block copolymer was well-dissolved for UV-visible analysis (i.e., to protonate the tertiary amino groups in the pH responsive block). The reaction vessel was covered with aluminium foil to exclude light. The crude product was analysed by ^{1}H NMR spectroscopy, UV-Visible spectrophotometry, and GPC. The formation of the S-nitrosothiol group was confirmed by UV-Visible spectrophotometry. Specifically, the appearance of an intense absorbance in the region 330-350 nm was noted, along with a weak band in the region 550-600 nm, as expected for these compounds.[23]

B.9 Synthesis of P[OEGMA-co-DMAEMA--block-DIPMA]-SNO micelles

Subsequent micelle formation was then conducted by injecting 1 mL of P[OEGMA-co-DMAEMA-block-DIPMA]-SNO (0.19 mM) into deoxygenated phosphate buffered saline (5 mL) under vigorous stirring at room temperature to afford a final pH of 7.4 or 6.0. The reaction mixture was stirred for a further 5 min under N_2. During this process every effort was made to exclude light to minimise photolysis of the S-nitrosothiol moiety. The micelle solution was then sampled for dynamic light scattering (DLS), UV-Visible spectrophotometry and fluorescence spectroscopy.

B.10 Determination of nitric oxide (NO) release from P[OEGMA]-SNO with fluorescent probe 5,6-Diaminofluorescein (DAF)

NO release was detected using 5,6-diaminofluorescein (DAF), a fluorescent indicator which is frequently used for measuring the presence of NO. A solution of DAF was prepared according to the procedure of Friedman and co-workers (see Friedman, A. J.; Han, G.; Navati, M. S.; Chacko, M.; Gunther, L.; Alfieri, A.; Friedman, J. M. *Nitric Oxide* **2008**, *19*, 12). Specifically, DAF was dissolved in DMSO to make a 23 μM solution which was stored in the dark. P[OEGMA]-SNO (13.7 mM) was dissolved in acetonitrile (13.7 mL). 500 μL of this solution was mixed with 500 μL DAF solution. Every effort was made to exclude light during this process. The presence of released NO was confirmed by fluorescence spectroscopy by observing the fluorescence emission signal between 500 and 550 nm (excitation wavelength at 492 nm).

C. Analysis Methods

C.1 ^{1}H Nuclear Magnetic Resonance Spectroscopy

^{1}H NMR spectra were recorded at 400 MHz on a Bruker UltraShield 400 MHz spectrometer

running Bruker Topspin, version 1.3. Spectra were recorded in $CDCl_3$, $(CD_3)_2SO$ or D_2O.

C.2 Gel Permeation Chromatography (GPC)

GPC was performed using a Shimadzu modular system comprised of a SIL-20AD automatic injector, a RID-10A differential refractive-index detector and a 50 × 7.8 mm guard column followed by three KF-805L columns (300 × 8 mm, bead size: 10 μm, pore size maximum: 5000 Å). *N,N'*-Dimethylacetamide (DMAc, HPLC grade, 0.03% w/v LiBr) at 50 °C was used for the analysis with a flow rate of 1 mL min^{-1}. Samples were filtered through 0.45 μm PTFE filters before injection. The GPC calibration was performed with narrow-polydispersity polystyrene standards ranging from 500 to 2×10^6 g mol^{-1}.

C.3 Dynamic Light Scattering (DLS)

DLS measurements were carried out on a Malvern Zetasizer Nano ZS Series running DTS software (laser, 4 mW, λ = 633 nm; angle 173°). The polydispersity index (PDI), used to describe the average diameters and size distribution of prepared micelles, was determined via a cumulants analysis of the measured intensity autocorrelation function using the DTS software. Samples were filtered using 0.45 μm PTFE syringe filter to remove contaminants / dust prior to measurement.

C.4 UV-vis spectroscopy

UV-Vis spectra were acquired on a Shimadzu UV-3600 UV-VIS-NIR spectrophotometer using quartz cuvettes with 10 mm path length.

C.5 Fluorescence spectroscopy

Fluorescence spectra were obtained using a fluorescence spectrophotometer (Shimadzu RF-5301 PC). Slit widths were set at 2.5 mm for both excitation and emission.

C.6 Amperometric NO Sensing

The NO-generating capability of polymers was examined via an amperometric approach using an NO-selective miniaturized Clark-type sensor manufactured by Unisense A/S. The working concept behind the sensor has been published by Schreiber and co-workers (see Schreiber, F.; Polerecky, L.; Beer, D. d. *Anal. Chem*. **2008**, *80*, 1152).

Calibration of the sensor was performed after allowing the sensor signal to stabilize over a pre-polarization period (usually 2 hours or more). A stock solution of an NO donor was prepared anaerobically by dissolving a known quantity of *S*-nitrosoglutathione (0.0229 g, 6.81×10^{-5}) into degassed PBS 7.4 (1.4 mL) in a closed container. 10 mL of PBS buffer was transferred to a nitrogen-flushed bottle equipped with a stirrer and the bottle capped with a modified septum for facilitating insertion of the probe. The sensor was then immersed into the solution via a specialized opening on the septum which enabled the bottle to be capped after the sensor tip had been carefully passed through. Once the signal stabilized to a low, stable reading, the value was recorded and assumed to correspond to the zero [NO] value. Calibration points within the expected range of measurement were collected by injecting known amounts of GSNO stock solution using a micro-syringe into the stirred calibration buffer solution. The current increased upon addition of the first aliquot and reached a plateau after several seconds. Further calibration values were obtained as subsequent aliquots were added (seven in total, ranging from 0 – 5000 μL). The recorded data was used to generate a linear calibration curve for [NO] vs. current (amps). All measurements were conducted at 37 °C.

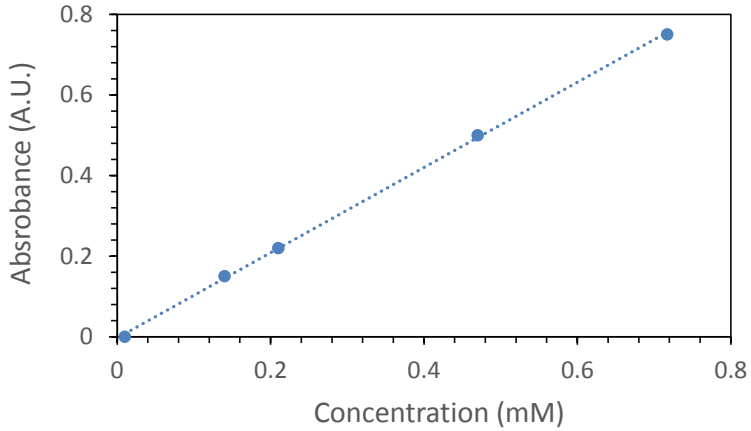

Figure S1. Standard curve for assessment of free thiol using the Ellman's assay: Absorbance at 412 nm versus concentration of cysteine.

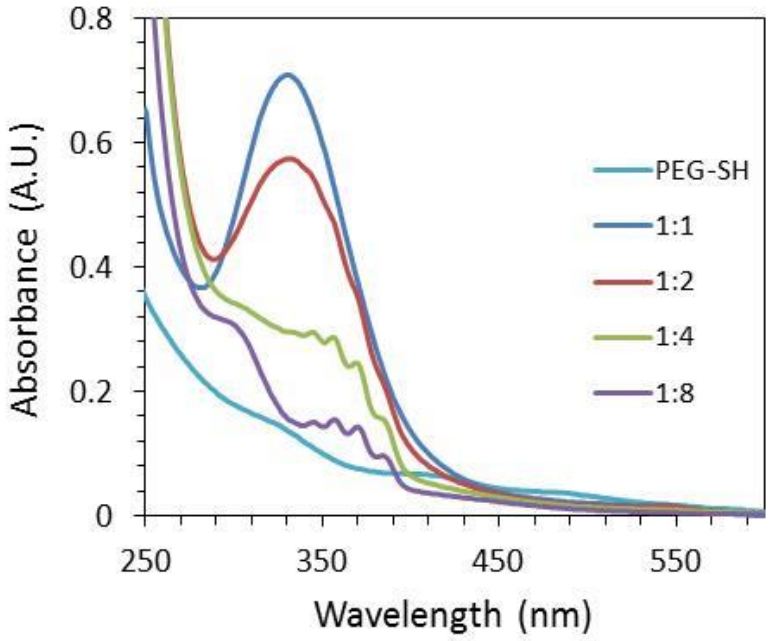

Figure S2 UV-visible spectra for PEG-SNO (M_n = 2000 g mol^{-1}) formed by the reaction of PEG-SH (M_n = 2000 g mol^{-1}) with varying stoichiometric amounts of nitrous acid. [PEG-SNO] = 1.04 mM.

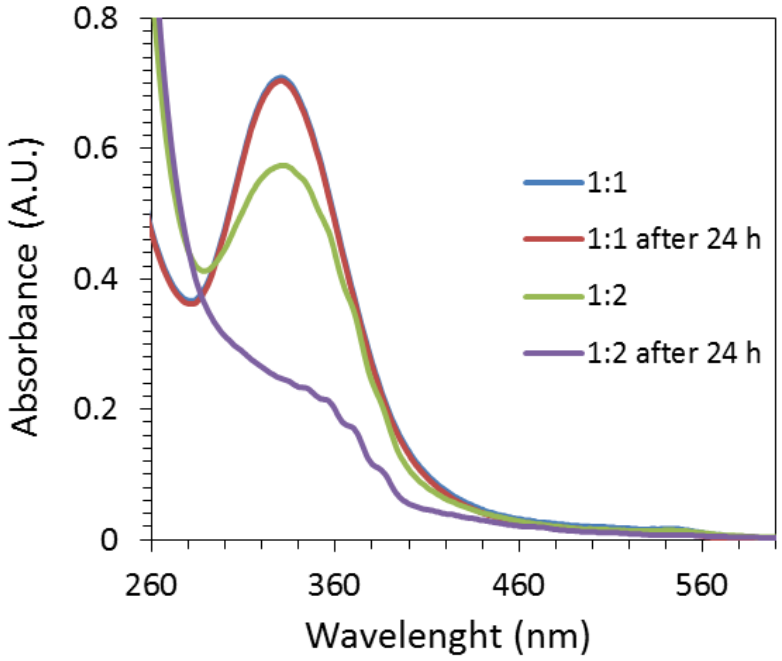

Figure S3. UV-visible spectra for PEG-SNO (M_n = 2000 g mol^{-1}) formed by the reaction of PEG-SH (M_n = 2000 g mol^{-1}) with nitrous acid at either PEG-SH:HNO_2 = 1:1 or PEG-SH:HNO_2 = 1:2. Spectra were collected immediately after reaction and after 24 hours. [PEG-SNO] = 1.04 mM.

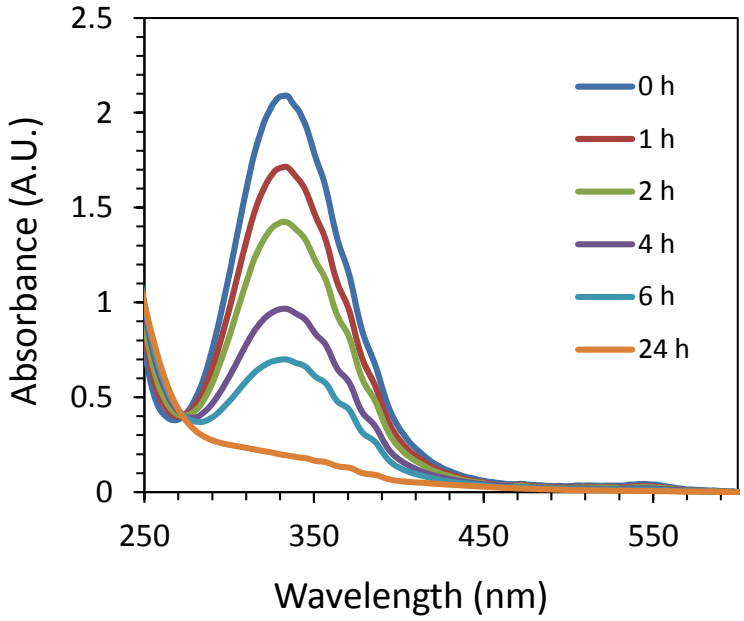

Figure S4. UV-visible spectra for PEG-SNO (M_n = 2000 g mol^{-1}) formed by the reaction of PEG-SH (M_n = 2000 g mol^{-1}) with nitrous acid at PEG-SH:HNO_2 = 1:1 before and after an additional equivalent of nitrous acid was added. Spectra were collected periodically over the 24 hours following addition of the extra nitrous acid. [PEG-SNO] = 2.60 mM.

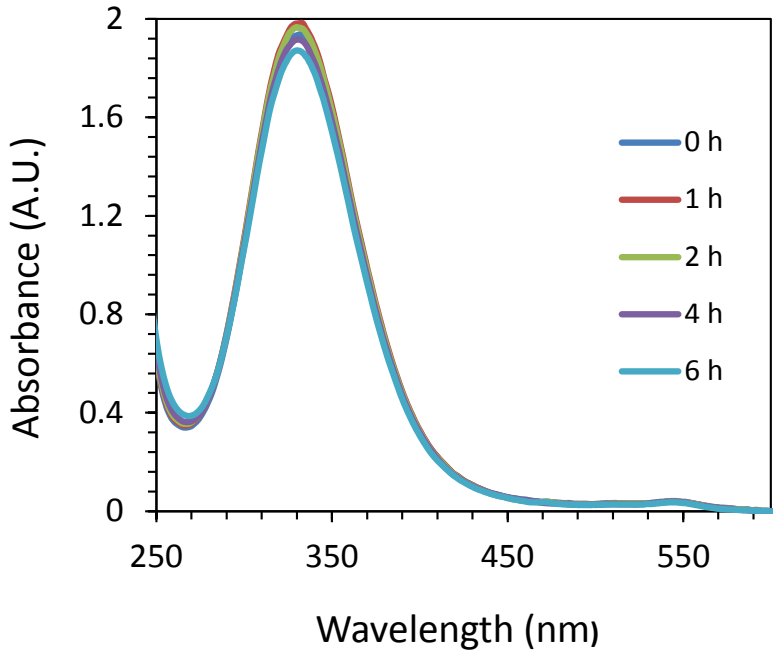

Figure S5. UV-visible spectra for PEG-SNO (M_n = 2000 g mol^{-1}) formed by the reaction of PEG-SH (M_n = 2000 g mol^{-1}) with nitrous acid at PEG-SH:HNO_2 = 1:1 before and after an additional equivalent of sulfuric acid was added. Spectra were collected periodically over the 24 hours following addition of the extra sulfuric acid. [PEG-SNO] = 2.60 mM.

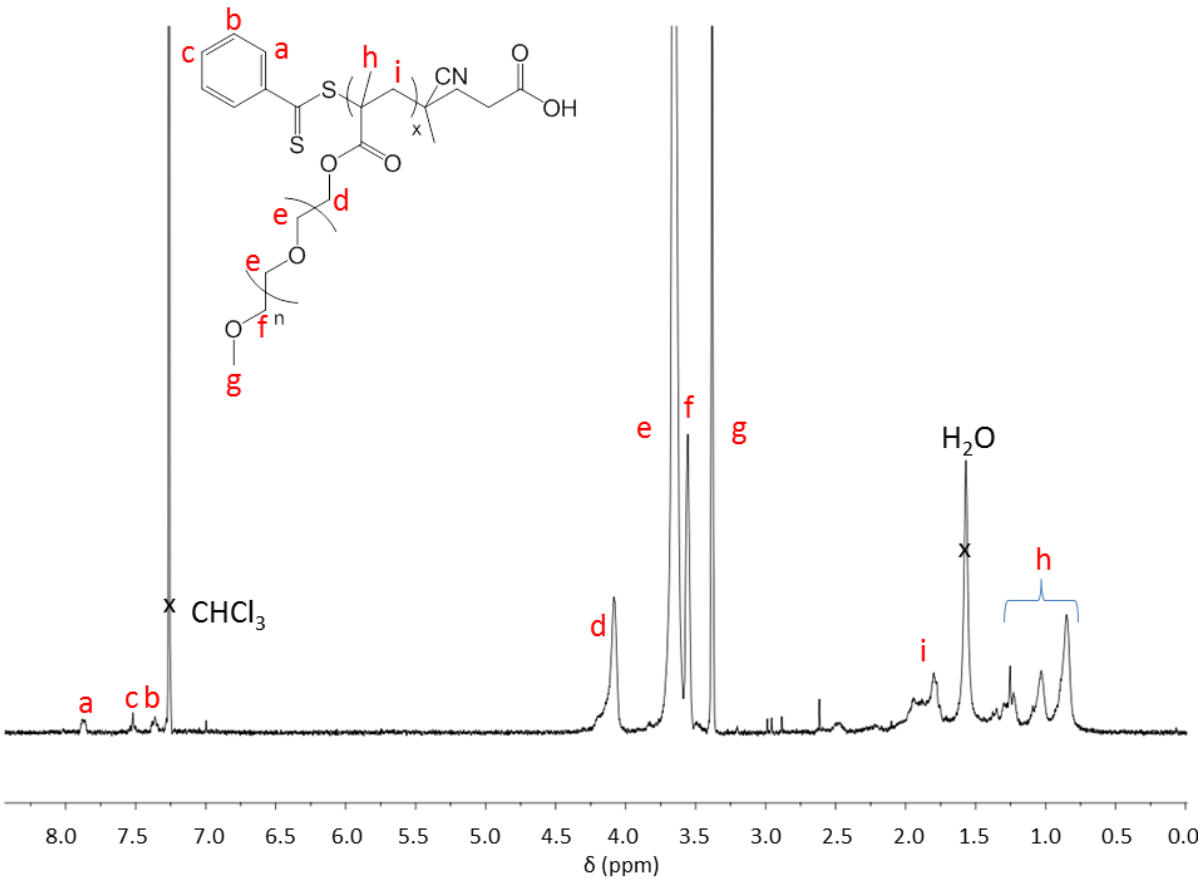

Figure S6. ^{1}H NMR spectrum of P[OEGMA]-S(C=S)Ph (Table, Entry 1), recorded in $CDCl_3$ (400 MHz).

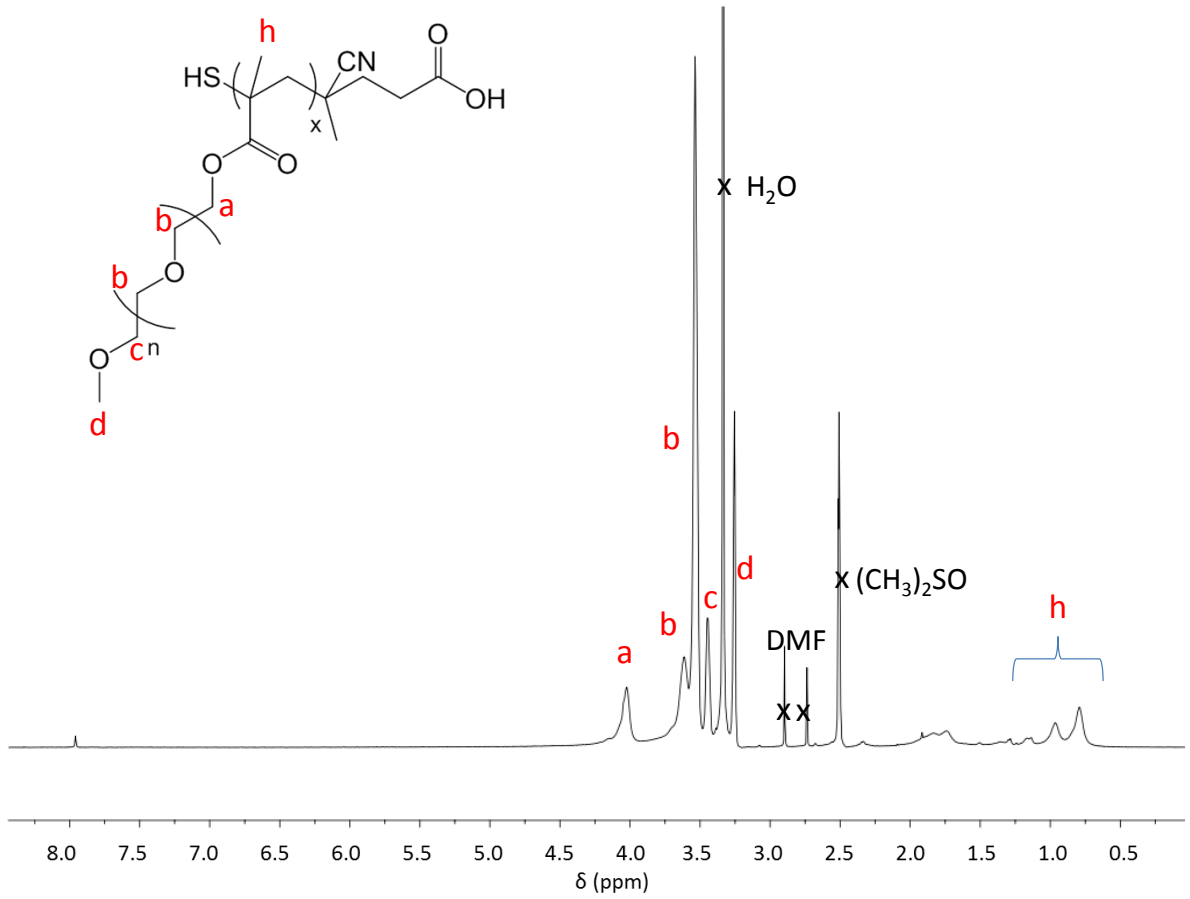

Figure S7. ^{1}H NMR spectrum of P[OEGMA]-SH (Table 1, Entry 2) after hydrazinolysis, recorded in $(CD_3)_2SO$ (400 MHz). Note: Three distinct signals (δ 7.3, 7.5 and 7.8 ppm, representing the aromatic benzodithioate end group of P[OEGMA]-S(C=S)Ph) are no longer evident following hydrazinolysis.

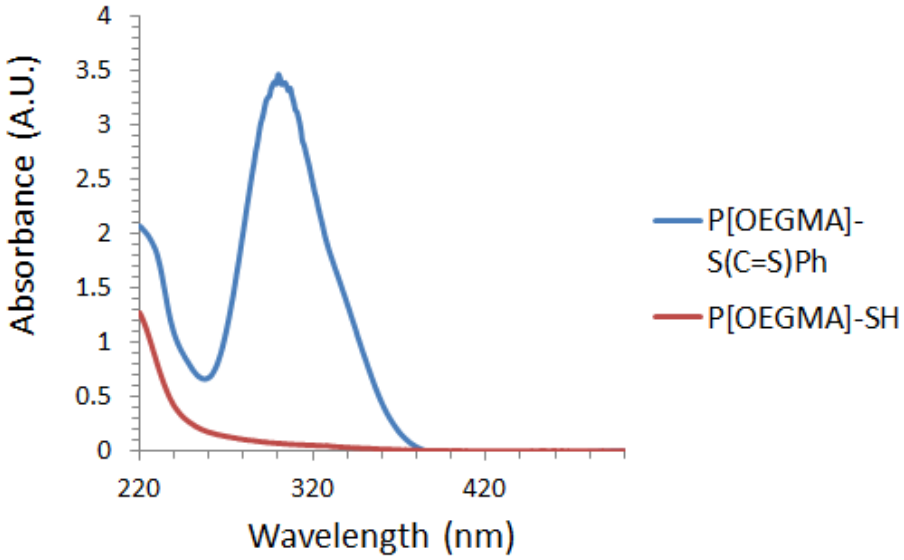

Figure S8. UV-visible spectra of P[OEGMA]-S(C=S)Ph before and after hydrazinolysis. The blue line represents P[OEGMA]-S(C=S)Ph (Table 1, Entry 1) before removal of the RAFT end group, while the red line represents P[OEGMA]-SH (Table 1, Entry 2) formed by removal of RAFT end group via hydrazinolysis. Polymer concentration = 67 mg ml^{-1}.

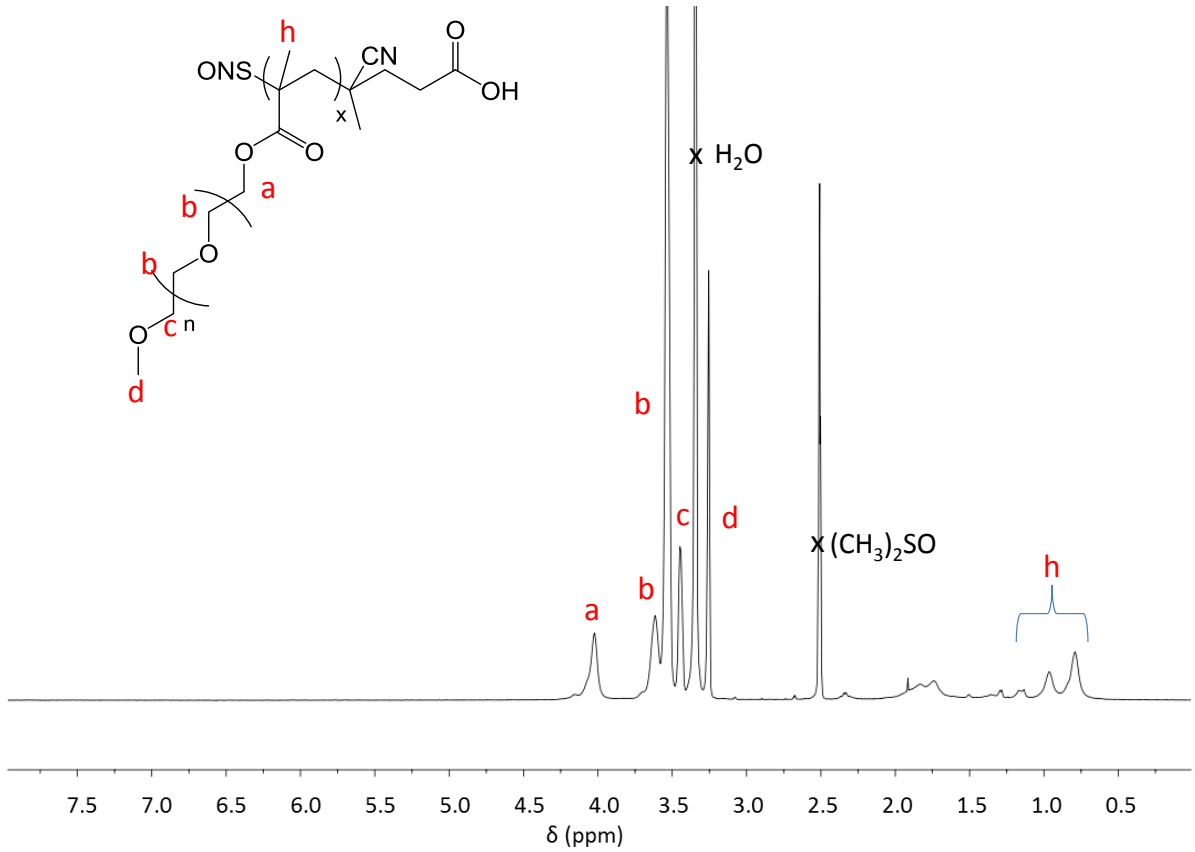

Figure S9. ^{1}H NMR spectrum of P[OEGMA]-SNO (Entry 3), recorded in $(CD_3)_2SO$ (400 MHz).

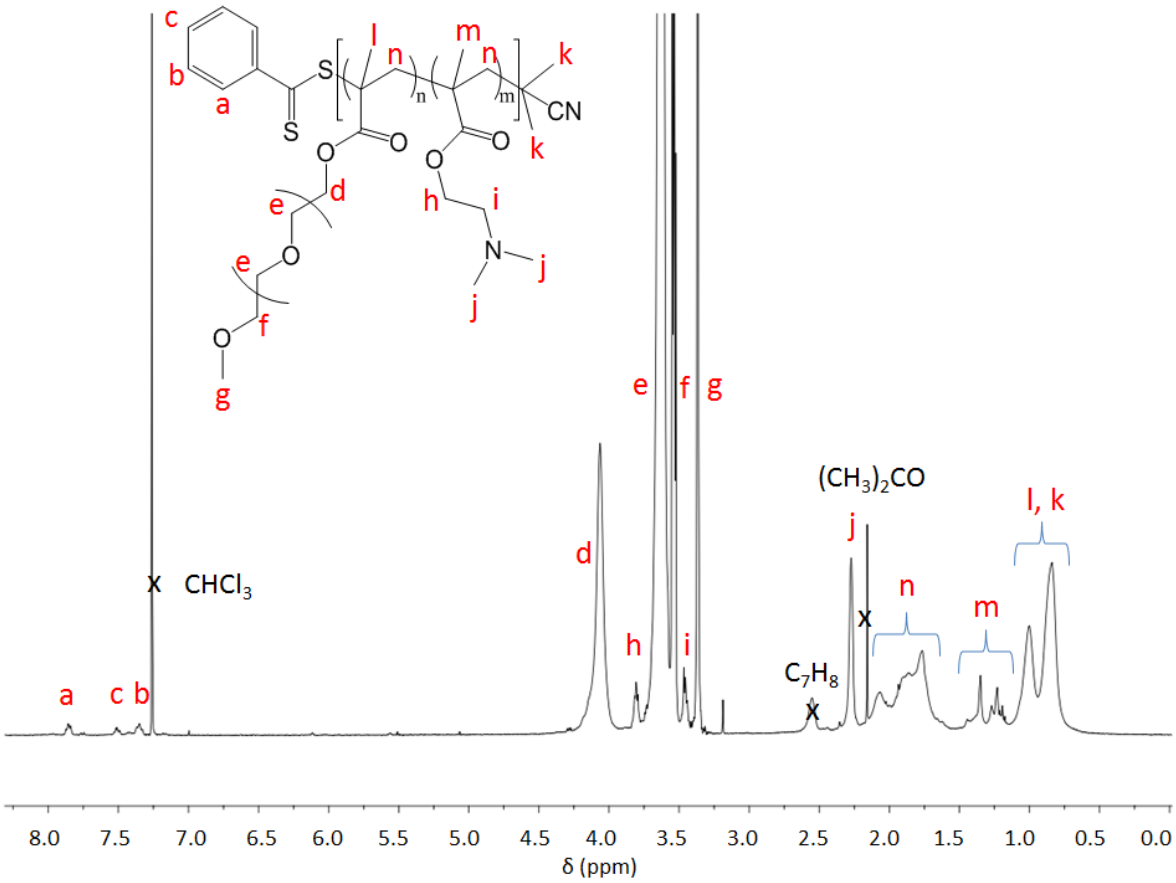

Figure S10. ^{1}H NMR spectrum of P[OEGMA-co-DMAEMA]-S(C=S)Ph, recorded in $CDCl_3$ (400 MHz)

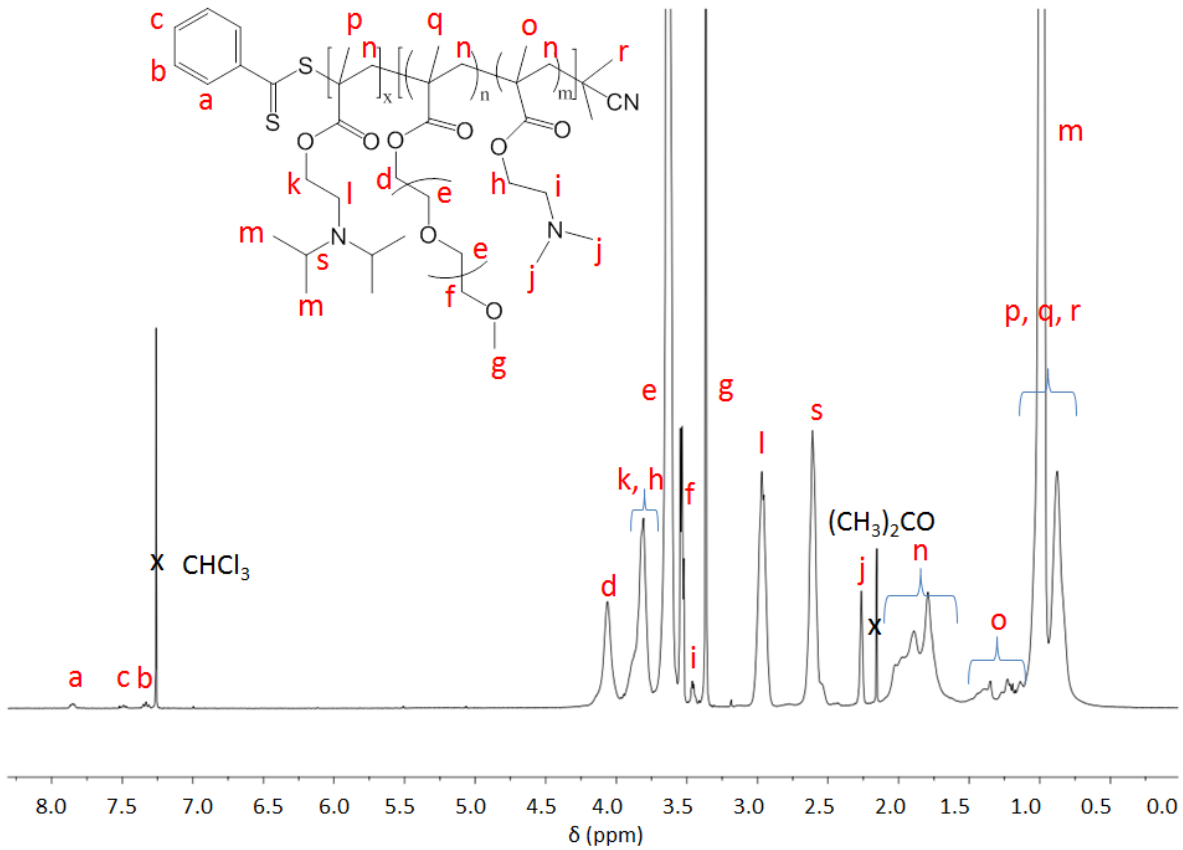

Figure S11. ^{1}H NMR spectrum of P[OEGMA-co-DMAEMA-block-DIPMA]-S(C=S)Ph (Table 1, Entry 4), recorded in $CDCl_3$ (400 MHz)

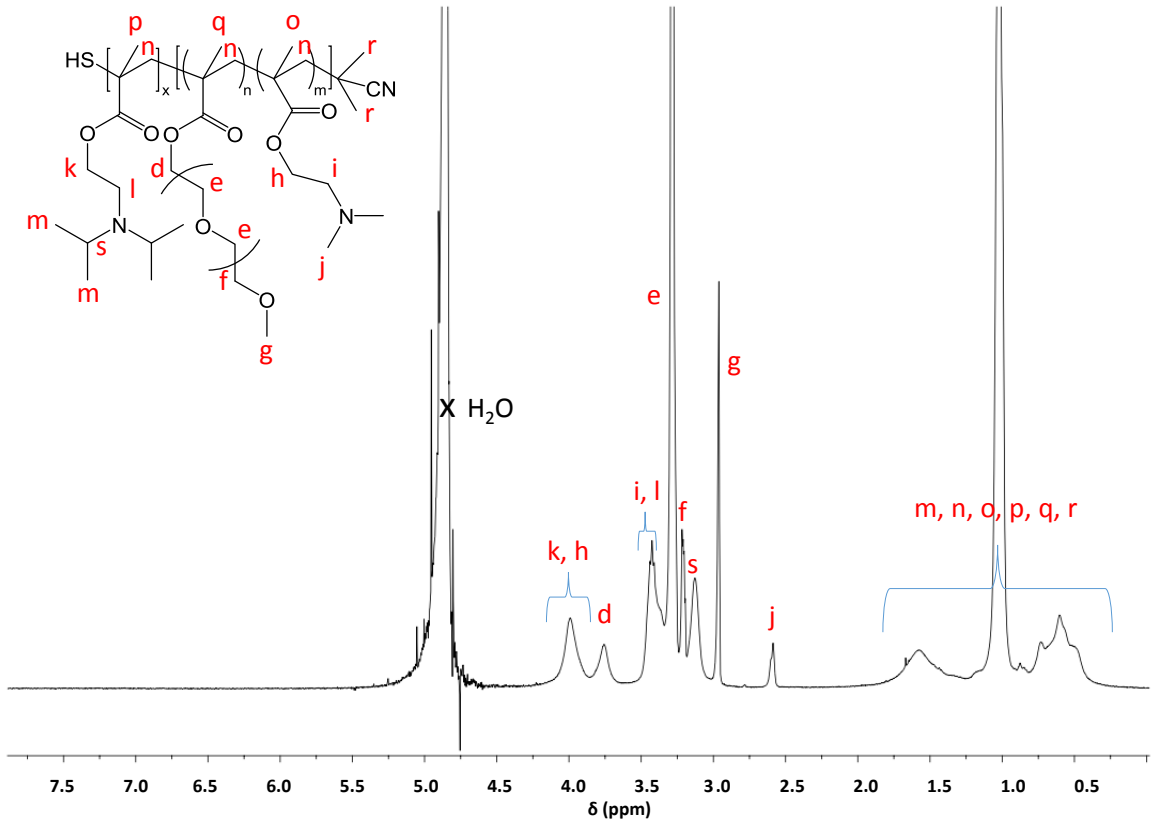

Figure S12. ^{1}H NMR spectrum of P[OEGMA-co-DMAEMA-block-DIPMA]-SH (Entry 5) after aminolysis, recorded in D_2O (400 MHz). The pH was adjusted to ~ 3 using 1 M HCl to solubilize the polymer prior to analysis. Note: Three distinct signals (δ 7.3, 7.5 and 7.8 ppm, representing the aromatic benzodithioate end group of P[PEGMA-block-DIPMA]-S(C=S)Ph) are no longer evident following hydrazinolysis.

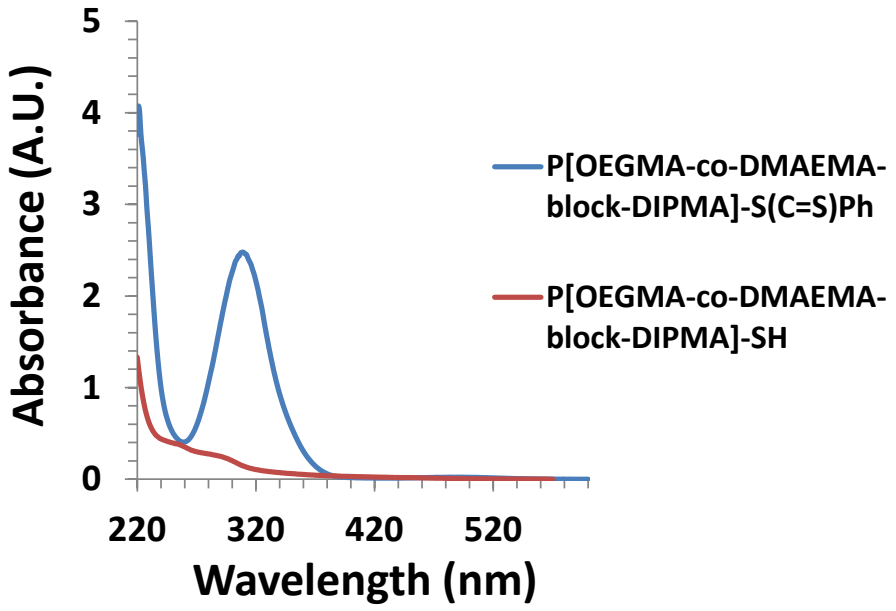

Figure S13. UV-visible spectra of P[OEGMA-co-DMAEMA-block-DIPMA]-S(C=S)Ph before and after hydrazinolysis. The blue line represents P[OEGMA-co-DMAEMA-block-DIPMA]-S(C=S)Ph (Table 1, Entry 4) before removal of the RAFT end group, while the red line represents P[OEGMA-co-DMAEMA-block-DIPMA]-SH (Table 1, Entry 5) formed by removal of RAFT end group via hydrazinolysis. Polymer concentration = 67 mg ml^{-1}.

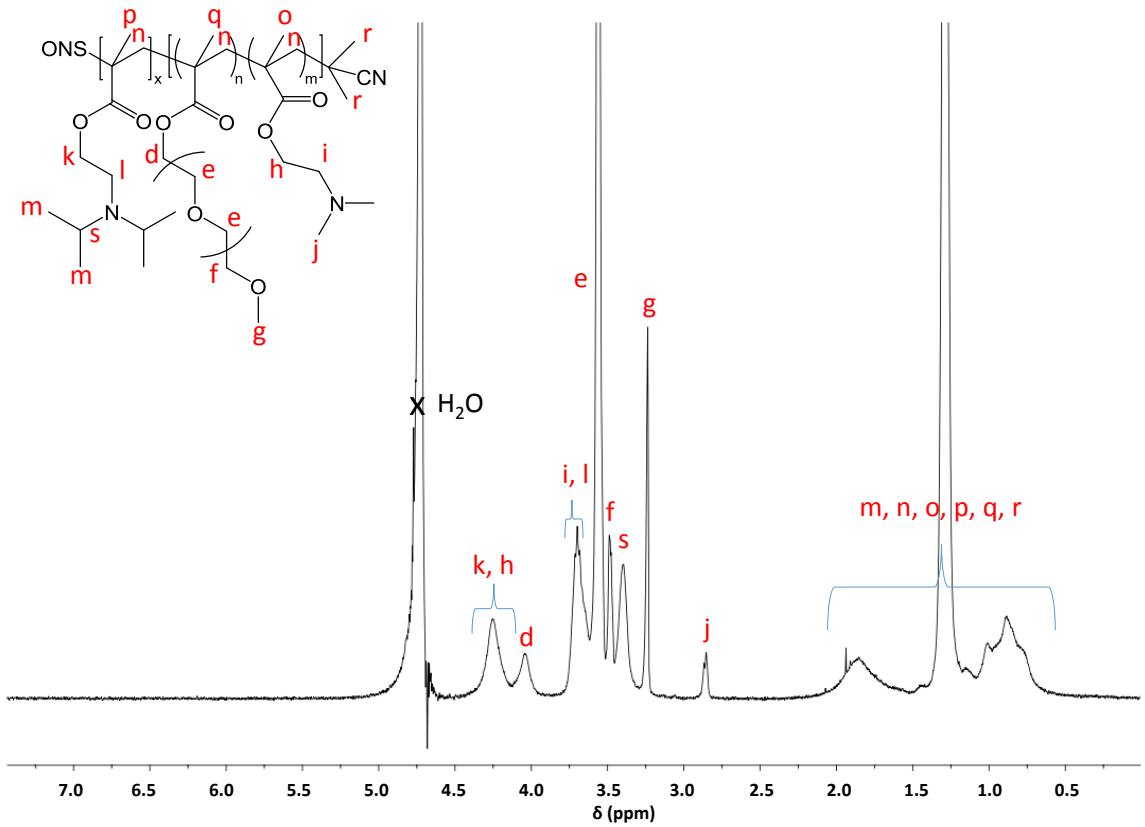

Figure S14. ^{1}H NMR spectrum of P[OEGMA-co-DMAEMA-block-DIPMA]-SNO (Entry 6), recorded in D_2O (400 MHz). The pH was adjusted to ~ 3 using 1 M HCl to solubilize the polymer prior to analysis.

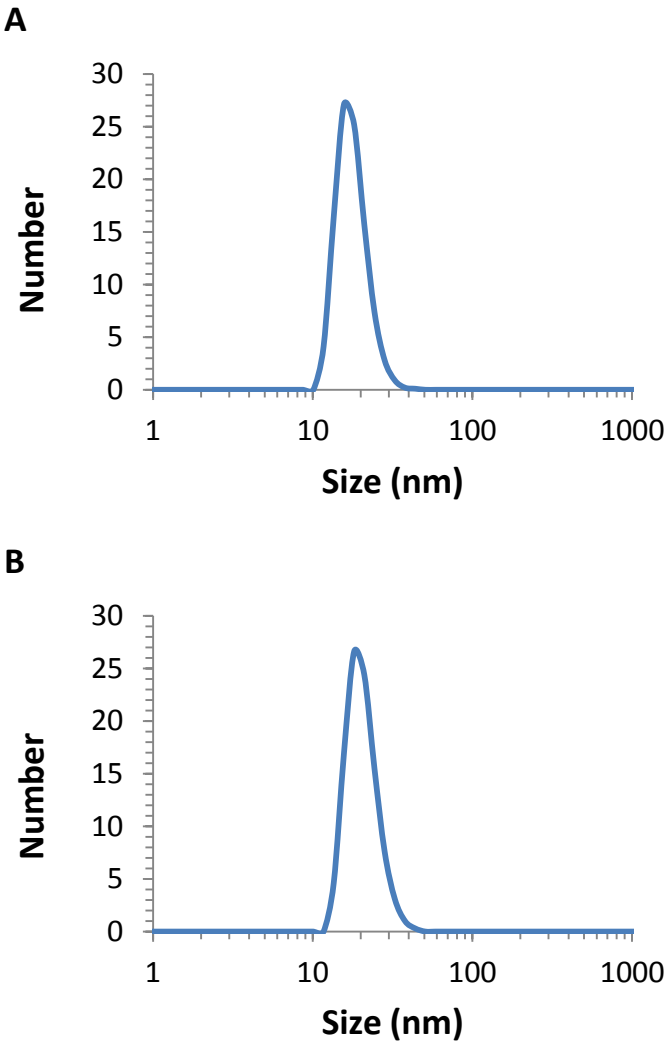

Figure S15. Size distribution (by number) for micelles in phosphate buffered saline at (A) pH 7.4 and (B) pH 6.0, as determined by dynamic light scattering. For pH 7.4 the average diameter was 17 nm and PSD = 0.1 - 0.2. For pH 6.0, the average diameter was 20 nm with PSD = 0.05.

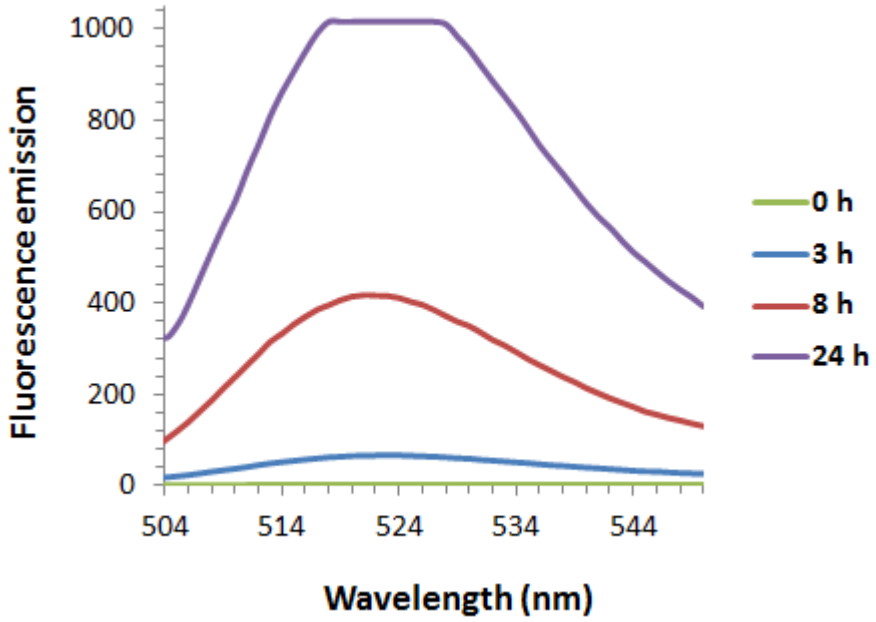

Figure S16. Evolution of fluorescence spectra generated by the release of nitric oxide from P[OEGMA]-SNO (10 μM) in the presence of 5,6-diaminofluorescein.

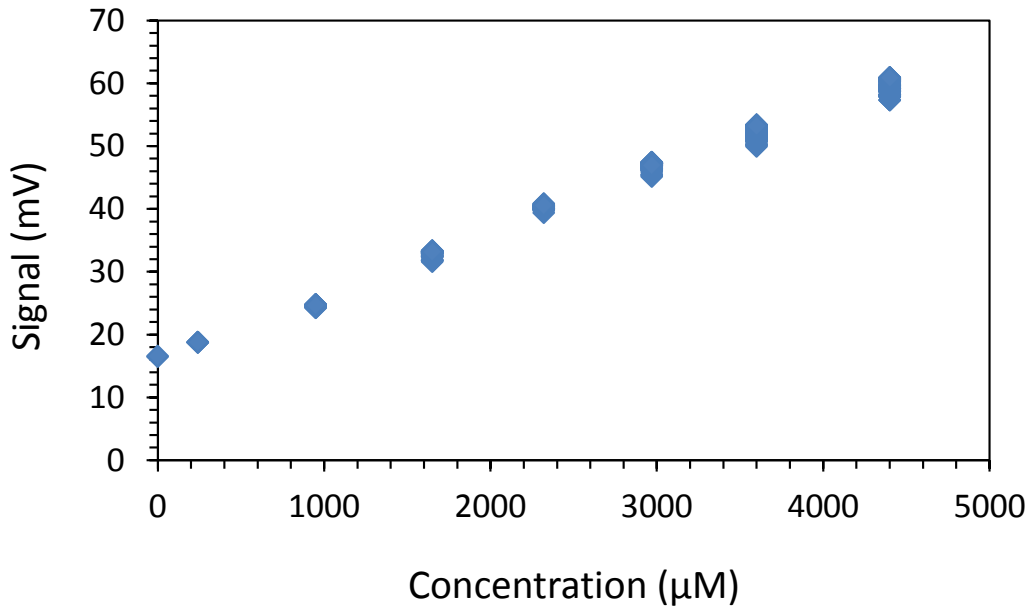

Figure S17. Calibration curve for the electrochemical sensing of nitric oxide from a known concentration of NO donor. S-nitrosoglutathione was used as the standard.

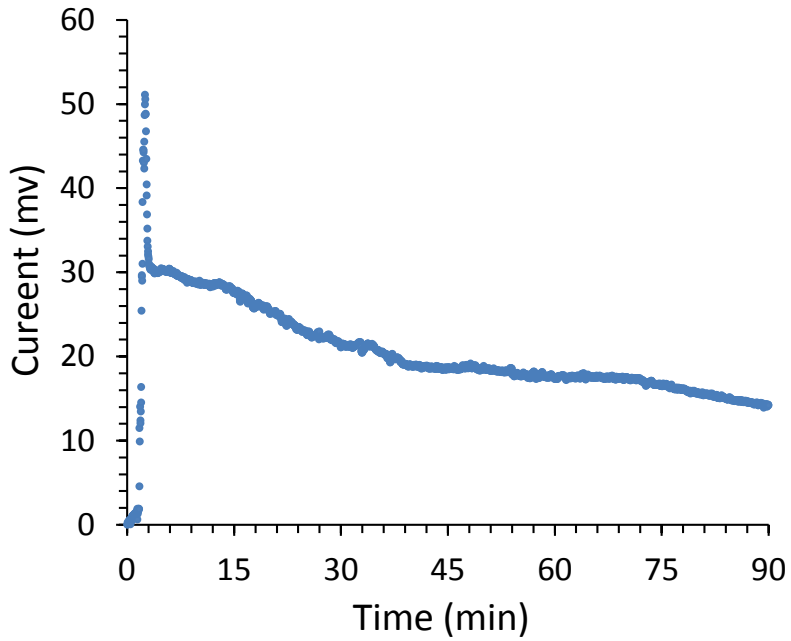

Figure S18. Electrochemical response from PEG-SNO at 0.58 mM in PBS at pH 7.4 and 37 °C.

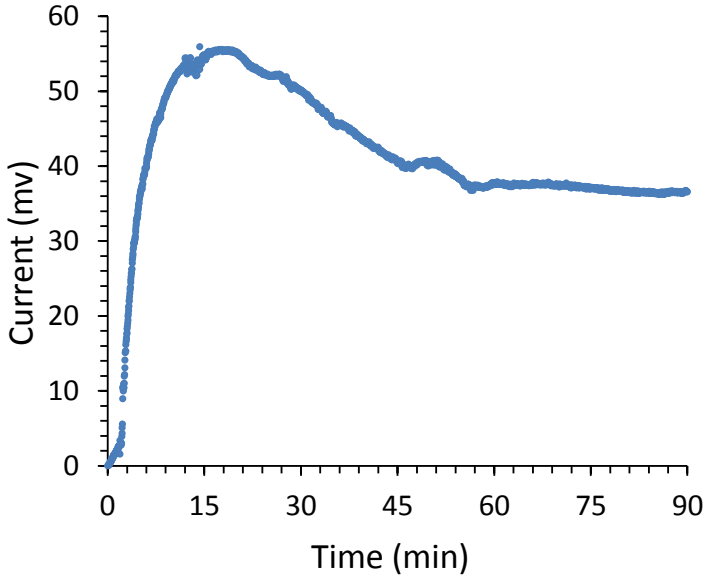

Figure S19. Electrochemical response from P[OEGMA]-SNO at 0.58 mM in PBS at pH 7.4 and 37 °C.

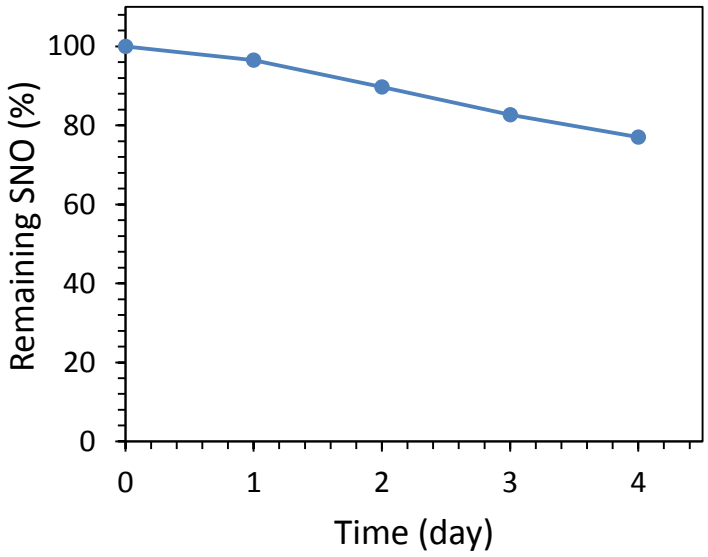

Figure S20. % SNO remaining for P[OEGMA]-SNO (2.28 mM) at room temperature with time. Data derived from the time dependent spectra in Figure 3A.

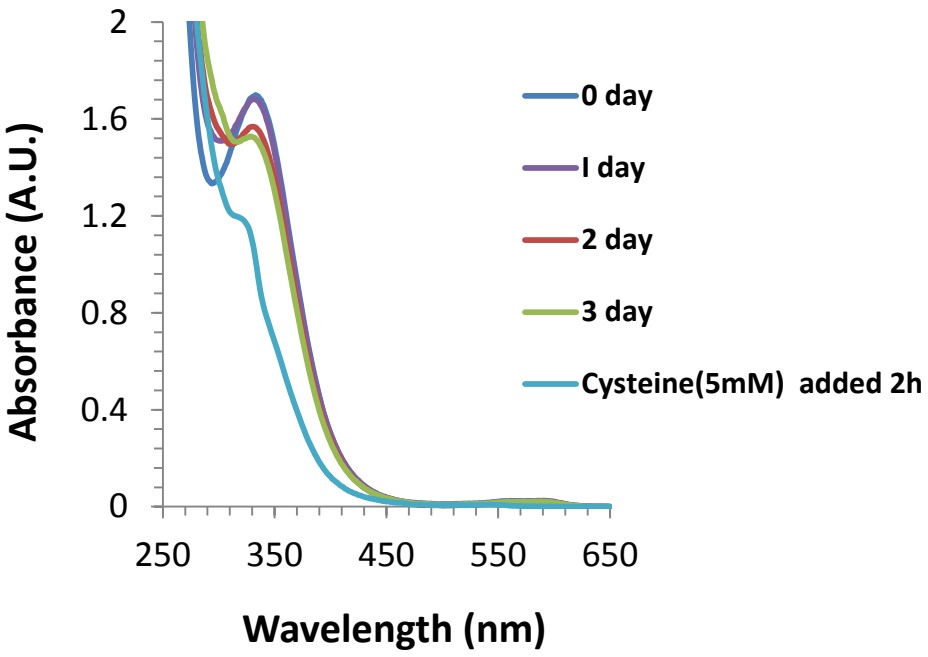

Figure S21. UV-Visible spectra for P[OEGMA]-SNO (2.28 mM) with time (or addition of cysteine) at room temperature. Figure 4A in the main manuscript shows the region from 450-650 nm in expanded view.

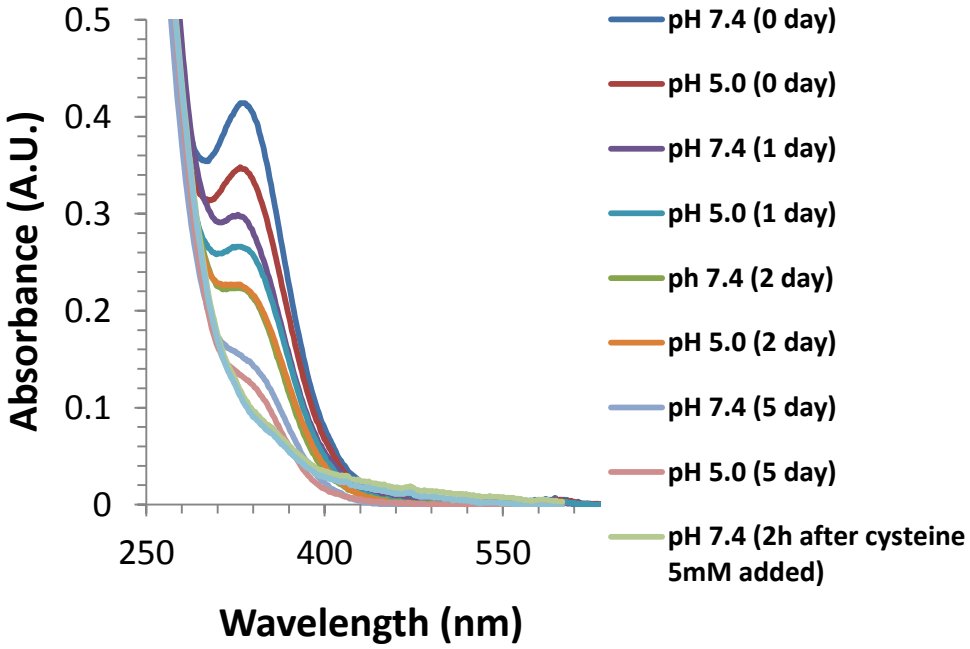

Figure S22. UV-Visible spectra of P[OEGMA]-SNO in different pH conditions (pH 7.4 and 5.0) at 37˚C (0.68 mM).

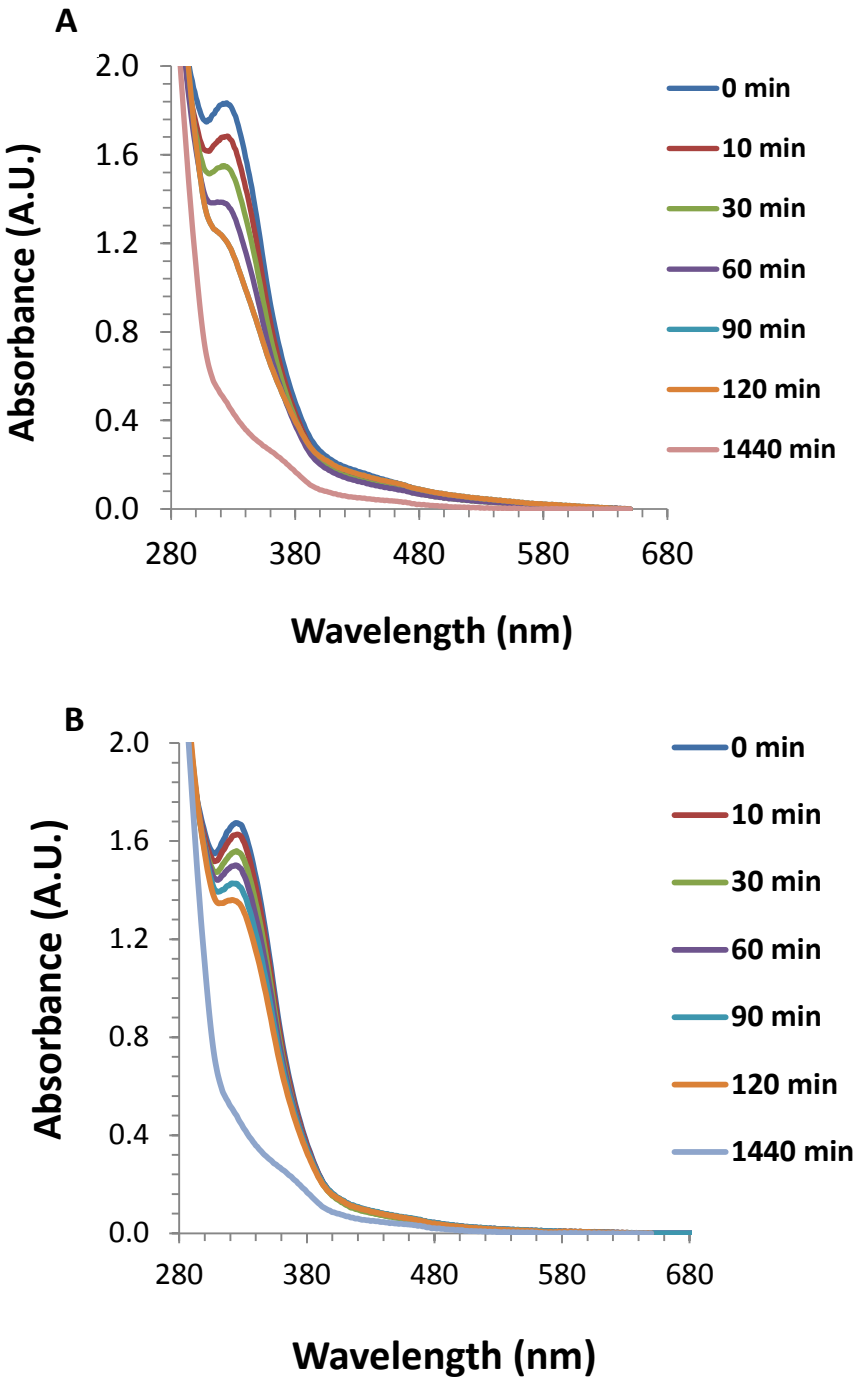

Figure S23. Evolution of UV-visible spectra with time for P[OEGMA-co-DMAEMA-block-DIPMA]-SNO (1.98 mM) at 37˚C and: (A) pH 7.4 or (B) pH 6.0.

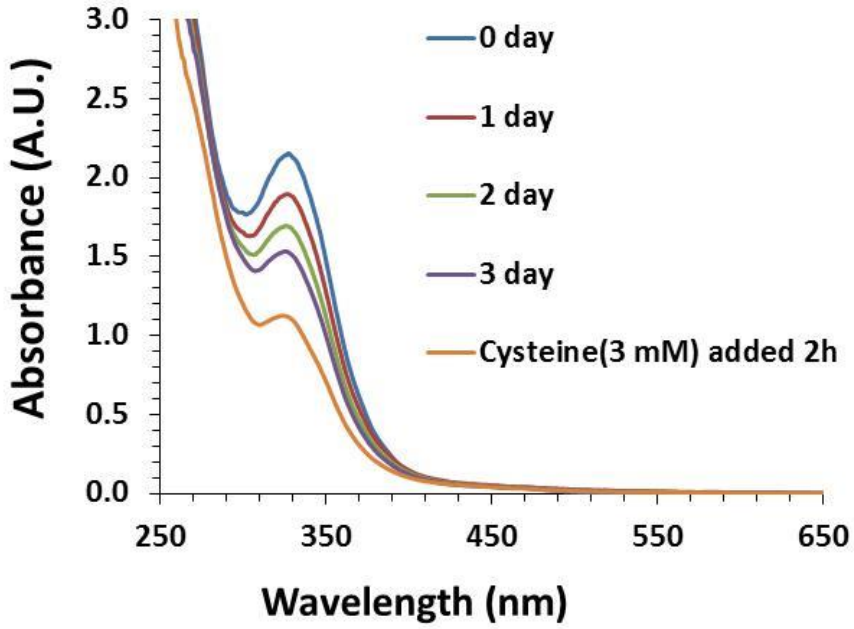

Figure S24. UV-Visible spectra of P[OEGMA-co-DMAEMA-block-DIPMA]-SNO (1.98 mM) at room temperature and pH 2-3.

CHAPTER 3: Polymers with acyl-protected perthiol chain termini as convenient building blocks for doubly responsive H_2S-donating nanoparticles

Polymer Chemistry

COMMUNICATION

View Article Online
View Journal | View Issue

Cite this: *Polym. Chem.*, 2017, **8**, 6362

Received 18th September 2017,
Accepted 21st September 2017

DOI: 10.1039/c7py01484h

rsc.li/polymers

Polymers with acyl-protected perthiol chain termini as convenient building blocks for doubly responsive H_2S-donating nanoparticles†

Sul Hwa Yu,[a] Francesca Ercole,[a] Nicholas A. Veldhuis,[a,b] Michael R. Whittaker,[a] Thomas P. Davis *[a,c] and John F. Quinn *[a]

H_2S-releasing polymers with an acyl-protected perthiol chain terminus were prepared using a simple, high yielding end-group modification process. Specifically, benzodithioate-terminated poly (oligoethylene glycol methyl ether) methacrylate (POEGMA) was first converted to pyridyl-2-disulfide-terminated polymer, after which a thiol–disulfide exchange reaction with thiobenzoic acid yielded an acyl protected perthiol at the chain terminus. The same approach was successfully applied to a hydrophilic–hydrophobic block polymer, P[OEGMA-*block*-*n*-butyl methacrylate], and a pH-responsive block copolymer, P[OEGMA-*co*-*N*,*N*-(dimethylamino) ethyl methacrylate-*block*-*N*,*N*-(diisopropylamino)ethyl methacrylate]. All polymers were shown to release H_2S when exposed to thiol (L-cysteine), with release rate dependent on polymer structure. In the case of the pH-responsive block copolymer there was minimal release of H_2S under conditions where the polymers were micellised, whereas there was rapid, sustained release when the block copolymers were in unimeric form. These materials were shown to increase the intracellular concentration of H_2S when applied to HEK cells, and may be useful for interrogating localized delivery of H_2S.

The transient production of hydrogen sulfide (H_2S) mediates a variety of essential biochemical processes.[1–3] For instance, H_2S has been shown to have important signaling functions in the gastrointestinal,[4] circulatory,[5] renal,[6] immune[7] and nervous[8] systems. To identify the biological function of H_2S, studies such as these typically employ sulfide salts (*e.g.*, Na_2S/NaSH) as exogenous donors of H_2S. However, these salts liberate H_2S in buffer with little control over the release profile,[9,10] which is not analogous to the continuous biosynthesis of H_2S *in vivo*. As a result, the biological functions of H_2S can be difficult to completely isolate from other, off-target, effects.

To address this issue, a range of organic H_2S-donors with superior release profiles have been synthesized, such as *S*-benzoylthiohydroxylamines,[11] *N*-benzoylthiobenzamides,[12] dithioperoxyanhydrides,[13] 1,2-dithiole-3-thiones,[14] phosphonamidothioates,[15] and acyl-protected perthiols.[16] One approach for further enhancing the release profile of such donors is to incorporate these moieties into responsive, nanoparticle-based H_2S delivery systems, thereby enabling more spatiotemporally defined delivery of the signaling molecule. As such, conjugating H_2S donors to polymers is attracting increasing attention.[17–19]

One strategy for incorporating a functional moiety into a polymer chain is *via* modification of the chain end-group. In particular, thiocarbonylthio end-groups which are present in polymers synthesized by reversible addition–fragmentation chain transfer (RAFT) polymerisation represent an excellent substrate for modification.[20–23] This has been exploited for various reactions, such as thiol–disulfide exchange,[24] azide–alkyne click reactions[25] or thiol–ene click reactions.[26] Recently, we reported the synthesis of *S*-nitrosothiol-terminated polymers *via* a simple two-step modification of the RAFT end-group.[27] This enabled the preparation of polymers with an end-group structure which mimics the biologically significant molecule *S*-nitrosoglutathione (GSNO).[28]

Inspired by the protected perthiol small molecule H_2S donors of Xian and coworkers,[16] we describe herein a straightforward, high-yielding end-group modification approach for incorporating H_2S donor moieties into polymers synthesized *via* RAFT polymerisation. By aminolysing the terminal thiocarbonylthio groups in the presence of dipyridyl disulfide, we first formed polymers with a terminal pyridyl disulfide group.[24] These could be easily converted to benzoyl-capped perthiols by reaction with a slight excess of thiobenzoic acid. The resulting polymers remain dormant in an aqueous environment and are only triggered to release H_2S by exposure to thiols. Moreover, these protected perthiol groups can be readily incorporated into both simple homopolymers and more sophisticated pH

[a]*ARC Centre of Excellence in Convergent Bio-Nano Science and Technology, Monash Institute of Pharmaceutical Sciences, Monash University, Parkville, VIC 3052, Australia. E-mail: thomas.p.davis@monash.edu, john.f.quinn@monash.edu*
[b]*Drug Discovery Biology Theme, Monash Institute of Pharmaceutical Sciences, Monash University, Parkville, VIC 3052, Australia*
[c]*Department of Chemistry, University of Warwick, Coventry, ULCV4 7AL, UK*
†Electronic supplementary information (ESI) available. See DOI: 10.1039/c7py01484h

responsive block copolymers, the latter of which can be employed to prepare stimuli-responsive nanoparticles. Such nanoparticles can be stimulated to release H_2S by exposure to thiols, with the release profile highly influenced by pH.

Benzodithioate-terminated poly(oligoethylene glycol methyl ether) methacrylate (P[OEGMA]-S(C═S)Ph, **1a**, Scheme 1) was first prepared by polymerising OEGMA (MW = 500 g mol^{-1}) in the presence of the RAFT agent 2-cyanoprop-2-yl benzodithioate. The resulting polymer was purified by precipitation (see ESI† for detailed procedures), and characterized using ^{1}H nuclear magnetic resonance spectroscopy (^{1}H NMR) and gel permeation chromatography (GPC) (Table S1,† Fig. 1A, B & S1†). The purified P[OEGMA]-S(C═S)Ph was then reacted with ethanolamine in the presence of dipyridyl disulfide under deoxygenated conditions to form pyridyl disulfide-terminated POEGMA (P[OEGMA]-S-S-Py) (Scheme 1, **1b**).[24] In essence, this reaction entails the rapid aminolysis of the thiocarbonylthio end-group by ethanolamine to form an intermediate thiol (P[OEGMA]-SH), which undergoes an immediate thiol–disulfide exchange reaction with the dipyridyl disulfide to form the P[OEGMA]-S-S-Py. The reaction mixture was allowed to stir for two hours, although the pink colour of the benzodithioate was lost within the first ten minutes, during which time yellow colour developed (associated with liberation of mercaptopyridine). The P[OEGMA]-S-S-Py was purified by dialysis and characterized using GPC and ^{1}H NMR (Table S1,† Fig. 1A, B & S2†). The ^{1}H NMR spectrum was consistent with complete conversion of the benzodithioate end-group to pyridyl disulfide (Fig. 1A). Specifically, the three characteristic resonances in the ^{1}H NMR spectrum associated with the aromatic benzodithioate end-group (δ = 7.40, 7.55 and 7.90 ppm) clearly shifted to new resonances associated with the aromatic pyridyl group (δ = 7.10, 7.65, 8.45 ppm) (Fig. 1A, S1 & S2†).

Moreover, GPC confirmed that conversion of the end-group to pyridyl disulfide had minimal impact on the molecular weight distribution of the polymer, with a low polydispersity maintained after the reaction (Fig. 1B, Table S1†). In the final step, the pyridyl disulfide end-group was converted to an acyl

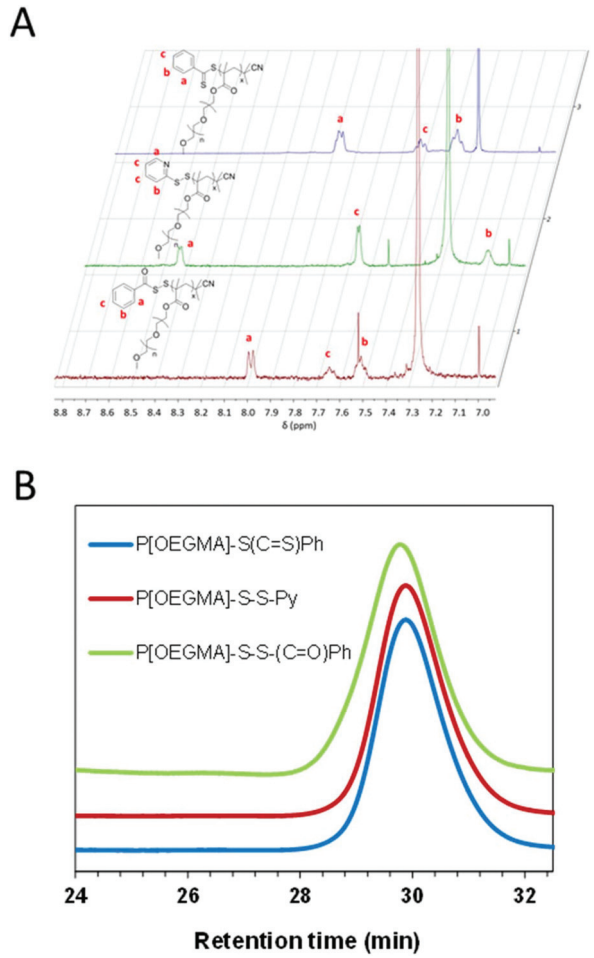

Fig. 1 (A) ^{1}H NMR spectra ($CDCl_3$, 400 MHz, δ 8.5–7.0 ppm) for (top) P[OEGMA]-S(C═S)Ph **1a**; (middle) P[OEGMA]-S-S-Py **1b**; and (bottom) P[OEGMA]-S-S-(C═O)Ph **1c** (B) GPC chromatograms for P[OEGMA]-S(C═S)Ph (**1a**, blue), P[OEGMA]-S-S-Py (**1b**, red) and P[OEGMA]-S-S-(C═O)Ph (**1c**, green). Refer to Table S1† for M_n values.

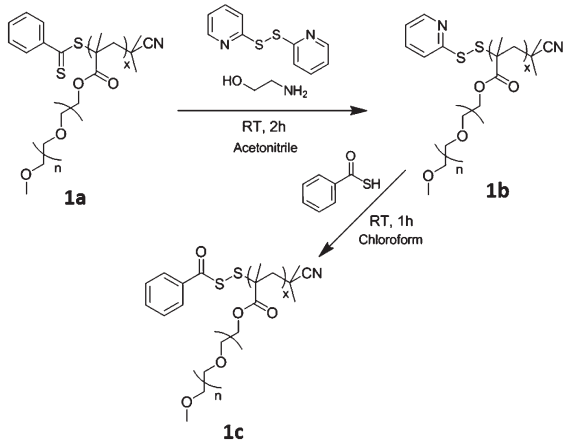

Scheme 1 Homopolymer end-group modification.

(benzoyl)-protected perthiol moiety, P[OEGMA]-S-S-(C═O)Ph, **1c** (Chart S1,† Scheme 1). Specifically, P[OEGMA]-S-S-Py was dissolved in chloroform and then reacted with 1.5 equivalents of thiobenzoic acid for 1 h. The resulting product was then purified by dialysis. The resulting acyl-protected perthiol terminated polymer (P[OEGMA]-S-S-(C═O)Ph) was characterized using GPC and ^{1}H NMR (Table S1,† Fig. 1A, B & S3†). Importantly, the thiol–disulfide exchange reaction led to minimal polymer coupling, as confirmed by maintenance of a low polydispersity index (1.15) as determined by GPC. Further, complete disappearance of the aromatic proton signals associated with the pyridyl group at δ = 7.10, 7.65, 8.45 ppm, together with the emergence of new resonance signals associated with the aromatic protons of the protecting benzoyl group (δ 7.5, 7.65, 8.0 ppm) (Fig. 1A, S2 & S3†) indicated successful conversion to the benzoyl protected perthiol. Importantly, the observed resonances are consistent with those observed in the corresponding small molecules.[16]

The POEGMA with benzoyl-protected perthiol end-groups was then examined for its ability to release H_2S upon exposure to a model thiol (L-cysteine). The putative donor (P[OEGMA]-S-S-(C═O)Ph) and the thiol-reactive intermediate (P[OEGMA]-S-S-Py) were each dissolved in phosphate buffered saline (PBS) solution at pH 7.4 with the chemoselective H_2S-responsive fluorescent probe SF4, which emits green fluorescence (λ = 520 nm) in the presence of H_2S.[29] In order to confirm that the probe could effectively detect H_2S under the particular conditions employed, a model test was conducted using the common inorganic donor, sodium sulfide (Na_2S). Exposure to Na_2S resulted in an immediate increase in fluorescent signal (λ = 520 nm) when the SF4 probe and Na_2S were incubated together (Fig. 2), confirming that the probe was suitable for detection of H_2S under the conditions employed. Subsequently, pyridyl terminated polymer (P[OEGMA]-S-S-Py) was tested with the SF4 probe in the presence and absence of L-cysteine. While this polymer might be expected to react with a thiol such as L-cysteine, the reaction would not be anticipated to liberate H_2S as no perthiol intermediate would be formed by the reaction. Indeed, this was the case: no fluorescence was observed when P[OEGMA]-S-S-Py was treated with L-cysteine, indicating that P[OEGMA]-S-S-Py did not function as an H_2S donor (Fig. 2). Identical experiments were then conducted using P[OEGMA]-S-S-(C═O)Ph. No H_2S release was observed in the absence of L-cysteine (Fig. 2) indicating that the donors do not release H_2S until they encounter the trigger molecule. However, treatment with L-cysteine stimulated immediate H_2S release from the P[OEGMA]-S-S-(C═O)Ph as indicated by the strong emission at 520 nm. These results clearly indicate that incorporating a benzoyl protected perthiol into the end-group of a polymer is an effective strategy for preparing H_2S releasing materials. We propose that these acyl-protected perthiol donors release H_2S by a comparable mechanism to the corresponding small molecule donors (Scheme 2).[16] In support of this mechanism, we observe some broadening of the MWD upon release of H_2S (Fig. S17†), consistent with the formation of coupled product through reaction of generated polymeric thiol with the protected perthiol. Moreover, release of H_2S also leads to the formation of a small amount of polymeric acyl capped thiol (*i.e.* thioester), as reflected in the ^{1}H NMR spectrum, Fig. S18.†

Additionally, real-time H_2S release from P[OEGMA]-S-S-(C═O)Ph was followed using an H_2S-selective amperometric microsensor, the working concept for which has been previously published by Jeroschewski *et al.*[30] H_2S release (μM) was measured over time for a solution of P[OEGMA]-S-S-(C═O)Ph in PBS at pH 7.4 (Fig. 3A). As expected, no response was detected in the absence of L-cysteine (*i.e.*, over the first 25 min). This is consistent with the data obtained using SF4, which indicates that the donors do not release H_2S in the absence of thiol. However, once L-cysteine was added to the solution of P[OEGMA]-S-S-(C═O)Ph, immediate evolution of H_2S was observed (Fig. 3A, with release characteristics tabulated in row 1, Table S2†). Altogether, these results confirmed the capacity of polymers with benzoyl-protected perthiol termini to function as macromolecular H_2S donors when triggered by a thiol-containing compound such as L-cysteine.

Having confirmed thiol-triggered H_2S release from the homopolymer P[OEGMA]-S-S-(C═O)Ph, **1c**, we extended this concept by synthesizing two more sophisticated structures, namely, block copolymers with protected perthiol termini: P[OEGMA-*block*-*n*-butyl methacrylate], P[OEGMA-*block*-BMA]-S-S-(C═O)Ph, and a pH-responsive block copolymer, P[OEGMA-*co*-*N*,*N*-(dimethylamino) ethyl methacrylate-*block*-*N*,*N*-(diiso-

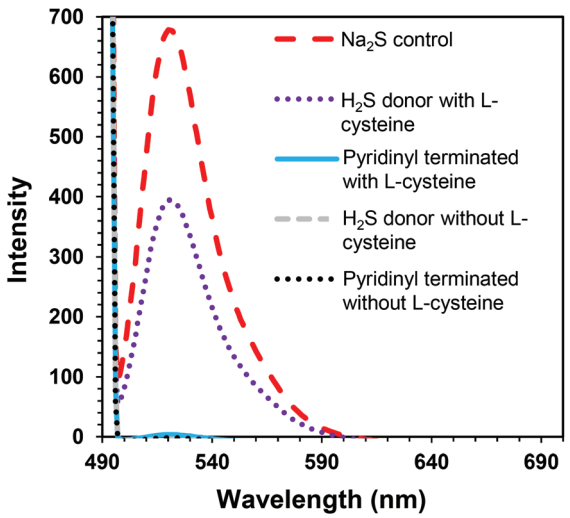

Fig. 2 Fluorescence spectra of fluorescent probe for H_2S detection SF4 (λ_{ex} = 488 nm; λ_{em} = 490–700 nm) with Na_2S, P[OEGMA]-S-S-Py **1b** (pyridinyl terminated) with/without L-cysteine and P[OEGMA]-S-S-(C═O)Ph **1c** (H_2S donor) with/without L-cysteine. [H_2S donor] = 0.460 mM; [pyridyl terminated] = 0.460 mM; [SF4] = 0.084 mM; [L-cysteine] = 0.825 mM; [Na_2S] = 0.063 mM.

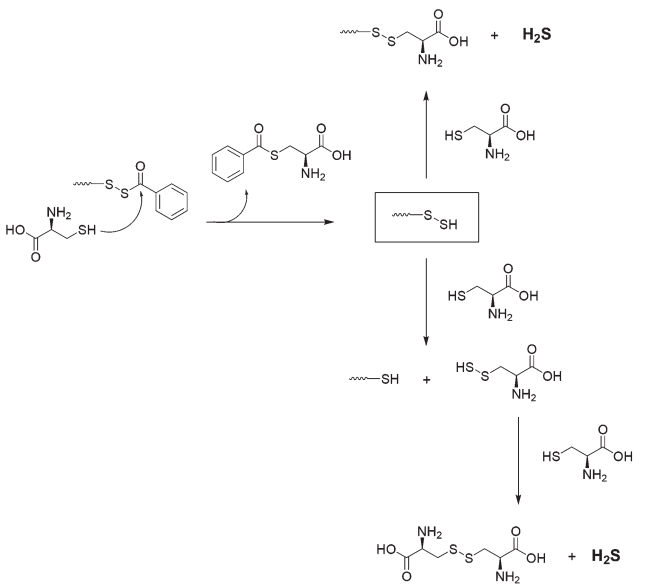

Scheme 2 Proposed mechanism of H_2S release from polymers with acyl-protected perthiol termini.

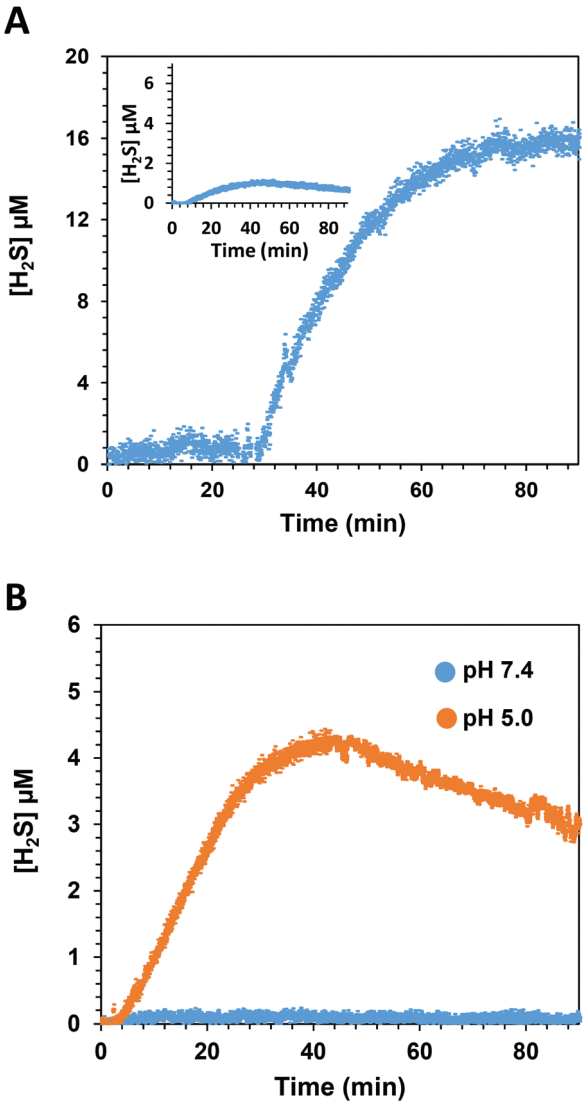

Fig. 3 (A) Electrochemical H_2S release response from P[OEGMA]-S-S-(C═O)Ph **1c** (5 mg, 0.71 μmoles, 143 μM) in the presence of L-cysteine (4.65 molar equiv., 3.3 μmoles, 660 μM) in PBS at pH 7.4 (5 mL). Note: L-Cysteine was added at t = 25 min. Inset shows electrochemical H_2S release from P[OEGMA-*block*-BMA]-S-S-(C═O)Ph **2c** (7 mg, 0.71 μmoles, 143 μM) in PBS at pH 7.4 (5 mL) in the presence of L-cysteine (33 mM, 100 μL, 3.3 μmoles, 660 μM). Note: L-Cysteine was added at t = 2 min. (B) Electrochemical H_2S release response from P[OEGMA-*co*-DMAEMA-*block*-DIPMA]-S-S-(C═O)Ph **3c** (15.8 mg, 0.71 μmoles, 143 μM) in PBS at pH 7.4 and pH 5.0 solution in the presence of L-cysteine (33 mM, 100 μL, 3.3 μmoles, 660 μM). Note: L-Cysteine was added at t = 2 min.

propylamino)ethyl methacrylate], P[OEGMA-*co*-DMAEMA-*block*-DIPMA]-S-S-(C═O)Ph (**2c** and **3c** respectively in Chart S1†). The same end-group post-modification procedure was employed to prepare the H_2S donating block copolymers as was used for the homopolymer, as described in the ESI.† We envisaged that, based on the different structures of these amphiphiles, it would be possible to prepare micelles with different H_2S release capability.

The block polymer, P[OEGMA-*block*-BMA]-S-S-(C═O)Ph, **2c**, could subsequently be dispersed in phosphate buffered saline (pH 7.4), enabling the formation of micelles. Characterization by dynamic light scattering (DLS) revealed a number average hydrodynamic particle diameter of 9.1 nm, with a polydispersity of 0.17 (Fig. S9†). P[OEGMA-*co*-DMAEMA-*block*-DIPMA]-S-S-(C═O)Ph **3c** incorporates ionizable tertiary amine groups which are known to be hydrophobic units in pH 7.4 buffer, thus imparting pH sensitivity to the block copolymer system.[31] As such, the pH responsive block polymer was able to form micelles with a low polydispersity of 0.03 (Fig. S15,† D = 22 nm) when dispersed in phosphate buffered saline pH 7.4, despite that some broadening of its GPC molecular weight distribution occurred during polymer modification steps (Fig. S14†).

We then examined whether these block copolymer nanoassemblies could be employed to modulate the release of H_2S under various conditions. Upon treatment with L-cysteine, the generated H_2S flux from the P[OEGMA-*block*-BMA]-S-S-(C═O)Ph micelles was found to be much lower than that from P[OEGMA]-S-S-(C═O)Ph homopolymer (peaking H_2S concentration 17 times less, Table S2,† Fig. 3A). This provides evidence that the H_2S donor end-group was substantially shielded in the core of the micelle, therefore reducing accessibility of the release trigger (L-cysteine) to the H_2S donor moiety. As shown in Fig. 3B, in case of P[OEGMA-*co*-DMAEMA-*block*-DIPMA]-S-S-(C═O)Ph, the flux generated was dependent on the pH of PBS. The self-assembly profile *vs.* pH, as monitored using DLS, is displayed as Fig. S19 in the ESI.† At pH 7.4, deprotonation increases the hydrophobicity of the DIPMA moieties, which leads to the formation of P[OEGMA-*co*-DMAEMA-*block*-DIPMA]-S-S-(C═O)Ph micelles. As a result, there is negligible H_2S release when L-cysteine is introduced under these conditions (similarly to the non-pH responsive P[OEGMA-*block*-BMA]-S-S-(C═O)Ph micelles). In contrast, exposing P[OEGMA-*co*-DMAEMA-*block*-DIPMA]-S-S-(C═O)Ph to L-cysteine at pH 5.0 led to a more significant thiol-triggered release which was sustained over the ensuing 90 min. In order to make relative assessments of H_2S donation from P[OEGMA-*co*-DMAEMA-*block*-DIPMA]-S-S-(C═O)Ph at different pH conditions, the total concentration of dissolved sulfide species was calculated from $[\text{sulfides}]_{\text{total}} = [H_2S] \times (10^{\text{pH}-\text{p}K1} + 1)$ in different pH solutions, as summarized in the ESI (C.6 and Table S2†). The total sulfide concentration, $[\text{sulfides}]_{\text{total}}$, generated in PBS at pH 5 was 7.5 times higher than pH 7.4 solution. This is due to protonation of the tertiary amine groups facilitating micelle disassembly: the block copolymer is essentially hydrophilic under these conditions, thus increasing accessibility of the thiol to H_2S donor moiety. However, we believe that the reason that the disassembled polymer does not achieve the same levels of H_2S release compared to the hydrophilic P[OEGMA]-S-S-(C═O)Ph homopolymer (Fig. 3A) is due to higher molecular weight dithiol coupled products which were formed during the synthesis of the pH-responsive polymer (obvious in the GPC trace, Fig. S14†). Overall, these results indicate that it is possible to modulate the release of

H_2S using pH-responsive building blocks by variation of the local environment. Such an approach could be used to deliver H_2S more specifically to subcellular compartments such as the endosome.

Finally, we tested the suitability of the materials synthesized to deliver H_2S in a cellular environment without the addition of exogenous thiol. To this end, we applied (i) a polymer with the acyl protected perthiol end-group (P[OEGMA-*co*-DMAEMA-*block*-DIPMA]-S-S-(C═O)Ph, **3c**) and (ii) a control polymer with no acyl protected perthiol end-group, essentially removed by pre-exposure of L-cysteine to **1c** to HEK cells (Thermo Fisher Scientific, Scoresby, Victoria, Australia). As described further in the ESI,† the latter forms a mixture of P[OEGMA]-S(C═O)Ph, P[OEGMA]-S-S-$C_3H_7NO_2$ and P[OEGMA]-S-S-P[OEGMA] (Scheme S1, Fig. S17 & S18†). The fluorescent H_2S-selective chemosensor SF4 was employed to detect the evolution of H_2S in the cells. From Fig. 4 it is clear that application of the H_2S donor leads to increased SF4 fluorescence, corresponding to H_2S evolution in the cells, even without the administration of exogenous thiol. In cells treated with control polymer, some background SF4 fluorescence was still detected, though much less, which we believe could be due to the endogenous H_2S production. As such, the donor reported herein is clearly capable of releasing H_2S to live cells upon exposure to thiol even at intracellular levels.

In conclusion, we report a high-yielding, straightforward approach for incorporating H_2S donors into polymer end-groups by the modification of thiocarbonylthio chain termini. The polymers formed are able to release H_2S upon exposure to thiols such as L-cysteine. The modification is applicable to both homopolymers and block copolymers, the latter enabling the formation of H_2S releasing micelles with a substantially slower release profile. Moreover, pH-responsive block copolymers enable the preparation of novel, intelligent particles capable of delivering H_2S when triggered by both the presence of thiol and by subtle changes in environmental pH. These materials maybe useful research tools for interrogating the delivery of H_2S with subcellular precision.

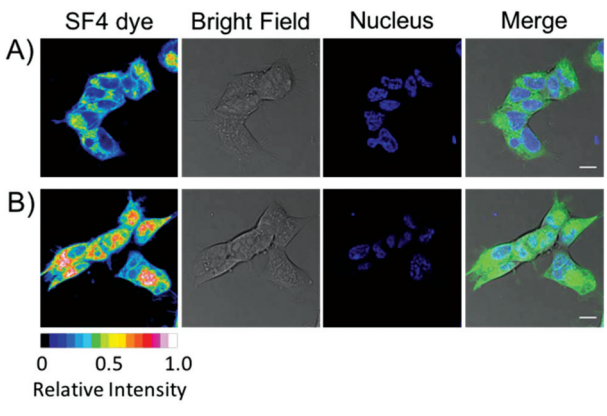

Fig. 4 Confocal microscopy images of HEK cells treated with (A) control polymer (mixture of P[OEGMA]-S(C═O)Ph, P[OEGMA]-S-S-$C_3H_7NO_2$ and P[OEGMA]-S-S-P[OEGMA]) (100 nM, 0.8 ng mL^{-1}); (B) treated with H_2S donor pH-responsive block copolymer **3c** P[OEGMA-*co*-DMAEMA-*block*-DIPMA]-S-S-(C═O)Ph (100 nM, 2.2 ng mL^{-1}), using H_2S fluorescent probe SF4. SF4 dye represented with 16-colour scale to indicate relative dye intensity. Scale bar, 10 μm.

Conflicts of interest

There are no conflicts to declare.

Acknowledgements

This work was carried out within the Australian Research Council (ARC) Centre of Excellence in Convergent Bio-Nano Science and Technology (CE140100036). T. P. D. is grateful for the award of an Australian Laureate Fellowship from the ARC. T. P. D., M. R. W. and J. F. Q. acknowledge financial support from the Faculty of Pharmacy and Pharmaceutical Sciences, Monash University and from the Monash-Warwick Alliance.

Notes and references

1 R. Wang, *Trends Biochem. Sci.*, 2014, **39**, 232.
2 R. Wang, *Sci. Am.*, 2010, **302**, 66.
3 L. Li and P. K. Moore, *Trends Pharmacol. Sci.*, 2008, **29**, 84.
4 L. R. Schicho, D. Krueger, F. Zeller, C. W. H. von Weyhern, T. Frieling, H. Kimura, I. Ishii, R. de Giorgio, B. Campi and M. Schemann, *Gastroenterology*, 2006, **131**, 1542–1552.
5 Y. Cheng, J. F. Ndisang, G. Tang, K. Cao and R. Wang, *Am. J. Physiol.: Heart Circ. Physiol.*, 2004, **287**, H2316–H2323.
6 M. Xia, L. Chen, R. W. Muh, P. L. Li and N. Li, *J. Pharmacol. Exp. Ther.*, 2009, **329**, 1056–1062.
7 R. Yang, C. Qu, Y. Zhou, J. E. Konkel, S. Shi, Y. Liu, C. Chen, S. Liu, D. Liu, Y. Chen, E. Zandi, W. Chen, Y. Zhou and S. Shi, *Immunity*, 2015, **43**, 251–263.
8 L. F. Hu, M. Lu, P. T. H. Wong and J. S. Bian, *Antioxid. Redox Signaling*, 2011, **15**, 405–419.
9 L. Li, M. Whiteman, Y. Guan, K. L. Neo, Y. Cheng, S. W. Lee, Y. Zhao, R. Baskar, C. H. Tan and P. K. Moore, *Circulation*, 2008, **117**, 2351.
10 X. Gu and Y. Z. Zhu, *Expert Rev. Clin. Pharmacol.*, 2011, **4**, 123.
11 J. C. Foster and J. B. Matson, *Org. Lett.*, 2014, **47**, 5089.
12 Y. Zhao, H. Wang and M. Xian, *J. Am. Chem. Soc.*, 2011, **133**, 15.
13 T. Roger, F. Raynaud, F. Bouillaud, C. Ransy, S. Simonet, C. Crespo, M.-P. Bourguignon, N. Villeneuve, J. P. Vilaine, I. Artaud and E. Galardon, *ChemBioChem*, 2013, **14**, 2268.
14 J. L. Wallace, G. Caliendo, V. Santagada, G. Cirino and S. Fiorucci, *Gastroenterology*, 2007, **132**, 261–271.
15 J. Kang, Z. Li, C. L. Organ, C. M. Park, C. T. Yang, A. Pacheco, D. Wang, D. J. Lefer and M. Xian, *J. Am. Chem. Soc.*, 2016, **138**, 6336–6339.

16 Y. Zhao, S. Bhushan, C. T. Yang, H. Otsuka, J. D. Stein, A. Pacheco, B. Peng, N. O. Devarie-Baez, H. C. Aguilar, D. J. Lefer and M. Xian, *ACS Chem. Biol.*, 2013, **8**, 1283–1290.
17 U. Hasegawa and A. J. van der Vlies, *Bioconjugate Chem.*, 2014, **25**, 1290–1300.
18 J. C. Foster and J. B. Matson, *Macromolecules*, 2014, **47**, 5089–5095.
19 F. Ercole, F. M. Mansfeld, M. Kavallaris, M. R. Whittaker, J. F. Quinn, M. L. Halls and T. P. Davis, *Biomacromolecules*, 2016, **17**, 371.
20 S. Perrier and P. Takolpuckdee, *J. Polym. Sci., Part A: Polym. Chem.*, 2005, **43**, 5347.
21 H. Willcock and R. K. O'Reilly, *Polym. Chem.*, 2010, **2**, 149.
22 S. Sinnwell, A. J. Inglis, T. P. Davis, M. H. Stenzel and C. Barner-Kowollik, *Chem. Commun.*, 2008, 2052.
23 P. J. Roth, C. Boyer, A. B. Lowe and T. P. Davis, *Macromol. Rapid Commun.*, 2011, **32**, 1123.
24 C. Boyer, J. Q. Liu, V. Bulmus and T. P. Davis, *Aust. J. Chem.*, 2009, **62**, 830.
25 C. Boyer and T. P. Davis, *Chem. Commun.*, 2011, **47**, 6029.
26 D. Quemener, T. P. Davis, C. Barner-Kowollik and M. H. Stenzel, *Chem. Commun.*, 2006, 5051.
27 S. H. Yu, J. Hu, F. Ercole, N. P. Truong, T. P. Davis, M. R. Whittaker and J. F. Quinn, *ACS Macro Lett.*, 2015, **4**, 1278.
28 P. G. Wang, M. Xian, X. P. Tang, X. J. Wu, Z. Wen, T. W. Cai and A. J. Janczuk, *Chem. Rev.*, 2002, **102**, 1091.
29 V. S. Lin, A. R. Lippert and C. J. Chang, *Proc. Natl. Acad. Sci. U. S. A.*, 2013, **110**, 7131.
30 P. Jeroschewski, C. Steuckart and M. Kuhl, *Anal. Chem.*, 1996, **68**, 4351.
31 K. Zhou, Y. Wang, X. Huang, K. Luby-Phelps, B. D. Sumer and J. Gao, *Angew. Chem., Int. Ed.*, 2011, **50**, 6109.

Supporting Information

Polymers with acyl-protected perthiol chain termini as convenient building blocks for doubly responsive H_2S-donating nanoparticles

Sul Hwa Yu,[†] *Francesca Ercole,*[†] *Nicholas Veldhuis,*[†] *Thomas P. Davis,*[†‡*] *Michael R. Whittaker*[†*] *and John F. Quinn*[†*]

[†] *ARC Centre of Excellence in Convergent Bio-Nano Science and Technology, Monash Institute of Pharmaceutical Sciences, Monash University, Parkville, VIC 3052, Australia;*

[‡] *Chemistry Department, University of Warwick, Coventry, ULCV4 7AL, UK*

Synthesis and Characterization Methods

A. Materials

Oligo(ethylene glycol) methyl ether methacrylate (OEGMA) with M_n = 500 g mol^{-1} (denoted as $OEGMA_{500}$ where relevant) was purchased from Sigma-Aldrich and deinhibited by percolating over a column of basic alumina. 2-(dimethylamino)ethyl methacrylate (DMAEMA), butyl methacrylate (BMA) 2-(diisopropylamino)ethyl methacrylate (DIPMA) were purchased from Sigma-Aldrich and passed through a column of basic alumina in order to remove inhibitor prior to polymerization. Azobisisobutyronitrile (AIBN) was purified by recrystallization from methanol before use. 2-cyanoprop-2-yl benzodithioate (CPBD), ethanolamine, L-cysteine and dipyridyl disulfide (aldrithiol^{TM}-2) were purchased from Sigma-Aldrich at the highest purity available and used as received. Thiobenzoic acid (94%) was purchased from Alfa Aesar and used as received. Petroleum ether (b.p. 40 - 60 °C), diethyl ether, toluene, acetonitrile, chloroform and dioxane were purchased from Merck Millipore and used as received.

B. Synthetic Methods

B.1 Synthesis of P[OEGMA]-S(C=S)Ph, ***1a***

The synthesis of P[OEGMA]-S(C=S)Ph was carried out using the following stoichiometry: $[CPBD]_0$:$[OEGMA_{500}]_0$:$[AIBN]_0$=1:14.5:0.1. Briefly, $OEGMA_{500}$ (2.00 g, 4.01 × 10^{-3} mol), CPBD RAFT agent (6.14× 10^{-2} g, 2.77 × 10^{-4} mol), AIBN (0.45 × 10^{-2} g, 2.74 × 10^{-5} mol) and toluene (3 mL) were placed in a glass vial equipped with a magnetic stirrer bar and capped with a rubber septum. The reaction mixture was deoxygenated for 25 min at 0 °C by sparging with N_2. The deoxygenated and sealed reaction vessel was placed into a pre-heated oil bath at 70 °C and the polymerization was run with stirring for 4 h. The resulting mixture was then allowed to cool to 0 °C for about 15 min to halt polymerization. The monomer conversion was determined by ^{1}H NMR. The polymer was purified of unreacted monomer by first precipitating into a 50/50 (v/v) mixture of diethyl ether and petroleum ether (bp 40-60 °C), followed by two subsequent precipitations into petroleum ether (bp 40-60 °C). The product was then placed in a vacuum oven overnight to remove remaining solvent. The final product was analysed by ^{1}H NMR and GPC. The molecular weight and average monomer chain length calculated from ^{1}H NMR were determined to be 6813 g mol^{-1} and 13 units, respectively. The polydispersity index (determined by GPC) was 1.13.

B.2 Synthesis of P[OEGMA-block-BMA]-S(C=S)Ph, ***2a***

The synthesis of P[OEGMA-*block*-BMA]-S(C=S)Ph was carried out using the following stoichiometry: $[P[OEGMA]\text{-}S(C=S)Ph]_0:[BMA]_0:[AIBN]_0=1:50:0.13$. P[OEGMA]-S(C=S)Ph (0.104 g, 1.49×10^{-5} mol), BMA (0.10 g, 7.14×10^{-4} mol), and AIBN (0.32×10^{-3} g, 1.92×10^{-6} mol) were added to a glass vial equipped with a magnetic stirrer bar and capped with a rubber septum. The reaction mixture was deoxygenated for 30 min by sparging with N_2. The deoxygenated and sealed reaction vessel was placed into a pre-heated oil bath at 70 °C and the polymerisation was run with stirring for 4 h. The resulting mixture was then allowed to cool to 0 °C for about 15 min to halt polymerisation. The monomer conversion was determined by ^{1}H NMR. The polymer was purified via three precipitation and centrifugation steps (using a 50/50 (v/v) mixture of petroleum ether (bp 40-60 °C) and diethyl ether as the precipitant) to remove any traces of unreacted monomer. The product was then placed in a vacuum oven overnight to remove remaining solvent. The final product was analysed by ^{1}H NMR and GPC. The molecular weight and average monomer chain length calculated from ^{1}H NMR were determined to be 9710 g mol^{-1} and 19 units, respectively. The polydispersity index determined by GPC was 1.11.

B.3 Synthesis of P[OEGMA-co-DMAEMA]-S(C=S)Ph (Precursor for block polymer)

P[OEGMA-*co*-DMAEMA]-S(C=S)Ph was synthesized according to a previously reported procedure[1]. The stoichiometry was $[CPADB]_0:[OEGMA_{500}]_0:[DMAEMA]_0:[AIBN]_0$ = 1:50:6:0.08. Briefly, $OEGMA_{500}$ (10.0 g, 2×10^{-2} mol), DMAEMA (0.38 g, 2.40×10^{-3} mol), CPADB RAFT agent (0.09 g, 4.00×10^{-4} mol), AIBN (0.52×10^{-2} g, 3.20×10^{-5} mol) and toluene (20 mL) were placed in a glass vial equipped with a magnetic stirrer bar and capped with a rubber septum. The reaction mixture was deoxygenated for 1 h by sparging with N_2. The deoxygenated and sealed reaction vessel was placed into a pre-heated oil bath at 70 °C and the polymerisation was run with stirring for 6.15 h. The resulting mixture was then allowed to cool to 0 °C for about 15 min to halt polymerisation. The monomer conversion was determined by ^{1}H NMR. The polymer was purified via three precipitation and centrifugation steps (using a 50/50 (v/v) mixture of petroleum ether (bp 40-60 °C) and diethyl ether as the precipitant) to remove any traces of unreacted monomer. The product was then placed in a vacuum oven overnight to remove any remaining solvent. The final product was analysed by ^{1}H NMR and GPC. The molecular weight and average monomer chain lengths calculated from ^{1}H NMR

were determined to be 14,200 g mol^{-1}, and 27 units of OEGMA and 3 units of DMAEMA, respectively. The polydispersity index determined by GPC was 1.12.

B.4 Synthesis of P[OEGMA-co-DMAEMA-block-DIPMA]-S(C=S)Ph, ***3a***

The synthesis of P[OEGMA-*co*-DMAEMA-*block*-DIPMA]-S(C=S)Ph was conducted according to a previously reported procedure[1]. The stoichiometry was [P[OEGMA-*co*-DMAEMA]-S(C=S)Ph]$_0$:[DIPMA]$_0$:[AIBN]$_0$=1:100:0.08. P[OEGMA-*co*-DMAEMA]-S(C=S)Ph (1.31 g, 9.38×10^{-5} mol), DIPMA (2.00 g, 9.38×10^{-3} mol), and AIBN (0.12×10^{-2} g, 7.50×10^{-6} mol) were added to a glass vial equipped with a magnetic stirrer bar and capped with a rubber septum. The reaction mixture was deoxygenated by sparging with nitrogen for 1 h. The deoxygenated solution was placed into a pre-heated oil bath at 70 °C and the polymerisation was allowed to proceed with stirring for 12 h. The polymerisation was stopped by placing the sample in an ice bath for 15 min. The product was recovered by dialysis with acetone. The purified block polymer was then dried in vacuo. P[OEGMA-*co*-DMAEMA-*block*-DIPMA]-S(C=S)Ph was analysed by ^{1}H NMR and GPC.

B.5 Modification of the thiocarbonylthio end group from P[OEGMA]-S(C=S)Ph to form P[OEGMA]-S-S-Py, ***1b***

A mixture of P[OEGMA]-S(C=S)Ph (0.10 g, 1.43×10^{-5} mol) and aldrithiol^{TM}-2 (0.03 g, 1.43×10^{-4} mol) in acetonitrile (1 mL) was deoxygenated with nitrogen for 15 min. A solution of ethanolamine (35 μL, 5.71×10^{-4} mol) in acetonitrile (965μL) was deoxygenated with nitrogen for 15 min. The solution of ethanolamine in acetonitrile (100 μL) was transferred into the mixture of P[OEGMA]-S(C=S)Ph and aldrithiol^{TM}-2 in acetonitrile. The deoxygenated reaction mixture was then stirred for 2 h at room temperature to convert the P[OEGMA]-S(C=S)Ph to P[OEGMA]-S-S-Py (i.e. convert the dithioester endgroup to pyridyl-2-dithiol endgroup). Dialysis was conducted overnight to ensure removal of the *N*-(2-hydroxyethyl)benzothioamide side product and the excess aldrithiol/ethanolamine. The resulting polymer was dried under air and in vacuo, and then analysed by ^{1}H NMR spectroscopy to confirm the removal of the dithioester end group and the formation of pyridyl-2-dithiol endgroup. Three distinct signals in the ^{1}H NMR spectrum (δ 7.4, 7.55 and 7.9 ppm, corresponding to the aromatic benzodithioate) were lost, while three new peaks appeared (δ 7.1, 7.65, 8.45 ppm, representing the aromatic pyridyl group).

B.6 Modification of the thiocarbonylthio end group from P[OEGMA-block-BMA]-S(C=S)Ph to form P[OEGMA-block-BMA]-S-S-Py, ***2b***

A mixture of P[OEGMA-*block*-BMA]-S(C=S)Ph (0.10 g, 9.63×10^{-6} mol) and aldrithiol^{TM}-2 (0.02 g, 9.62×10^{-5} mol) in acetonitrile (1 mL) was deoxygenated with nitrogen for 15 min. A solution of ethanolamine (233 μL, 3.85×10^{-4} mol) in acetonitrile (9767 μL) was deoxygenated with nitrogen for 15 min. The solution of ethanolamine in acetonitrile (100 μL) was transferred into the mixture of P[OEGMA-*block*-BMA]-S(C=S)Ph and aldrithiol^{TM}-2 in acetonitrile. The deoxygenated reaction mixture was then stirred for 2 h at room temperature to convert the P[OEGMA-*block*-BMA]-S(C=S)Ph to P[OEGMA-*block*-BMA]-S-S-Py (i.e. convert the dithioester endgroup to pyridyl-2-dithiol endgroup). Dialysis was conducted overnight to ensure removal of the *N*-(2-hydroxyethyl)benzothioamide side product and the excess aldrithiol and ethanolamine. The resulting polymer was dried under air and in vacuo, and then analysed by ^{1}H NMR spectroscopy to confirm the removal of the dithioester end group and the formation of pyridyl-2-dithiol endgroup. Three distinct signals in the ^{1}H NMR spectrum (δ 7.35, 7.5 and 7.85 ppm, corresponding to the aromatic benzodithioate) were lost and replaced with three new peaks (δ 7.1, 7.6, 8.45 ppm, corresponding to the aromatic pyridyl group).

B.7 Modification of the thiocarbonylthio end group from P[OEGMA-co-DMAEMA-block-DIPMA]-S(C=S)Ph to form P[OEGMA-co-DMAEMA-block-DIPMA]-S-S-Py, ***3b***

A mixture of P[OEGMA-*co*-DMAEMA-*block*-DIPMA]-S(C=S)Ph (1.00 g, 4.51×10^{-5} mol) and aldrithiol^{TM}-2 (0.10 g, 4.51×10^{-4} mol) in acetonitrile (1 mL) was deoxygenated with nitrogen for 15 min. A solution of ethanolamine (110 μL, 1.80×10^{-3} mol) in acetonitrile (890 μL) was deoxygenated with nitrogen for 15 min. The solution of ethanolamine in acetonitrile (100 μL) was transferred into the mixture of P[OEGMA-*co*-DMAEMA-*block*-DIPMA]-S(C=S)Ph and aldrithiol^{TM}-2 in acetonitrile. The deoxygenated reaction mixture was then stirred for 2 h at room temperature to convert the P[OEGMA-*co*-DMAEMA-*block*-DIPMA]-S(C=S)Ph to P[OEGMA-*co*-DMAEMA-*block*-DIPMA]-S-S-Py (i.e. convert the dithioester endgroup to pyridyl-2-dithiol endgroup). Dialysis was conducted overnight to ensure removal of the *N*-(2-hydroxyethyl)benzothioamide side product and the excess aldrithiol and ethanolamine. The resulting polymer was dried under air and in vacuo, and then analysed by ^{1}H NMR spectroscopy to confirm the removal of the dithioester end group and the formation of pyridyl-2-dithio endgroup. Three distinct signals in the ^{1}H NMR spectrum (δ 7.3, 7.5 and 7.85

ppm, corresponding to the aromatic benzodithioate) were lost and replaced with new peaks (δ 7.1, 7.55-7.7, 8.45 ppm, corresponding to the aromatic pyridyl group).

B.8 Thiol-disulfide exchange reaction of P[OEGMA]-S-S-Py with thiobenzoic acid to form P[OEGMA]-S-S-(C=O)Ph, ***1c***

P[OEGMA]-S-S-Py prepared as above (B.5) (0.06 g, 8.79×10^{-6} mol) was dissolved in chloroform (900 µL). Thiobenzoic acid (1.94 mg, 1.40×10^{-5} mol) was added into the solution with stirring and allowed to react at room temperature for 1 h to convert the P[OEGMA]-S-S-Py to P[OEGMA]-S-S-(C=O)Ph (i.e., to convert the pyridyl-2-thiol endgroup to the acyl-protected perthiol endgroup). Dialysis was conducted overnight to ensure removal of the 2-mercaptopyridine side product and the excess thiobenzoic acid. The resulting polymer was dried under air and in vacuo, and then analysed by ^{1}H NMR spectroscopy to confirm the removal of the pyridyl-2-thiol endgroup and the formation of the acyl-protected perthiol endgroup. Three distinct signals in the ^{1}H NMR spectrum (δ 7.1, 7.65, 8.45 ppm corresponding to the aromatic pyridyl group) were lost and replaced with new peaks (δ 7.5, 7.65, 8.0 ppm, corresponding to the benzoyl protecting group).

B.9 Thiol-disulfide exchange reactions of P[OEGMA-block-BMA]-S-S-Py with thiobenzoic acid to form P[OEGMA-block-BMA]-S-S-(C=O)Ph, ***2c***

P[OEGMA-*block*-BMA]-S-S-Py prepared as above (B.6) (0.05 g, 5.15×10^{-6} mol) was dissolved in chloroform (1 mL). Thiobenzoic acid (1.14 mg, 8.22×10^{-6} mol) was added into the solution with stirring and allowed to react at room temperature for 1h to convert the P[OEGMA-*block*-BMA]-S-S-Py to P[OEGMA-*block*-BMA]-S-S-(C=O)Ph (i.e. convert pyridyl-2-thiol endgroup to the acyl-protected perthiol endgroup). Dialysis was conducted overnight to ensure removal of the 2-mercaptopyridine side product and the excess thiobenzoic acid. The resulting polymer was dried under air and in vacuo, and then analysed by ^{1}H NMR spectroscopy to confirm the removal of the pyridyl-2-thiol endgroup and the formation of the acyl-protected perthiol endgroup. Three distinct signals in the ^{1}H NMR spectrum (δ 7.1, 7.6, 8.45 ppm, corresponding to the aromatic pyridyl group) were lost and replaced with new peaks (δ 7.5, 7.6, 8.0 ppm, corresponding to the aromatic benzoyl protecting group).

Micelles were formed in pH 7.4 PBS buffer by dissolving 7 mg (0.71 µmoles) of polymer directly into PBS at pH 7.4 (5 mL) and then confirming formation by DLS.

B.10 Thiol-disulfide exchange reactions of P[OEGMA-co-DMAEMA-block-DIPMA]-S-S-Py with thiobenzoic acid to form P[OEGMA-co-DMAEMA-block-DIPMA]-S-S-(C=O)Ph, ***3c***

P[OEGMA-*co*-DMAEMA-*block*-DIPMA]-S-S-Py prepared as above (B.7) (0.46 g, 2.08×10^{-5} mol) was dissolved in chloroform (2 mL). Thiobenzoic acid (4.58 mg, 3.32×10^{-5} mol) was added into the solution with stirring and allowed to react at room temperature for 1h to convert the P[OEGMA-*co*-DMAEMA-*block*-DIPMA]-S-S-Py to P[OEGMA-*co*-DMAEMA-*block*-DIPMA]-S-S-(C=O)Ph (i.e., to convert the pyridyl-2-thiol endgroup to the acyl-protected perthiol endgroup). Dialysis was conducted overnight to ensure removal of the 2-mercaptopyridine side product and the excess thiobenzoic acid. The resulting polymer was dried under air and in vacuo, and then analysed by ^{1}H NMR spectroscopy to confirm the removal of the pyridyl-2-thiol endgroup and the formation of the acyl-protected perthiol endgroup. Three distinct signals in the ^{1}H NMR spectrum (δ 7.1, 7.55-7.7, 8.45 ppm, corresponding to the aromatic pyridyl group) were lost and replaced with new peaks (δ7.4-7.6, 8.0, 8.2 ppm, corresponding to the aromatic benzoyl protecting group). Micelle formation was conducted in pH 7.4 PBS buffer. 25 mg of polymer was dissolved in acetone (0.3 mL) and then added into 5 mL of buffer solution with stirring. Acetone was removed by evaporation with a stream of air. Micelle formation was confirmed by DLS.

B.11 Control polymer (mixture of P[OEGMA]-S(C=O)Ph, P[OEGMA]-S-S-$C_3H_7NO_2$ and P[OEGMA]-S-S-P[OEGMA]) formed via exposure of P[OEGMA]-S-S-(C=O)Ph, ***1c****, to L-cysteine.*

H_2S-donating homopolymer P[OEGMA]-S-S-(C=O)Ph (5 mg, 0.71 µmoles, 143 µM) was dissolved in PBS at pH 7.4 in the presence of L-cysteine (4.65 molar equiv., 3.3 µmoles, 660 µM) over 72 h in an open open vessel. Dialysis was then conducted to ensure removal of the side products and the excess L-cysteine. The resulting polymer was dried under air and in vacuo, and then analysed by ^{1}H NMR spectroscopy to confirm the final products (mixture of P[OEGMA]-S(C=O)Ph, P[OEGMA]-S-S-$C_3H_7NO_2$ and P[OEGMA]-S-S-P[OEGMA]).

C. Analysis Methods

C.1 ^{1}H Nuclear Magnetic Resonance Spectroscopy

^{1}H NMR spectra were recorded at 400 MHz on a Bruker UltraShield 400 MHz spectrometer 7 running Bruker Topspin, version 1.3. Spectra were recorded in $CDCl_3$.

C.2 Gel Permeation Chromatography (GPC)

GPC was performed using a Shimadzu modular system comprised of a SIL-20AD automatic injector, a RID-10A differential refractive-index detector and a 50 × 7.8 mm guard column followed by three KF-805L columns (300 × 8 mm, bead size: 10 μm, pore size maximum: 5000 Å). *N*,*N*-Dimethylacetamide (DMAc, HPLC grade, 0.03% w/v LiBr) at 50 °C was used as the eluent with a flow rate of 1 mL min^{-1} . Samples were filtered through 0.45 μm PTFE filters before injection. The GPC calibration was performed with narrow-polydispersity polystyrene standards ranging from 500 to 2×10^6 g mol^{-1} .

C.3 Dynamic Light Scattering (DLS)

DLS measurements were carried out on a Malvern Zetasizer Nano ZS Series running DTS software (laser, 4 mW, λ = 633 nm; angle 173°). The polydispersity index (PDI), used to describe the average diameters and size distribution of prepared micelles, was determined via a cumulants analysis of the measured intensity autocorrelation function using the DTS software. Samples were filtered using 0.45 μm PTFE syringe filter to remove contaminants / dust prior to measurement.

C.4 Fluorescence spectroscopy

Fluorescence spectra were obtained using a fluorescence spectrophotometer (Shimadzu RF-5301 PC). Slit widths were set at 5 nm for excitation and at 3 or 5 nm for emission, with sensitivity set at low.

C.5 Amperometric H_2S Sensing

The H_2S-generating capability of the polymers was examined using an amperometric H_2S microsensor manufactured by Unisense A/S.

Calibration of the sensor was performed after the sensor signal had stabilized over a prepolarization period (usually 2 hours or more). A 2.0 mM stock solution of Na_2S was prepared anaerobically by dissolving a known quantity of the salt into N_2-flushed, deionized water in a closed container. The acidic calibration buffer prepared by adding aqueous HCl to PBS at pH 7.4, giving a pH value < 4 (normally 3.8). This was deoxygenated for 20 minutes by bubbling with N_2 gas. 20 mL of the acidic buffer was then transferred to a nitrogen-flushed bottle equipped with a stirrer, which was capped with a septum. The sensor was then immersed

into the solution via a specialized opening on the septum which enabled the bottle to be capped after the sensor tip had been passed through. Once the signal stabilized to a low, stable reading, the value was recorded and assumed to correspond to the zero [H_2S] value. Calibration points within the expected range of measurement were collected by injecting known amounts of Na_2S stock solution into the stirred calibration buffer solution using a micro-syringe. The current increased upon addition of the first aliquot and reached a plateau after several seconds. Further calibration values were obtained as subsequent aliquots were added (six in total, ranging from 10 – 160 µL). The recorded data was used to generate a linear calibration plot for [H_2S] vs. current (amps)[2].

L-cysteine mediated H_2S-generating capability of polymers was examined as follows. Polymer (0.71 µmoles) in deoxygenated pH 7.4 PBS (5 mL) and L-cysteine (3.3 µmoles) in deoxygenated PBS at pH 7.4 were prepared separately. The sensor was immersed into the polymer solution, using the septum to minimize exposure to air on immersing the sensor into the solution. 50 µL of L-cysteine solution was then injected slowly into the stirring polymer solution using a micro-syringe. The time of cysteine addition was recorded.

C.6 H_2S kinetics considerations

H_2S is a weak acid, which can be ionized into HS^- and S^{2-}. The ionization equilibrium between H_2S and HS^-/S^{2-} has to be established.[2]

The total concentration of sulfides in solution can be described as $[sulfides]_{tot} = [H_2S] + [HS^-]$. By using the equilibrium constants K_1 and K_2 (K_1= equilibrium constant between H_2S and HS^- , K_2= equilibrium constant between HS^- and S^{2-}), the total concentration of dissolved sulfide species generated in solution was simplified into $[sulfides]_{tot} = [H_2S] \times (10^{pH-pK1} +1)$. The pK_1 value was also affected by temperature measurement[2]: $pK_1 = 32.55 + (1519.44/T) - 15.672\log(T) + 0.02722T$. T is in Kelvin. All amperometric H_2S release measurements were conducted at 25°C (298.15 K).

Measurement in pH 7.4 at 25°C (298.15 K) is calculated from $[sulfides]_{tot} = [H_2S]_{detected} \times 3.40$.
Measurement in pH 5.0 at 25°C (298.15 K) is calculated from $[sulfides]_{tot} = [H_2S]_{detected} \times 1.01$

*C.7 H_2S release test from P[OEGMA]-S-S-(C=O)Ph (**1c**) using SF4 probe*

A stock solution of SF4 was prepared fresh in a 1:1 mixture of DMF and DMSO (6.1 mM). An aliquot (110 µL) was then diluted into water to a final volume of 5 mL and concentration

of 0.134 mM. Separately, 5.0 mg of homopolymer was dissolved into 300 µL of THF and this was mixed with 1 mL of SF4 solution (0.134 mM) and 300 µL of PBS (7.4), the final volume was therefore 1.6 mL. The solution was transferred to a quartz cuvette and the fluorescence measured (λ_{ex} = 488 nm; λ_{em} = 490-700 nm), representing the H_2S donor without added L-cysteine. L-cysteine-mediated H_2S release from the polymers was then was investigated by adding 40 µL of L-cysteine solution (5 mL stock solution with a concentration of 33 mM in degassed PBS at pH 7.4). The solution was left to mix for 2 minutes and then the fluorescence re-measured. Negative controls were also measured using pyridyl terminated polymer (with and without cysteine), in place of the H_2S-donating homopolymer. As a positive control, a sample was measured using Na_2S: A stock solution of Na_2S was initially prepared fresh in degassed PBS 7.4 (10 mM) and then an aliquot (10 µL) of this was mixed with 1 mL of SF4 solution (0.134 mM) and 600 µL of PBS (7.4).

C.8 SF4 detection of H_2S donating polymer (B.10) in human embryonic kidney (HEK) cells.

Human embryonic kidney (HEK293) cells were cultured in DMEM supplemented with 5% heat-inactivated FBS. Cell were plated onto poly-D-lysine (5µg/cm^2) coated 8-well optical µ-slides (Ibidi, Germany) 24 h prior to imaging. On the day of imaging, cells were labelled with 10µM SF4 fluorescent probe and Hoechst nuclear stain 33342 in OptiMem media for 30 min at 37°C.

H_2S donor polymer (acyl protected perthiol end-group (P[OEGMA-*co*-DMAEMA-*block*-DIPMA]-S-S-(C=O)Ph) **3c**) or control polymer (formed by previous exposure of **1c** to L-cysteine to) were diluted to 10µM in OptiMem media and added to cells at a final concentration of 100nM (2.2 ng/ml and 0.8 ng/ml for H_2S donor and control polymer, respectively) for 60 min at 37°C in 5% CO_2. Cells were then transferred to physiological saline (HBSS, pH7.4, supplemented with Mg^{2+} and Ca^{2+}) and imaged on Leica SP8 confocal microscope (humidified, 37°C) with a HCX PL APO 63x (NA 1.40) oil objective (Pinhole 2AU). Images were acquired by sequential excitation with UV (405 diode) and Argon (488 nm) lasers and emission at 450±40m (NucBlue Hoechst stain, blue) and 550±50nm (SF4 dye, green), using identical laser intensity and gain settings.

Chart S1. Various protected perthiol end-group modified polymers synthesized during this study: (**1c**) poly(oligoethylene glycol methyl ether methacrylate)-S-S-(C=O)Ph; (**2c**) poly(oligoethylene glycol methyl ether methacrylate-*block*-butyl methacrylate)-S-S-(C=O)Ph; (**3c**) poly(oligoethylene glycol methyl ether methacrylate-*co*-*N*,*N*-(dimethylamino)ethyl methacrylate-*block*- *N*,*N*-(diisopropylamino)ethyl methacrylate)-S-S-(C=O)Ph.

1c	**2c**	**3c**
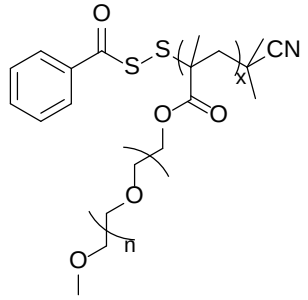	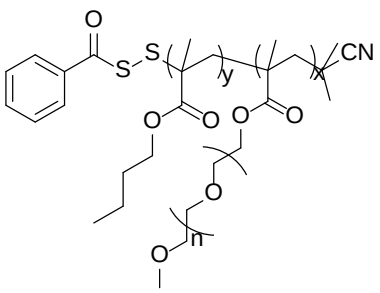	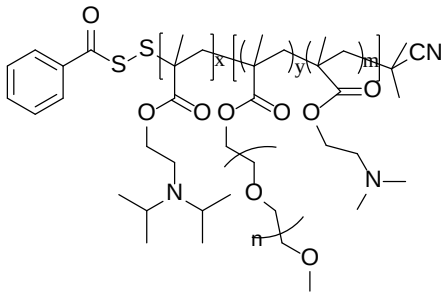

Table S1. Characterisation of polymers synthesized

Polymer	M_n (g mol^{-1})[a]	M_n (g mol^{-1})[b]	PDI
P[OEGMA]-S(C=S)Ph, **1a**	6813	7041	1.13
P[OEGMA]-S-S-Py, **1b**	-	7041	1.13
P[OEGMA]-S-S-(C=O)Ph, **1c**	-	7844	1.15
P[OEGMA-b-BMA]-S(C=S)Ph, **2a**	9710	10672	1.11
P[OEGMA-*b*-BMA]-S-S-Py, **2b**	-	10625	1.12
P[OEGMA-*b*-BMA]-S-S-(C=O)Ph, **2c**	-	11564	1.15
P[OEGMA-co-DMAEMA-b-DIPMA]-S(C=S)Ph, **3a**	22200	21280	1.24
P[OEGMA-*co*-DMAEMA-*b*-DIPMA]-S-S-Py, **3b**	-	22803	1.22
P[OEGMA-*co*-DMAEMA-*b*-DIPMA]-S-S-(C=O)Ph, **3c**	-	25847	1.30

[a] Molecular weight determined by ^{1}H NMR spectroscopy.

[b] Molecular weight determined by gel permeation chromatography.

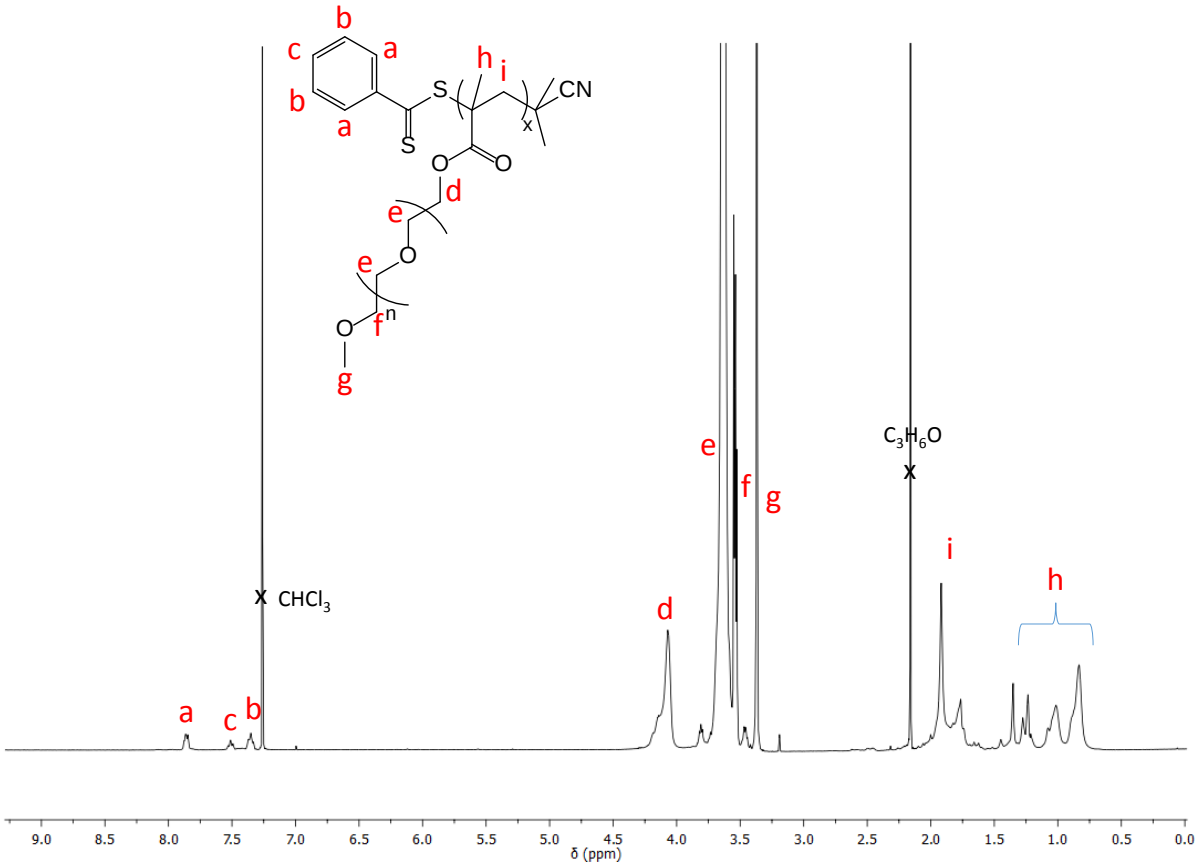

Figure S1. ^{1}H NMR spectrum of P[OEGMA]-S(C=S)Ph (Table S1, **1a**), recorded in $CDCl_3$ (400 MHz).

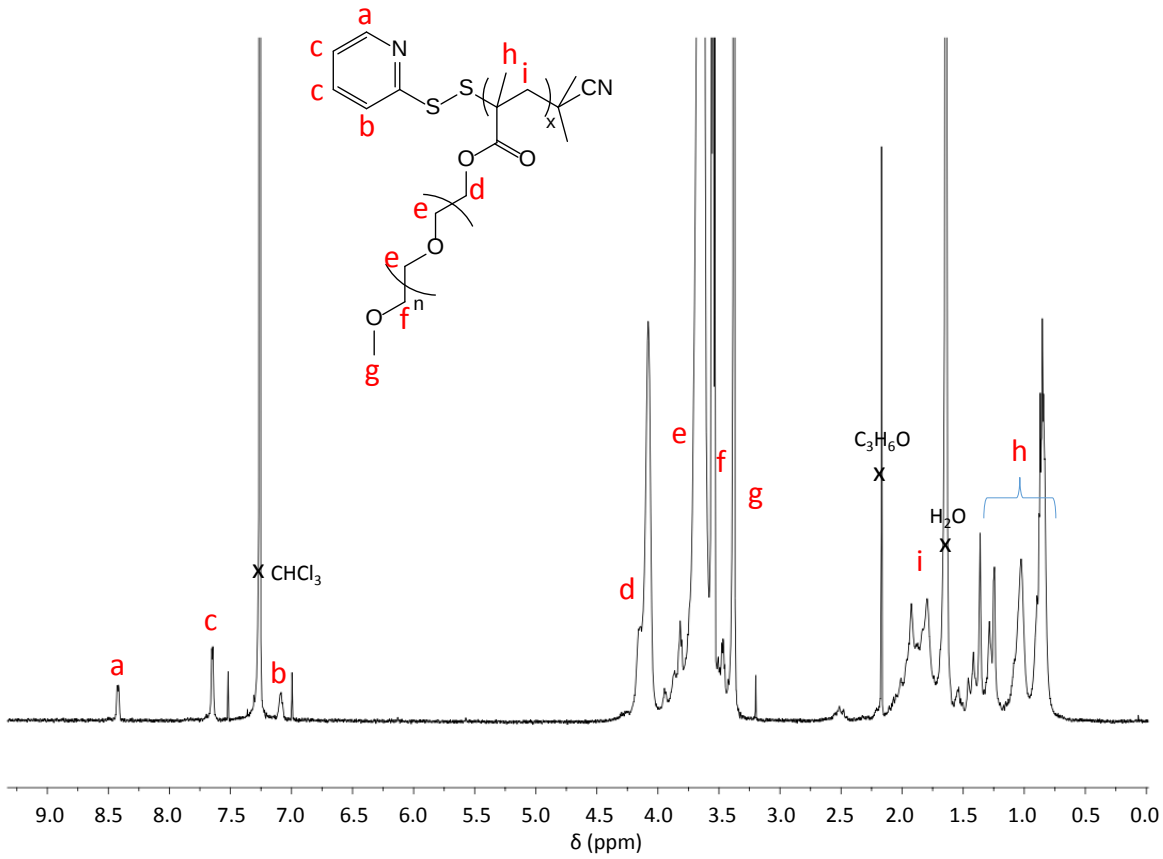

Figure S2. ^{1}H NMR spectrum of P[OEGMA]-S-S-Py (Table S1, **1b**), recorded in $CDCl_3$ (400 MHz).

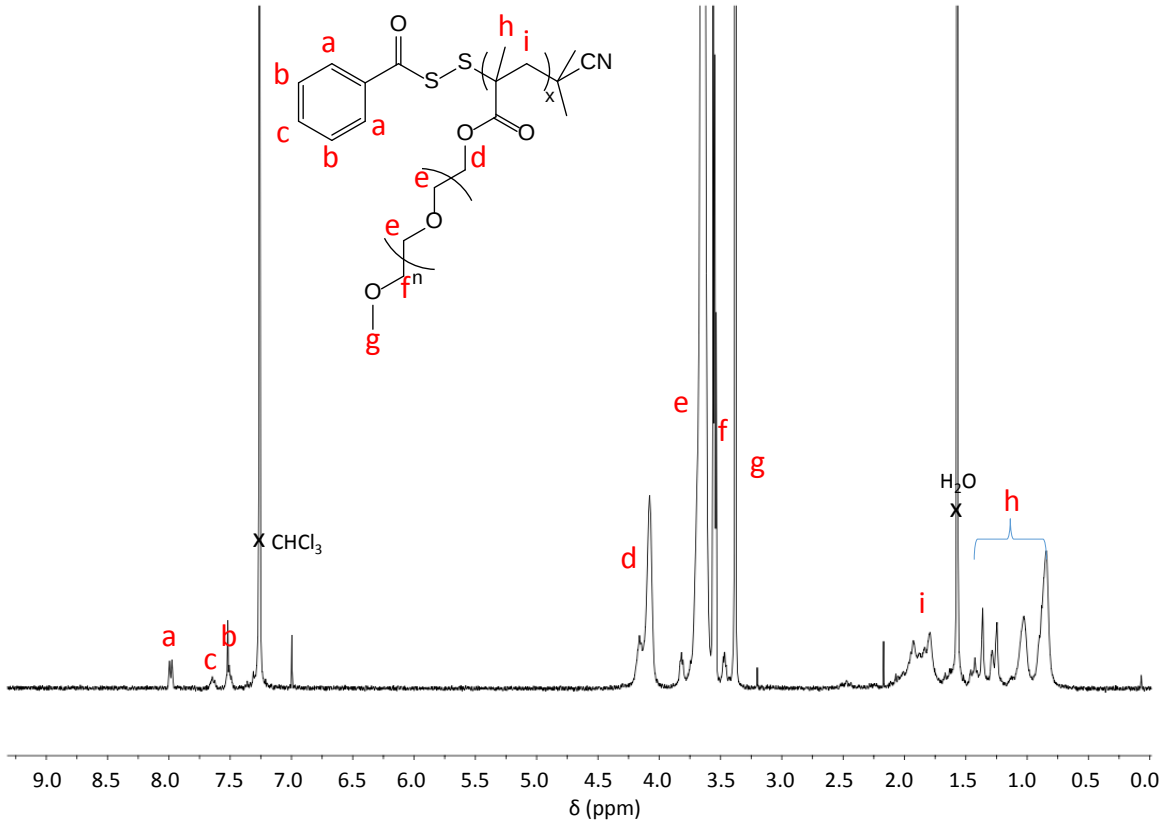

Figure S3. ^{1}H NMR spectrum of P[OEGMA]-S-S-(C=O)Ph (Table S1, **1c**), recorded in $CDCl_3$ (400 MHz).

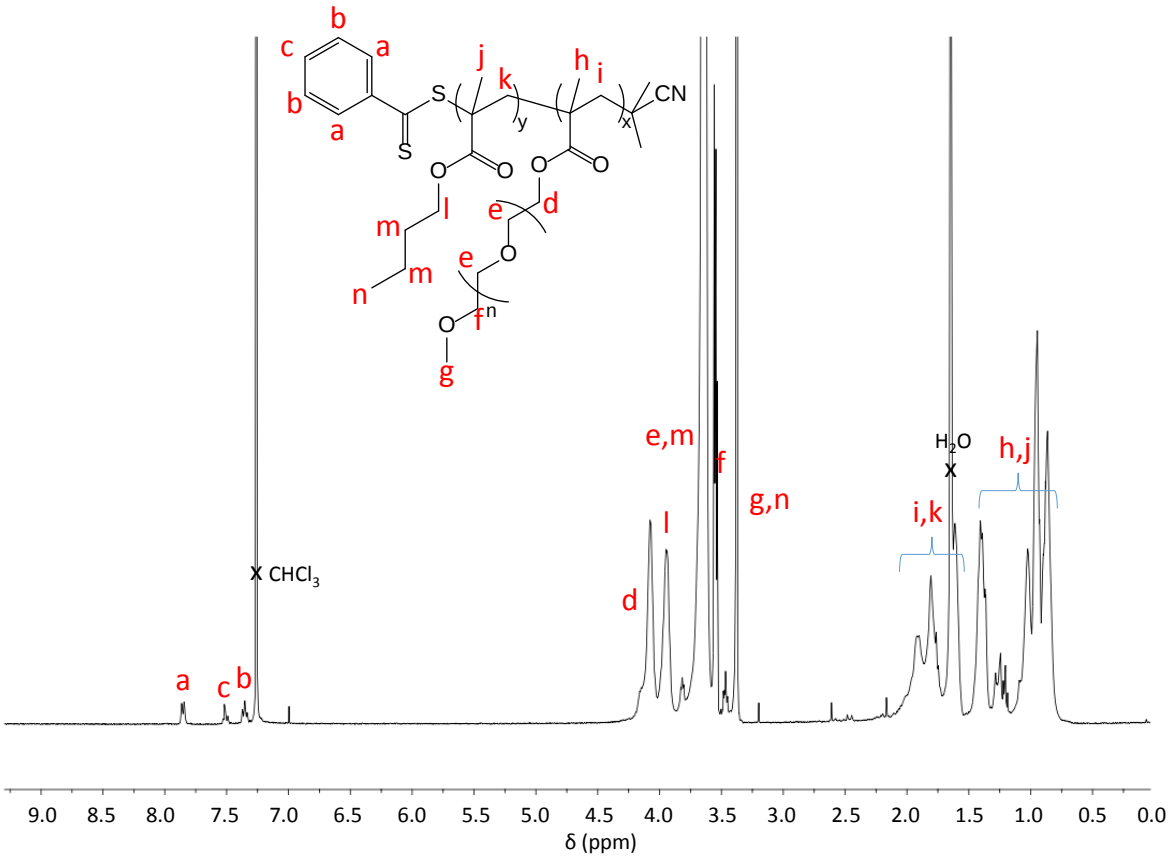

Figure S4. ^{1}H NMR spectrum of P[OEGMA-*block*-BMA]-S(C=S)Ph (Table S1, **2a**), recorded in $CDCl_3$ (400 MHz).

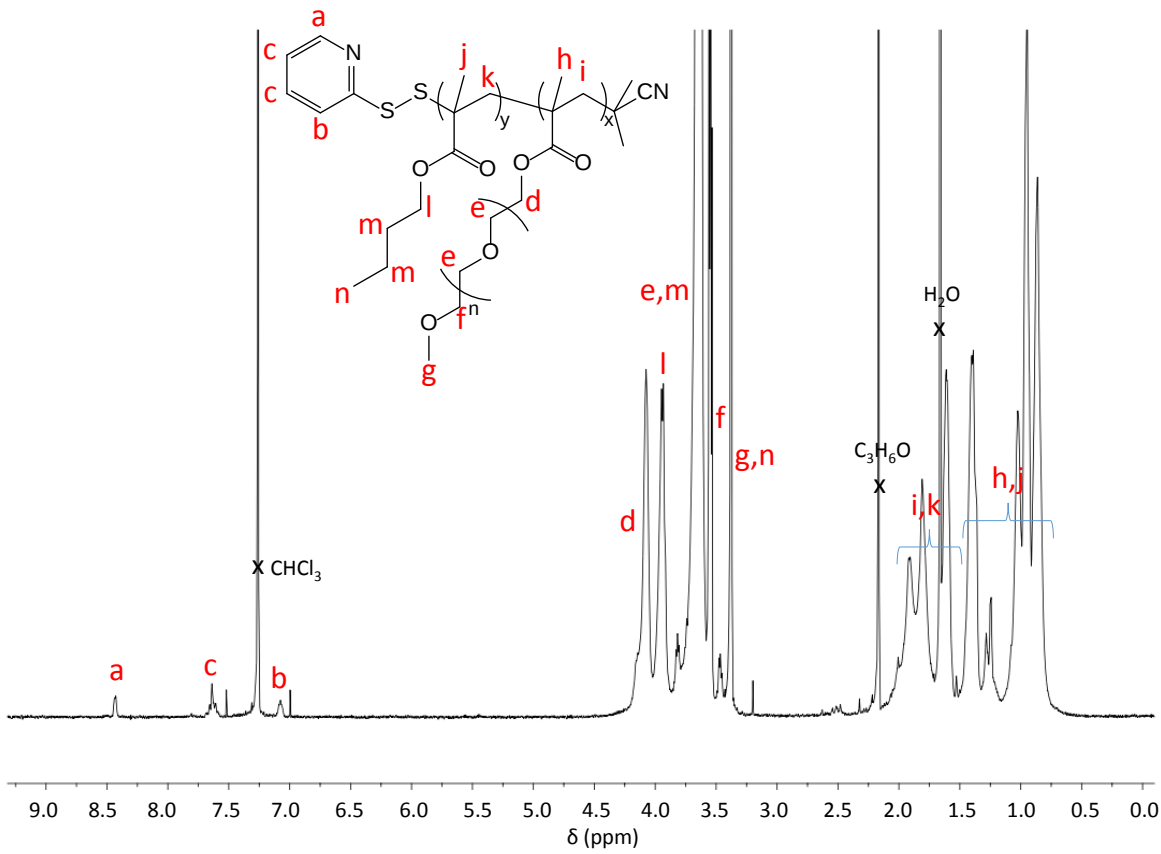

Figure S5. ^{1}H NMR spectrum of P[OEGMA-*block*-BMA]-S-S-Py (Table S1, **2b**), recorded in $CDCl_3$ (400 MHz).

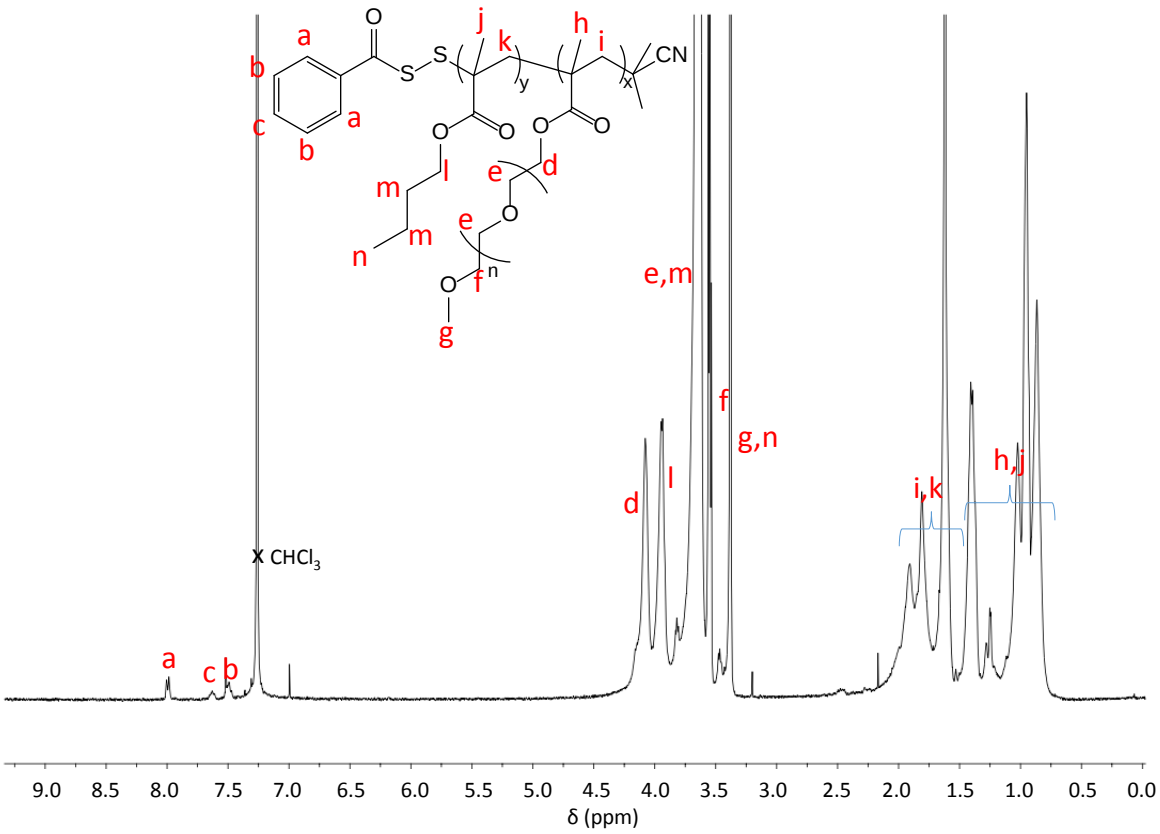

Figure S6. ^{1}H NMR spectrum of P[OEGMA-*block*-BMA]-S-S-(C=O)Ph (Table S1, **2c**), recorded in $CDCl_3$ (400 MHz).

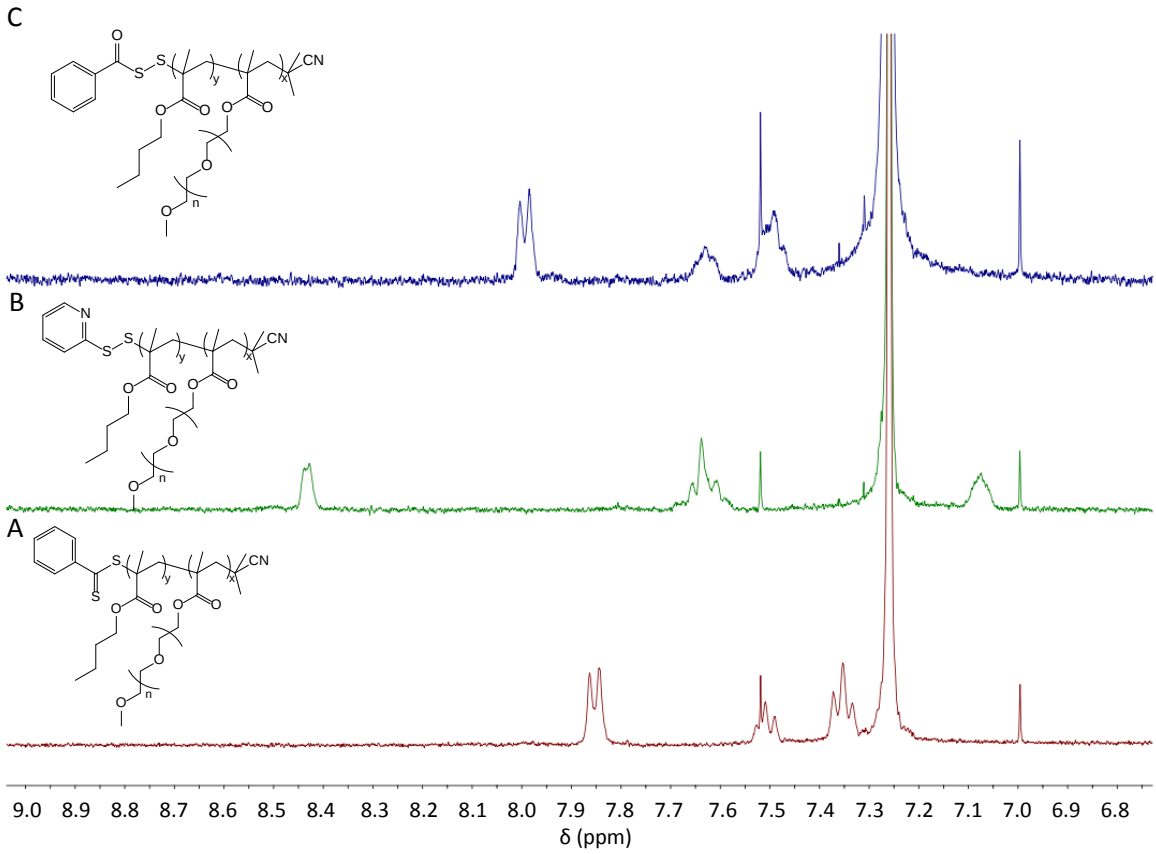

Figure S7. Enlarged ^{1}H NMR spectra (δ 9.0 - 6.8 ppm) corresponding to end-groups protons of (A) P[OEGMA-*block*-BMA]-S(C=S)Ph, **2a** (B) P[OEGMA-*block*-BMA]-S-S-Py, **2b** (C) P[OEGMA-*block*-BMA]-S-S-(C=O)Ph, **2c**, recorded in $CDCl_3$ (400 MHz). Refer to Table S1 for GPC characterisation of polymers.

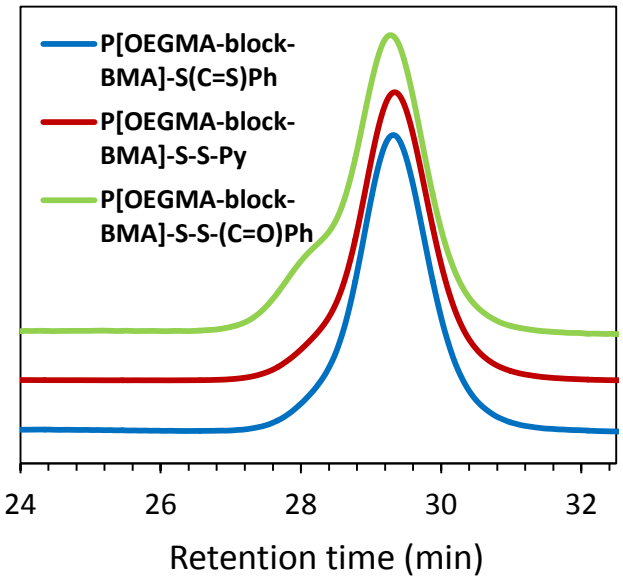

Figure S8. GPC chromatograms for P[OEGMA-*block*-BMA]-S(C=S)Ph (**2a**, blue line), P[OEGMA-*block*-BMA]-S-S-Py (**2b**, red line), P[OEGMA-*block*-BMA]-S-S-(C=O)Ph (**2c**, green line). Refer to Table S1 for GPC characterization of polymer.

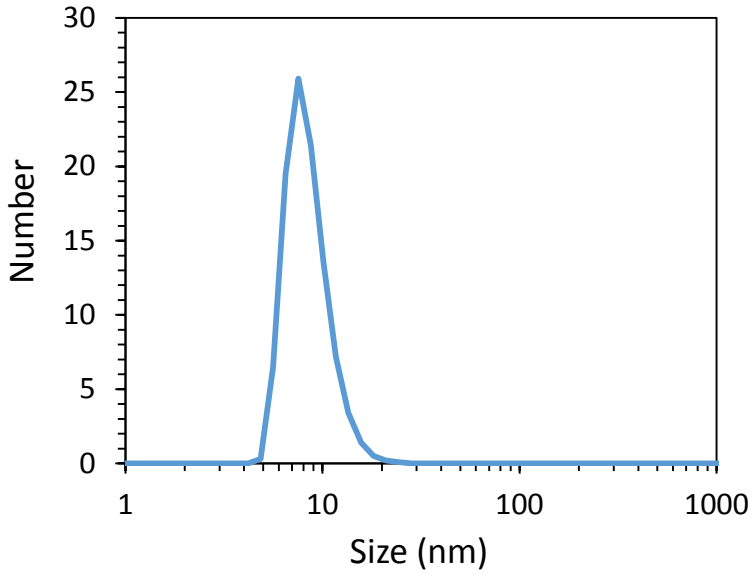

Figure S9. Size distribution (by number) for micelles of P[OEGMA-*block*-BMA]-S-S-(C=O)Ph (**2c**) in phosphate buffered saline at pH 7.4, as determined by dynamic light scattering. The average diameter was 9.1 nm with PDI = 0.17.

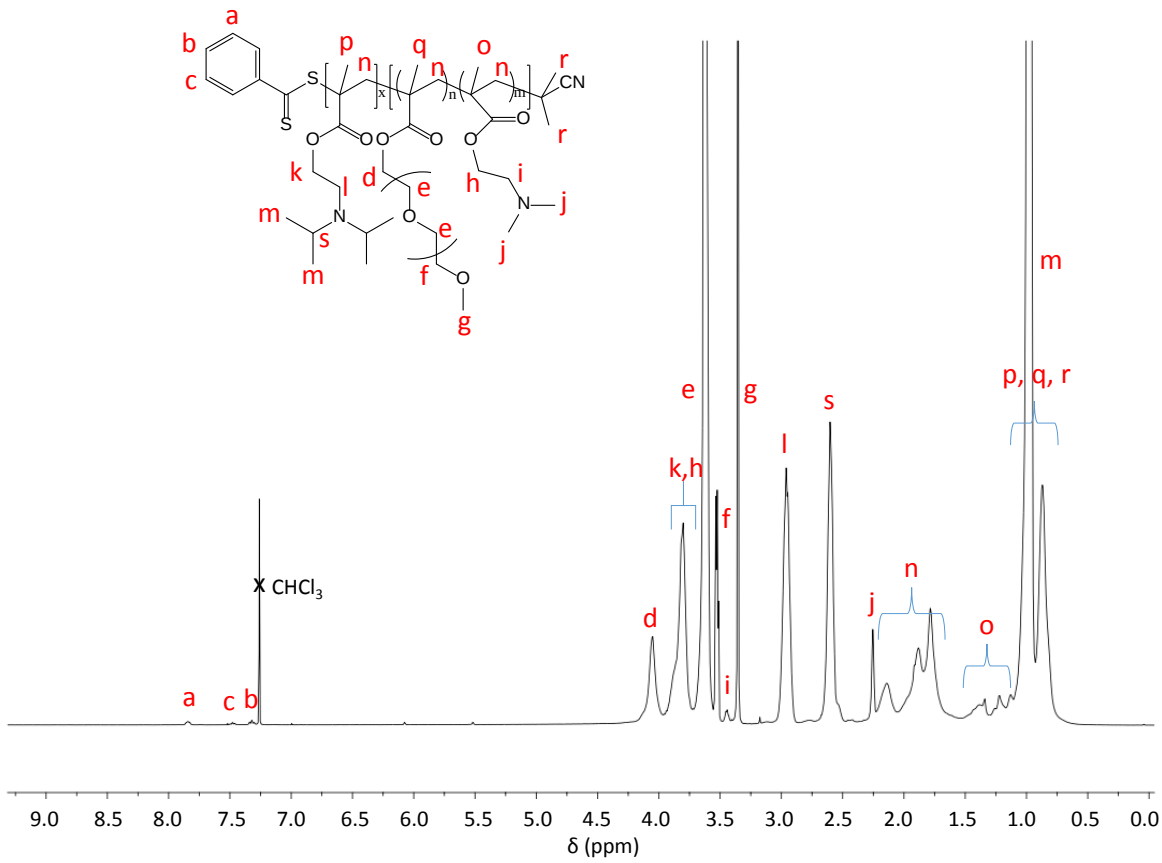

Figure S10. ^{1}H NMR spectrum of P[OEGMA-*co*-DMAEMA-*block*-DIPMA]-S(C=S)Ph (**3a**, Table S1), recorded in $CDCl_3$ (400 MHz).

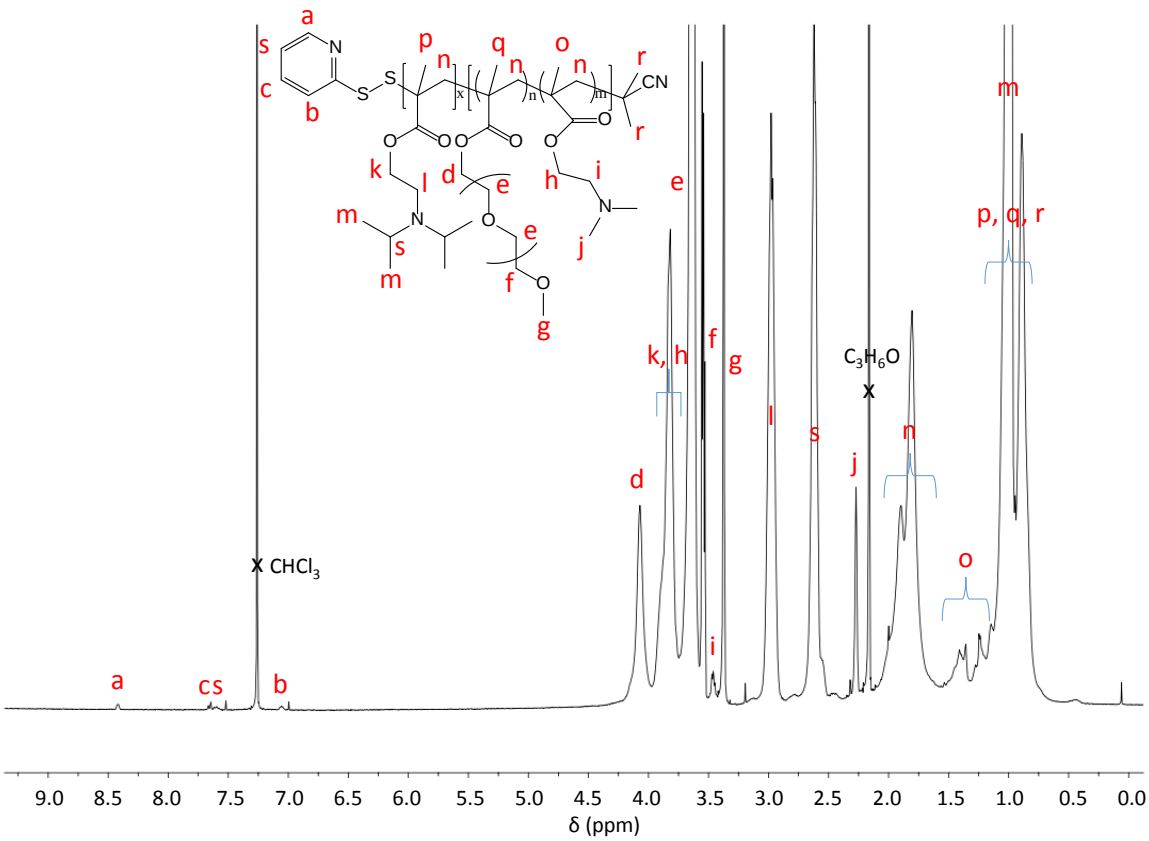

Figure S11. ^{1}H NMR spectrum of P[OEGMA-*co*-DMAEMA-*block*-DIPMA]-S-S-Py (**3b**, Table S1), recorded in $CDCl_3$ (400 MHz).

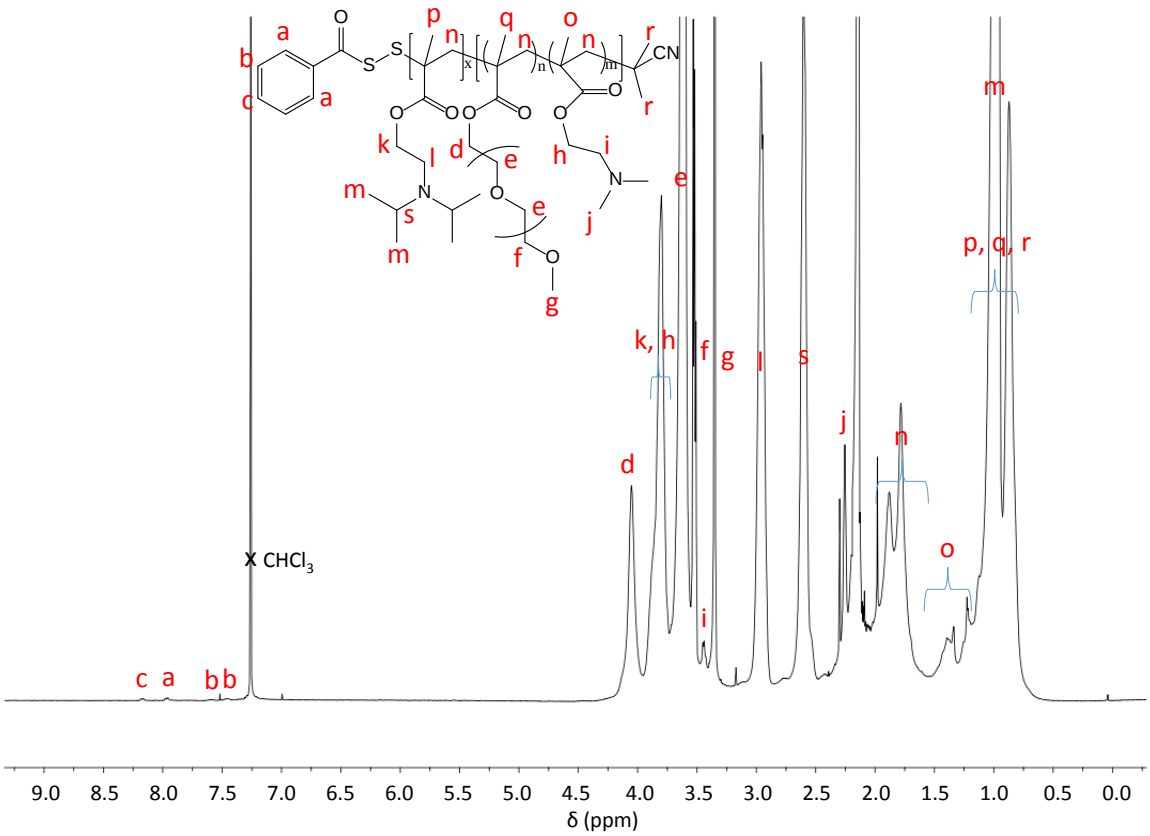

Figure S12. ^{1}H NMR spectrum of P[OEGMA-*co*-DMAEMA-*block*-DIPMA]-S-S-(C=O)Ph (**3c**, Table S1), recorded in $CDCl_3$ (400 MHz).

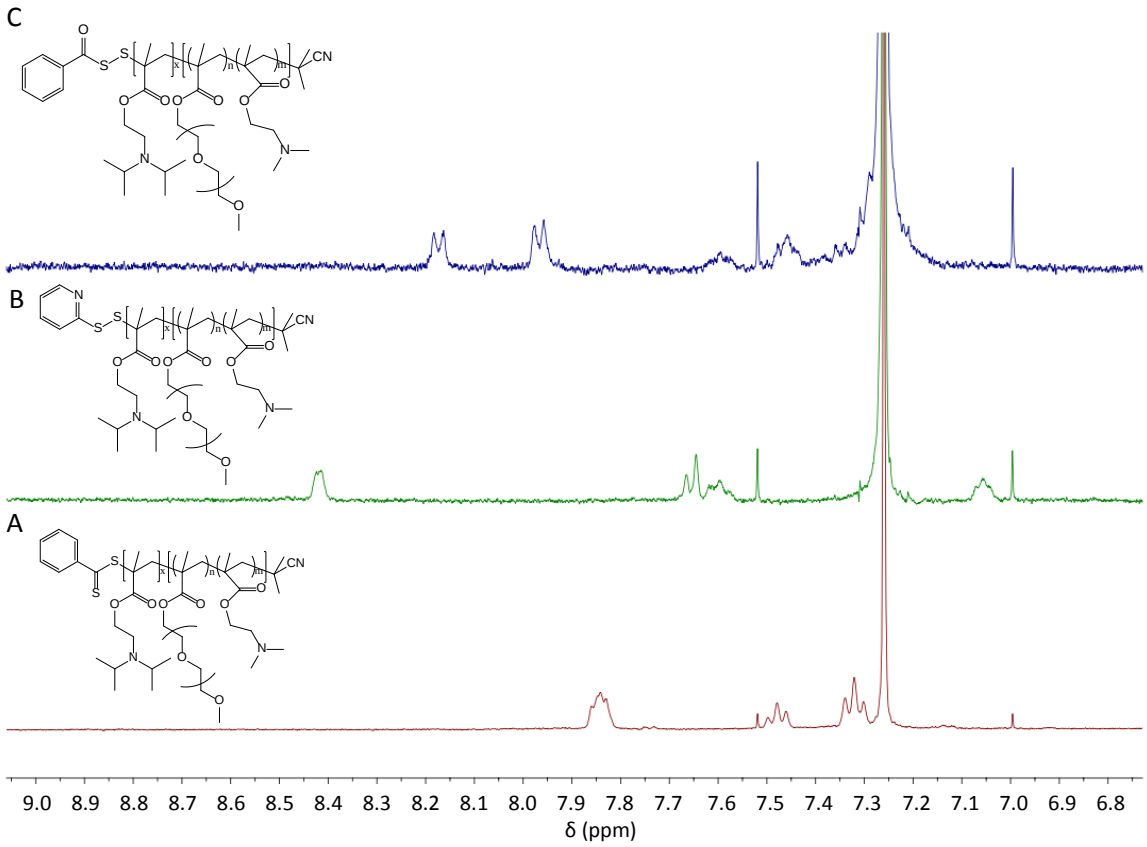

Figure S13. Enlarged ^{1}H NMR spectra (δ 9.0 - 6.8 ppm) corresponding to end-groups protons of (A) P[OEGMA-*co*-DMAEMA-*block*-DIPMA]-S(C=S)Ph, **3a** (B) P[OEGMA-*co*-DMAEMA-*block*-DIPMA]-S-S-Py, **3b** (C) P[OEGMA-*co*-DMAEMA-*block*-DIPMA]-S-S-(C=O)Ph, **3c**, recorded in $CDCl_3$ (400 MHz). Refer to Table S1 for GPC characterization of polymers.

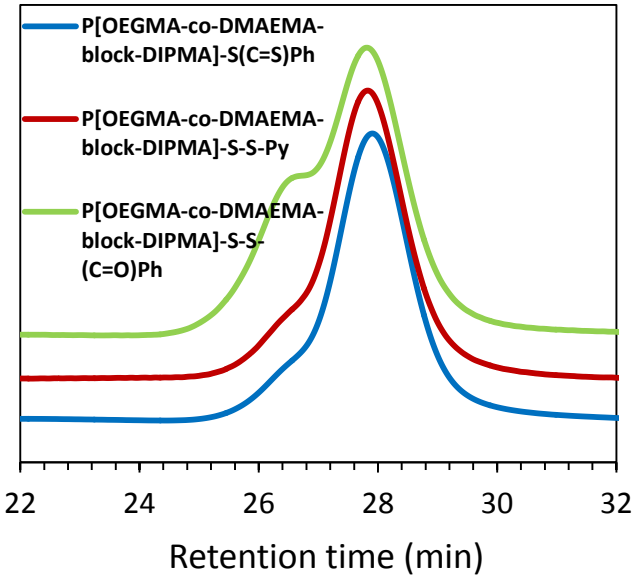

Figure S14. GPC chromatograms for P[OEGMA-*co*-DMAEMA-*block*-DIPMA]-S(C=S)Ph (**3a**, blue line), P[OEGMA-*co*-DMAEMA-*block*-DIPMA]-S-S-Py (**3b**, red line), P[OEGMA-*co*-DMAEMA-*block*-DIPMA]-S-S-(C=O)Ph (**3c**, green line). Refer to Table S1 for GPC characterisation of polymer.

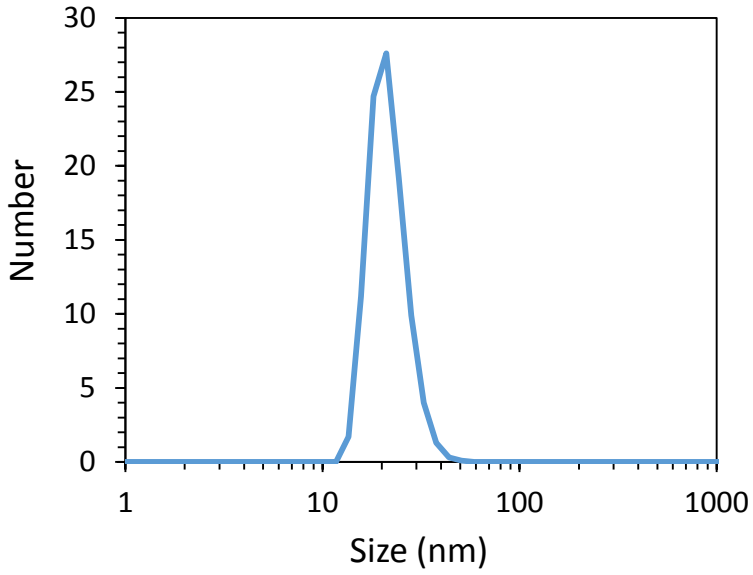

Figure S15. Size distribution (by number) for micelles of P[OEGMA-*co*-DMAEMA-*block*-DIPMA]-S-S-(C=O)Ph, **3c**, in phosphate buffered saline at pH 7.4, as determined by dynamic light scattering. The average diameter was 22 nm with PDI = 0.03.

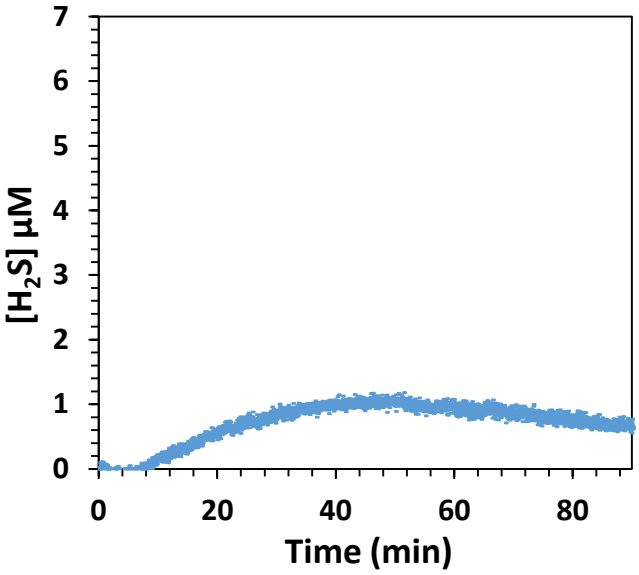

Figure S16. H_2S release from P[OEGMA-*block*-BMA]-S-S-(C=O)Ph, **2c**, (0.71 µmoles, 143 µM) in the presence of L-cysteine (33 mM, 100 µL, 3.3 µmoles). Note: L-cysteine was added at t = 2 min.

Table S2. Release characteristics of H_2S donor polymers, measured by Amperometry.

Polymer	L-cys[a] (Y/N)	pH[b]	P*eaking time*[c] (min)	P*eaking* $[H_2S]$[d] (μmol/L)	$[sulfides]_{tot}$[e] (μmol/L)	$[H_2S$ donors$]$[f] (μmol/L)	Sulfides (MPC) released[g] (%)
Chart S1, **1c**	Y	7.4	50	17	58	143	41
Chart S1, **2c**	Y	7.4	51	1	3.4	143	2.4
Chart S1, **3c**	Y	7.4	38	0.2	0.6	143	0.4
Chart S1, **3c**	Y	5.0	42	4.4	4.5	143	3.1

[a]Y = L-cysteine added (3.3 μmoles) during microsensor recording; N = L-cysteine not added. [b]Measured PBS pH condition. [c]Time taken to reach highest value of μmol/L on the curve of $[H_2S]$ vs time after L-cysteine added. [d]Highest μmol/L H_2S value attained on the curve of $[H_2S]$ vs time. [e]Total sulfides concentration = $[sulfides]_{tot} = [H_2S] + [HS^-]$, where $[sulfides]_{tot} = [H_2S] \times (10^{pH-pK1} + 1)$, (see supporting information C.6). [f]$[H_2S$ donors$] = n(H_2S$ donor polymers)/0.005, where 5mL = total volume in reaction vessel for microsensor testing. [g]% sulfides released (measured at peaking concentration) = $[sulfides]_{tot}/[H_2S$ donors$]$.

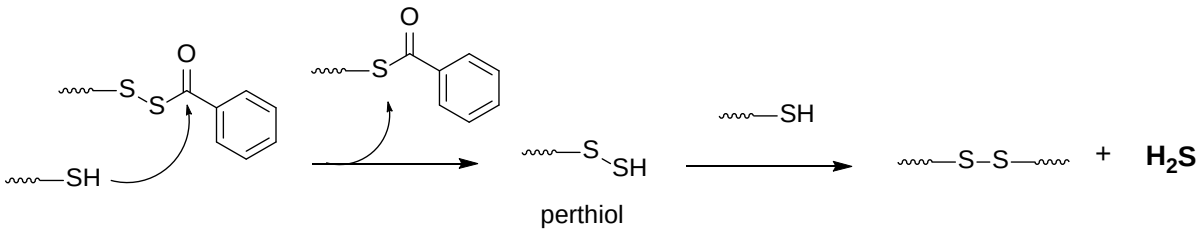

Scheme S1. Possible mechanism for formation of P[OEGMA]-S(C=O)Ph and P[OEGMA]-S-S-P[OEGMA] after H_2S is released from homopolymer P[OEGMA]-S-S-(C=O)Ph **1c**.

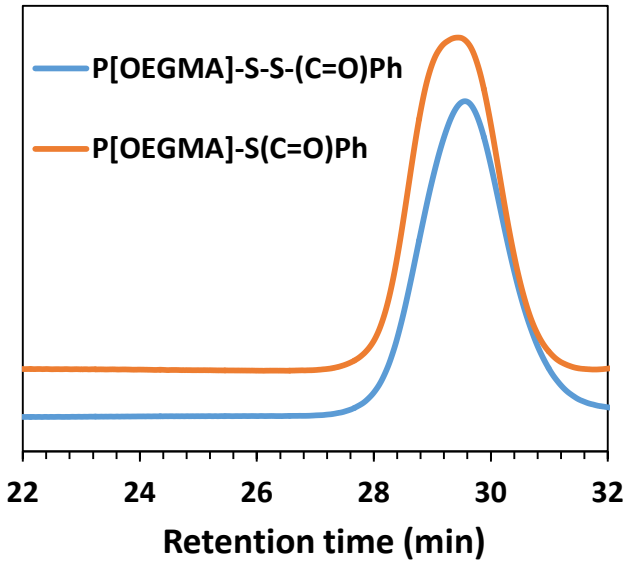

Figure S17. GPC chromatograms: blue line is P[OEGMA]-S-S-(C=O)Ph (**1c)** before exposure to L-cysteine; orange line is P[OEGMA]-S-S-(C=O)Ph (**1c)** after exposure to L-cysteine which forms a mixture of P[OEGMA]-S(C=O)Ph, P[OEGMA]-S-S-$C_3H_7NO_2$ and P[OEGMA]-S-S-P[OEGMA] (M_n = 9627 g mol^{-1} before and 10644 g mol^{-1} after treatment).

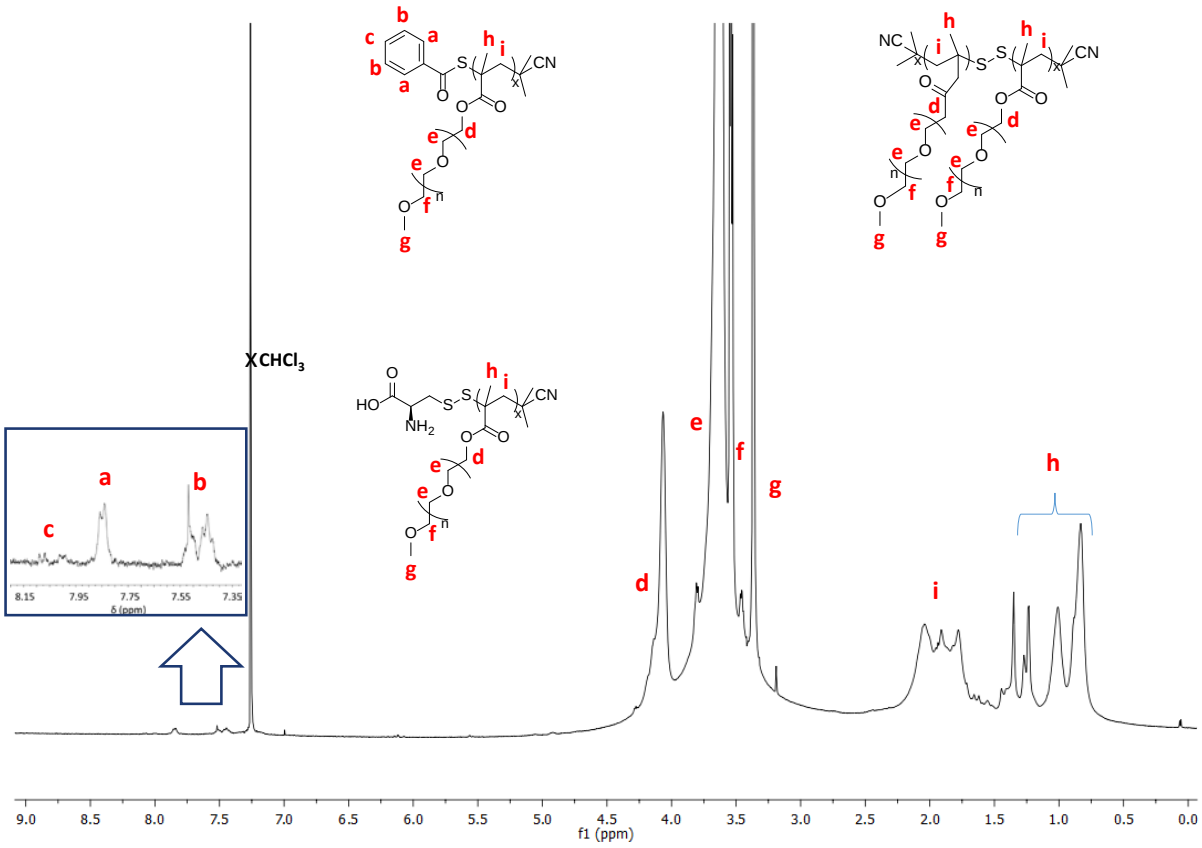

Figure S18. ^{1}H NMR spectrum of mixture of P[OEGMA]-S(C=O)Ph, P[OEGMA]-S-S-$C_3H_7NO_2$ and P[OEGMA]-S-S-P[OEGMA] after exposure of P[OEGMA]-S-S-(C=O)Ph, **1c**, to L-cysteine to release H_2S, recorded in $CDCl_3$ (400 MHz).

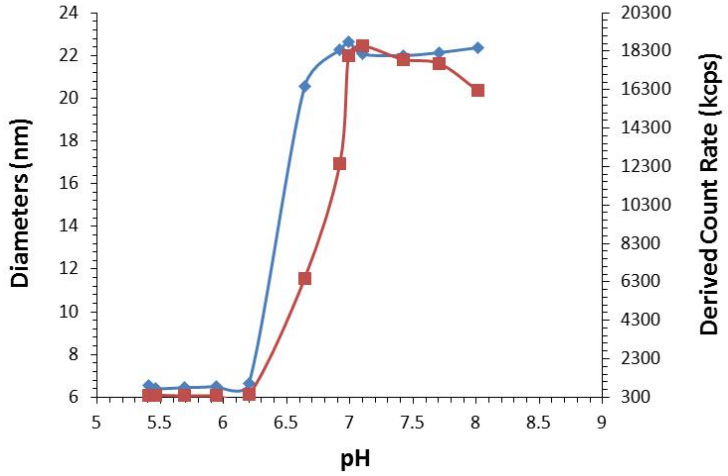

Figure S19. Hydrodynamic diameters (blue line) and derived count rate (red line) of P[OEGMA-*co*-DMAEMA-*block*-DIPMA]-S-S-(C=O)Ph, **3c**, self-assemblies as a function of solution pH.

References

(1) Yu, S. H.; Hu, J.; Ercole, F.; Truong N. P.; Davis, T. P.; Whittaker, M. R.; Quinn, J. F. *Macro Lett.*, **2015**, *4*, 1278.

(2) Ercole, F.; Mansfeld, F. M.; Kavallaris, M.; Whittaker, M. R.; Quinn, J. F.; Halls, M. L.; Davis, T. P. *Biomacromolecules*. **2016**, 17, 371.

CHAPTER 4: Development of a shape-controlled H_2S delivery system using epoxide-functional nanoparticles for improving chemosensitive in osteosarcoma cells

Development of a shape-controlled H_2S delivery system using epoxide-functional nanoparticles for improving chemosensitivity in osteosarcoma cells.

Sul hwa Yu,[a] Lars Esser,[a] Song Yang Khor,[a] Danielle Senyschyn,[a] *Nicholas A. Veldhuis,[a,b] Michael R. Whittaker,[a] Francesca Ercole,[a] John F. Quinn[a]* and Thomas P. Davis[a,c]**

[a] ARC Centre of Excellence in Convergent Bio-Nano Science & Technology, Monash Institute of Pharmaceutical Sciences, Monash University, Parkville, VIC 3052, Australia

[b] Drug Discovery Biology Theme, Monash Institute of Pharmaceutical Sciences, Monash University, Parkville, VIC 3052, Australia

[c] Department of Chemistry, University of Warwick, Coventry CV4 7AL, United Kingdom

Abstract: Hydrogen sulfide (H_2S), an endogenous modulator of signalling processes, has potential as a therapeutic drug or in combination drug therapies. As such, the controlled delivery of H_2S has received an increasing amount of attention to elicit specific biological effects. Herein we report post-polymerisation modification of polymers incorporating glycidyl methacrylate (GMA) units to form thiol-triggered macromolecular H_2S donors. This methodology allows the facile preparation of polymeric nano-particulate donors with different morphologies by dovetailing with polymerization-induced self-assembly. The thiol-reactive epoxide functional groups in PGMA were chemically transformed into acyl-protected perthiol groups using a series of sulfhydryl reactions. The morphologies were found to be unaffected during all post-polymerization modification processes and their H_2S releasing properties studied in detail. Both spherical and worm-like nano-particulate donors were shown to successfully release H_2S in the presence of the model thiol, L-cysteine. In addition, the donor polymers were shown to effectively increase H_2S inside the cells upon exposure to thiol even at endogenous levels. Finally, the co-administration of H_2S donor nanoparticles and doxorubicin (DOX) was found to enhance DOX cytotoxicity in osteosarcoma cells. These results indicate that H_2S-donating polymers may have potential for combination chemotherapy, particularly in cases where chemoresistance has developed.

4.1 Introduction

The gasotransmitters (nitric oxide, carbon monoxide and hydrogen sulfide) are a family of otherwise gaseous molecules that are produced in controlled concentrations in all organs, cells and intracellular organelles.[1] Hydrogen sulfide (H_2S), described as the third gaseous modulator,[2] was previously considered to be a toxic compound[3] but has recently gained attention due to its identified contribution to important biological processes,[4] including the regulation of inflammation and blood pressure,[5] as well as gastroprotective,[6] cardioprotective[7] and neuroprotective effects.[6, 8-13]

H_2S elicits its effects in cells by altering the function and activity of a diverse range of signalling proteins, including ion channels and kinases.[14] While these endogenous processes are typically tightly controlled to avoid unwanted H_2S-mediated signalling

events or toxicity, [15] donor-mediated release of H_2S has recently gained traction for its ability to exogenously regulate specific cellular processes[16] and even cell death[17]. This has implications for targeting cancer, where H_2S donors may offer a single treatment option, or provide a combinatorial approach with established chemotherapeutic agents. Previous studies, for example, have demonstrated the synergistic effect between exogenous H_2S and the antineoplastic drug doxorubicin (DOX) by studying the effect of H_2S donor-DOX conjugate drugs.[18] Whilst the mechanisms remain unclear, the combination drugs were found to increase intracellular DOX retention and cytotoxicity in U2OS osteosarcoma cells, when compared to DOX treatment alone.[18]

To date, a range of donor compounds have been utilised in biological investigations for delivering H_2S, including the inorganic sulfide salts (e.g., Na_2S/NaSH) which conveniently produce HS^- and H_2S instantaneously in buffer. However, release profile of salts are unlikely to reproduce the effects of continuous biosynthesis required in the presence of high cellular H_2S turnover,[15] nor allow H_2S to interact with particular intracellular targets in a reproducible or practical manner.[12, 19-21] To overcome these challenges, organic H_2S donors with slower release profiles have been developed and these are shown to produce protective and beneficial effects in a biological setting.[22] For example, non-steroidal anti-inflammatory drugs (NSAIDs) conjugated with H_2S releasing molecules provide both potent anti-inflammatory effects and reduced gastrointestinal bleeding.[23] Several other H_2S donating small molecules have been synthesized based on aryl dithiole-3-thione (ADT),[12] acyl-protected perthiols,[24] dithioperoxyanhydrides,[25] 1,2-dithiole-3-thiones[26] and phosphonamidothioates[27]. Further, nanoparticle-based H_2S delivery systems have been developed which have shown improved stabilities and subsequently more controlled release profiles, along with less toxic effects associated with excessive H_2S exposure[28, 29] Another approach is to use polymeric carriers in which side chains have been modified, post-polymerisation, with different moieties such as *S*-benzoylthiohydroxylamines or dithioperoxyanhydride compounds, giving rise to H_2S release under thiol-triggered conditions (e.g., L-cysteine/glutathione).[30-33] Furthermore, the backbone of poly(lactic acid) has been functionalized with different loadings of thiobenzamide, resulting in functionalized macromolecular H_2S donors that can release H_2S over days to weeks.[34] Thiobenzamide-functionalized block copolymers

have also been prepared that effectively release H_2S under thiol-triggered conditions as well as hydrolytically, with their release profile further enhanced when the donor groups were incorporated into the micelle corona, rather than the core.[16] More recently, a self-assembling PEG–cholesterol conjugate incorporating a garlic-inspired trisulfide linkage between the two segments was developed that releases H_2S in the presence of thiols (even at intracellular levels), with simultaneous solubility changes.[35]

Inspired by the previous report of perthiol based H_2S donating small molecules (as reported by Xian *et al*.[24]), we have previously explored[36] the synthesis of protected perthiol-functionalised polymers by modifying the end-group of polymers made using reversible addition-fragmentation chain transfer (RAFT) polymerization[37]. In this work we provide an approach of using post-polymerization transformation of poly(glycidyl methacrylate) (PGMA) units into side-chain, acyl-protected perthiol functional polymers (H_2S donors), by transformation of pendant epoxide groups. Simple block copolymer, self-assembled nanoparticles with different morphologies (spherical and worm-like micelles) containing PGMA domains were prepared via RAFT polymerization. PGMA was chemically modified into benzoyl-protected perthiol groups using a series of sulfhydryl modification reactions. The polymers displayed a controlled H_2S release profile under triggered conditions, and intracellular H_2S release was confirmed using a fluorescent probe for H_2S detection. Finally we demonstrated that the delivery of H_2S using nanoparticles with different morphologies, in combination with DOX, enhanced the cytotoxic effects in U2OS osteosarcoma cells relative to native DOX treatment.

4.2 Experimental Section

4.2.1 Materials. Oligo(ethylene glycol) methyl ether methacrylate (OEGMA) with M_n = 300 g mol^{-1} (denoted as $OEGMA_{300}$ where relevant) was purchased from Sigma-Aldrich and de-inhibited by percolating over a column of basic alumina. Glycidyl methacrylate (GMA) and styrene (St) were purchased from Sigma-Aldrich and passed through a column of basic alumina in order to remove inhibitor. Azobisisobutyronitrile (AIBN) was purified by recrystallization from methanol before use. 4-Cyano-4-(thiobenzoylthio)pentanoic acid (CPADB), ethanolamine, triethylamine (TEA) and Aldrithiol™-2 were purchased from Sigma-Aldrich at the highest purity available and

were used as received. Thiobenzoic acid (94%) was purchased from Alfa Aesar and used as received. Petroleum ether (b.p. 40 - 60 °C), diethyl ether, toluene, acetonitrile, chloroform, methanol and dioxane were purchased from Merck Millipore and used as received.

4.2.2 Instruments. ^{1}H NMR spectra were recorded at 400 MHz on a Bruker UltraShield 400 MHz spectrometer 7 running Bruker Topspin, version 1.3. Spectra were recorded in $CDCl_3$.

Gel permeation chromatography (GPC) was performed using a Shimadzu modular system comprised of a SIL-20AD automatic injector, an RID-10A differential refractive-index detector and a 50 × 7.8 mm guard column followed by three KF-805L columns (300 × 8 mm, bead size: 10 µm, pore size maximum: 5000 Å). *N,N*-Dimethylacetamide (DMAc, HPLC grade, 0.03% w/v LiBr) at 50 °C was used for the analysis with a flow rate of 1 mL min^{-1}. Samples were filtered through 0.45 µm PTFE filters before injection. The GPC calibration was performed with narrow-polydispersity polystyrene standards ranging from 500 to 2 × 10^6 g mol^{-1}.

Dynamic light scattering (DLS) measurements were carried out on a Malvern Zetasizer Nano ZS Series running DTS software (laser, 4 mW, λ = 633 nm; angle 173°). The polydispersity index (PDI), used to describe the average diameters and size distribution of prepared micelles, was determined via a cumulants analysis of the measured intensity autocorrelation function using the DTS software. Samples were filtered using 0.45 µm PTFE syringe filter to remove contaminants / dust prior to measurement. The morphologies of the block copolymers were observed by transmission electron microscopy (TEM), taking micrographs on a Tecnai F20 electron microscope (Advanced Microscopy Facility at the Bio21 Advanced Microscopy Facility, The University of Melbourne) at an accelerating voltage of 200 kV at ambient temperature. An aliquot (5 µL) of 0.5 wt% block copolymer solution (in methanol) was placed on a Formvar coated copper grid (GSCu100F-50, Proscitech) and dried in air at ambient temperature for 4 h before TEM imaging.

4.2.3 Synthesis. The characterization of all polymers containing pendant repeat units: oligo(ethylene glycol) methyl ether methacrylate (OEGMA), glycidyl methacrylate (GMA), styrene (St)**,** 3-(pyridyldisulfanyl)-2-hydroxypropyl methacrylate (PDHMA), 3-(benzoylthio)-2-hydroxypropyl methacrylate (BTHMA) and 3-(benzoyldisulfanyl)-2-

hydroxypropyl methacrylate (BDTHMA); methods for amperometric H_2S sensing are fully described in the supporting information.

4.2.4 Synthesis of P[OEGMA-*co*-GMA]-S(C=S)Ph, 1a (Table 1, Entry 1). The synthesis was carried out using the following stoichiometry: $[CPADB]_0:[OEGMA_{300}]_0:[GMA]_0:[AIBN]_0=1:50:10:0.1$. Briefly, $OEGMA_{300}$ (2.69 g, 8.97×10^{-3} mol), GMA (0.25 g, 1.76×10^{-3} mol), CPADB RAFT agent (0.05 g, 1.79×10^{-4} mol), AIBN (0.29×10^{-2} g, 1.79×10^{-5} mol) and toluene (14 mL) were placed in a glass vial equipped with a magnetic stirrer bar and capped with a rubber septum. The reaction mixture was deoxygenated for 25 min at 0 °C by sparging with N_2. The deoxygenated and sealed reaction vessel was placed into a pre-heated oil bath at 70 °C and the polymerization was run with stirring for 5 h. The resulting mixture was then allowed to cool to 0 °C for about 15 min to stop polymerization. The monomer conversion was determined by ^{1}H NMR. The polymer was purified via three precipitation and centrifugation steps (using a 50/50 (v/v) mixture of petroleum ether (bp 40-60 °C) and diethyl ether as the precipitant) to remove any traces of unreacted monomer. The product was then placed in a vacuum oven overnight to remove remaining solvent. The final product was analysed by ^{1}H NMR and GPC. The molecular weight and GMA average monomer chain length calculated from ^{1}H NMR were determined to be 8000 g mol^{-1} and 7 units, respectively. The polydispersity index (determined by GPC) was 1.14.

4.2.5 Thiocarbonylthio end group removal from P[OEGMA-*co*-GMA]-S(C=S)Ph, 1a, to form P[OEGMA-*co*-GMA] 1b (Table 1, Entry 2). A radical-induced process for the removal of the thiocarbonylthio group of P[OEGMA-*co*-GMA]-S(C=S)Ph was performed according to a previously reported procedure.[39] A mixture of P[OEGMA-*co*-GMA]-S(C=S)Ph **1a** (0.11 g, 1.38×10^{-5} mol), AIBN (0.23×10^{-2} g, 2.75×10^{-4} mol) and toluene (3.5 mL) was placed in a glass vial equipped with a magnetic stirrer bar and capped with a rubber septum. The reaction mixture was deoxygenated for 40 min at 0 °C by sparging with N_2. The deoxygenated and sealed reaction vessel was placed into a pre-heated oil bath at 80 °C with stirring for 4 h. The resulting mixture was then allowed to cool to 0 °C for about 15 min to stop the radical reaction. The polymer was purified via three precipitation and centrifugation steps (using a 50/50 (v/v) mixture of petroleum ether (bp 40-60 °C) and diethyl ether as the precipitant) to ensure removal of the recycled CPADB side product. This whole process was performed twice to

remove all thiocarbonylthio end groups from P[OEGMA-*co*-GMA]-S(C=S)Ph. The product was then placed in a vacuum oven overnight to remove remaining solvent. The final product was analysed by ^{1}H NMR and GPC. Three distinct signals in the ^{1}H NMR spectrum (δ 7.3, 7.5 and 7.8 ppm, corresponding to the aromatic benzodithioate) were lost upon radical reaction. The polydispersity index (determined by GPC) was 1.21.

4.2.6 Ring opening reaction of PGMA to form P[OEGMA-*co*-BTHMA] 1c (Table 1, Entry 3). P[OEGMA-*co*-GMA] **1b** prepared as above (0.08 g, 1.08×10^{-5} mol) was dissolved in methanol (6 mL). Thiobenzoic acid (0.09 g, 6.57×10^{-4} mol) and triethylamine (0.04 g, 3.94×10^{-4} mol) were added into the solution with stirring and allowed to react at 50 °C overnight. The dialysis was conducted overnight to ensure complete removal of the excess amount of thiobenzoic acid and TEA. The resulting polymer was dried under air and in vacuo, which were then analysed by ^{1}H NMR spectroscopy to confirm the complete ring opening of PGMA with thiobenzoic acid. Three distinct signals in the ^{1}H NMR spectrum (δ 3.3, 2.9, 2.7 ppm, corresponding to the glycidyl methacrylate epoxide group) disappeared, and new peaks emerged corresponding to the aromatic benzothioate group (δ 7.5, 7.6, 8.0 ppm).

4.2.7 Modification of P[OEGMA-*co*-BTHMA] 1c, to form P[OEGMA-*co*-BTHMA-*co*-PDHMA] 1d (Table 1, Entry 4). A mixture of P[OEGMA-*co*-BTHMA] **1c**, prepared as above (0.06 g, 7.64×10^{-6} mol) and Aldrithiol^{TM}-2 (0.12 g, 5.45×10^{-4} mol) in acetonitrile (5 mL) was deoxygenated by sparging with nitrogen for 15 min. A solution of ethanolamine (127 µL, 2.10×10^{-3} mol) in acetonitrile (873 µL) was deoxygenated with by sparging with nitrogen for 15 min. The solution of ethanolamine in acetonitrile (300 µL) was transferred into the mixture. The deoxygenated reaction mixture was then stirred for 3 h at room temperature to convert the P[OEGMA-*co*-BTHMA] **1c** into P[OEGMA-*co*-BTHMA-*co*-PDHMA] **1d** (i.e. convert the benzoylthio group to pyridy-2-dithiol group). The resulting mixture was then dialysed overnight against acetone and water (50/50 (v/v)), using a dialysis membrane with molecular weight cut-off 3.5 kDa, to ensure removal of side products, excess aldrithiol and ethanolamine. The resulting polymer was dried under air and in vacuo, and then analysed by ^{1}H NMR spectroscopy to confirm formation of pyridy-2-dithiol group. The characteristic signals of the benzothioate aromatic protons (δ 7.5, 7.6, 8.0 ppm) in the ^{1}H NMR spectrum were

partially replaced with new resonance peaks (δ 7.1, 7.7, 8.5 ppm) associated with the aromatic pyridyl group (Figure S4, S6). This indicated a conversion of 60% to the final product P[OEGMA-*co*-BTHMA-*co*-PDHMA] **1d.**

4.2.8 Thiol-disulfide exchange reactions of P[OEGMA-*co*-BTHMA-*co*-PDHMA] 1d with thiobenzoic acid to form P[OEGMA-*co*-BTHMA-*co*-BDTHMA] 1e. P[OEGMA-*co*-BTHMA-*co*-PDHMA] **1d** prepared as above (0.05 g, 6.89×10^{-6} mol) was dissolved in chloroform (5 mL). Thiobenzoic acid (1.52 mg, 1.10×10^{-5} mol) was added into the solution with stirring and the mixture allowed to react at room temperature for 2 h to convert pyridy-2-dithiol groups to benzoyl-protected perthiol groups. The resulting mixture was then dialysed overnight against acetone and water (50/50 (v/v)), using a dialysis membrane with molecular weight cut-off 3.5 kDa, to ensure removal of aldrithiol/pyridine-2-thiol side products and excess thiobenzoic acid. The resulting polymer was dried under air and in vacuo, and then analysed by ^{1}H NMR spectroscopy to confirm the removal of the pyridyl disulfide group and the formation of the benzoyl-protected perthiol moiety. The reaction was monitored via the disappearance of the pyridyl aromatic proton signals and the appearance of new aromatic benzodithioate proton resonances (δ 7.6, 7.7, 8.1 ppm) which overlapped with the peaks of residual benzothioate groups (40% left from the previous reaction) as shown in Figure S5. Self-assembly was monitored using DLS by dissolving 5 mg of polymer into PBS pH 7.4 PBS (5 mL).

4.2.9 Preparation of P[GMA]-S(C=S)Ph 2a. The synthesis of PGMA was performed according to a previously reported procedure.[44] The purified polymer was then carefully dried at 30 °C under vacuum overnight to give 381 mg of a pink solid which was characterized by GPC and ^{1}H NMR.

4.2.10 Preparation of P[GMA-*b*-OEGMA]-S(C=S)Ph 2b. P[GMA]-S(C=S)Ph **2a** (80 mg, M_n ~ 1406 g/mol (based on ^{1}H NMR), i.e. 5.7×10^{-5} mol of polymer), in the presence of oligo(ethylene glycol) methyl ether methacrylate] (OEGMA) 0.81 mL, M_n ~ 300 g mol^{-1}, 2.8×10^{-3} mol), and AIBN (1.2 mg, 7.1×10^{-6} mol) as initiator. The compounds were dissolved in 4.1 mL acetonitrile in a septa-sealed vial, which was then purged with nitrogen for 30 min while cooling in an ice bath. The ratio between the monomer, macro-RAFT agent and initiator in the polymerization mixture was 50 : 1 : 0.125. After deoxygenation, the reaction medium was placed in an oil bath at 70 °C.

After 6 h the reaction was quenched via rapid cooling and exposure to air. The polymer was concentrated by partial evaporation of solvent and purified by precipitation four times with a 25 : 25 : 1 mixture of diethyl ether, petroleum spirit (BR 40 – 60 °C) and chloroform. The purified polymer was then dried at 30 °C in vacuo overnight to give 379 mg of a red gelatinous solid.

4.2.11 Preparation of P[GMA-*b*-OEGMA-*b*-St]-S(C=S)Ph spherical 3a and worm-like 4a micelles. P[GMA-*b*-OEGMA]-S(C=S)Ph **2b** was used as a macro-CTA for the preparation of micelles via Polymerization Induced Self Assembly (PISA). The ratio between the styrene, macro-CTA and initiator in the polymerization mixture was 5000 : 1.0 : 0.5, with the styrene to solvent (methanol) set to 1 : 1.1 (%w/w). Specifically, **2b** (146 mg, M_n ~ 9,400 g mol^{-1} (based on ^{1}H NMR), i.e. 1.6 x 10^{-5} mol of polymer), styrene (de-inhibited using basic alumina, 8.9 mL, 7.8 x 10^{-2} mol), AIBN (1.3 mg, 7.9 x 10^{-6} mol), and methanol (12.3 ml) were added to a septa-sealed vial, and purged with nitrogen for 30 minutes in an ice-bath to limit methanol evaporation. After deoxygenation, the vial was placed in an oil bath at 70 °C. For spherical micelles, the reaction was stopped after 4 hour by rapid cooling and exposure to air. For worm-like micelles, the reaction was quenched after 22 h. The self-assembled nanoparticles were purified by dialysis (using a dialysis membrane with molecular weight cut-off 12-14 kDa), against methanol and the solvent was changed three times to remove all monomer. The purified polymers were characterized by ^{1}H NMR, GPC, DLS and TEM.

4.2.12 Ring opening reaction of P[GMA-*b*-OEGMA-*b*-St]-S(C=S)Ph 3a spherical micelles to form P[BTHMA-*b*-OEGMA-*b*-St] 3b spherical micelles. PGMA-*b*-POEGMA-*b*-PSt spherical micelles (0.1 g, 3.63 × 10^{-6} mol) in methanol (2 mL), thiobenzoic acid (0.04 g, 3.20 × 10^{-4} mol) and triethylamine (0.02 g, 1.92 × 10^{-4} mol) were combined with stirring and allowed to react at 50 °C overnight. The resulting mixture was then dialysed against methanol overnight, using a dialysis membrane with molecular weight cut-off 12-14 kDa, to ensure removal of the excess thiobenzoic acid and TEA. The resulting polymer was then analysed by ^{1}H NMR, DLS and TEM. ^{1}H NMR spectroscopy was used to confirm the complete ring opening of PGMA with thiobenzoic acid. Three distinct signals in the ^{1}H NMR spectrum (δ 3.25, 2.85, 2.65 ppm), representing the glycidyl methacrylate epoxide group disappeared, and new

peaks emerged at δ 7.4, 7.6 and 8.0 ppm, representing the aromatic benzothioate group).

4.2.13 Modification of the benzothioate group from P[BTHMA-*b*-OEGMA-*b*-St] 3b to form P[BTHMA-*co*-PDHMA-*b*-OEGMA-*b*-St] 3c spherical micelles. A mixture of P[BTHMA-*b*-OEGMA-*b*-St] **3b** spherical micelles prepared as above (0.09 g, 3.38 × 10^{-6} mol) and Aldrithiol^{TM}-2 (0.06 g, 2.70 × 10^{-4} mol) in methanol (2 mL) was deoxygenated with nitrogen for 15 min. A solution of ethanolamine (65 µL, 1.08 × 10^{-3} mol) in methanol (935 µL) was deoxygenated with nitrogen for 15 min. An aliquot of the ethanolamine solution in methanol (300 µL) was transferred into the mixture of P[BTHMA-*b*-OEGMA-*b*-St] **3b** and Aldrithiol^{TM}-2 in methanol, and the deoxygenated reaction mixture was then stirred for 3 h at room temperature to convert the benzothioate groups to pyridy-2-dithiol groups. The resulting mixture was then dialysed against methanol overnight, using a dialysis membrane with molecular weight cut-off 12-14 kDa, to ensure removal of side products and the excess aldrithiol/ethanolamine. The resulting polymer was then analysed by ^{1}H NMR spectroscopy to confirm formation of pyridyl disulfide group.

The characteristic signals in the ^{1}H NMR spectrum of the benzothioate aromatic protons (δ 7.4, 7.6, 8.0 ppm) in the ^{1}H NMR spectrum were partially replaced with new resonance peaks associated with the aromatic pyridyl group, of which the 8.50 ppm peak was the only one fully resolved (Figure S13). This indicated a conversion of 50 % for the formation of P[BTHMA-*co*-PDHMA-*b*-OEGMA-*b*-St] **3c** spherical micelles.

4.2.14 Thiol-disulfide exchange reactions of P[BTHMA-*co*-PDHMA-*b*-OEGMA-*b*-St] 3c spherical micelles with thiobenzoic acid to form P[BTHMA-*co*-BDTHMA-*b*-OEGMA-*b*-St] 3d spherical micelles. A mixture of P[BTHMA-*co*-PDHMA-*b*-OEGMA-*b*-St] **3c** spherical micelles in methanol (3 mL) was prepared as above (0.08 g, 3.16 × 10^{-6} mol). Thiobenzoic acid (12.3 mg, 8.91 × 10^{-5} mol) was added into the solution with stirring and allowed to react at room temperature for 3h to convert pyridyl disulfide groups to acyl-protected perthiol groups. The resulting mixture was then dialysed against methanol overnight, using a dialysis membrane with molecular weight cut-off 12-14 kDa, to ensure removal of side products and excess thiobenzoic acid. The resulting polymer was then analysed by ^{1}H NMR spectroscopy to confirm the removal of the pyridyl disulfide group and the formation of acyl-protected perthiol.

As previously, the pyridyl aromatic proton signals disappeared and new aromatic benzodithioate proton resonances appeared (δ 7.4, 7.6, 7.9-8.1 ppm), which overlapped with those of residual benzothioate groups left from the previous reaction (50 % left from the previous reaction) as shown in Figure S14.

4.2.15 Ring opening reaction P[GMA-*b*-OEGMA-*b*-St]-S(C=S)Ph 4a worm-like micelles to form P[BTHMA-*b*-OEGMA-*b*-St] 4b worm-like micelles. A mixture of P[GMA-*b*-OEGMA-*b*-St]-S(C=S)Ph **4a** worm-like micelles (0.06 g, 1.70×10^{-6} mol) in methanol (1 mL) was prepared as above. Thiobenzoic acid (0.02 g, 1.19×10^{-4} mol) and triethylamine (7.23 mg, 7.14×10^{-5} mol) were added into the solution with stirring and allowed to react at 50 °C overnight. The resulting mixture was then dialysed against methanol overnight, using a dialysis membrane with molecular weight cut-off 12-14 kDa, to ensure complete removal of the excess thiobenzoic acid and TEA. The resulting polymer was then analysed by ^{1}H NMR spectroscopy to confirm that complete ring opening of PGMA with thiobenzoic acid had occured. Three distinct signals in the ^{1}H NMR spectrum (δ 3.3, 2.9 and 2.7 ppm, corresponding to the glycidyl methacrylate epoxide group) disappeared, with the formation of new peaks (δ 7.4, 7.6 and 8.0 ppm), representing the aromatic benzothioate group.

4.2.16 Modification of the benzothioate group from P[BTHMA-*b*-OEGMA-*b*-St] 4b to form P[BTHMA-*co*-PDHMA-*b*-OEGMA-*b*-St] 4c worm-like micelles. A mixture of P[BTHMA-*b*-OEGMA-*b*-St] **4b** worm-like micelles (46 mg, 1.28×10^{-6} mol) and Aldrithiol^{TM}-2 (20 mg, 0.90×10^{-4} mol) in methanol (1 mL) was prepared and deoxygenated with nitrogen for 15 min. A solution of ethanolamine (20 µL, 3.35×10^{-4} mol) in methanol (980 µL) was deoxygenated with nitrogen for 15 min. An aliquot of the methanolic ethanolamine solution (300 µL) was transferred into the mixture of P[BTHMA-*b*-OEGMA-*b*-St] **4b** and Aldrithiol^{TM}-2. The deoxygenated reaction mixture was then stirred for 3 h at room temperature to convert the benzothioate group to pyridy-2-dithiol group. The resulting mixture was then dialysed against methanol overnight, using a dialysis membrane with molecular weight cut-off 12-14 kDa, to ensure removal of side products and the excess aldrithiol/ethanolamine. The resulting polymer was then analysed by ^{1}H NMR spectroscopy to confirm formation of pyridyl disulfide group. Three distinct signals in the ^{1}H NMR spectrum (δ 7.4, 7.6 and 8.0 ppm), corresponding to the aromatic benzothioate group were partially shifted to the new

peaks; δ 8.5 ppm represents the aromatic pyridyl group. This indicated a conversion of 25 % for the formation of P[BTHMA-*co*-PDHMA-*b*-OEGMA-*b*-St] **4c** worm-like micelles.

4.2.17 Thiol-disulfide exchange reactions of P[BTHMA-*co*-PDHMA-*b*-OEGMA-*b*-St] 4c worm-like micelles with thiobenzoic acid to form P[BTHMA-*co*-BDTHMA-*b*-OEGMA-*b*-St] 4d worm-like micelles. A solution of P[BTHMA-*co*-PDHMA-*b*-OEGMA-*b*-St] **4c** worm-like micelles in methanol (1 mL) was prepared as above (38.5 g, 1.08×10^{-6} mol). Thiobenzoic acid (1.66 mg, 1.20×10^{-5} mol) was added into the solution with stirring and allowed to react at room temperature for 3h to convert the pyridy-2-dithiol groups into acyl-protected perthiol groups. The resulting mixture was then dialysed against methanol, using a dialysis membrane with molecular weight cut-off 12-14 kDa, overnight to ensure removal of side products and the excess thiobenzoic acid. The resulting polymer was then analysed by ^{1}H NMR spectroscopy to confirm the removal of the pyridyl disulfide group and the formation of the benzoyl-protected perthiol group. As previously, the pyridyl aromatic proton signals disappeared and new aromatic benzodithioate proton resonances appeared (δ 7.4, 7.6, 7.9-8.1 ppm), which overlapped with those of residual benzothioate groups left from the previous reaction (75 % left from the previous reaction) as shown in Figure S17.

Finally, the worm-like micelles **4d** were scissioned by sonification (Sonics Vibracell with tapered microtip 1/8") to produce short worm-like micelles **4e**. The dispersion was sonicated for 10 minutes (5 seconds on, 5 seconds off at 20% amplitude) whilst in a water bath to prevent heating.

4.2.18 Preparation of non-H_2S donating control polymers (3e and 4f) via exposure of P[BTHMA-*co*-BDTHMA-*b*-OEGMA-*b*-St] polymers (3d and 4e) to L-cysteine. H_2S-donating self-assembled spherical micelles **3d** (4.73 mg, 0.71 μmoles, 143 μM) and short worm-like micelles **4e** (15.6 mg, 0.71 μmoles, 143 μM) were dissolved separately in PBS at pH 7.4 in the presence of L-cysteine (4.65 molar equiv., 3.3 μmoles, 660 μM) over 72 h in each open vessel. Dialysis (dialysis membrane with the molecular weight cut-off 12-14 kDa) was then conducted to ensure removal of the side products and the excess L-cysteine. The resulting control polymers: **3e** (non-H_2S donating, spherical micelles) and **4f** (non-H_2S donating, short worm-like micelles)

were dried under air and in vacuo, and then analysed by ^{1}H NMR spectroscopy to confirm the final products. Refer to supporting information figures (Figure S21 and Figure S22) for ^{1}H NMR of resulting non-H_2S donating products formed.

4.2.19 Measurement of L-Cysteine mediated H_2S release profile using an amperometric H_2S sensor. The H_2S-generating capability of polymers was examined via an amperometric sensor using a H_2S microsensor manufactured by Unisense A/S. The complete method is described in the supporting information. L-cysteine mediated H_2S-generation was examined as follows: Polymer (0.71 µmoles of H_2S releasing groups) in deoxygenated pH 7.4 PBS (5 mL) and L-cysteine (3.3 µmoles) in deoxygenated PBS at pH 7.4 were prepared separately. The sensor was immersed into the polymer solution, using a septum to minimize exposure to air. 50 µL of L-cysteine solution was then injected slowly into the stirring polymer solution using a micro-syringe. The time of cysteine addition was recorded.

4.2.20 Cell culture. Human DOX-sensitive U-2 OS cells (ATCC® HTB-96™) were purchased from ATCC and maintained in McCoy's 5A medium (Sigma-Aldrich, NSW, Australia) supplemented with 10% v/v fetal bovine serum (FBS; ThermoFisher Scientific, Victoria, Australia) in a humidified atmosphere at 37 °C with 5% CO_2.

4.2.21 Cell viability assays. The cytotoxicity of DOX was tested in-vitro using the RealTime-Glo™ MT Luminescent Cell Viability Assay (Promega, NSW, Australia) according to manufacturer instructions. Cells were seeded at 7500 per well in white walled 96 well tissue culture plates and incubated for 24 h, then co-incubated with DOX (9 µM) and H_2S releasing P[BTHMA-*co*-BDTHMA-*b*-OEGMA-*b*-St] **3d** spherical micelles with the concentration range of 0.06 – 0.60 mg/mL (i.e., 9 - 90 µM of H_2S releasing acyl protected perthiol groups) or non-H_2S donating control spherical micelles in the same concentration range (0.06 – 0.60 mg/mL) for 24 h at 37 °C and 5% CO_2. The control micelles were H_2S-donating micelles **3d** that had been previously exposed to L-cysteine (See Supporting Information section A.3) to ensure that their H_2S-releasing capability was exhausted. For H_2S releasing worm-like micelles **4d**, the aggregated long worm-like micelles were initially sonicated under mild condition to produce short worm-like micelles. The cells were then co-incubated with DOX (9 µM) and H_2S-releasing P[BTHMA-*co*-BDTHMA-*b*-OEGMA-*b*-St] short worm-like micelles (0.99 mg/mL, i.e., 45 µM of H_2S releasing acyl protected perthiol groups) or control

short worm-like micelles with the same concentration for 24 h at 37 °C and 5% CO_2. Control short worm-like micelles were H_2S donating micelles previously exposed to L-cysteine (See supporting information section A.3). For the non-H_2S control experiment, cells were only incubated with DOX (9 µM) for 24 h at 37 °C and 5% CO_2.

After incubation for 24h, the supernatant was removed and 2 x Real Time Glo™ was added to each well. This reagent was prepared by adding 2 µL of MT Cell Viability Substrate and 2 µl of NanoLuc® Enzyme to 996 µl of cell culture medium. Cells were incubated for 15 min at 37 °C and 5% CO_2 before reading luminescence on a Perkin Elmer EnSight™ Multimode Plate Reader with an integration time of 0.25 seconds per well. Data was normalized to the absorbance of untreated control cells, which were expected to maintain maximal cell viability.

4.2.22 Preparation of SF4. The synthesis and characterization of SF4 fluorogenic probe has been previously reported.[38]

4.2.23 High-Content SF4 time course cell based study. The cell based high content H_2S release time course study was performed according to previous reported procedures.[16, 35] H_2S donor short worm-like micelles (1.98 mg/mL, 90 µM), control short worm-like micelles (1.98 mg/mL, 90 µM), H_2S donor spherical micelles **3d** (0.60 mg/mL, 90 µM) and control spherical micelles (0.60 mg/mL, 90 µM) were prepared in PBS at pH 7.4. A stock solution of SF4 was prepared fresh in a 1:1 mixture of DMF and DMSO (5 mM), which was then diluted to give a 5 µM solution in Hank's Balanced Salt Solution (HBSS). U2OS cells were seeded at 10000 cells per well in triplicate in optically clear blank 96 well plates and grown to 70-80 % confluency for 24 h at 37 °C and 5% CO_2. A high-content PerkinElmer Operetta with an Olympus LUCPlanFLN 20 x (NA 0.45) objective was employed to measure the fluorescence imaging. SF4 fluorescence SF4 (λ_{ex} = 460-490 nm, λ_{em} = 500-550 nm) was visualised using an EGFP filter set. Images were detected every 4 min. Cells were washed with HBSS, then loaded with SF4 (5 µM) for 10 min at 37 °C. Baseline fluorescence was measured for 8 min, followed by addition of polymeric solution in each well. The images were then taken every 4 min for 80 min at 37 °C. All data were analysed by determining the mean SF4 fluorescence per well using Harmony High Content Imaging and Analysis software (v3.5.2). For each experimental condition, SF4 fluorescence was PBS (pH 7.4) vehicle-subtracted and expressed relative to the baseline fluorescence. Data were

expressed as the mean ± SEM from three independent experiments.

4.3 Results and Discussion

4.3.1 Synthesis of H_2S-releasing Polymeric Donors. Poly(glycidyl methacrylate)-based copolymers are versatile precursors, useful in the preparation of a range of functional materials, underpinned by the ability of side-chain epoxide rings to undergo ring opening reactions with a number of nucleophiles.[39-41] The general synthetic strategy used in this study for the synthesis of PGMA-based copolymers, followed by modification to yield the H_2S delivery system, is summarised in Scheme 1. Initially, benzodithioate-terminated poly((oligoethylene glycol methyl ether) methacrylate-*co*-glycidyl methacrylate) (P[OEGMA-*co*-GMA]-S(C=S)Ph) **1a** (Table 1, Entry 1) was prepared by co-polymerising oligo(ethylene glycol methyl ether) methacrylate and glycidyl methacrylate in the presence of 4-cyano-4-(thiobenzoylthio)pentanoic acid. The resulting polymer was purified and characterised by gel permeation chromatography (GPC) and ^1H nuclear magnetic resonance (NMR) spectroscopy (Figure S1 and S6, Table 1).

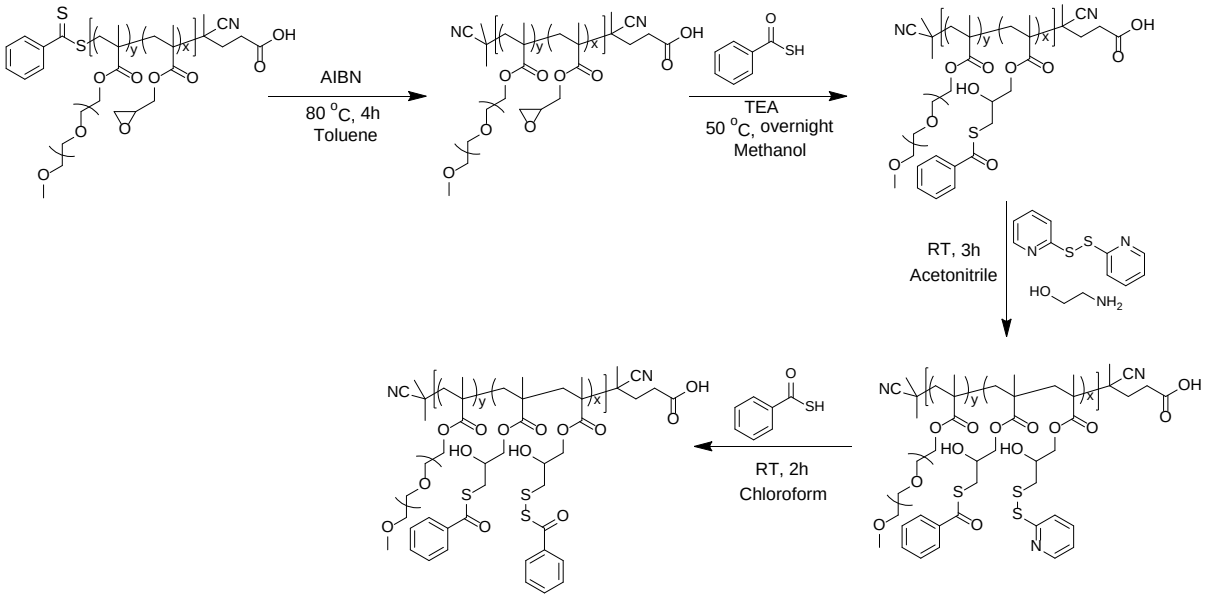

Scheme 1. Synthesis of H_2S donor **1e** by successive post-modifications of copolymer PGMA-*co*-POEGMA **1a**.

The thiocarbonylthio end-group of P[OEGMA-*co*-GMA]-S(C=S)Ph **1a** was then removed using an excess of cyano-isopropyl radicals[42] to give (P[OEGMA-*co*-GMA]) **1b** (Table 1, entry 2, Figure S2 and S6). The ring opening of the PGMA epoxide groups

was then performed with an excess of the nucleophilic reagent, thiobenzoic acid in the presence of triethylamine as the base in order to introduce -S(C=O)Ph groups (Scheme 1, step 2). Due to steric factors predominating the base catalysed nucleophilic ring opening reaction, attachment of the thiolate nucleophile is thought to occur at the least substituted and hindered carbon atom, as depicted in polymeric structures shown in Scheme 1.[40] The resulting polymer **1c,** containing 3-(benzoylthio)-2-hydroxypropyl methacrylate (BTHMA) pendant groups (which are essentially protected thiols), was confirmed by ^{1}H NMR and GPC (Table 1, Figure S3 and S6). The disappearance of NMR signals at δ 3.3, 2.9 and 2.7 ppm indicated that epoxide-ring opening had gone to completion, along with the appearance of new resonance signals (δ 7.5, 7.6, 8.0 ppm) attributed to (-S(C=O)Ph) benzothioate aromatic protons.

Table 1. Molecular weight of modified P[OEGMA-*co*-GMA] polymers.

	Polymer	$\mathbf{M_n}^a$ **(g mol^{-1})**	$\mathbf{M_n}^b$ **(g mol^{-1})**	$\boldsymbol{Đ}^c$
1a	P[OEGMA$_{22}$-*co*-GMA$_7$]-S(C=S)Ph	8000	8197	1.14
1b	P[OEGMA$_{22}$-*co*-GMA$_7$]	-	9057	1.21
1c	P[OEGMA$_{22}$-*co*-BTHMA$_7$]	-	10051	1.20
1d	P[OEGMA$_{22}$-*co*-BTHMA$_{2.8}$-*co*-PDHMA$_{4.2}$]	-	9689	1.22
1e	P[OEGMA$_{22}$-*co*-BTHMA$_{2.8}$-*co*-BDTHMA$_{4.2}$]	-	-	-

[a] Molecular weight determined by ^{1}H NMR spectroscopy. [b] Molecular weight determined by gel permeation chromatography. [c] dispersity index, ***Đ***, as determined by GPC analysis in DMAc.

In the next step, the -S(C=O)Ph groups of **1c** were converted to pyridyl disulfides, to introduce 3-(pyridyldisulfanyl)-2-hydroxypropyl methacrylate (PDHMA) repeat units into the polymer chain (**1d,** Table 1, Entry 4). Specifically, in a one-pot, deoxygenated reaction at room temperature, the benzothioate -S(C=O)Ph groups of **1c** were deprotected via aminolysis with ethanolamine into thiols -SH which then undergo thiol-disulfide exchange with the dipyridyl disulphide. The resulting polymer **1d** was purified by dialysis and characterized using GPC and ^{1}H NMR spectroscopy (Table 1, Figure S4 and S6). The characteristic signals of the benzothioate aromatic protons (δ 7.5, 7.6, 8.0 ppm) in the ^{1}H NMR spectrum are partially replaced with new resonance peaks (δ 7.1, 7.7 and 8.5 ppm) associated with the aromatic pyridyl group (Figure S4, S6). The

conversion of benzothioate to pendant pyridyl disulfides was calculated to be approximately 60%. The benzothioate peaks still evident in the ^{1}H NMR indicated that the aminolysis was incomplete. Given that there was minimal impact on the molecular weight distribution of the polymer at this step, (as reflected by the relatively unchanged polydispersity index (PDI)), this suggested that there is little loss of thiols to disulfide coupling (Table 1, Figure S6). Non-quantitative conversion of benzothioate to pyridyl disulfide could instead be due to less accessible benzothioate isomers having formed during the epoxide ring opening reaction with thiobenzoic acid, although this could not be confirmed by ^{1}H NMR. However, this is unlikely based on previous published studies looking at nucleophilic, base catalysed ring opening of epoxides using thiols. Another more likely explanation could be that hydroxyl groups formed upon epoxide ring opening could become hydrogen bonded to vicinal POEGMA brushes to create a sterically hindered environment for nucleophilic attack, a factor that would depend on the density of the OEGMA side chains. In the final step, acyl-protected perthiol donor groups (-S-S(C=O)Ph), or more specifically, 3-(benzoyldisulfanyl)-2-hydroxypropyl methacrylate (BDTHMA) groups were introduced into the polymers via the exchange reaction of pyridyl disulfide groups with thiobenzoic acid, to give **1e**. The success of the exchange reaction was monitored via the disappearance of the pyridyl aromatic proton signals and the appearance of new aromatic benzothioate proton resonances (Figure S5). The new proton resonances are consistent with those observed for the corresponding small molecule H_2S donors as well as -S-S(C=O)Ph end-functional polymers.[24, 36]

The resulting copolymer, P[OEGMA$_{22}$-*co*-BTHMA$_{2.8}$-*co*-BDTHMA$_{4.2}$] **1e** was then dispersed in phosphate buffered saline (pH 7.4) and the potential formation of self-assemblies was assessed using dynamic light scattering (DLS) giving a number average hydrodynamic particle diameter of 4.5 nm with a polydispersity of 0.22 over successive measurements (Figure S7). Given the small size, we reasoned that these particles were likely to be either single polymer chains or aggregates of 2-3 chains, however more tests would be needed to confirm this.

Having confirmed the formation of the model H_2S donor copolymer system, the same synthetic approach was applied to the block copolymer system, poly(glycidyl methacrylate)-*block*-poly(oligo(ethylene glycol) methyl ether methacrylate)-*block*-poly(styrene), P[GMA-*b*-POEGMA-*b*-PSt], which assembles into spherical and worm-

like micelles. In this system the functionalisation of the PGMA domains is confined to the surface of the micelles, which we reasoned would have a strong impact on subsequent H_2S release kinetics. Firstly, PGMA, homopolymer **2a** (Table 2) was prepared and characterised (GPC and ^{1}H NMR, Table S1, Figures S8 and S11). The purified PGMA was then chain extended with OEGMA (MW = 300 g mol^{-1}) to give P[GMA-*b*-OEGMA] block copolymer **2b** (Table 2 and S1, Figure S9 and S11). Spherical and worm-like micelles were then prepared using P[GMA-*b*-OEGMA] **2b** as the macromolecular RAFT agent, via polymerization-induced self-assembly (PISA) with styrene as both monomer and co-solvent (Table S1, Figure S10 and S11).[43] The PISA process facilitated the incorporation of 132 and 282 units of styrene per P[GMA-*b*-OEGMA] chain, to form spherical (**3a**) and worm-like (**4a**) micelles respectively, with size and shape examined using DLS and transmission electron microscopy (TEM) (Figure 1 and S15, Table S1). After purification by dialysis against methanol the nanoparticles underwent the epoxide ring opening reaction to yield **3b**, spherical micelles functionalised with benzothioate (-S(C=O)Ph) moieties, as confirmed by ^{1}H NMR. Retention of shape and size was confirmed by DLS and TEM (Figures 1, S12 and S15). The benzothioate functionality was then converted into pyridyl disulfide units to give **3c**, with a conversion of approx. 50 %. As previously, this was approximated by comparing the aromatic pyridyl resonances at δ 8.5 ppm to the benzothioate proton signals at δ 8.0 ppm (Figure S13). Pyridyl-conjugated polymers were then modified by thiol-disulfide exchange to BDTHMA-functional spherical micelles, **3d**, as characterised by ^{1}H NMR (Figures S14 and S15). The stability of the polymeric spherical micelle was confirmed by TEM and DLS after each reaction step (Figure 1 and S15). Importantly, TEM analysis (Figure 1) revealed that the spherical morphology remained unchanged during the post-polymerization modifications, and DLS showed that a number average particle size of ~ 25 nm was maintained throughout the modifications (Figure S15, Table S1).

Table 2. Polymers prepared with PISA and subsequently functionalised with H_2S donating groups

	Polymers	s/w[a]	M_n[b] (g mol^{-1})	M_n[c] (g mol^{-1})	$Đ$[d]
2a	P[GMA_7]-S(C=S)Ph	-	1259	2691	1.20
2b	P[GMA_7-*b*-$OEGMA_{29}$]-S(C=S)Ph	-	9959	9157	1.12
3a	P[GMA_7-*b*-$OEGMA_{29}$-*b*-St_{132}]-S(C=S)Ph	s	23317	23773	1.22
3b	P[$BTHMA_7$-*b*-$OEGMA_{29}$-*b*-St_{132}]	s	-	-	-
3c	P[$BTHMA_{3.5}$-*co*-$PDHMA_{3.5}$-*b*-$OEGMA_{29}$-*b*-St_{132}]	s	-	-	-
3d	P[$BTHMA_{3.5}$-*co*-$BDTHMA_{3.5}$-*b*-$OEGMA_{29}$-*b*-St_{132}]	s	-	-	-
4a	P[GMA_7-*b*-$OEGMA_{29}$-*b*-St_{282}]-S(C=S)Ph	w	38441	27092	1.41
4b	P[$BTHMA_7$-*b*-$OEGMA_{29}$-*b*-St_{282}]	w	-	-	-
4c	P[$BTHMA_{1.8}$-*co*-$PDHMA_{5.2}$-*b*-$OEGMA_{29}$-*b*-St_{282}]	w	-	-	-
4d	P[$BTHMA_{1.8}$-*co*-$BDTHMA_{5.2}$-*b*-$OEGMA_{29}$-*b*-St_{282}]	w	-	-	-

[a] 's' refers to spherical micelles produced by PISA and 'w' refers to worm-like micelles as produced PISA [b] M_n determined by ^{1}H NMR spectroscopy via integration of aromatic RAFT end groups versus individual monomer resonances, as described in the experimental section.[c] M_n determined by GPC in *N*,*N*-dimethylacetamide (DMAc, 0.03 % w/v LiBr, 0.05 % BHT) using a conventional calibration curve with polystyrene standards. [d] dispersity index, $Đ$, as determined by GPC analysis in DMAc.

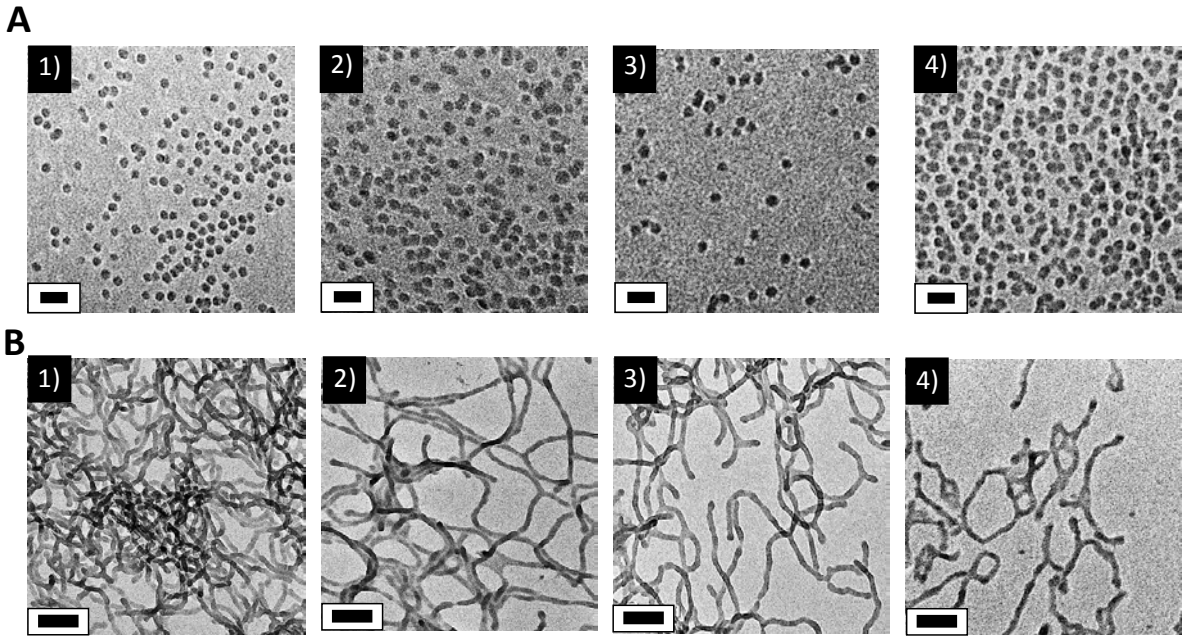

Figure 1. Representative TEM images of individual surface-functional spherical (A, top) and worm-like (B, bottom) micelles after each post-polymerization step (scale bar: (A): 50 nm, (B): 100 nm): 1) initial spherical **3a** (22.5 ± 3.03 nm) and worm-like **4a** micelles (26.1 ± 3.97 nm); 2) After epoxide-ring opening reaction to form spherical **3b** (20.7 ± 3.62 nm) and worm-like **4b** micelles (27.8 ± 4.57 nm); 3) After aminolysis of benzothioate groups by ethanolamine in the presence of dipyridyl disulfide to form pyridyl disulfide-conjugated spherical **3c** (24.2 ± 5.18 nm) and worm-like **4c** micelles (29.1 ± 4.68 nm); 4) After thiol-disulfide exchange reaction with an excess of thiobenzoic acid to produce H_2S donating spherical **3d** (20.8 ± 2.88 nm) and worm-like **4d** micelles (22.8 ± 3.91 nm).

The same post-modification procedure was employed to prepare H_2S releasing, self-assembled worm-like micelles, P[BTHMA-*co*-BDTHMA-*b*-OEGMA-*b*-St] **4d** from **2b**, as described in greater detail in the experimental section and supporting information. As for the spherical micelles, similar TEM observations were also made for the worm-like morphology: the particle shape and size remained largely unaffected after each post-polymerization process. It is possible that purification via dialysis was a contributing factor to maintenance of morphology and size.

4.3.2 Examination of H_2S Releasing Capacity from Post-Modified Polymer System. The H_2S releasing polymer and polymeric nanoparticles were then examined for their propensity to release H_2S when triggered by exposure to the model thiol, L-cysteine, using an H_2S-selective amperometric microsensor.[44]

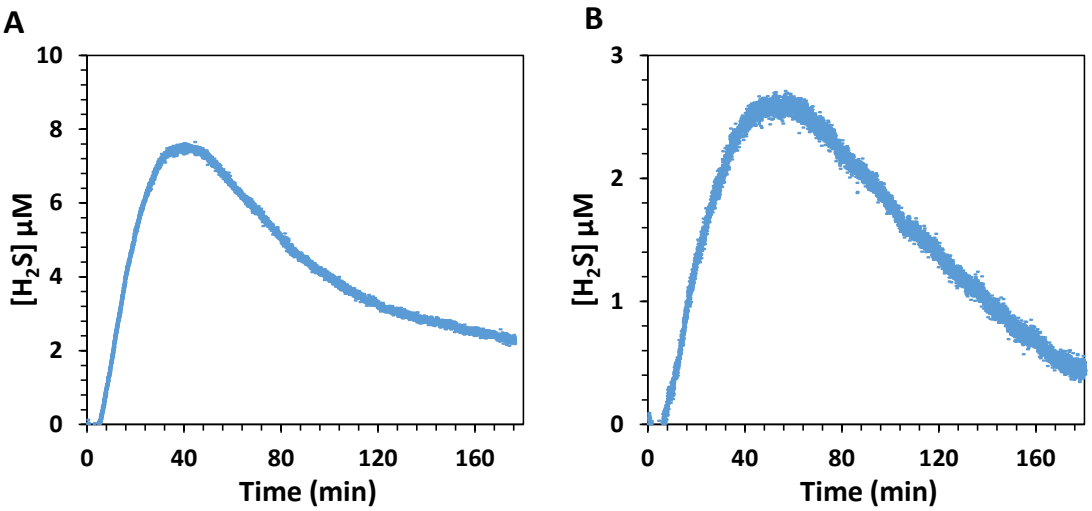

Figure 2. (A) Electrochemical H_2S release from **1e** (1.4 mg of polymer, 0.71 µmoles, 143 µM = [H_2S donors]) in the presence of L-cysteine (4.65 molar equiv., 3.3 µmoles, 660 µM) in PBS at pH 7.4 (5 mL). Note: L-cysteine was added at t = 5 min. (B) Electrochemical H_2S release response from **3d** spherical micelles (4.73 mg polymer, 0.71 µmoles, 143 µM = [H_2S donors]) in the presence of L-cysteine (4.65 molar equiv., 3.3 µmoles, 660 µM) in PBS at pH 7.4 (5 mL). Note: L-cysteine was added at t = 5 min.

H_2S release (in µM) was measured over time for a solution of BDTHMA-modified copolymer **1e,** dissolved in PBS pH 7.4. Figure 2(A) shows that H_2S was not detected in the absence of L-cysteine (first 5 minutes). When exposed to L-cysteine, the evolution of H_2S is observed, increasing to a peaking time of 41 min (Table 3) followed by a gradual decrease in H_2S signal. We then examined whether the self-assembled BDTHMA-surface functionalised nanoparticles, **3d** and **4d**, could also release H_2S under the same conditions. Upon treatment with L-cysteine, a similar surge in H_2S concentration is detected from **3d** spherical micelles (Figure 2B). A similar thiol-triggered H_2S release profile was also detected for worm-like micelles **4d** (Figure S20). Altogether, these results indicated that nanoparticles were successfully modified into thiol-stimulated H_2S donor systems.

Table 3. Release characteristics of H_2S donor polymers with L-Cys[a] at pH 7.4[b] as measured by Amperometry.

Polymer	Peaking time[c] (min)	Peaking $[H_2S]$[d] (µmol/L)	$[sulfides]_{tot}$[e] (µmol/L)	$[H_2S$ donors$]$[f] (µmol/L)	Sulfides released (MPC) (%) [g]
1e	41	7.6	25.8	142	18
3d	48	2.6	8.8	142	6.2
4d	48	1.3	4.4	142	3.1

[a] 3.3 µmole aliquot of L-Cys added, final concentration = 660 µM. [b] Measured in PBS pH 7.4 [c] Time taken to reach highest concentration value on the curve of $[H_2S]$ vs time after L-cysteine added. [d] Highest µmol/L H_2S value attained on the curve of $[H_2S]$ vs time. [e] Total sulfides concentration = $[sulfides]_{tot} = [H_2S] + [HS^-]$, where $[sulfides]_{tot} = [H_2S] \times (10^{pH-pK1} + 1) = 3.40 \times [H_2S]$ (see Supporting Information for explanation of equations). [f] $[H_2S$ donors$] = n(H_2S$ donors$)/0.005$, where 5mL = total volume in reaction vessel for microsensor testing. $n(H_2S$ donors$)$ = (average number of units in each chain) × n(polymer); average number of units in each chain is estimated from conversion by ^{1}H NMR as displayed in Tables 1 and 2 and n(polymer) = mass polymer (g) /M_n (^{1}H NMR) where M_n (1e, 3d and 4d) = 8000, 23317, 38441 g/mol respectively. Mass of polymer is varied per measurement so that $[H_2S$ donor$]$ is the same. [g] % sulfides released (measured at peaking concentration, MPC) = $[sulfides]_{tot}/[H_2S$ donors$]$.

In aqueous buffer an ionization equilibrium exists between H_2S and HS^- which is taken into consideration in order to make relative quantitative assessments of H_2S donation. The total concentration of dissolved sulfide species in solution, $[sulfides]_{tot}$, encompasses both species $[H_2S] + [HS^-]$ which exist in relative proportions as determined by pH. The amperometric sensor only detects partial pressure of H_2S and thus accounts for only one component of the total sulfides. Using the known equilibrium constant K_1 for the dissociation of H_2S in water, $[sulfides]_{tot}$ can be calculated from $[H_2S] \times (10^{pH-pK1} + 1)$, which simplifies to $[H_2S]_{detected} \times 3.40$ (as defined further in the Supporting Information (section A.1/2). The $[sulfides]_{tot}$ measured at peaking concentration (MPC), with respect to initial $[H_2S$ donors$]$, can be taken as a measure of efficiency of H_2S donation (column 6, table 3), as calculated for the three polymer systems.

Referring to Table 3, the highest peaking $[sulfides]_{tot}$ was produced from the H_2S donor copolymer, **1e**, followed by spherical particles **3d** and then worm-like micelles **4d**. Since the same concentration of H_2S donor was used in each measurement, this translated to the same scale of % Sulfides released (MPC), with **1e** > **3d** > **4d**. This result correlated with what we observed for the conversion of PGMA functional group eventually into H_2S donating BDTHMA functionalised copolymer, with **1e** conversion

(65%) > **3d** conversion (50%) > **4d** (25%). We reason that a sterically hindered environment for nucleophilic attack had been produced in the PISA self-assemblies due to a higher density of OEGMA side chains, and that this could also correlate to there being less accessible (to thiol attack) H_2S donating groups present in these assemblies.

As previously indicated, H_2S donating BDTHMA -S-S(C=O)Ph groups are acyl-protected perthiol donors that release H_2S by a comparable mechanism to the corresponding small molecule donors (as shown in Scheme S1). In our previous work supporting this mechanism, we observed some broadening of the MWD of polymers upon release of H_2S, consistent with the formation of polymeric coupled product. These products can form through reaction of generated polymeric thiol with the protected perthiol (as shown in Scheme S2). We reason that such coupled polymeric bi-products which form during the reaction of -S-S(C=O)Ph groups with cysteine may also create an impenetrable environment for further thiol attack. Furthermore, higher molecular weight coupled products are formed during the synthesis of spherical and worm-like micelles (**3a** and **4a**) which could also enhance this effect.[36]
All three H_2S donor polymers showed a comparable H_2S releasing peaking time, which is the time to reach the maximum [H_2S], with the PISA-derived self-assemblies showing slightly longer times to reach a maximum value.

4.3.3 Intracellular H_2S release U2OS Live-Cell Imaging. We examined the ability of these self-assembled nanoparticles to efficiently deliver H_2S into a cellular environment. In these cell studies, no exogenous thiol compounds were added since the aim was to confirm whether there were sufficient intracellular thiols present to stimulate the release. The chemoselective H_2S-responsive fluorescent probe SF4, which becomes fluorescent (λ=520 nm) in the presence of H_2S, was used.[38] We applied 4 different self-assembled nanoparticles to the cells: (i) H_2S donor spherical micelles P[BTHMA-*co*-BDTHMA-*b*-OEGMA-*b*-St] **3d** (ii) non-H_2S donating control spherical micelles (formed by pre-exposure of **3d** to L-cysteine, described above and in the supporting information **3e** (Figure S21)), (iii) H_2S donor short-worm like micelles **4e** (formed by sonicating P[BTHMA-*co*-BDTHMA-*b*-OEGMA-*b*-St] **4d**, described above and in the supporting information (Figure S19)), and (iv) control short worm-like micelles **4f** (described above and in the supporting information (Figure S22)). All experiments were conducted both with and without SF4 probe.

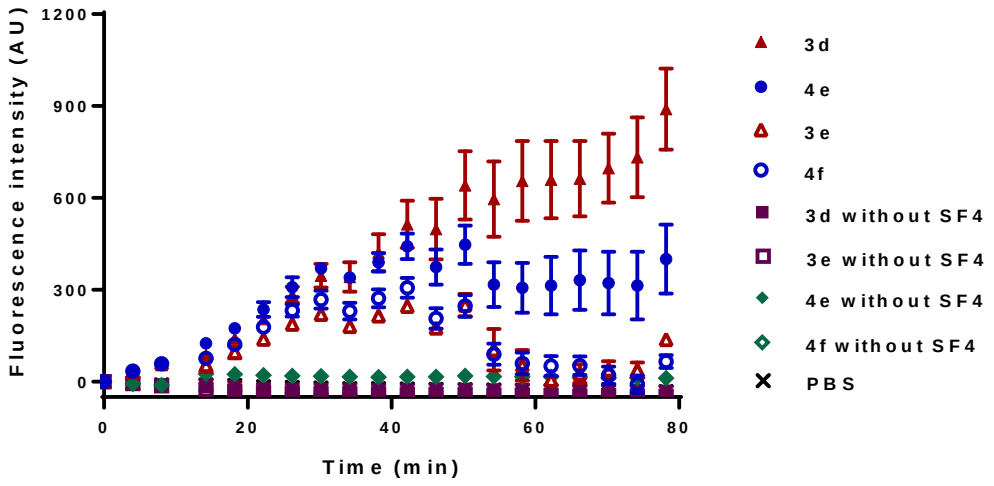

Figure 3. Fluorescence intensity of SF4 probe (5 µM) for H_2S detection over time in U2OS cells in response to the addition of PBS (pH 7.4), H_2S donor spherical micelles **3d** (0.60 mg/mL, 90 µM), control spherical micelles **3e** (0.60 mg/mL, 90 µM), H_2S donor short worm-like micelles **4e** (1.98 mg/mL, 90 µM) and control short worm-like micelles **4f**, made from **4d** (1.98 mg/mL, 90 µM), all prepared in PBS (pH 7.4). Note: Symbols represent means and error bars SEM from each independent experiment conducted in triplicate. ***$p < 0.01$ vs PBS, one-way ANOVA with Dunnett's multiple comparison test.

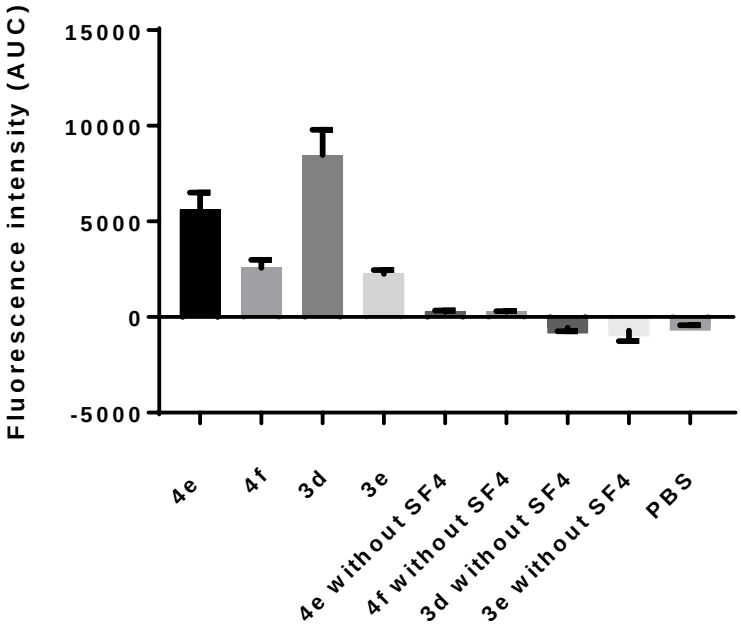

Figure 4. Fluorescence intensity (AUC, Area Under the Curve) derived from the time course SF4 probe test in U2OS cells (Figure 5). Note: bars represent means and error bars SEM from each independent experiment conducted in triplicate. ***$p < 0.01$ vs PBS, one-way ANOVA with Dunnett's multiple comparison test.

Firstly, cells were pre-loaded with SF4 for 10 min to measure the baseline fluorescence, followed by the addition of the different polymers. Fluorescence intensity

was detected every 4 min for 90 min. Figure 3 and Figure 4 show that H_2S donor spherical micelles **3d** and H_2S donor short worm-like micelles **4e** (formed from **4d**) were able to cause a substantial increase in intracellular SF4 fluorescence over time, as compared to control polymers (**3e**, **4f**) and polymers (**3d**, **4e**) without added SF4, even in the absence of exogenous thiol compounds. Moreover, H_2S donor spherical micelles **3d** showed higher fluorescence signals compared to H_2S donor short worm-like micelles **4e** over time, without any addition of exogenous thiol. In the control experiments, there was no change in SF4 fluorescence when PBS was added, as well as when no SF4 was applied (Figure 3). Notably some SF4 fluorescence was still observed, though much less, in the cells treated with control polymers in the presence of SF4 probe (Figure 3 and Figure 4). Indeed it is possible for SF4's azide groups to be reduced by endogenous reducing agents including thiols to elicit some background fluorescence.[45] Furthermore, endogenous production of H_2S could elicit some intracellular fluorescence. Importantly, the SF4 fluorescence from these control polymers attenuated over time to near zero fluorescence (Figure 3). As such, these results demonstrate that the H_2S donor spherical micelles **3d** and short worm-like micelles **4e** are capable of releasing H_2S inside the live U2OS cells, in a sustained and prolonged manner. Moreover, this release of H_2S is triggered by intracellular thiols and does not require the application of any exogenous trigger.

4.3.4 Effects of H_2S Donating Self-Assembled Nanoparticles to Improve DOX sensitivity on U2OS Cells. Doxorubicin (DOX), also known as Adriamycin, is a chemotherapy medication used to clinically treat a range of cancers.[46] However, along with side effects such as cardiotoxicity, the effectiveness of DOX in treating cancer is limited by the ease with which cancer cells develop resistance to it. Such resistance occurs via through a number of mechanisms. One such mechanism is through the cancer cells effluxing the drug using their highly expressed protein pumps, such as P-glycoprotein and MRP pumps, thus limiting intracellular concentration and toxicity.[47]

Nitric oxide has been shown to revert the resistance to DOX in human colon cancer cells by inhibiting the efflux pumps,[48] and therefore, nitric oxide donors conjugated to DOX have been explored for increasing accumulation of DOX and cytotoxicity.[49] Interestingly, H_2S donating compounds conjugated to DOX have been applied to U-2OS osteosarcoma cells with increasing degrees of DOX-resistance, with a number displaying significantly more potent cytotoxic effects compared to DOX alone.[18] On

the basis of these results, we postulated that H_2S-donating polymers might have potential as adjuvants in combination with doxorubicin. Specifically, we investigated the cytotoxic effect of combined delivery of H_2S with DOX on U2OS osteosarcoma cells using our self-assembled H_2S-donating nanoparticles. The cells were co-incubated with DOX (9 µM) and a range of concentrations of H_2S releasing, self-assembled spherical micelles **3d** 0.06 – 0.60 mg/mL (9 - 90 µM of H_2S releasing groups) and non-H_2S releasing, control spherical micelles **3e**. The control nanoparticles **3e** were prepared by pre-exposing the donor particles to L-cysteine to ensure that the H_2S donors had been exhausted prior to applying the particles to cells, as described in supporting information (section A.3)). As described further in Supporting Information, pre-exposure to L-cysteine produces a mixture of non-H_2S donors, (Scheme S1, S2, and Figure S21).

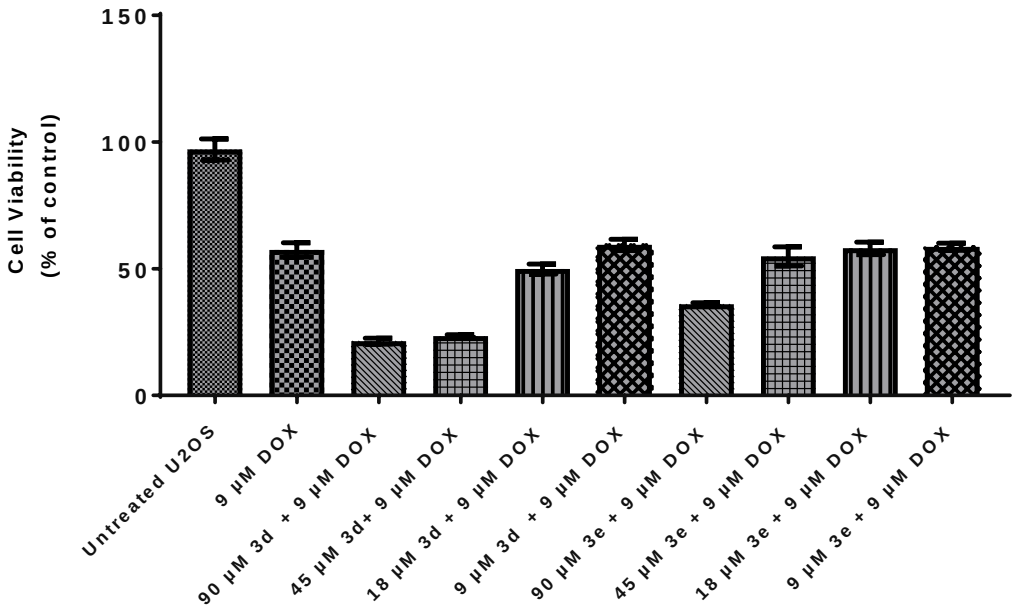

Figure 5. Cytotoxicity of doxorubicin (DOX) on U2OS cells co-incubated with and without self-assembled H_2S donor **3d** spherical micelles (0.06 – 0.60 mg/mL, 9 - 90 µM of H_2S releasing groups), and non-H_2S donating control **3e** spherical micelles (0.06 – 0.60 mg/mL, 9 - 90 µM of non-H_2S releasing groups), as determined by Real-time Luminescent cell viability assay. Note: all toxicity studies have been repeated in triplicate.

Cells co-incubated with H_2S donor spherical micelles **3d** and DOX were more sensitive to DOX toxicity compared to control spherical micelles **3e** and native DOX treatment (Figure 5). This synergistic cytotoxic effect was more profound when higher concentrations (90 µM, 45 µM) of H_2S donor spherical micelles were used in the co-incubation with DOX (9 µM). Specifically, co-treatment of 45 µM H_2S donor spherical

micelles **3d** with DOX (9 μM) inhibited cell viability (%) twice as much as when the same concentration of control spherical micelles **3e** was used. In contrast, co-administration of the control particles **3e** at an equivalent concentration with DOX (9 μM) gave no further decrease in cell viability compared to native DOX treatment. Overall this indicates that H_2S releasing nanoparticles increase the susceptibility of U2OS cells to DOX cytotoxicity, a result consistent with earlier results using DOX-H_2S-donor conjugates.

Following confirmation that H_2S releasing spherical micelles can enhance DOX toxicity to U2OS cells, we decided to investigate the cytotoxicity of H_2S donor worm-like micelles **4d** and control worm-like micelles with the same concentration of DOX (9 μM) (Figure 6). Prior to testing, the long worm-like micelles were sonicated under mild conditions to produce shorter worm-like micelles **4e**, in order to facilitate cell uptake (Figure S19).[50, 51] Similar results were obtained with H_2S-donor short worm-like micelles as for the spherical micelles. Specifically, co-incubation of H_2S donor short worm-like micelles **4e** (45 μM) with DOX (9 μM) resulted in higher cytotoxic effects than co-treatment of control short worm-like micelles **4f** (45 μM) with DOX and native DOX treatment. A 2× reduction in cell viability (%) was observed with co-treatment of H_2S releasing short worm-like micelles **4e** with DOX as compared to control short worm-like polymer nanoparticles **4f** with DOX. Interestingly, the control worm-like micelles **4f** did lead to some enhancement in toxicity above native DOX treatment, although this was nowhere near as profound as that observed with the H_2S-releasing worm-like nanoparticles.

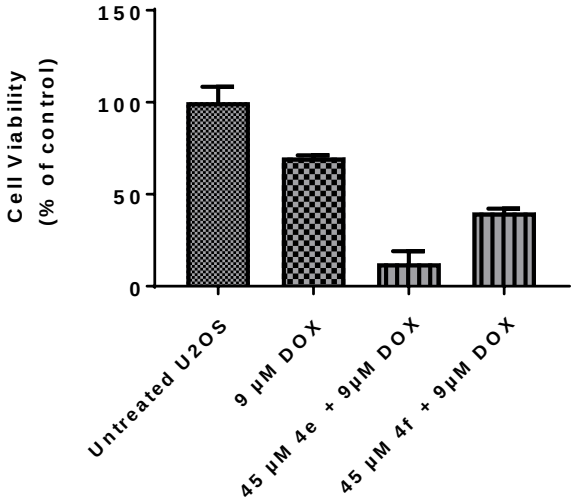

Figure 6. Cytotoxicity of doxorubicin (DOX) on U2OS cells co-incubated with and without H_2S donor, self-assembled, short worm-like micelles **4e** (made from **4d)** (0.99 mg/mL, 45 µM = H_2S releasing groups), and control short worm-like micelles **4f**. (as in Figure S22, 0.99 mg/mL, 45 µM = non H_2S releasing groups) as determined by real-time Luminescent Cell Viability Assay. Note: all toxicity studies have been repeated in triplicate.

4.4 Conclusion

In this study, post-polymerization transformations of poly(glycidyl methacrylate) (PGMA) were exploited to prepare H_2S donor polymers. Epoxide functional polymer-based nanoparticles with different morphologies were first synthesized, and then modified through a series of post-modification processes using several thiol chemistry reactions. These chemically modified polymers were found to successfully release H_2S in the presence of L-cysteine. This facile methodology provides the first approach of post-polymerisation modification of PGMA into thiol-triggerable H_2S polymeric donor systems. Moreover, these H_2S donor polymers were effective at releasing H_2S inside cells upon exposure to endogenous thiols. Delivery of H_2S from the self-assembled nanoparticles in combination with DOX was also examined on U2OS osteosarcoma cells, with higher cytotoxicity observed compared to control polymers with DOX or native DOX treatment. This indicated that H_2S releasing nanoparticles strongly influenced DOX cytotoxicity in U2OS cell lines with decreasing degree of DOX resistance via through increasing H_2S inside the cells. The results presented here demonstrate that H_2S-donating polymeric nanoparticles, combined with chemotherapeutics, may provide a promising avenue for treatment of chemoresistant cells.

Acknowledgements

This work was supported by the Australian Research Council (ARC) Centre of Excellence in Convergent Bio-Nano Science and Technology (Project No. CE140100036). J.F.Q. acknowledges receipt of a Future Fellowship from the ARC (FT170100144), and T.P.D. the award of an Australian Laureate Fellowship from the ARC (FL140100052). Electron microscopy was performed at the Bio21 Advanced Microscopy Facility, The University of Melbourne.

Associated Content

Supporting Information

The Supporting Information is available free of charge on the ACS Publications website at DOI: 10.1021/acs.biomac,XXXXX.

Author Information

Corresponding Author

*E-mail: thomas.p.davis@monash.edu, john.f.quinn@monash.edu.

Author Contributions

The manuscript was written through contributions of all authors. All authors have given approval to the final version of the manuscript.

Notes

The authors declare no competing financial interest.

4.5 Reference

1. R. Wang, *Trends Biochem. Sci.*, 2014, **39**, 227-232.
2. R. Wang, *FASEB J.*, 2002, **16**, 1792-1798.
3. R. O. Beauchamp, J. S. Bus, J. A. Popp, C. J. Boreiko and D. A. Andjelkovich, *CRC Crit. Rev. Toxicol.*, 1984, **13**, 25-97.
4. R. Wang, *Sci. Am.*, 2010, **302**, 66-71.
5. G. D. Yang, L. Y. Wu, B. Jiang, W. Yang, J. S. Qi, K. Cao, Q. H. Meng, A. K. Mustafa, W. T. Mu, S. M. Zhang, S. H. Snyder and R. Wang, *Science*, 2008, **322**, 587-590.
6. J. V. R. Medeiros, V. H. Bezerra, A. S. Gomes, A. L. R. Barbosa, R. C. P. Lima, P. M. G. Soares, G. A. C. Brito, R. A. Ribeiro, F. Q. Cunha and M. Souza, *J Pharmacol. Exp. Ther.*, 2009, **330**, 764-770.
7. X. L. Wang, Q. Wang, W. Guo and Y. Z. Zhu, *Biosci. Rep.*, 2011, **31**, 87-98.
8. H. Kimura, Y. Nagai, K. Umemura and Y. Kimura, *Antioxid. Redox Signal.*, 2005, **7**, 795-803.
9. K. Qu, S. W. Lee, J. S. Bian, C. M. Low and P. T. H. Wong, *Neurochem. Int.*, 2008, **52**, 155-165.
10. L. Y. Wu, W. Yang, X. M. Jia, G. D. Yang, D. Duridanova, K. Cao and R. Wang, *Lab. Investig.*, 2009, **89**, 59-67.
11. J. L. Wallace, M. Dicay, W. McKnight and G. R. Martin, *FASEB J.*, 2007, **21**, 4070-4076.
12. G. Caliendo, G. Cirino, V. Santagada and J. L. Wallace, *J. Med. Chem.*, 2010, **53**, 6275-6286.
13. L. Li and P. K. Moore, *Trends Pharmacol. Sci.*, 2008, **29**, 84-90.
14. L. Li, P. Rose and P. K. Moore, in *Annu. Rev. Pharmacol. Toxicol., Vol 51, 2011*, ed. A. K. Cho, 2011, vol. 51, pp. 169-187.
15. J. Furne, A. Saeed and M. D. Levitt, *American Journal of Physiology-Regulatory Integrative and Comparative Physiology*, 2008, **295**, R1479-R1485.
16. F. Ercole, F. M. Mansfeld, M. Kavallaris, M. R. Whittaker, J. F. Quinn, M. L. Halls and T. P. Davis, *Biomacromolecules*, 2016, **17**, 371-383.
17. Z. W. Lee, J. B. Zhou, C. S. Chen, Y. J. Zhao, C. H. Tan, L. Li, P. K. Moore and L. W. Deng, *Plos One*, 2011, **6**.
18. K. Chegaev, B. Rolando, D. Cortese, E. Gazzano, I. Buondonno, L. Lazzarato, M. Fanelli, C. M. Hattinger, M. Serra, C. Riganti, R. Fruttero, D. Ghigo and A. Gasco, *J Med. Chem.*, 2016, **59**, 4881-4889.
19. A. Sparatore, G. Santus, D. Giustarini, R. Rossi and P. Del Soldato, *Expert Rev. Clin. Pharmacol.*, 2011, **4**, 109-121.
20. X. Gu and Y. Z. Zhu, *Expert Rev. Clin. Pharmacol.*, 2011, **4**, 123-133.
21. L. Li, M. Whiteman, Y. Y. Guan, K. L. Neo, Y. Cheng, S. W. Lee, Y. Zhao, R. Baskar, C.-H. Tan and P. K. Moore, *Circulation*, 2008, **117**, 2351.
22. Y. Zhao, T. D. Biggs and M. Xian, *Chem. Commun.*, 2014, **50**, 11788-11805.
23. J. L. Wallace, *Trends Pharmacol. Sci.*, **28**, 501-505.
24. Y. Zhao, S. Bhushan, C. Yang, H. Otsuka, J. D. Stein, A. Pacheco, B. Peng, N. O. Devarie-Baez, H. C. Aguilar, D. J. Lefer and M. Xian, *ACS Chem. Biol.*, 2013, **8**, 1283-1290.
25. T. Roger, F. Raynaud, F. Bouillaud, C. Ransy, S. Simonet, C. Crespo, M.-P. Bourguignon, N. Villeneuve, J.-P. Vilaine, I. Artaud and E. Galardon,

ChemBioChem, 2013, **14**, 2268-2271.
26. J. L. Wallace, G. Caliendo, V. Santagada, G. Cirino and S. Fiorucci, *Gastroenterology*, **132**, 261-271.
27. J. Kang, Z. Li, C. L. Organ, C.-M. Park, C.-t. Yang, A. Pacheco, D. Wang, D. J. Lefer and M. Xian, *J. Am. Chem. Soc.*, 2016, **138**, 6336-6339.
28. U. Hasegawa and A. J. van der Vlies, *Bioconjugate Chem.*, 2014, **25**, 1290-1300.
29. U. Hasegawa and A. J. van der Vlies, *MedChemComm*, 2015, **6**, 273-276.
30. K. Kashfi and K. R. Olson, *Biochem. Pharmacol.*, 2013, **85**, 689-703.
31. J. C. Foster, C. R. Powell, S. C. Radzinski and J. B. Matson, *Org. Lett.*, 2014, **16**, 1558-1561.
32. Y. Zhao, J. Kang, C.-M. Park, P. E. Bagdon, B. Peng and M. Xian, *Org. Lett.*,, 2014, **16**, 4536-4539.
33. Y. Zhao, H. Wang and M. Xian, *J. Am. Chem. Soc.*, 2011, **133**, 15-17.
34. T. R. Long, A. Wongrakpanich, A.-V. Do, A. K. Salem and N. B. Bowden, *Polym. Chem.* 2015, **6**, 7188-7195.
35. F. Ercole, M. R. Whittaker, M. L. Halls, B. J. Boyd, T. P. Davis and J. F. Quinn, *Chem. Commun.*, 2017, **53**, 8030-8033.
36. S. H. Yu, F. Ercole, N. A. Veldhuis, M. R. Whittaker, T. P. Davis and J. F. Quinn, *Polym. Chem.*, 2017, **8**, 6362-6367.
37. J. Chiefari, Y. K. Chong, F. Ercole, J. Krstina, J. Jeffery, T. P. T. Le, R. T. A. Mayadunne, G. F. Meijs, C. L. Moad, G. Moad, E. Rizzardo and S. H. Thang, *Macromolecules*, 1998, **31**, 5559-5562S.
38. V. S. Lin, A. R. Lippert and C. J. Chang, *Proc. Natl. Acad. Sci. U S A*, 2013, **110**, 7131-7135.
39. Q. L. Li, W. X. Gu, H. Gao and Y. W. Yang, *Chem. Commun.*, 2014, **50**, 13201-13215.
40. I. Gadwal, M. C. Stuparu and A. Khan, *Polym. Chem.*, 2015, **6**, 1393-1404.
41. E. M. Muzammil, A. Khan and M. C. Stuparu, *RSC Adv.*, 2017, **7**, 55874-55884
42. S. Perrier, P. Takolpuckdee and C. A. Mars, *Macromolecules*, 2005, **38**, 2033-2036.
43. L. Esser, N. P. Truong, B. Karagoz, B. A. Moffat, C. Boyer, J. F. Quinn, M. R. Whittaker and T. P. Davis, *Polym. Chem.*, 2016, **7**, 7325-7337.
44. P. Jeroschewski, C. Steuckart and M. Kuhl, *Anal. Chem.*, 1996, **68**, 4351-4357.
45. J. V. Staros, H. Bayley, D. N. Standring and J. R. Knowles, *Biochem. Biophys. Res. Commun.* 1978, **80**, 568-572.
46. O. Tacar, P. Sriamornsak and C. R. Dass, *J. Pharm. Pharmacol.*, 2013, **65**, 157-170.
47. M. M. Gottesman, *Annu. Rev. Med.*, 2002, **53**, 615-627.
48. C. Riganti, E. Miraglia, D. Viarisio, C. Costamagna, G. Pescarmona, D. Ghigo and A. Bosia, *Cancer Res.*, 2005, **65**, 516.
49. K. Chegaev, C. Riganti, L. Lazzarato, B. Rolando, S. Guglielmo, I. Campia, R. Fruttero, A. Bosia and A. Gasco, *ACS Med. Chem. Lett.* 2011, **2**, 494-497.
50. N. P. Truong, J. F. Quinn, M. R. Whittaker and T. P. Davis, *Polym. Chem.*, 2016, **7**, 4295-4312.
51. N. P. Truong, M. R. Whittaker, C. W. Mak and T. P. Davis, *Expert Opin. Drug. Deliv.*, 2015, **12**, 129-142.

Supporting Information

Development of a shape-controlled H_2S delivery system using epoxide-functional nanoparticles for improving chemosensitivity in osteosarcoma cells.

Sul hwa Yu,[a] Lars Esser,[a] Song Yang Khor,[a] Danielle Senyschyn,[a] *Nicholas A. Veldhuis,[a,b] Michael R. Whittaker,[a] Francesca Ercole,[a] John F. Quinn[a]* and Thomas P. Davis[a,c]**

[a] ARC Centre of Excellence in Convergent Bio-Nano Science & Technology, Monash Institute of Pharmaceutical Sciences, Monash University, Parkville, VIC 3052, Australia

[b]Drug Discovery Biology Theme, Monash Institute of Pharmaceutical Sciences, Monash University, Parkville, VIC 3052, Australia

[c] Department of Chemistry, University of Warwick, Coventry CV4 7AL, United Kingdom

A.1 Amperometric H_2S Sensing

The H_2S-generating capability of polymers was examined via an amperometric sensor using a H_2S microsensor manufactured by Unisense A/S.

Calibration of the sensor was performed after the sensor signal had stabilized over a prepolarization period (usually 2 hours or more). A 2.0 mM stock solution of Na_2S was prepared anaerobically by dissolving a known quantity of the salt into N_2-flushed, deionized water in a closed container. The acidic calibration buffer prepared by adding aqueous HCl to PBS at pH 7.4. A pH value < 4 (normally 3.8) was deoxygenated for 20 minutes by bubbling with N_2 gas. 20 mL of the acidic buffer was transferred to a nitrogen-flushed bottle equipped with a stirrer, which was capped with a septum. The sensor was then immersed into the solution via a specialized opening on the septum which enabled the bottle to be capped after the sensor tip had been passed through. Once the signal stabilized to a low, stable reading, the value was recorded and assumed to correspond to the zero [H_2S] value. Calibration points within the expected range of measurement were collected by injecting known amounts of Na_2S stock solution using a micro-syringe into the stirred calibration buffer solution. The current increased upon addition of the first aliquot and reached a plateau after several seconds. Further calibration values were obtained as subsequent aliquots were added (six in total, ranging from 10 – 160 µL). The recorded data was used to generate a linear calibration plot for [H_2S] vs. current (amps).[1,2]

L-cysteine mediated H_2S-generating capability of polymers was examined; polymer (0.71 µmoles) in deoxygenated pH 7.4 PBS (5 mL) and L-cysteine (33 mM) in deoxygenated PBS at pH 7.4 were prepared respectively. The sensor was immersed into the polymer solution, which then used the septum for minimizing exposure to air on immersing the sensor into the solution. Then, 50 µL of L-cysteine solution was injected slowly into the stirring polymer solution using a micro-syringe. All the time points were recorded when the experiments was started and the cysteine was added.

A.2 H_2S kinetics considerations

H_2S is a weak acid, which can be ionized into HS^- and S^{2-}. The ionization equilibrium between H_2S and HS^-/S^{2-} has to be established.[1]

The total concentration of sulfides in solution can be described as $[sulfides]_{tot} = [H_2S] + [HS^-]$. By using the equilibrium constants K_1 and K_2 (K_1= equilibrium constant between H_2S and HS^- , K_2= equilibrium constant between HS^- and S^{2-}), the total concentration of dissolved sulfide species generated in solution was simplified into $[sulfides]_{tot} = [H_2S] \times (10^{pH-pK1} +1)$. The pK_1 value was also affected by temperature measurement[2]: $pK_1 = 32.55 + (1519.44/T) -15.672\log(T) + 0.02722T$. T is in Kelvin. All amperometric H_2S release measurements were conducted at 25°C (298.15 K).

Measurement in pH 7.4 at 25°C (298.15 K) is calculated from $[sulfides]_{tot} = [H_2S]_{detected} \times 3.40$.

A.3 Control polymers after H_2S is released from P[BTHMA-*co*-BDTHMA-*b*-OEGMA-*b*-St] polymers via pre-exposure to L-cysteine

H_2S-donating self-assembled spherical micelles (4.73 mg, 0.71 µmoles, 143 µM) and worm-like micelles (15.6 mg, 0.71 µmoles, 143 µM) were dissolved separately in PBS at pH 7.4 in the presence of L-cysteine (4.65 molar equiv., 3.3 µmoles, 660 µM) over 72 h in each open vessel. Dialysis was then conducted to ensure removal of the side products and the excess L-cysteine. The resulting polymers were dried under air and in vacuo, and then analysed by ^1H NMR spectroscopy to confirm the final products.

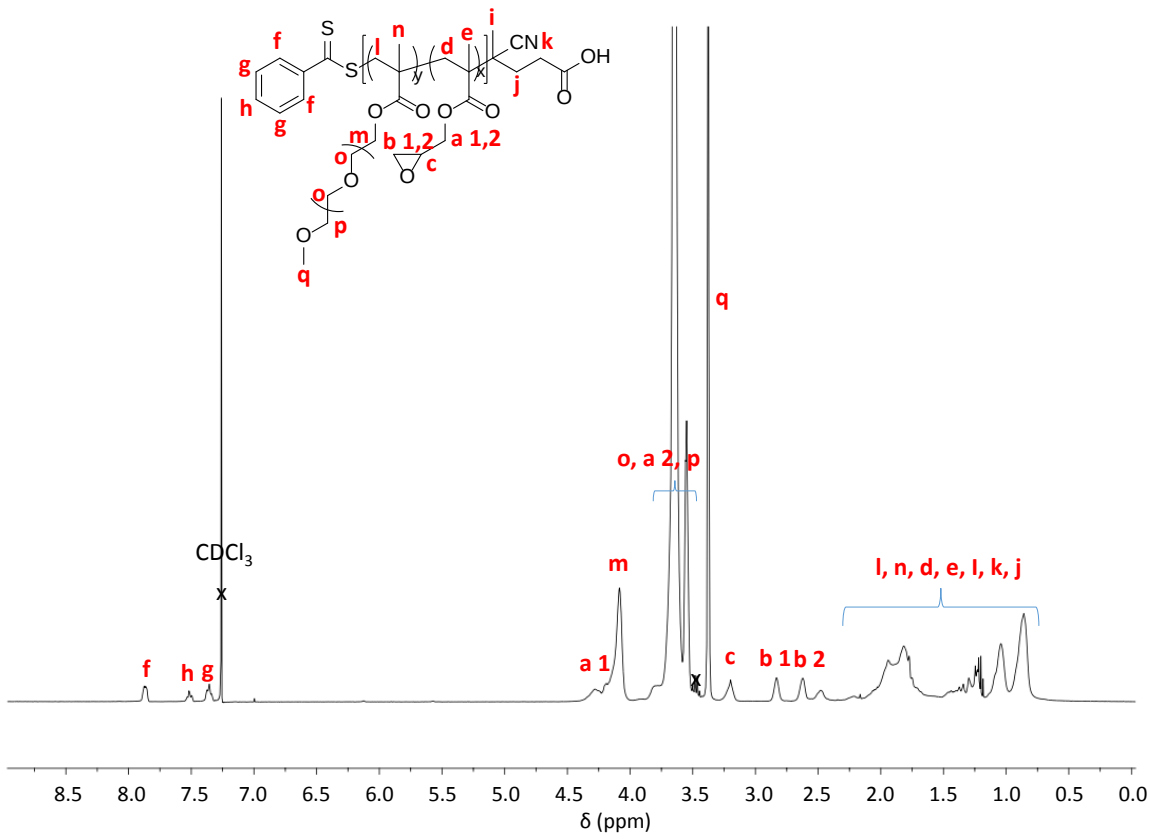

Figure S1. ^{1}H NMR spectrum of P[OEGMA-*co*-GMA]-S(C=S)Ph, **1a**, recorded in $CDCl_3$ (400 MHz).

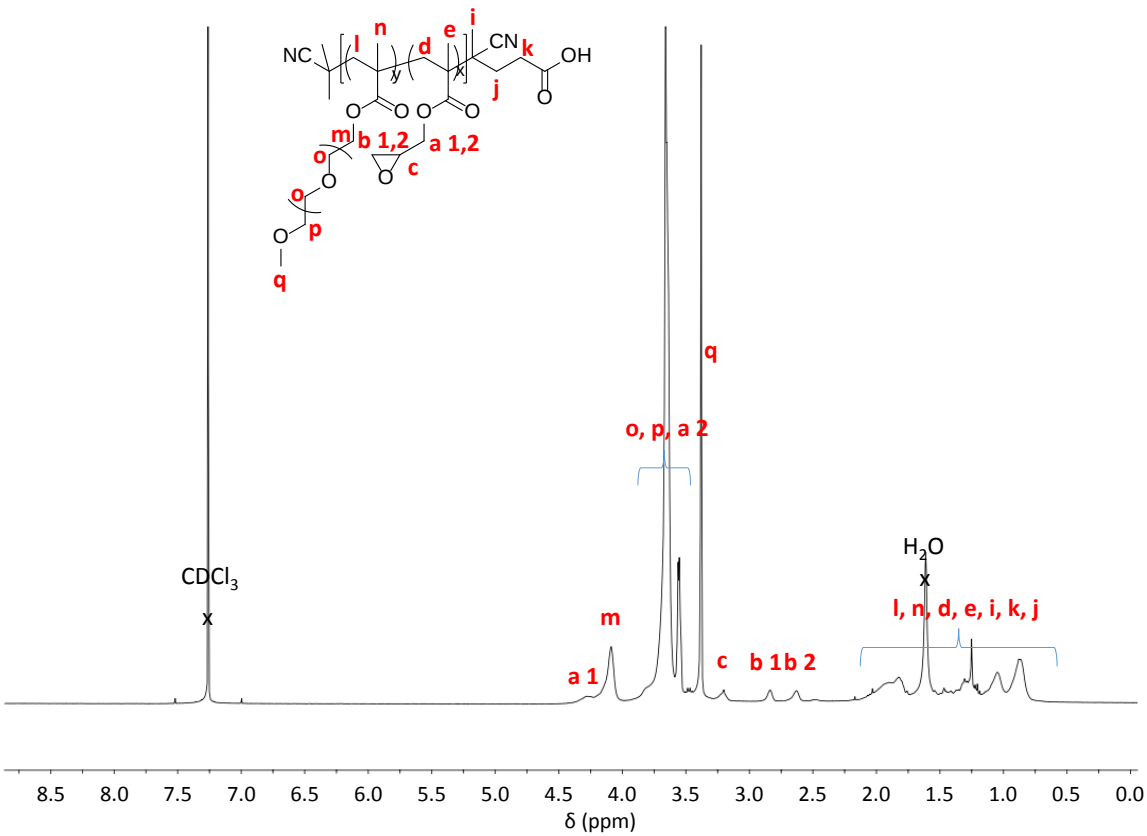

Figure S2. ^{1}H NMR spectrum of P[OEGMA-*co*-GMA] **1b** recorded in $CDCl_3$ (400 MHz).

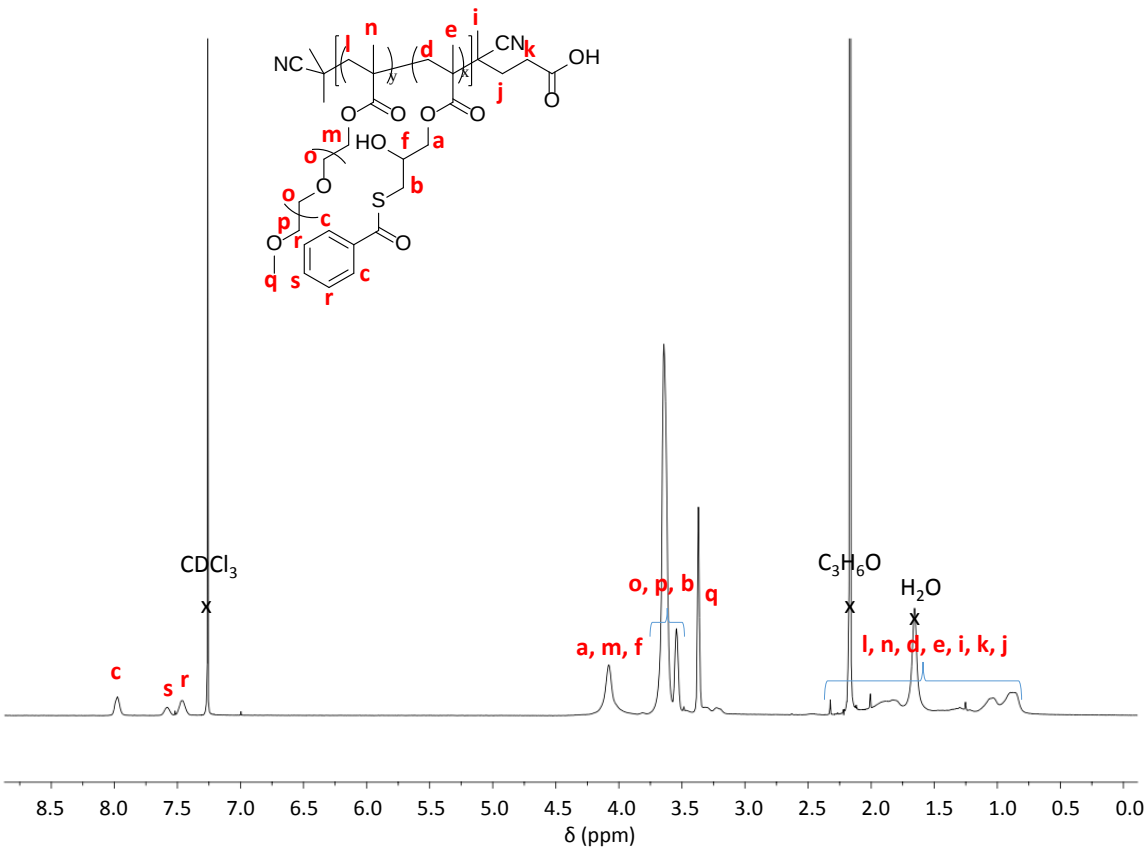

Figure S3. ^{1}H NMR spectrum of P[OEGMA-*co*-BTHMA] **1c**, recorded in $CDCl_3$ (400 MHz).

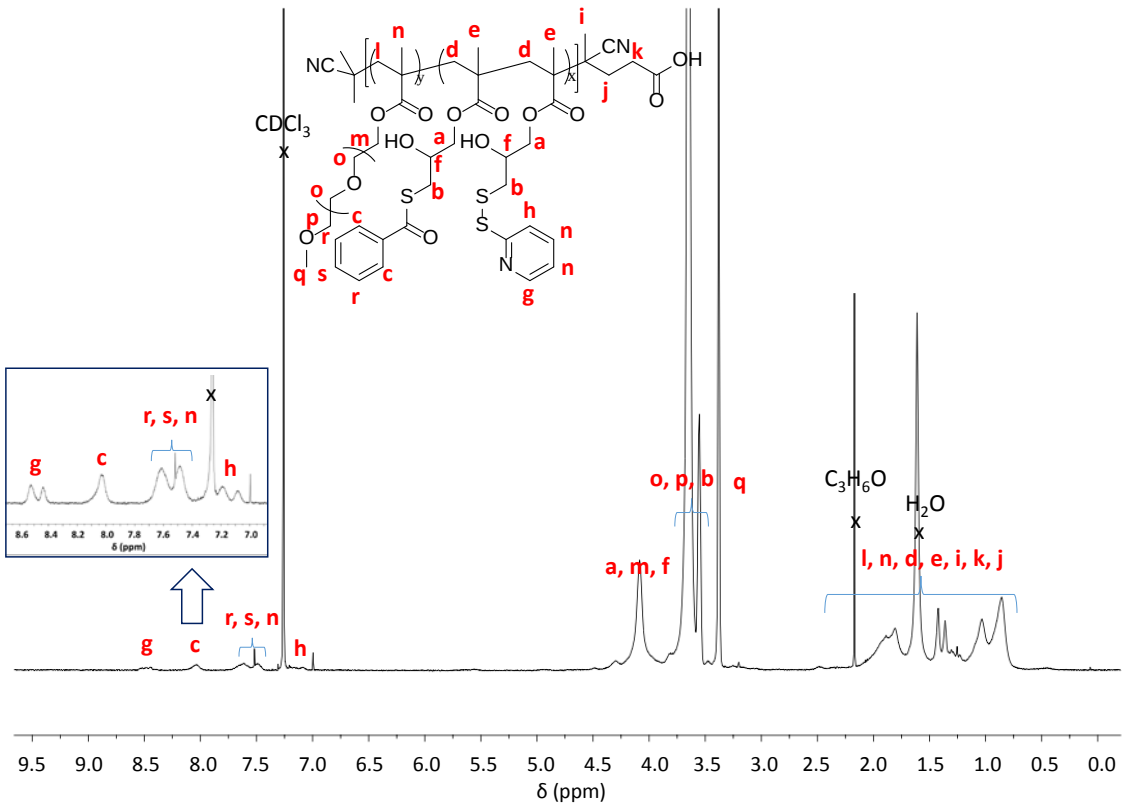

Figure S4. ^{1}H NMR spectrum of P[OEGMA-*co*-BTHMA-*co*-PDHMA] **1d**, recorded in $CDCl_3$ (400 MHz).

Note: Three distinct signals in the ^{1}H NMR spectrum (δ 7.45, 7.6 and 8.0 ppm, representing the aromatic benzothioate group) (Figure S3) were partially shifted to the new peaks (δ 7.1, 7.65, 8.5 ppm, representing the aromatic pyridyl group). The ^{1}H NMR indicates 60 % conversion from **1c**.

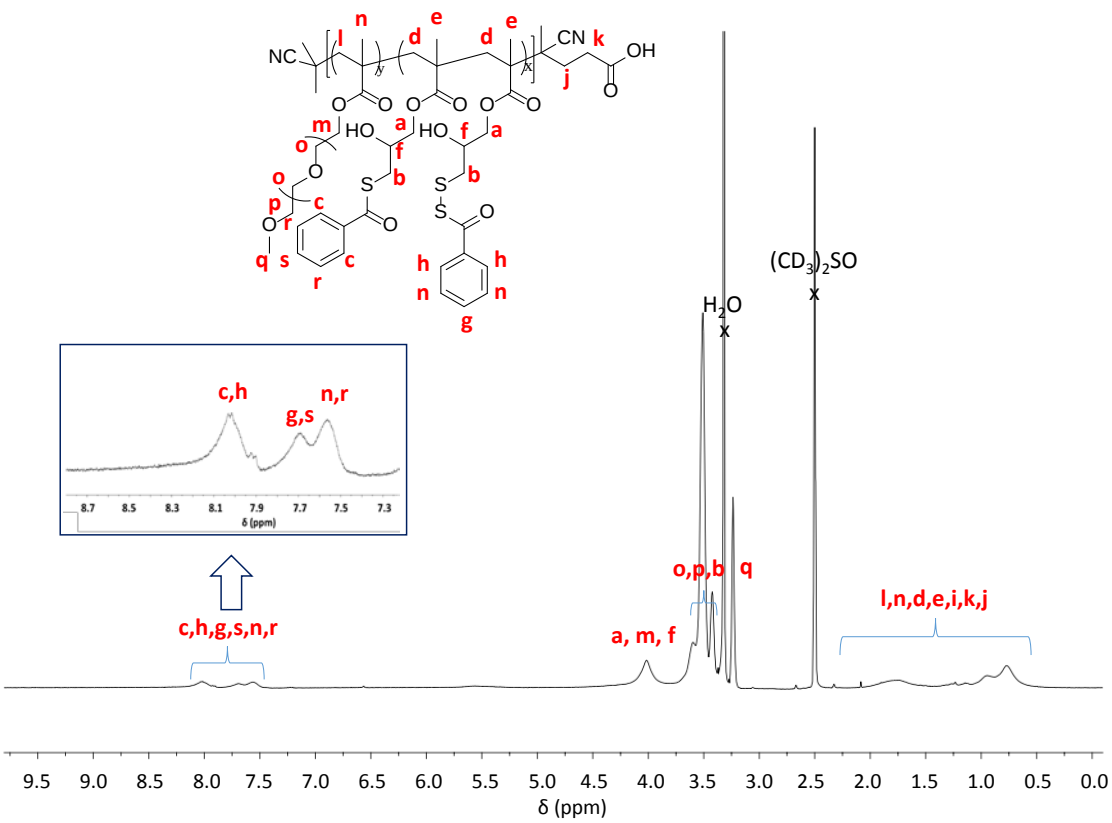

Figure S5. ^{1}H NMR spectrum of P[OEGMA-*co*-BTHMA-*co*-BDTHMA] **1e**, recorded in $(CD_3)_2SO$ (400 MHz).

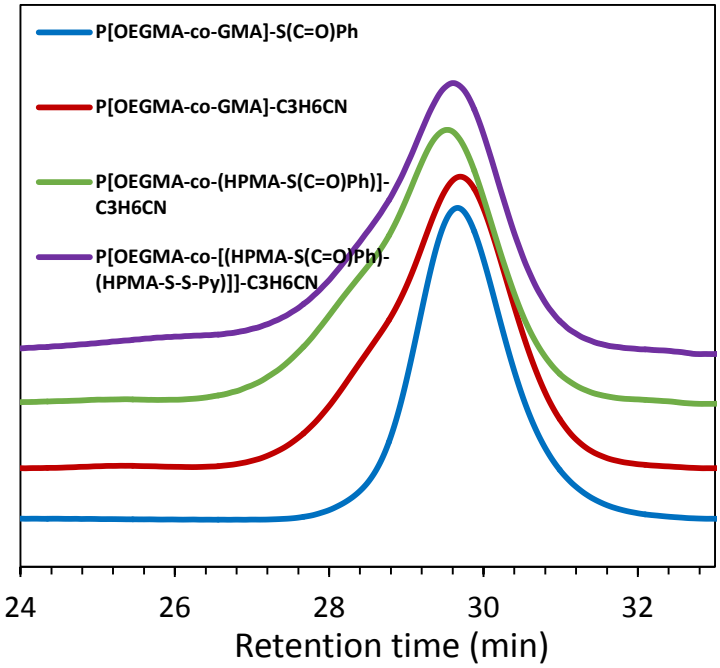

Figure S6. Normalized GPC spectra for P[OEGMA-*co*-GMA]-S(C=S)Ph **1a** (blue line), P[OEGMA-*co*-GMA] **1b** (red line), P[OEGMA-*co*-BTHMA] **1c** (green line), P[OEGMA-*co*-BTHMA-*co*-PDHMA] **1d** (purple line).

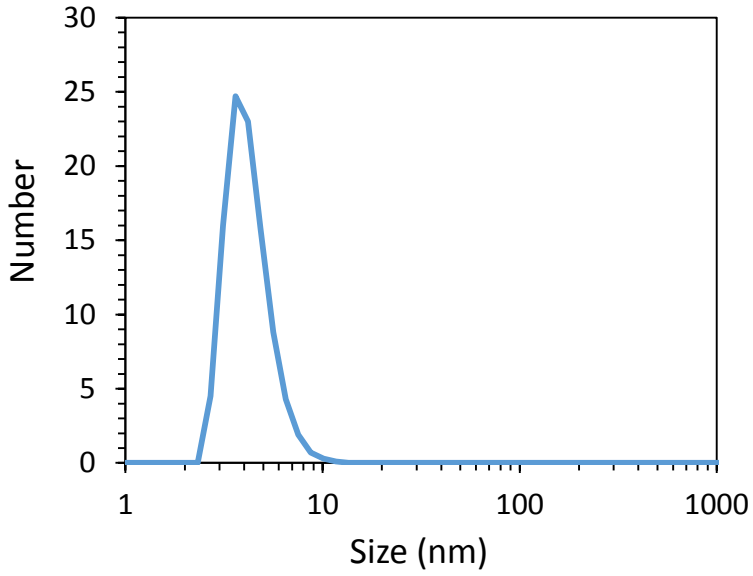

Figure S7. Size distribution (by number) for P[OEGMA-*co*-BTHMA-*co*-BDTHMA] **1e** in PBS (pH 7.4), as determined by dynamic light scattering. The average diameter was 4.5 nm with PDI = 0.22.

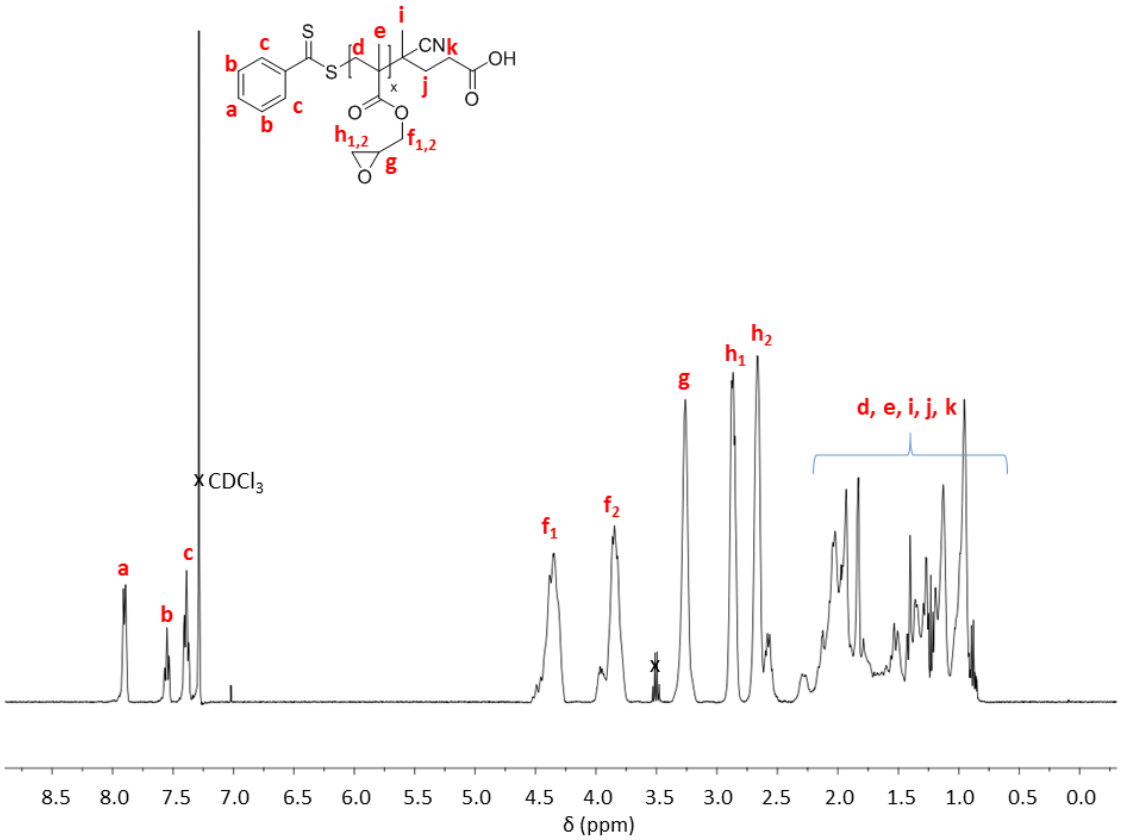

Figure S8. ^{1}H NMR spectrum of P[GMA]-S(C=S)Ph **2a**, recorded in $CDCl_3$ (400 MHz).

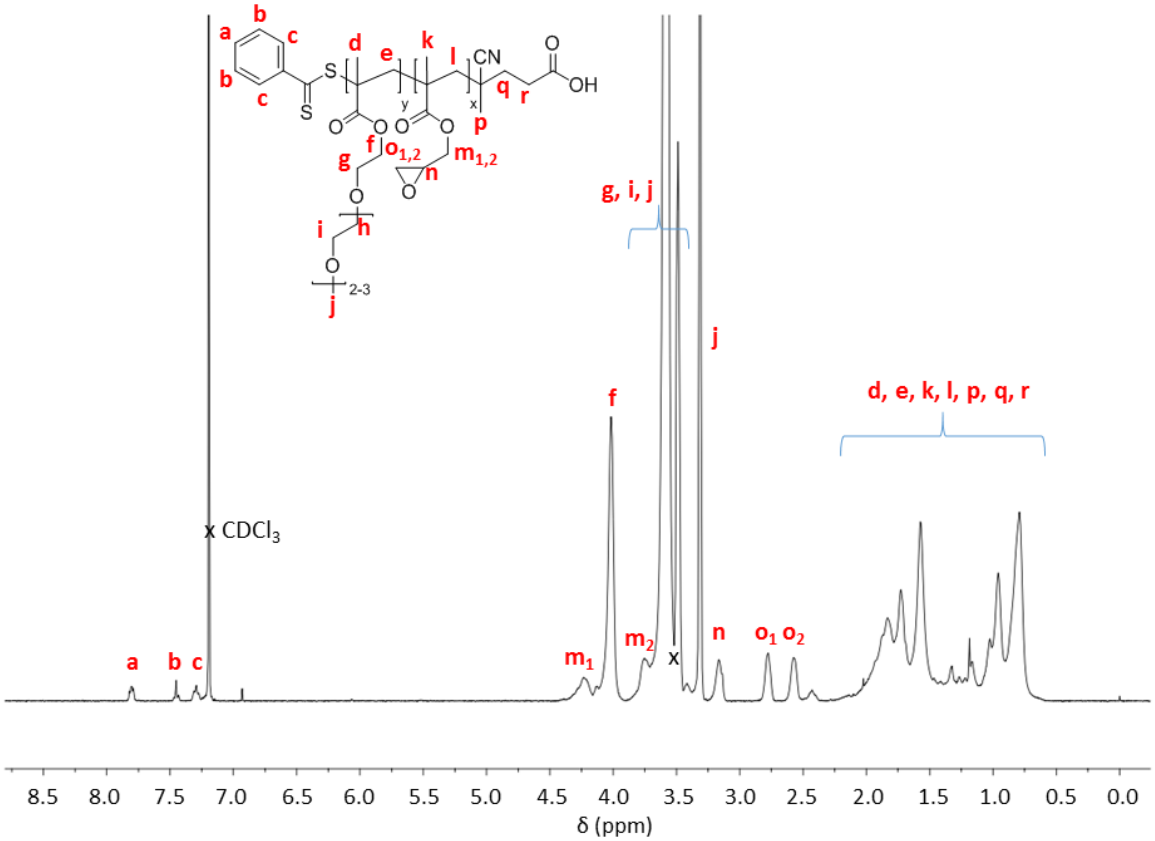

Figure S9. ^{1}H NMR spectrum of P[GMA-*b*-OEGMA]-S(C=S)Ph **2b**, recorded in $CDCl_3$ (400 MHz).

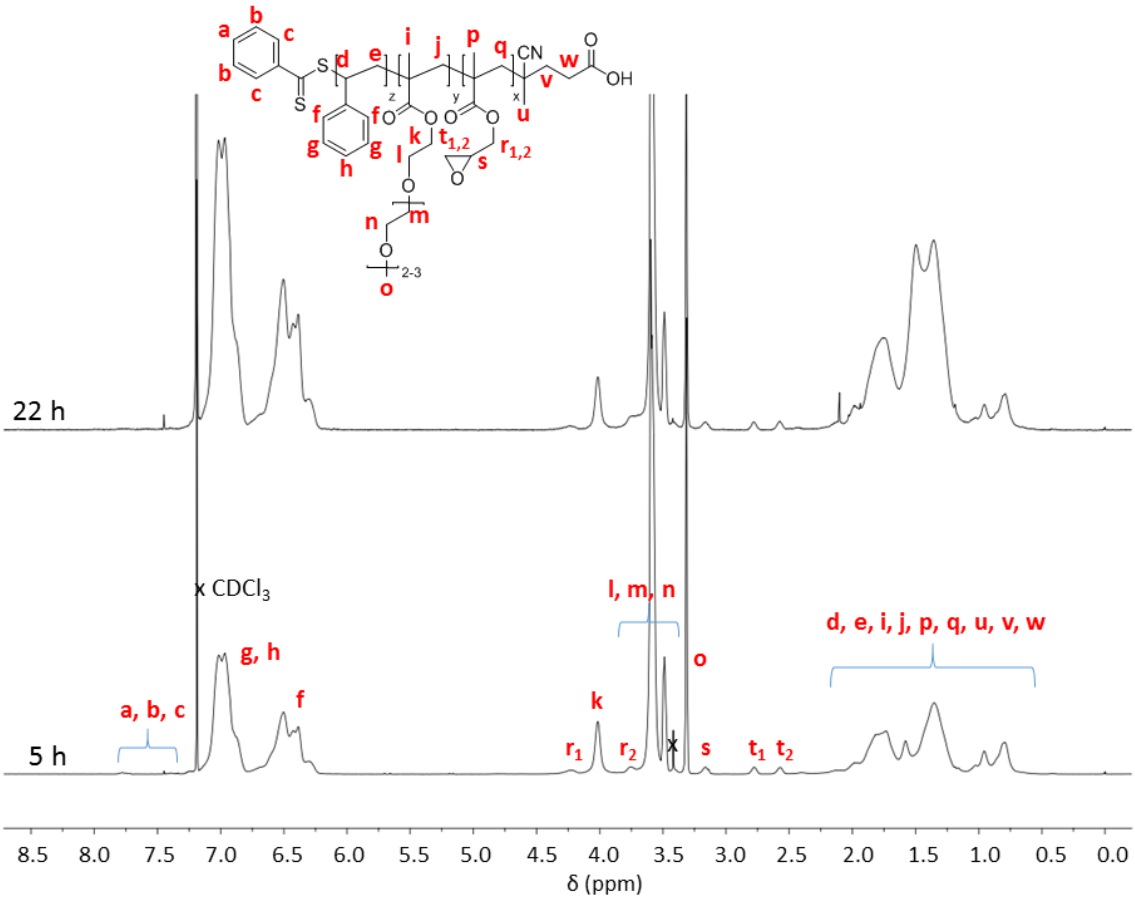

Figure S10. ^{1}H NMR spectra of P[GMA-*b*-OEGMA-*b*-St]-S(C=S)Ph **3a** (top) and **4a** (bottom) for different reaction times (5h and 22 h respectively), recorded in $CDCl_3$ (400 MHz).

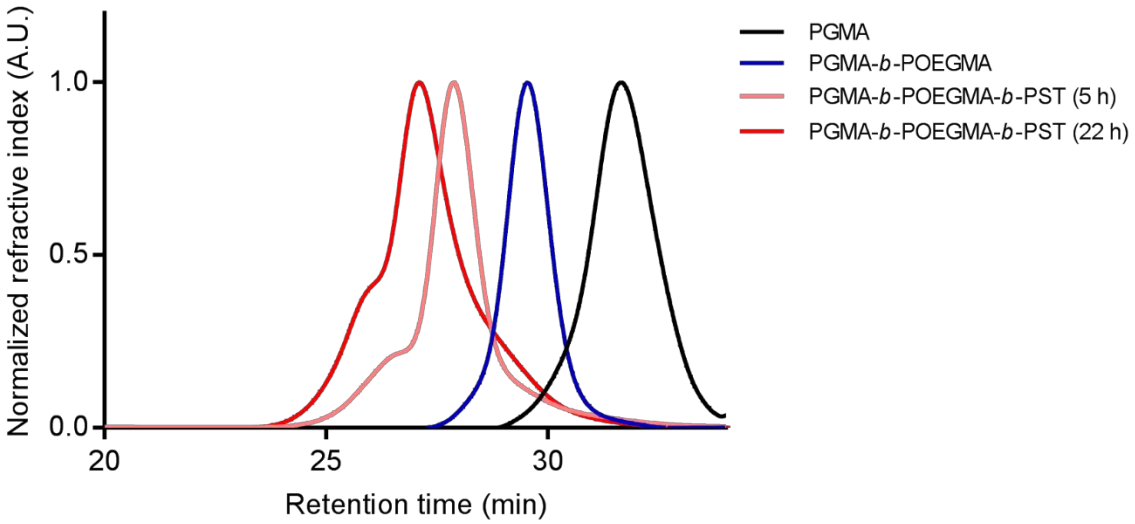

Figure S11. Normalized GPC spectra for P[GMA]-S(C=S)Ph **2a** (black), P[GMA-*b*-OEGMA]-S(C=S)Ph **2b** (blue) and P[GMA-*b*-OEGMA-*b*-St]-S(C=S)Ph polymers, **3a** (pink) and **4a** (red).

Table S1. Polymerisation Characteristics of synthesized PISA nanoparticles by ^{1}H NMR, GPC, DLS and TEM. The predominant morphologies observed in TEM were defined as spherical (S) and wormlike (W) micelles.

Polymer	Polym. Time (h)	Conv. (%)[a]	^{1}H NMR composition			GPC			DLS	
			GMA	OEGMA	ST	M_n[b] (g/mol)	M_n[c] (g/mol)	PDI	D_h (nm)	PDI
P[GMA]-S(C=S)Ph **2a**	1.5	25	7	-	-	1259	2691	1.20		-
P[GMA-*b*-OEGMA]-S(C=S)Ph **2b**	4	56	7	29	-	9959	9157	1.12		-
P[GMA-*b*-OEGMA-*b*-St]-S(C=S)Ph **3a**	5	2.6	7	29	132	23317	23773	1.22	23.2	0.11
P[GMA-*b*-OEGMA-*b*-St]-S(C=S)Ph **4a**	22	5.6	7	29	282	38441	27092	1.41		-

[a] All conversions were calculated using ^{1}H NMR spectra of the crude polymerisation mixtures. PGMA conversion: $[I^{4.43\text{-}4.21}] / [I^{4.52\text{-}4.21}] \cdot 100$ %, PGMA-*b*-POEGMA: $[I^{4.43\text{-}4.21}] / [I^{4.52\text{-}4.21}] \cdot 100$ %, and for PGMA-*b*-POEGMA-*b*-PSt: $[I^{7.2\text{-}6.9}] / [I^{6.7} + I^{5.8} + I^{5.3}] \cdot 100$ %.

[b] The molecular weight of each polymer was determined using the following formulas:

$M_{n,\,PGMA,NMR} = [(I^{2.7ppm} + I^{2.9ppm} + I^{3.3ppm} + I^{3.9ppm} + I^{4.ppm}) / 5] / \cdot [(I^{7.9ppm}) / 2] \cdot M_{n,\,PGMA} + M_{n,\,CPADB}$. Where $I^{7.9ppm}$ corresponds to the signal of two aromatic protons of the RAFT agent.

$M_{n,\,PGMA\text{-}b\text{-}POEGMA,NMR} = [I^{4.1ppm} / I^{7.9ppm}] \cdot M_{n,\,POEGMA} + M_{n,\,PGMA}$, with $I^{4.1\ ppm}$ corresponding to the ester signal of OEGMA,

$M_{n,\,PGMA\text{-}b\text{-}POEGMA\text{-}b\text{-}PSt,NMR} = [I^{6.3\text{-}6.9ppm} / I^{4.1ppm}] \cdot 2/3 \cdot M_{n,\,PS} + M_{n,\,PGMA\text{-}b\text{-}POEGMA}$, with $I^{4.1\ ppm}$

[c] Assessed by GPC in *N*,*N*-dimethylacetamide (DMAc, 0.03 % w/v LiBr, 0.05 % BHT) using a conventional calibration curve with narrow molecular weight distribution polystyrene standards.

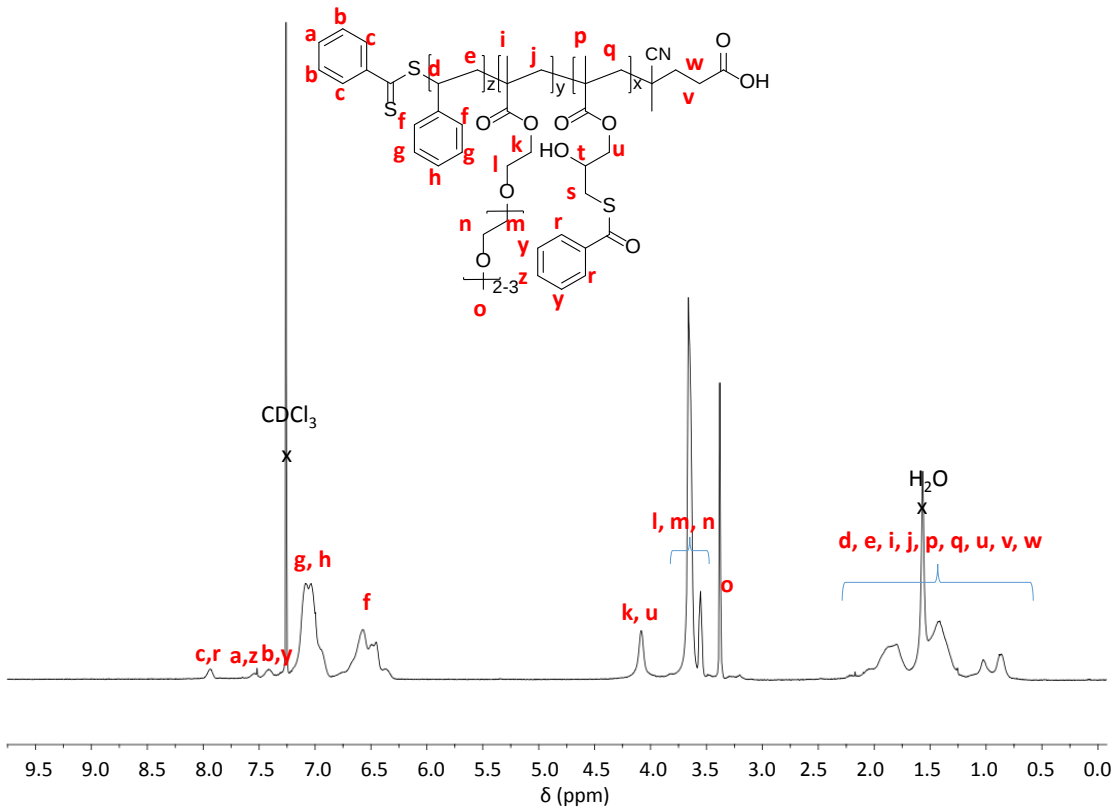

Figure S12. ^{1}H NMR spectrum of P[BTHMA-*b*-OEGMA-*b*-St] **3b**, spherical micelles, recorded in $CDCl_3$ (400 MHz).

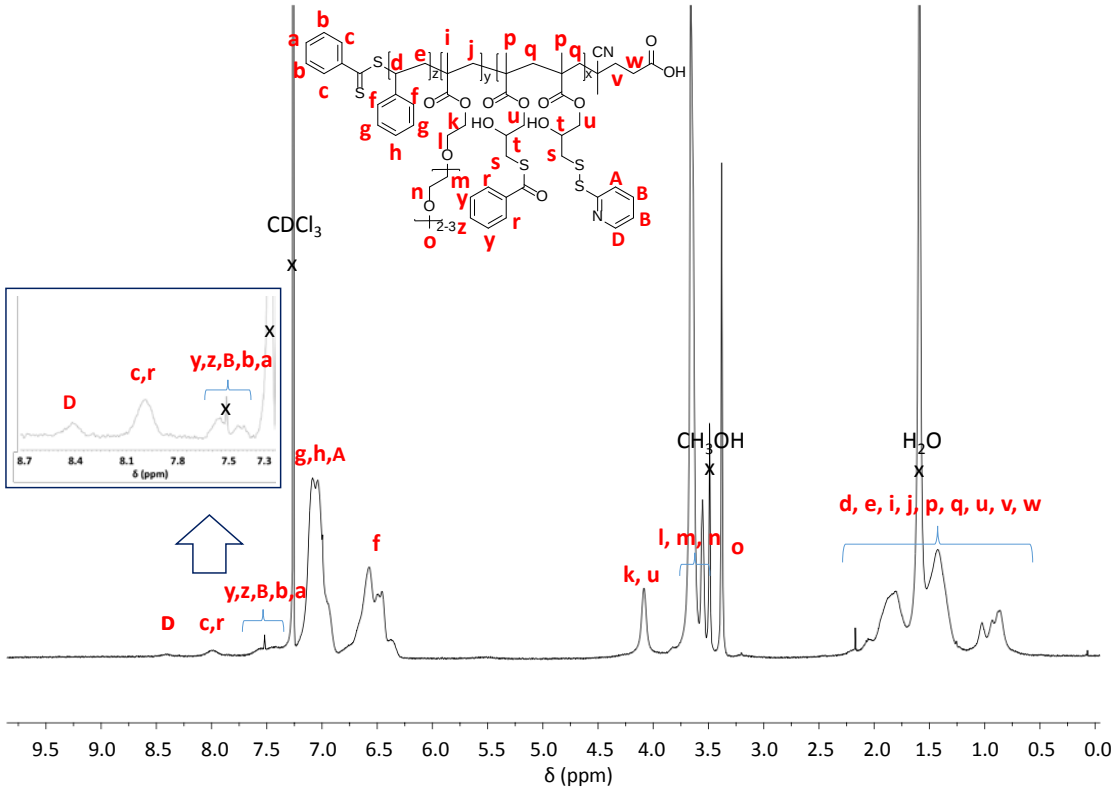

Figure S13. ^{1}H NMR spectrum of P[BTHMA-*co*-PDHMA-*b*-OEGMA-*b*-St] **3c** spherical micelles, recorded in $CDCl_3$ (400 MHz).

Note: Three distinct signals in the ^{1}H NMR spectrum (δ 7.4, 7.55 and 8.0 ppm, representing the aromatic benzothioate group) (as shown also in Figure S12) were partially shifted to the new peaks; δ 8.5 ppm represents the aromatic pyridinyl group. This indicates 50 % conversion was achieved to form P[BTHMA-*co*-PDHMA-*b*-OEGMA-*b*-St] **3c** spherical micelles.

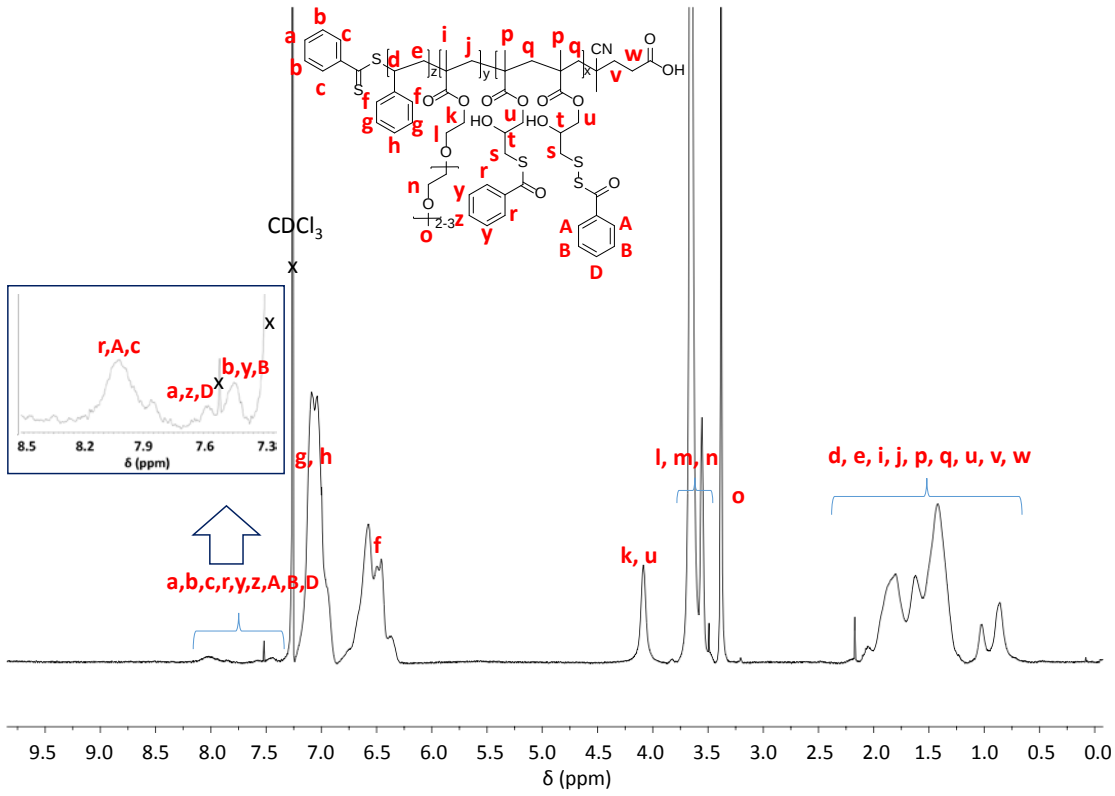

Figure S14. ^{1}H NMR spectrum of P[BTHMA-*co*-BDTHMA-*b*-OEGMA-*b*-St] **3d** spherical micelles, recorded in $CDCl_3$ (400 MHz).

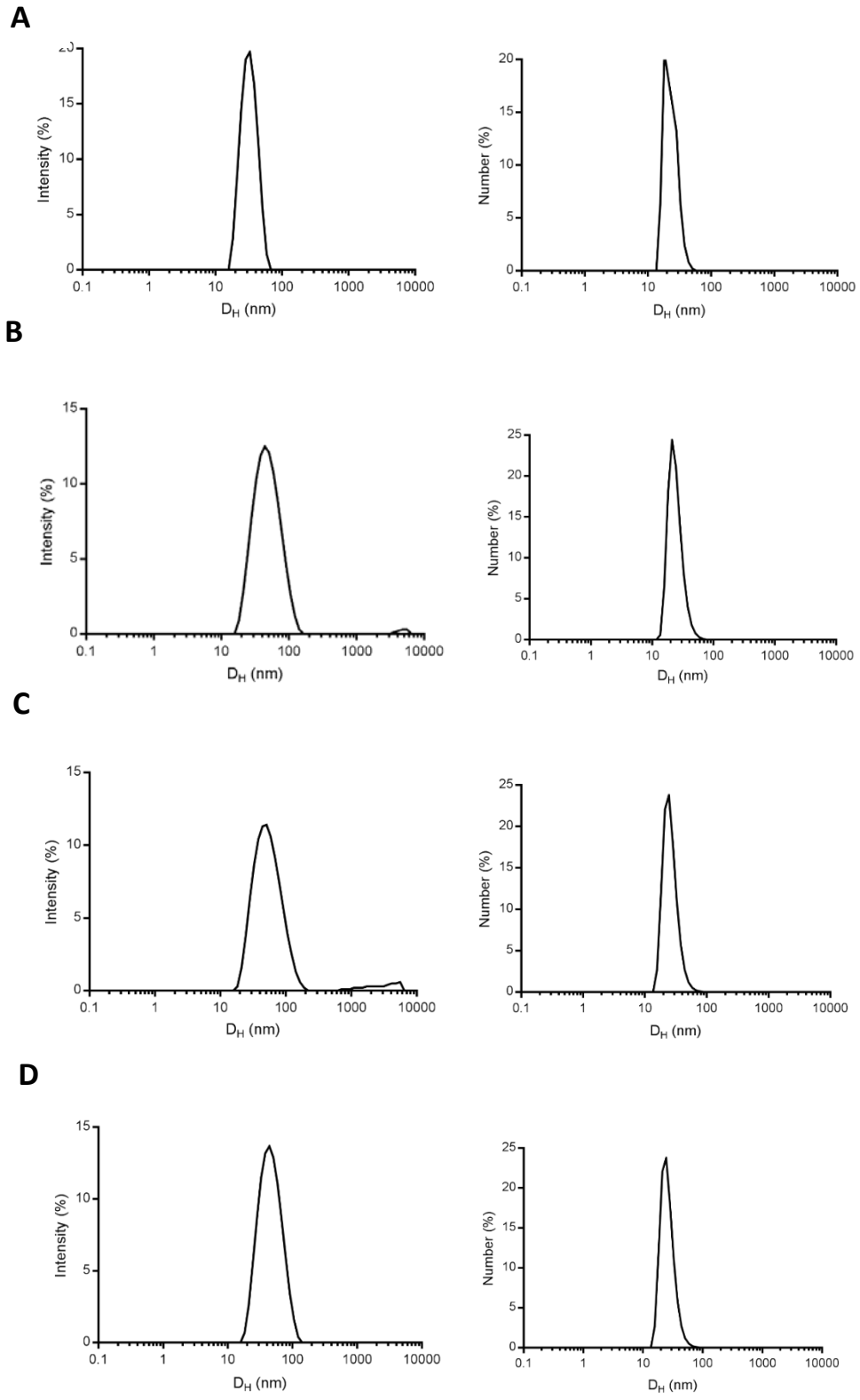

Figure S15. Determination of the hydrodynamic size of spherical micelles (A) P[GMA-*b*-OEGMA-*b*-St]-S(C=S)Ph **3a** (number average diameter: 23.1 ± 5.4, PDI: 0.11), (B) P[BTHMA-*b*-OEGMA-*b*-St] **3b** (number average diameter: 24.8 ± 7.1, PDI: 0.13), (C) P[BTHMA-*co*-PDHMA-*b*-OEGMA-*b*-St] **3c** (number average diameter: 25.3 ± 7.5, PDI: 0.23), (D) P[BTHMA-*co*-BDTHMA-*b*-OEGMA-*b*-St] **3d** (number average diameter: 24.9 ± 7.1, PDI: 0.16), by DLS with the intensity distribution (left) and number distribution (right).

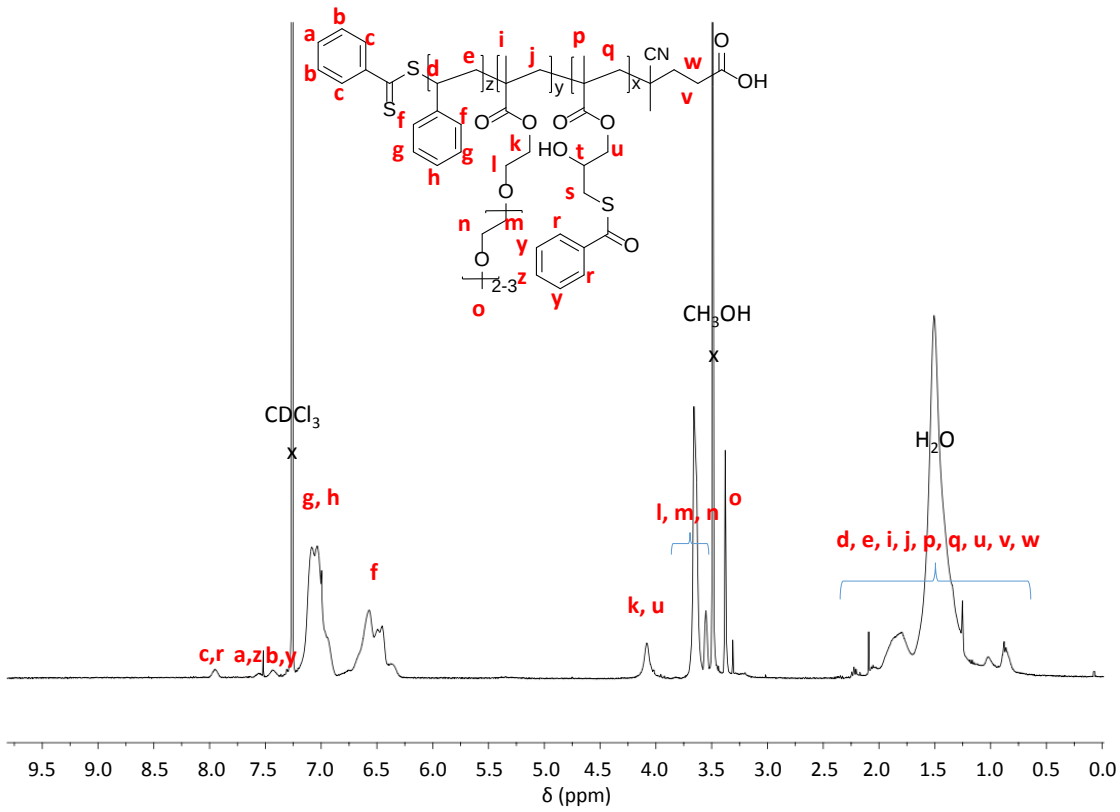

Figure S16. ^{1}H NMR spectrum of P[BTHMA-*b*-OEGMA-*b*-St] **4b** worm-like micelles, recorded in $CDCl_3$ (400 MHz).

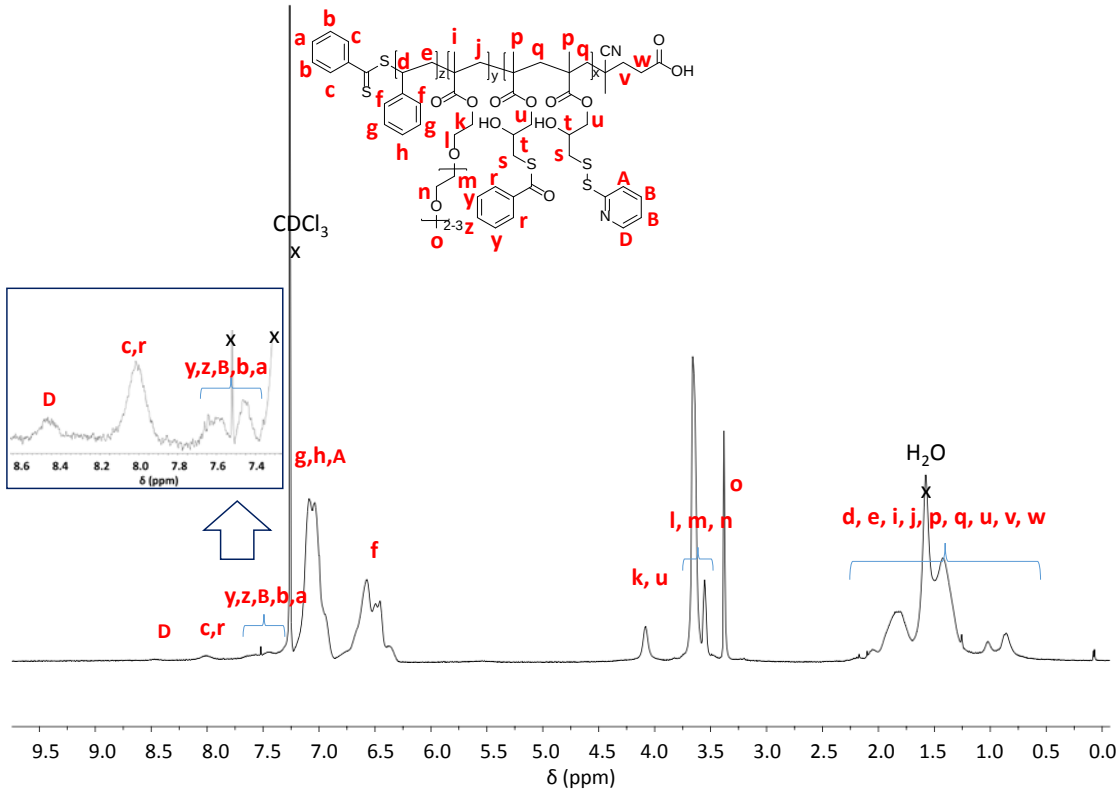

Figure S17. ^{1}H NMR spectrum of P[BTHMA-*co*-PDHMA-*b*-OEGMA-*b*-St] **4c** worm structure, recorded in $CDCl_3$ (400 MHz).

Note: Three distinct signals in the ^{1}H NMR spectrum (δ 7.4, 7.55 and 8.0 ppm, representing the aromatic benzothioate group) (as shown also in Figure S16) were partially shifted to the new peaks; δ 8.5 ppm represents the aromatic pyridinyl group. This indicates 25 % conversion was achieved to form P[BTHMA-*co*-PDHMA-*b*-OEGMA-*b*-St] **4c** worm-like micelles.

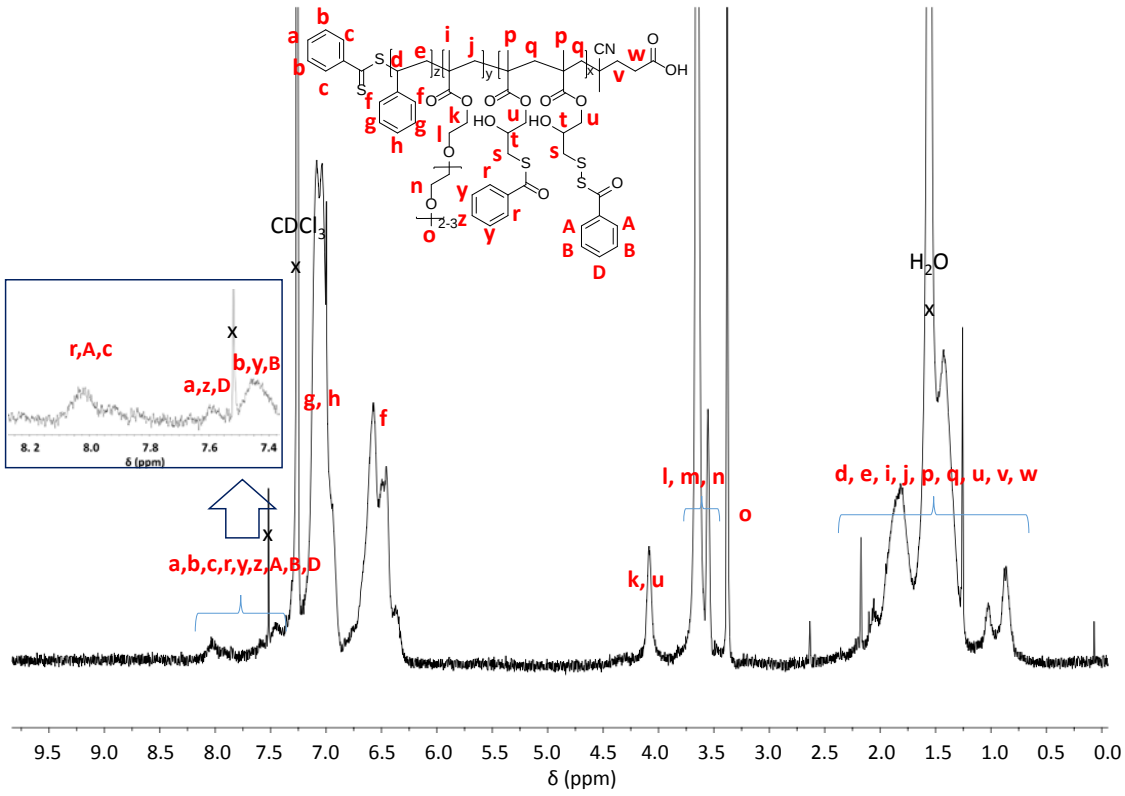

Figure S18. ^{1}H NMR spectrum of P[BTHMA-*co*-BDTHMA-*b*-OEGMA-*b*-St] **4d** worm-like micelles, recorded in $CDCl_3$ (400 MHz).

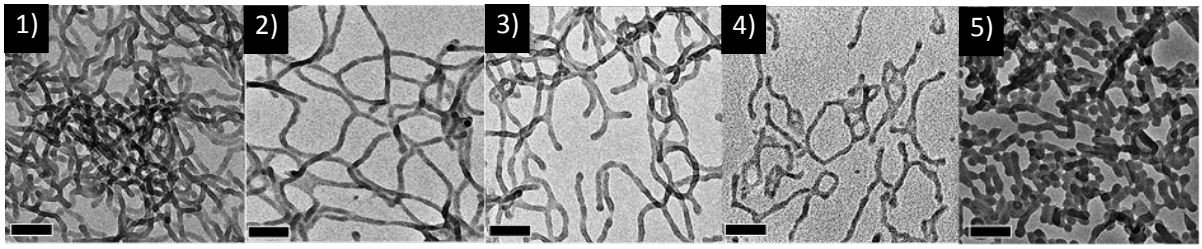

Figure S19. Representative TEM images (scale bar, 100 nm) of individual surface-functional worm-like micelles after each post-polymerization step: 1) initial P[GMA-*b*-OEGMA-*b*-St]-S(C=S)Ph worm-like micelles **4a** ; 2) Epoxy-ring opening to form P[BTHMA-*b*-OEGMA-*b*-St] **4b**; 3) Aminolysis of benzothioate groups by ethanolamine in the presence of dipyridyl disulfide to form pyridinyl disulfide-conjugated P[BTHMA-*co*-PDHMA-*b*-OEGMA-*b*-St] **4c** worm-like micelles; 4) Thiol-disulfide exchange reaction with an excess of thiobenzoic acid to produce H_2S donor, P[BTHMA-*co*-BDTHMA-*b*-OEGMA-*b*-St **4d**; 5) After sonication of worm-like micelles **4d** for 10 min (see method section for more information) to produce shorter worm-like micelles.

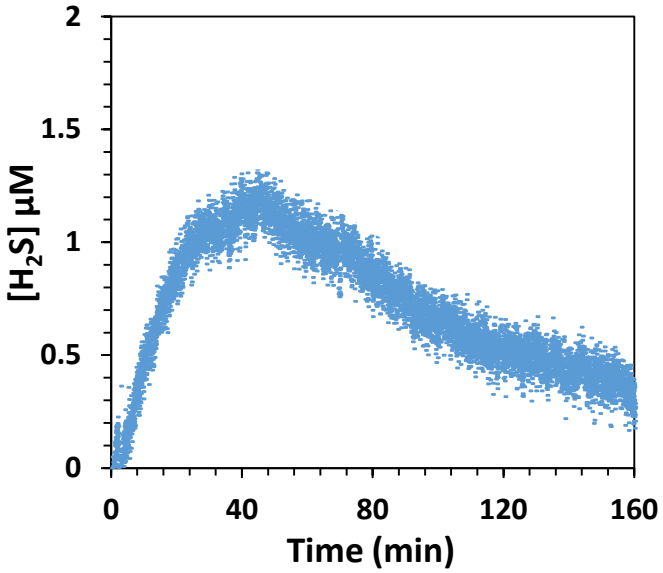

Figure S20. Electrochemical H_2S release response from P[BTHMA-*co*-BDTHMA-*b*-OEGMA-*b*-St **4d** worm-like micelles (11.7 mg, 0.71 µmoles, 143 µM) in the presence of L-cysteine (4.65 molar equiv., 3.3 µmoles, 660 µM) in PBS at pH 7.4 (5 mL). Note: L-cysteine was added at t = 2 min.

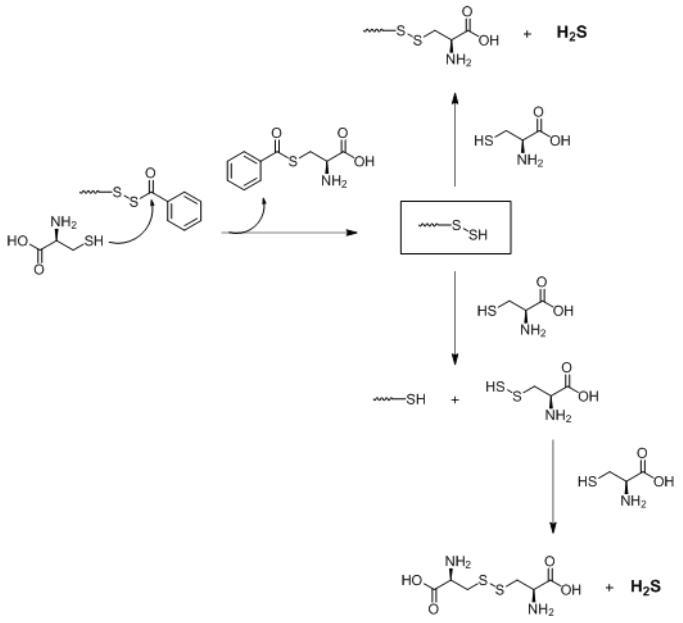

Scheme S1. Proposed mechanism of H_2S release from H_2S donor polymers functionalized with acyl-protected perthiol groups.[3]

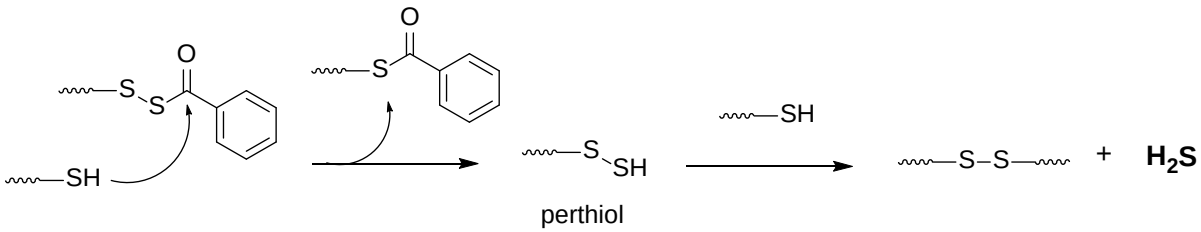

Scheme S2**.** Possible mechanism for the formation of thiol-coupled polymeric products after H_2S is released from BDTHMA functionalized polymers, **1e**, **3d** and **4d**.

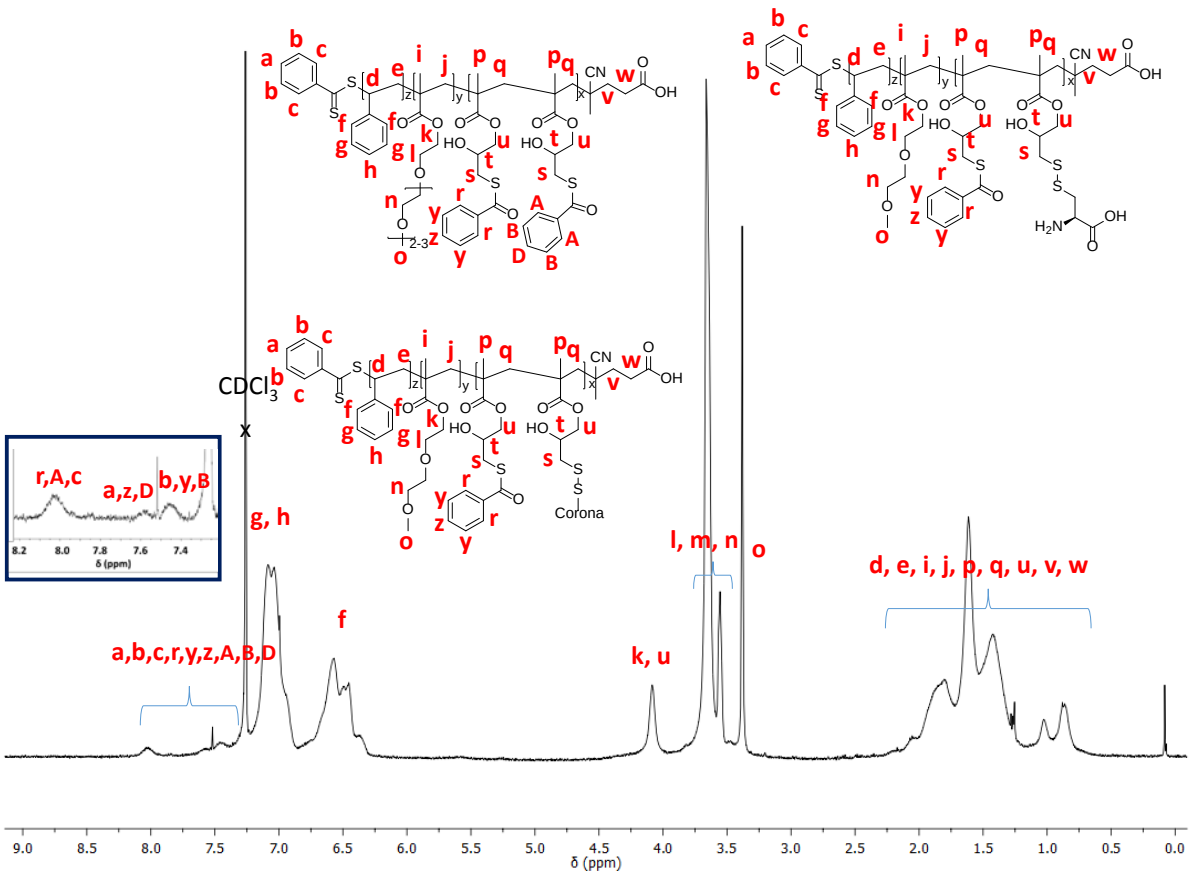

Figure S21. ^{1}H NMR spectrum of polymeric (non-H_2S donating) products formed after H_2S is released from P[BTHMA$_{3.5}$-*co*-BDTHMA$_{3.5}$-*b*-OEGMA$_{29}$-*b*-St$_{132}$] **3d** spherical micelles, recorded in $CDCl_3$ (400 MHz).

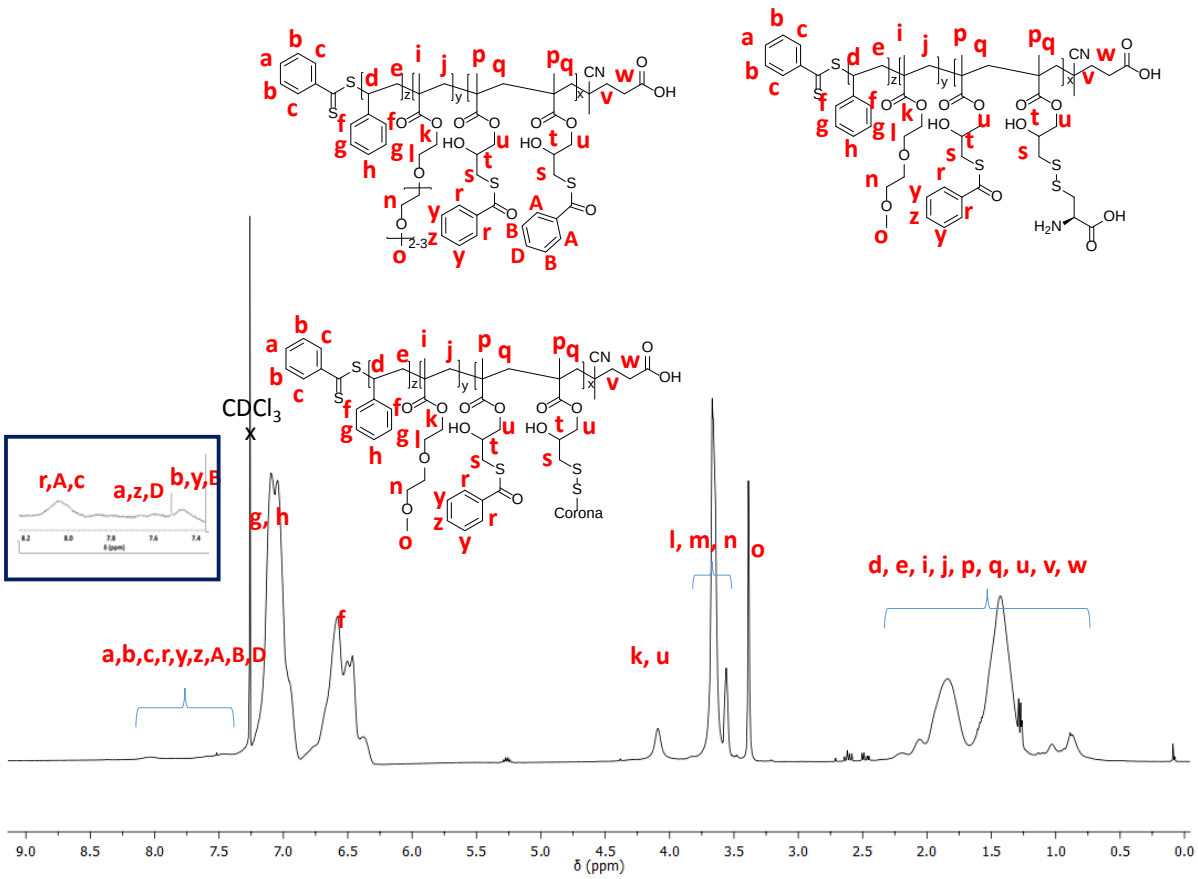

Figure S22. ^{1}H NMR spectrum of polymeric (non-H_2S donating) products formed after H_2S is released from P[BTHMA-*co*-BDTHMA-*b*-OEGMA-*b*-St] **4d** worm-like micelles, recorded in $CDCl_3$ (400 MHz).

References

(1) Ercole, F.; Mansfeld, F. M.; Kavallaris, M.; Whittaker, M. R.; Quinn, J. F.; Halls, M. L.; Davis, T. P. *Biomacromolecules*. **2016**, 17, 371.

(2) Ercole, F.; Whittaker, M. R.; Hall, M. L.; Boyd, B. J.; Davis, T. P.; Quinn, J. F. Chem Commun. 2017, 53, 8030.

(3) Zhao, Y.; Bhushan, S.; Yang, C. T.; Otsuka, H.; Stein, J. D.; Pacheco, A.; Peng, B.; Devarie-Baez, N. O.; Aguilar, H. C.; Lefer, D. J.; Xian, M. *ACS Chem. Biol*. **2013**, 8, 1283.

CHAPTER 5: Co-delivery system of NO using polymer nanoparticle with doxorubicin to combat drug resistant cancer cells

5.1 Introduction

Chemotherapeutics have contributed to high success rates in cancer treatment. However, killing all the cancer cells in a solid tumour remains a significant impediment to successful chemotherapy treatment.[1] Multidrug resistance (MDR) is one of the major obstacles to effective chemotherapy of cancers. Several mechanisms have been identified that lead to the development of MDR phenotypes, such as increased efflux or decreased uptake of drugs, the modification of drug specific targets or improved ability to repair DNA damage.[1–4] One of the most studied mechanisms of MDR is the overexpression of ATP binding cassette (ABC) transporter proteins, such as P-glycoprotein (Pgp) and the MDR–associated proteins (MRPs), on MDR cells. The cancer cells actively mediate drug efflux using these highly expressed integral membrane proteins, and thus limit intracellular drug concentration and therefore toxicity.[1,5] To reverse this effect, the most common strategy is the co-administration of anticancer agents with inhibitors of the transporters, resulting in improved intracellular drug accumulation and restoring the sensitivity of MDR tumour cells to therapeutic drugs. Co-treatment of anticancer drugs with various Pgp inhibitors including laniquidar, tariquidar or elacridar has been clinically investigated.[1,6–9]

Nitric oxide (NO) has been shown to reverse the resistance to chemotherapeutics in various MDR cancer cell lines.[10–15] Previous studies have suggested a relationship between endogenous nitric oxide production and antineoplastic drug resistance in human epithelial colon doxorubicin-resistant cancer cells (HT29-dx).[16,17] Doxorubicin-sensitive and –resistant cancer cells (HT29/HT29-dx) showed a different capacity to produce NO and that feature has been postulated to contribute to the observed drug resistance. During doxorubicin (DOX) treatment, nitrite production and nitric oxide synthase (NOS) expression were highly increased in HT29 cells, but not in HT29-dx cells. Furthermore, HT29-dx cells overexpress the transporters P-gp and MRP3, one of which has been identified as playing a significant role in the emergence of clinical drug resistance. Exogenously applied NO donors, such as *S*-nitrosopenicillamine (SNAP), sodium nitroprusside (SNP) or *S*-nitrosoglutathione (GSNO) induced greater nitration of tyrosine residues which are highly expressed in MRP3 transporters, which consequently led to increased doxorubicin (DOX) accumulation and cytotoxic effects in HT29-dx cells. This suggests that nitrosylation may reduce the number of

functionally active MPR3 transporters perhaps by altering the conformation of the proteins at a site crucial for drug transport: this in turn affects doxorubicin efflux and consequently increases intracellular DOX accumulation. A range of studies have been undertaken to demonstrate the enhanced cytotoxic effects of anticancer agents with exogenous NO delivery in different cancer cell lines. For example, NO-releasing furoxan derivatives were studied in Madin-Darby canine kidney MDK cells overexpressing Pgp and MRP1 transporters.[18] These NO donors were able to nitrate tyrosine residues of the transporters, resulting in increased activity of chemotherapeutic agents by inhibiting the efflux pumps. Additionally, Kuppusamy and co-workers have demonstrated that the delivery of NO followed by the administration of cisplatin showed significantly greater cytotoxicity in drug resistant ovarian cancer cells when compared with those treated with cisplatin alone.[19] On the basis of these results, a series of NO-releasing DOX drugs were prepared by conjugating DOX with different NO donor substructures. The NO-DOX conjugate drugs have been explored for increasing accumulation of DOX and cytotoxicity in HT29 and HT29-dx cancer cells through nitration of tyrosine residues of the MRP3 protein pumps.[20]

Despite having significant clinical therapeutic potential, the direct use of NO as a therapeutic agent has many limitations, largely related to poor stability, high reactivity, and lack of specificity which in combination results in poor pharmokinetics and short half-life in biological systems. Thus, the biological effects could not be reproduced. To overcome these issues, and the challenge of controlled and sustained NO release, NO-delivering nanoparticle systems have been developed which have shown improved stabilities and subsequently more controlled release profiles of NO. Stevens and coworkers investigated the first potential use of NO releasing nanoparticles in cancer therapy.[21] The authors observed that NO-releasing silica nanoparticles were more effective in inhibiting ovarian cancer cell growth compared to non-tumour ovarian cells. Furthermore, a hollow-microsphere NO-delivery system (HM) was developed which carried both the anticancer agent irinotecan (CPT-11) and the NO donor, diethylenetriamine diazeniumdiolate (DETA NONOate).[22] Under low pH conditions, like those found in solid tumours, protons can infiltrate the shell of HM and react with NONOate, producing NO bubbles. The high pressure of NO was then able to increase localised drug release by both disrupting the shell of the HM and blocking Pgp-mediated drug efflux in multidrug resistant human breast cancer cell lines

(MCF7/ADR). Another approach has involved the development of polymeric NO-delivering micelles, in which a commonly used donor molecule, GSNO, was conjugated into the self-assembled system.[23] The NO-releasing polymeric micelles showed significantly enhanced GSNO stability in aqueous media. Also, a greater cytotoxic effect of cisplatin was observed in BE(2)-C neuroblastoma cells pre-treated with GSNO-functionalised micelles, compared with non NO pre-treated cells.

The present work provides, for the first time, the synthesis of NO-releasing core cross-linked star polymer nanoparticles in which *S*-nitrosoglutathione (GSNO) was conjugated into the core of the star. A slower NO release profile from GSNO-conjugated star polymers was observed, compared to GNSO itself. We demonstrated that the delivery of NO using the GSNO-functionalised star polymers, in combination with DOX, enhanced the cytotoxic effects in drug-resistant human breast cancer MCF7/VP16 cells.

5.2 Experimental Section

5.2.1 Materials. Oligo(ethylene glycol) methyl ether acrylate (OEGA) with Mn = 480 g mol^{-1} (denoted as OEGA480 where relevant) was purchased from Sigma-Aldrich and deinhibited by percolating over a column of basic alumina. *N,N'*-methylenebis(acrylamide) (MBAA), *S*-nitrosoglutathione (GSNO), glutathione (GSH) and 2,2,2-trifluoroethanol (TFE) were purchased from Sigma-Aldrich at the highest purity available. Azobisisobutyronitrile (AIBN) was purified by recrystallization from methanol before use. 3-(benzyl sulfanyl thiocarbonyl sulfanyl)-propanoic acid (BSPA) and pentafluorophenyl acrylate (PFPA) were prepared according to previously reported procedures.[24,25] Petroleum ether (b.p. 40 - 60 °C), diethyl ether, toluene, chloroform, methanol and dimethyl sulfoxide were purchased from Merck Millipore and used as received.

5.2.2 Instruments. ^{1}H NMR and ^{19}F NMR spectra were recorded at 400 MHz on a Bruker UltraShield 400 MHz spectrometer 7 running Bruker Topspin, version 1.3. Spectra were recorded in $CDCl_3$ and C_2D_6OS (d_6-DMSO).

Gel permeation chromatography (GPC) was performed using a Shimadzu modular system comprised of a SIL-20AD automatic injector, an RID-10A differential refractive-

index detector and a 50 × 7.8 mm guard column followed by three KF-805L columns (300 × 8 mm, bead size: 10 μm, pore size maximum: 5000 Å). *N,N*-Dimethylacetamide (DMAc, HPLC grade, 0.03% w/v LiBr) at 50 °C was used for the analysis with a flow rate of 1 mL min^{-1}. Samples were filtered through 0.45 μm PTFE filters before injection. The GPC calibration was performed with narrow-polydispersity polystyrene standards ranging from 500 to 2 × 10^6 g mol^{-1}.

Dynamic light scattering (DLS) measurements were carried out on a Malvern Zetasizer Nano ZS Series running DTS software (laser, 4 mW, λ = 633 nm; angle 173°). The polydispersity index (PDI), used to describe the average diameters and size distribution of prepared micelles, was determined via a cumulants analysis of the measured intensity autocorrelation function using the DTS software. Samples were filtered using 0.45 μm PTFE syringe filter to remove contaminants / dust prior to measurement. Transmission electron microscopy (TEM) was carried out on a Tecnai F20 electron microscope (Advanced Microscopy Facility at the Bio21 Advanced Microscopy Facility, The University of Melbourne) at an accelerating voltage of 200 kV at ambient temperature. An aliquot (5 μL) of 0.5 wt% star polymer solution (in distilled water) was placed on a Formvar coated copper grid (GSCu100F-50, Proscitech) and dried in air at ambient temperature overnight before TEM imaging.

UV-Vis spectra were acquired on a Shimadzu UV-3600 UV-VIS-NIR spectrophotometer using quartz cuvettes with 10 mm path length. Fluorescence spectra were obtained using a fluorescence spectrophotometer (Shimadzu RF-5301 PC). Slit widths were set at 2.5 nm for both excitation and emission. The photomultiplier voltage was set at 950 V.

The details of amperometric NO sensing are fully described in the supporting information.

5.2.3 Synthesis of POEGA (10K arm polymer) (Table S1, Entry 1) *b*. The synthesis of POEGA was carried out using the following stoichiometry: $[BSPA]_0$:$[OEGA_{480}]_0$:$[AIBN]_0$=1:20:0.1. Briefly, $OEGA_{480}$ (4.00 g, 8.33 × 10^{-3} mol), BSPA RAFT agent (0.112 g, 4.11 × 10^{-4} mol), AIBN (6.75 mg, 4.11 × 10^{-5} mol) and toluene (8 mL) were placed in a glass vial equipped with a magnetic stirrer bar and capped with a rubber septum. The reaction mixture was deoxygenated for 25 min at 0 °C by sparging with N_2. The deoxygenated and sealed reaction vessel was placed

into a pre-heated oil bath at 70 °C and the polymerization was run with stirring for 6 h. The resulting mixture was then allowed to cool to 0 °C for about 15 min to terminate polymerization. The monomer conversion was determined by ^{1}H NMR. The polymer was purified of unreacted monomer by precipitating into diethyl ether three times. The product was then placed in a vacuum oven overnight to remove remaining solvent. The final product was analysed by ^{1}H NMR and GPC. The molecular weight and average monomer chain length calculated from ^{1}H NMR were determined to be 9551 g mol^{-1} and 19 units of OEGA, respectively. The polydispersity index (determined by GPC) was 1.10.

5.2.4 Synthesis of Star polymer POEGA-block-P(MBAA-co-PFPA) (Table S1, Entry 2) *c*. The synthesis of Star polymer POEGA-block-P(MBAA-co-PFPA) was carried out using the following stoichiometry: $[POEGA]_0$:$[MBAA]_0$:$[PFPA]_0$:$[AIBN]_0$=1:8:10:0.3. POEGA (0.50 g, 5.24 × 10^{-5} mol), MBAA (0.06 g, 4.18 × 10^{-4} mol), AIBN (2.57 mg, 1.56 × 10^{-5} mol), PFPA (0.12 g, 5.23 × 10^{-4} mol) and toluene (5 mL) were added to a glass vial equipped with a magnetic stirrer bar and capped with a rubber septum. The reaction mixture was deoxygenated for 30 min by sparging with N_2. The deoxygenated and sealed reaction vessel was placed into a pre-heated oil bath at 70 °C and the polymerisation was run with stirring for 24 h. The resulting mixture was then allowed to cool to 0 °C for about 15 min to halt polymerisation. The polymer was purified via three precipitation and centrifugation steps (using a mixture of petroleum ether (bp 40-60 °C) and chloroform as the precipitant) to remove any traces of unreacted cross-linker, arm polymer and PFPA monomer. The product was then placed in a vacuum oven overnight to remove remaining solvent. The final composition of the product determined by ^{1}H NMR and ^{19}F NMR is equal to 31.0/69.0 mol % in PFPA and OEGA, which calculation (using TFE as a reference peak) was reported in previous paper.[26] The polydispersity index determined by GPC was 1.13.

5.2.5 Post-modification of POEGA-block-P(MBAA-co-PFPA) with GSNO *d*. POEGA-block-P(MBAA-co-PFPA) prepared as above (0.01 g,) was dissolved in DMSO (500 µL). GSNO (9.00 mg, 2.68 × 10^{-5} mol) was added into the solution with stirring and allowed to react at room temperature overnight. The resulting mixture was then dialysed overnight against water, using a dialysis membrane with molecular weight cut-off of 12-14 kDa, to ensure removal of side products and the excess amount

of GSNO. The resulting polymer was dried under air and in vacuo, which were then analysed by ^{1}H NMR and ^{19}F NMR spectroscopy. All reactions with GSNO were performed in the dark condition to avoid degradation of GSNO by light.

5.2.6 Detection of nitric oxide (NO) release from GSNO-conjugated star polymers using 5,6-diaminofluorescein (DAF). NO release was detected using a NO responsive fluorescent indicator, 5,6-diaminofluorescein (DAF). A solution of DAF was prepared according to the procedure of Friedman and co-workers.[27] Specifically, DAF was dissolved in DMSO to make a 23 μM solution which was stored in the dark. GSNO (0.048 mg/mL) and GSNO-conjugated star polymers ***d*** (0.200 mg/mL) were dissolved in PBS at pH 7.4. 500 μL of each solution was mixed with 500 μL DAF solution. Every effort was made to exclude light during this process. The presence of released NO was confirmed by fluorescence spectroscopy by observing the fluorescence emission signal between 500 and 550 nm (excitation wavelength at 492 nm).

5.2.7 Cell culture. Breast Cancer Cell Line MCF7 was purchased from CellBank Australia and etoposide resistant MCF7/VP16 were generated from the parental cell line according to the previous paper.[28] Both cells were cultured in Dulbecco's Modified Eagle's medium (DMEM; Sigma-Aldrich, NSW, Australia) supplemented with 10% v/v fetal bovine serum (FBS; ThermoFisher Scientific, Victoria, Australia). Cell cultures were maintained in a humidified atmosphere at 37 °C and 5% CO_2.

5.2.8 Cell viability assays. The cytotoxicity of DOX was tested in-vitro using a standard cell viability Alamar Blue Assay. The assay is used to quantitatively measure the viability of living cells based on their reducing capabilities; Oxidized non-fluorescent Alamar blue reagent was reduced to fluorescent red colour.[29] The fluorescent intensity is directly proportional to the number of living cells.

The cells were plated at 3000 per well into 96-well plates and incubated for 24 h. Different concentrations of doxorubicin were treated and plates were then incubated for 72 h at 37 °C and 5% CO_2. After 72 h the media was removed and replaced with 100 μL of a 10% Alamar Blue solution comprising of Alamar Blue diluted in complete media (DMEM and 10% FBS). Cells were returned to the incubator and maintained at a humidified atmosphere of 37 °C and 5% CO_2 for three hours and protected from direct light. After the three hour incubation, plates were read at 575 nm and data was

plotted relative to untreated cells and analysed in GraphPad Prism.

To test the cytotoxic effects of NO to improve DOX sensitivity in MCF7 and MCF7/VP16 cells, the cells were initially seeded at 3000 cells per well for MCF7 and 4000 cells per well for the MCF7/VP16 cell line in white walled 96 well plate tissue culture plates and incubated for 24 h. The cells were then co-incubated with DOX (0 – 0.8 µM) and GSNO (1 mM), GSNO-conjugated star polymer ***d*** (1.40 mg/mL, inside [GSNO] = 1 mM), GSH (1mM), GSH-conjugated star polymer ***e*** (1.38 mg/mL, inside [GSH] = 1 mM) or empty star polymer ***b*** (1.06 mg/mL) separately for 24 h at 37 °C and 5% CO_2. The synthesis of GSH-conjugated star polymer ***e*** is described in the supporting information (See Supporting Information section A.2). These stars would be the final product after NO was released from GSNO-conjugated star polymers. Empty star polymer ***b*** was not incorporated with any other functional groups.

Cells were co-incubated for 24 hours, after which point the media was removed and replaced with 100 µL of a 10% Alamar Blue solution comprising of Alamar Blue diluted in complete media (DMEM and 10% FBS).

Cells were returned to the incubator and maintained in a humidified atmosphere of 37 °C and 5% CO_2 for three hours protected from direct light. After the three hour incubation the fluorescence was determined using the Perkin Elmer Ensight plate reader. Fluorescence was read using a fluorescence excitation wavelength of 570 nm and emission wavelength of 585nm.

Data was normalized to the absorbance of untreated control cells, was considered which were expected to maintain maximal cell 100 % viability.

5.2.9 Western Blot Analysis. Cells were directly solubilized in the RIPA lysis buffer (25 mM Tris•HCl pH 7.6, 150 mM NaCl, 1 % NP-40, 1 % sodium deoxycholate, 0.1 % SDS). After centrifugation (13,000 × g for 3 min), the protease inhibitor cocktail tablet (cOmplete™, Mini protease inhibitor cocktail tablets) were added to the supernatant. Lysed samples containing laemmli sample buffer (x 4, Bio-Rad) and 2-mercaptoethanol were heated at 37 °C for 30 minutes. Whole cell extracts contacting equal amounts of proteins (28 - 30 µg) were then separated by SDS-PAGE (4-15 %), and transferred to polyvinylidene difluoride membrane sheets (Immobilon-P, Millipore, Bedford, MA). The membrane sheets were blocked with 5 % (w/v) non-fat dry milk in

TBST (Tris-buffered saline with 0.1 % of Tween20) overnight, and then probed with anti-MRP1 (rabbit monoclonal, rabbit IgG, diluted 1:1000 in blocker non-fat dry milk 5%, Cell Signaling Technology, Inc.) and anti-glyceraldehyde-3-phosphate dehydrogenase (GAPDH, mouse monoclonal, diluted 1 to 5000 in blocker non-fat dry milk 1%). After overnight incubation, the membrane was washed with TBS-Tween 0.1% and subjected for 1 hour to secondary anti-rabbit IgG (ThermoFisher Scientific, diluted 1:5000 in TBS-Tween 0.1%) and anti-mouse IgG (ThermoFisher Scientific, diluted 1:5000 in TBS-Tween 0.1%) at room temperature. The membrane was washed again with TBS-Tween 0.1% and proteins were detected by enhanced chemiluminescence (Bio-Rad) after chemiluminescent substrate (SuperSignal™ West Pico, Thermo Scientific) was added into the membrane for 1-2 minutes.

5.3 Results and Discussion

5.3.1 Synthesis of GSNO-conjugated Core Cross-linked Star polymers. Core cross-linked star polymer nanoparticles were prepared using the ‘arm-first’ method, which was previously developed and reported from our group for a number of applications including drug delivery, magnetic resonance imaging (MRI) and siRNA delivery.[30–36] In particular, NO-releasing star polymer was developed in which the secondary amine groups were reacted with NO gas to produce NO-core cross linked star polymers. These NO-releasing star polymers were observed to prevent *Pseudomonas aeruginosa* biofilm formation.[37] Herein, we extended and developed our previous work on star polymers. The general synthetic strategy applied in this study, the ‘arm-first’ synthesis of core cross-linked star polymers followed by conjugation with a small NO donor (*S*-nitrosoglutathione (GSNO)) to yield a NO-delivery nanoparticle system, is summarised in Scheme 1.

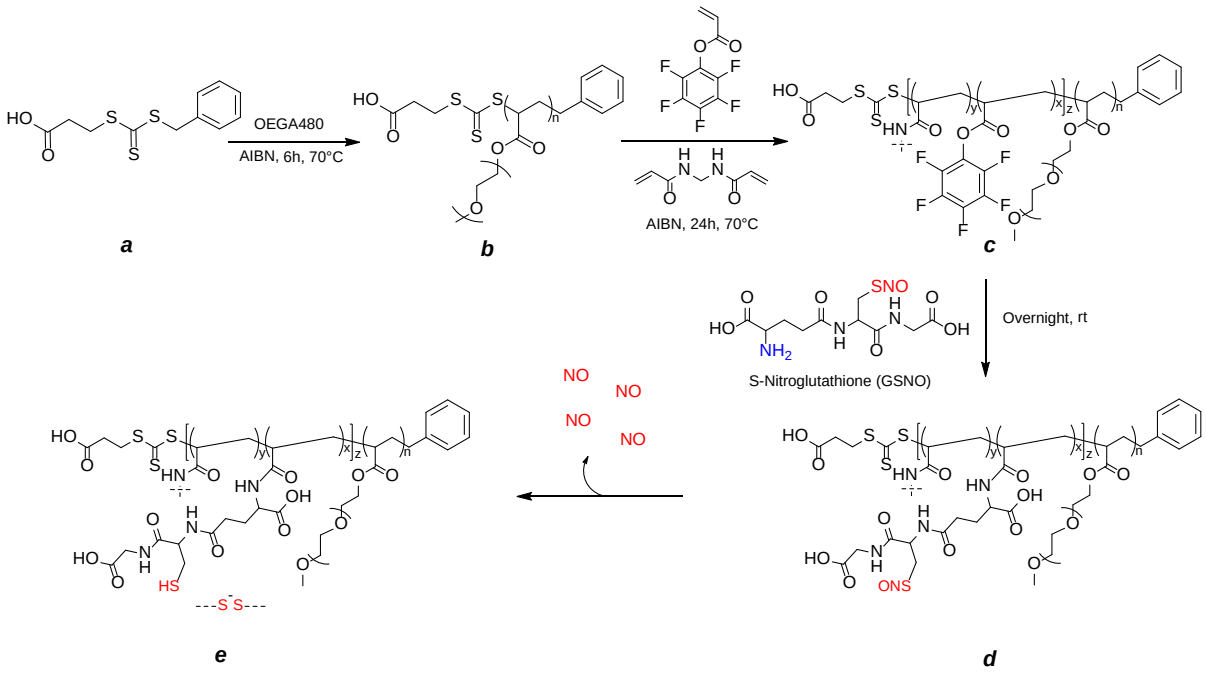

Scheme 1. Synthesis of POEGA-*block*-P(MBAA-*co*-PFPA) core cross-linked star polymer ***c*** using the 'arm first' method of POEGA ***b***, followed by the conjugation with S-nitrosoglutathione (GSNO) to yield NO-delivery star polymer system ***d***. Once NO is released, sulfhydryl groups (GSH) or disulfide bonds (GS-SG) ***e*** would be formed.

Initially, poly(ethylene glycol) methyl ether acrylate (POEGA) linear polymer ***b*** was prepared by reversible addition fragmentation transfer polymerization (RAFT) in the presence of 3-(benzyl sulfanyl thiocarbonyl sulfanyl)-propanoic acid, which was then purified and characterized by gel permeation chromatography (GPC) and ^{1}H nuclear magnetic resonance (NMR) spectroscopy (Figure 1 and S1, Table S1). The molecular weight of the POEGA based on ^{1}H NMR was determined to be 9551g mol^{-1} (calculated using the following equation: $M_n = [(I^{3.37ppm}/3)/(I^{7.2ppm}/2)] \times MW^{OEGA} + MW^{RAFT}$).

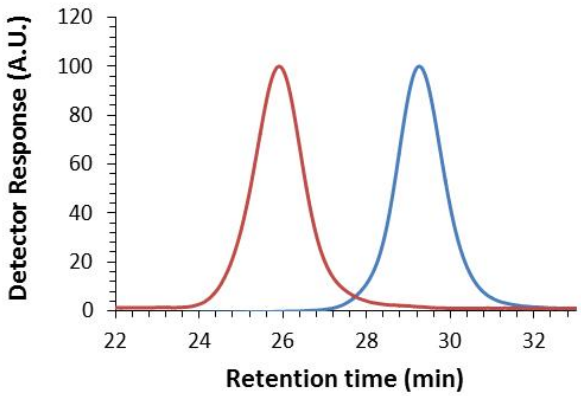

Figure 1. GPC chromatograms for POEGA (10K arm polymer) (blue line) and POEGA-block-P(MBAA-co-PFPA) (red line) (Table S1, Entry 1, 2).

The linear arm polymer was then chain extended with pentafluorophenyl acrylate (PFPA) in the presence of the cross-linker *N,N'*-methylenebis(acrylamide) (MBAA) (Scheme 1, Step 2). The resulting core-cross linked star polymer ***c*** was purified from residual unreacted arms by precipitation and characterised via ^{1}H NMR, ^{19}F NMR, GPC, dynamic light scattering (DLS) and transmission electron microscopy (TEM) (Figure 1, 2, S2 and S3, Table S1). GPC traces confirmed a low polydispersity (PDI: 1.13) maintained after the star formation (Figure 1, Table S1). DLS revealed a number average hydrodynamic particle diameter of 10.7 nm, with a polydispersity of 0.17 (Figure 2).

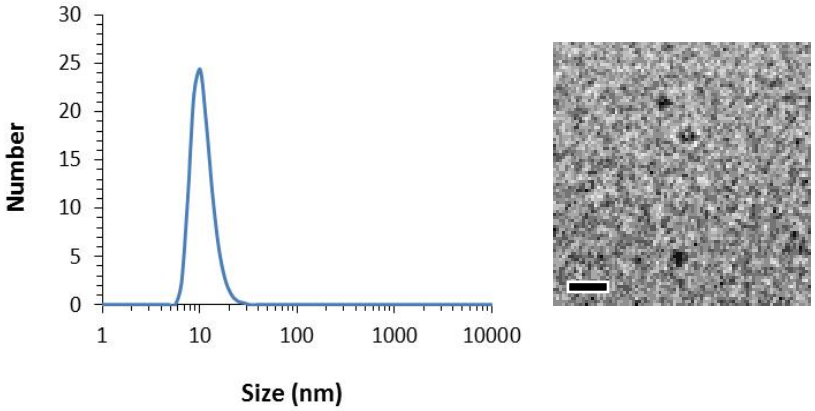

Figure 2. Size distribution (by number) for star polymer POEGA-block-P(MBAA-co-PFPA) as determined by dynamic light scattering with number average diameter, and transmission electron microscopy (TEM) images with 100 nm scale bar; average diameter = 10.7 nm and PDI = 0.17 in PBS pH 7.4 determined by DLS.

^{1}H NMR and ^{19}F NMR analyses showed the successful incorporation of PFPA functional groups and cross-linker into the star polymers. In particular, the molar

composition of PFPA and OEGA moieties in the star polymer were determined to be 31 % and 69 % respectively using 2,2,2-trifluoroethanol (TFE) as an integral reference peak in ^{1}H NMR and ^{19}F NMR, which calculation was further described in the supporting information (Figure S2 and S3). The molar composition of PFPA was determined to be 31 % using ^{19}F NMR and 2,2,2-trifluoroethanol (TFE) as an internal reference peak (Figure S2). The OEGA moieties in the star polymer were determined to be a 69 % quantified via ^{1}H NMR (Figure S3).

Finally, GSNO modified star polymers ***d*** were prepared (Scheme 1, Step 3) via conjugation of the GNSO to PFPA moieties in the core. Briefly, the pentafluoro-activated ester group (PFP) of POEGA-*block*-P(MBAA-*co*-PFPA) was reacted with the amino group (NH_2) of GSNO forming a covalent linkage into the core of the stars as described fully in the experimental section. By using the molar composition of PFPA and OEGA moieties, the amount of GSNO for an equimolar ratio of [GSNO]:[PFPA] was calculated using the following equation: the amount of PFPA inside the stars (g) = the amount of POEGA-*block*-P(MBAA-*co*-PFPA) (g) × {(MW^{PFPA} × 31 %)/[(MW^{PFPA} × 31 %) + (MW^{OEGA} × 69 %)]}, the amount of GSNO fully conjugated inside the star (g) = the amount of PFPA inside the stars (g) × (MW^{GSNO}/MW^{PFPA}). An excess (× 3.5) of GSNO was used to optimize the functionalization reaction with PFP, resulting in full conjugation into the star. All the reactions were performed carefully under dark conditions designed to prevent the degradation of GSNO due to light. Quantitative conjugation of GSNO into the star core was confirmed by both ^{1}H NMR and ^{19}F NMR analysis. Conveniently, on reaction with GSNO the side product, pentafluorophenol is released, resulting in a shift of the corresponding ^{19}F NMR signals (Figure S4): to -162, -166 and -174 ppm. After purification by exhaustive dialysis against distilled water, the excess of GSNO and pentafluorophenol were removed, as evidenced by the absence of their ^{19}F NMR and ^{1}H NMR spectra (Figure S4, B).

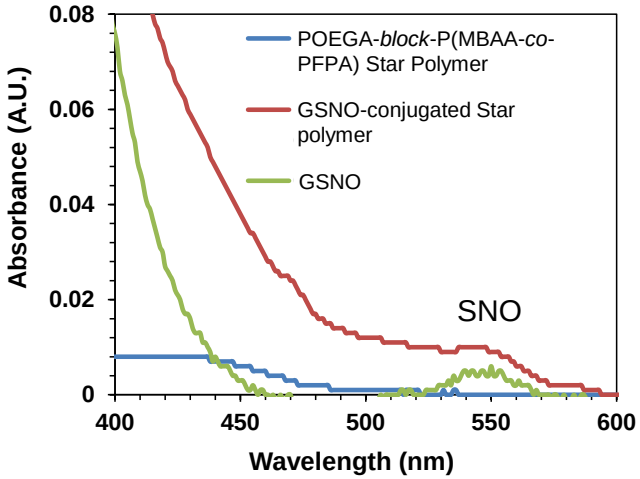

Figure 3. UV-visible spectra for POEGA-*block*-P(MBAA-*co*-PFPA) star polymer, GSNO conjugated star polymer and GSNO for the characteristic band (500-600 nm) of S-nitrosothiol (SNO) structure. (POEGA-*block*-P(MBAA-*co*-PFPA) star polymer = 1.9 mg/mL, GSNO conjugated star polymer = 15 mg/mL, GSNO = 2.0 mg/mL).

The successful conjugation of GSNO into stars was also confirmed by UV-visible spectrophotometry. GSNO has an *S*-nitrosothiol (SNO) structure which has two characteristic UV-vis bands between 330-350 nm and 500-600 nm.[38] The first band (330-350 nm) could not be used to provide evidence for the conjugation due to the overlap with the benzyl and thiocarbonylthio group absorbance of the star polymers (Figure S6). However, the GSNO-conjugated star polymer ***d*** and GSNO both showed the distinctive second band in the region of 500-600 nm, corresponding to the SNO structure (Figure 3). A UV-vis absorbance band in the same region (500-600 nm) was not detected in the neat star polymers, POEGA-*block*-P(MBAA-*co*-PFPA) ***c***. After conjugation with GSNO, DLS analysis indicated a slight increase in size (10.9nm) with a polydispersity of 0.22 (Figure S7).

5.3.2 Determination of NO release from GSNO conjugated star polymer using 5,6-diaminofluorescein (DAF). GSNO-conjugated star polymers ***d*** were then examined for their capacity to release NO, using a NO responsive fluorescent probe, 5,6-diaminofluorescein (DAF). DAF is commonly used for the detection of NO as it is ordinarily non-fluorescent but becomes fluorescent in the presence of NO, therefore providing evidence for NO release (as shown in Figure 4).[39–41]

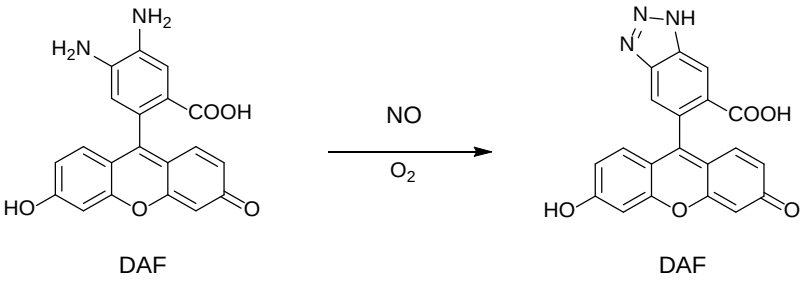

DAF DAF

Figure 4. Fluorescent probe DAF for NO detection. NO reacts with DAF to yield a green fluorescence emission at 524 nm.

In addition, DAF is highly selective and sensitive for the detection of nitric oxide release, being non-fluorescent in the presence of other reactive nitrogen species including nitrate, nitrite, hydrogen peroxide or peroxynitrite.[40] While it is known that DAF may cross react with ascorbic acid or dehydroascorbic acid,[42] these compounds are not present in the model system used herein. A sample of GSNO-conjugated star polymer ***d*** was dissolved in phosphate buffered saline (PBS) solution containing DAF (Figure 5A). The fluorescence intensity was found to increase over time following the addition of the NO-releasing GSNO-conjugated star polymer ***d***, indicating that NO was indeed generated from GSNO-conjugated star polymer ***d***. Furthermore, the NO release profiles were compared between GSNO and the GSNO-conjugated polymeric systems ***d*** using DAF dye. The GSNO-polymeric donor ***d*** showed a substantially slower NO release profile, compared to the small molecule, GSNO (Figure 5A, S8 (A)), indicating that the hydrophobic core of star polymers could improve GSNO stability.

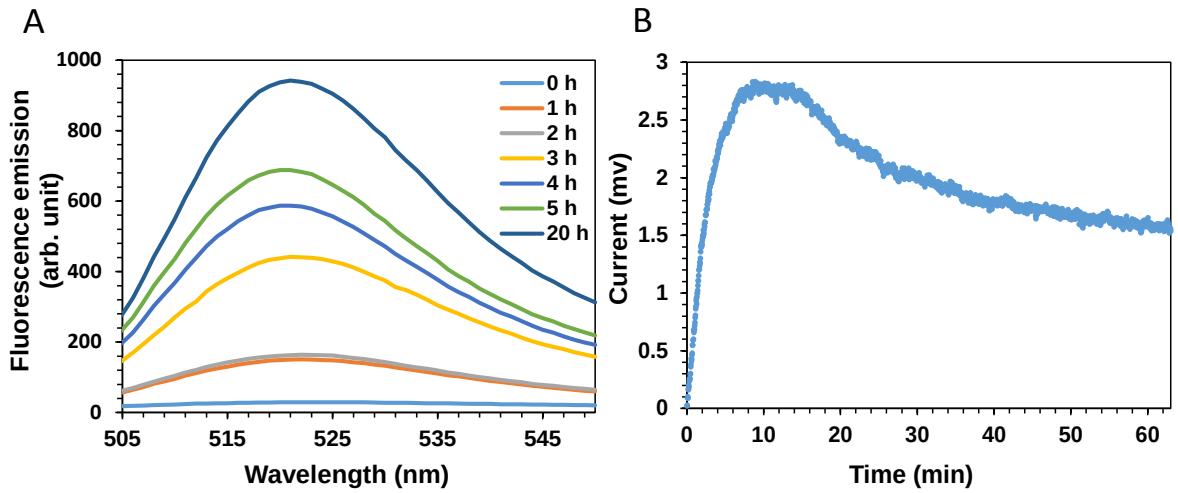

Figure 5. (A) Fluorescence spectra generated by the release of nitric oxide in the presence of 5,6-diaminofluorescein (23 µM). Evolution of fluorescence emission spectra at 524 nm caused by NO release from GSNO-conjugated star polymer dissolved in PBS at pH 7.4 (0.100 mg/mL, equivalent [GSNO] = 0.024 mg/mL). (B) Electrochemical response from GSNO-conjugated star polymer ***d*** (0.071 mg/mL, inside [GSNO] = 50 µM, 0.017 mg/mL) in PBS at pH 7.4 at 37 °C.

Additionally, the release of NO from GSNO-conjugated star polymers ***d*** was examined via an NO-selective amperometric sensor manufactured by Unisense A/S.[43] The evolution of NO was observed, increasing over the first 10 min (Figure 5B), followed by a relatively constant NO signal. A similar maximum amount of NO release was detected from GSNO and GSNO-conjugated star polymers ***d*** (Figure 5B, S8 (B)), indicating that GSNO-conjugated star polymers successfully contained the expected amount of GSNO inside the core. Altogether, these results demonstrated that GSNO-conjugated star polymers ***d*** were successfully prepared, and exhibited a substantially slower NO release profile than small molecule GSNO.

5.3.3 Biological evaluation of the effects of NO and DOX on different cell lines. Initial investigations were made on human ovarian carcinoma (SKOV3) and DOX resistant ovarian carcinoma (SKOVCR) cell.

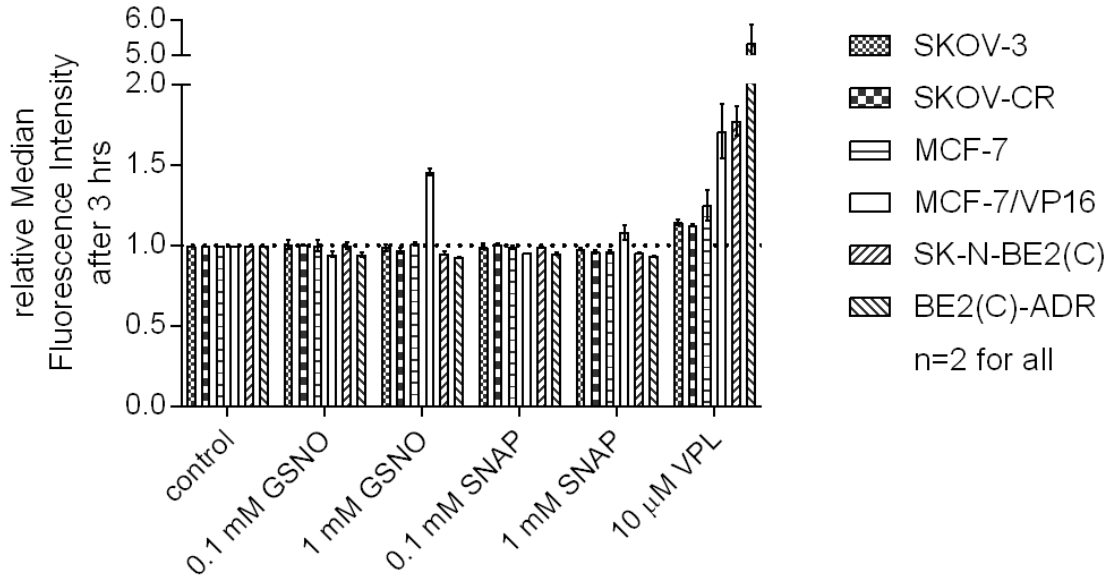

Figure 6. Normalised intracellular doxorubicin content measured as median fluorescence intensity in six different cell lines after co-treatment with 4 µM DOX and NO donors S-nitrosoglutathione (GSNO) or S-nitroso penicillamine (SNAP) at two different concentrations and 10 µM verapamil as positive control for 3 hours. Data was normalised to cells incubated with 4 µM doxorubicin only (control). Data is shown as mean ± SD (n=2).

Although intracellular NO release and nitrated drug efflux transporters modification could be observed (Figure S13-S16), there was no apparent improvement in DOX accumulation and cytotoxicity with NO treatment (Figure 6, S17, S18). This led to screening a number of cell lines (Figure 6, S18). The synergistic cytotoxic effect of DOX and NO was not detected in any of the tested cell lines, whereas co-incubation of GSNO with DOX increased DOX accumulation in MCF-7/VP16 cells (Figure 6, S18), leading to the change in cell line used for more detailed investigations.

5.3.4 Western blot detection of MRP1 transporters in MCF7 and MCF7/VP16 cells. As previously described, MCF7/VP16 cells highly expressed MRP1 transporters, compared to MCF7 cells.[28,44,45] In order to validate the presence of MRP1 transporters, western blot detection of the protein expression was conducted in both cell lines. Whole cell extracts containing similar amounts of proteins (28 – 30 µg) were subjected to western blotting using an anti-MRP1 antibody. The expression of housekeeping protein GAPDH (glyceraldehydes-3-phosphate dehydrogenase) was measured as a control of equal loading. Figure 7 shows that significant overexpression of MRP1

protein was detected in MCF7/VP16 cells, whereas MCF7 cells showed negligible expression of MRP1 transporters.

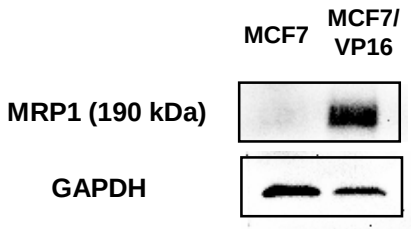

Figure 7. Western blot detection after MRP1 immunoprecipitation in MCF7 and MCF7/VP16 cells.

5.3.5 Application of GSNO and GSNO-conjugated Star Polymers to improve the DOX sensitivity of Human breast cancer cells (MCF7) and resistant cells (MCF7/VP16). Doxorubicin (DOX), also known as adriamycin, is an anticancer chemotherapy drug used to clinically treat a range of cancers.[46] The effectiveness of DOX can be reduced due to multidrug resistance (MDR) effects in various cancer cell lines. Many mechanisms are involved in these effects. One such mechanism is the overexpression of efflux pumps which limit intracellular drug concentration and toxicity.[2] As described previously, NO has been shown to reverse the DOX resistance in various cancer cells by inhibiting functional efflux transporters through nitration of the tyrosine residues in the proteins. In this study, human breast cancer cells (MCF7) and etoposide-resistant cancer cells (MCF7/VP16) were examined. MCF7/VP16 cells are 9-fold more resistant to doxorubicin (Figure S10), and overexpress MRP1 transporters, compared to the MCF7 cell line.[28,44,45,47] We decided to investigate the effect of delivering either GSNO or GSNO-conjugated star polymer ***d*** both with and without DOX on these cancer cell lines using the Alamar blue Assay. MCF7/VP16 cells were initially co-incubated with DOX (0 – 0.8 µM) and empty star polymers ***b*** (1.06 mg/mL), GSNO-conjugated star polymers ***d*** (1.40 mg/mL, corresponding to [GSNO] = 1 mM) or GSNO (1 mM) (Figure 8). The empty star polymers were POEGA stars ***b***, as described in the experimental section. The cells co-treated with GSNO or GSNO stars ***d*** separately with different concentrations of DOX showed lower cell viability (%) effects over the concentration range of 0.2 to 0.8 µM of DOX, compared to the native DOX treatment and co-treatment with empty stars ***b***. These synergistic cytotoxic effects were more pronounced when the cells were co-incubated with GSNO and DOX, as opposed to GSNO-conjugated stars ***d*** with DOX. Additionally, side products from

GSNO and GSNO-conjugated star polymers ***d*** might be involved in causing some of the observed cytotoxic effects on these cancer cell lines, which is further illustrated in Figure 9. In the absence of DOX, GSNO and GSNO-conjugated star polymers ***d*** were marginally more toxic than empty star polymer treatment ***b***, which resulted in almost 100 % cell viability.

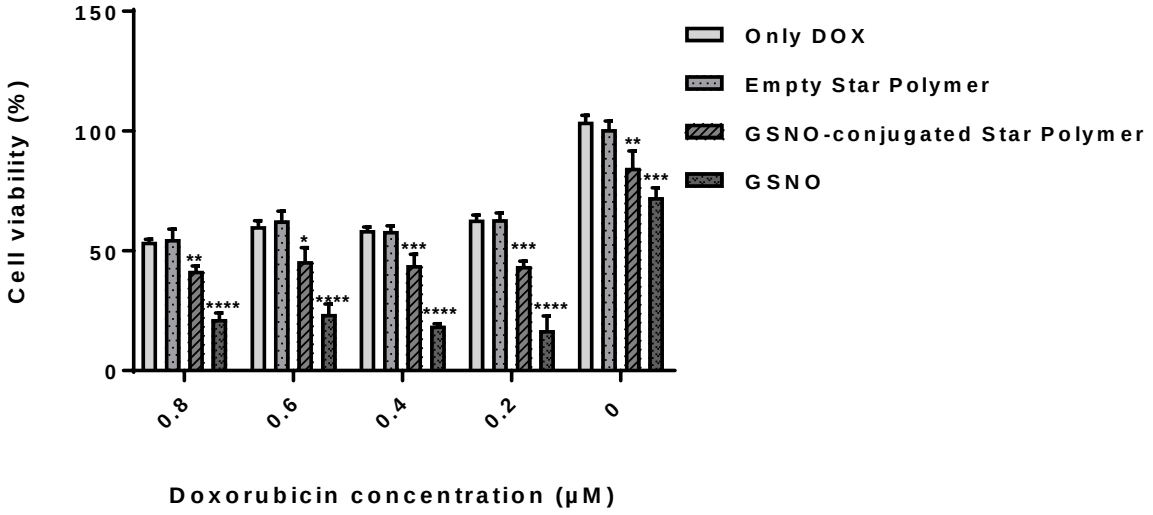

Figure 8. Cell viability (%) of MCF7/VP16 cells in the presence of empty star polymer (1.06 mg/mL), GSNO-conjugated star polymer (1.40 mg/mL, inside [GSNO] = 1 mM), and GSNO (1 mM) with and without co-treatment of DOX (0 – 0.8 μM). Note: all toxicity studies have been repeated in 3 distinct experiments in triplicate. **** $p < 0.0001$, *** $p < 0.001$, ** $p < 0.01$, * $p < 0.05$, error = SD, n = 3.

Furthermore, we performed further control experiments to confirm whether NO can indeed enhance cytotoxicity toward MCF7/VP16 cells. The control experiments included GSH (glutathione) and GSH-conjugated star polymers ***e***, which are the side products formed after NO was released from GSNO and GSNO-conjugated star polymers ***d*** respectively. In particular, GSH is highly reactive and is involved in various cellular signalling effects due to its function as an intracellular reducing agent.[48,49] In order to observe whether these reactive control particles exert any cytotoxic effects on these cancer cell lines, cells were co-incubated with GSH or GSH-conjugated star polymers ***e*** with and without DOX. GSH-conjugated star polymers ***e*** were prepared and described in supporting information (A.2).

Co-administration of these particles with a range of DOX concentrations (0 – 0.8 μM) gave no decrease in cell viability (%), relative to co-treatment of empty stars ***b*** with DOX and the native DOX treatment (Figure 9). Overall these results indicate that NO

delivered from GSNO and GSNO-conjugated star polymers ***d*** did increase susceptibility of MCF7/VP16 cells to DOX cytotoxicity.

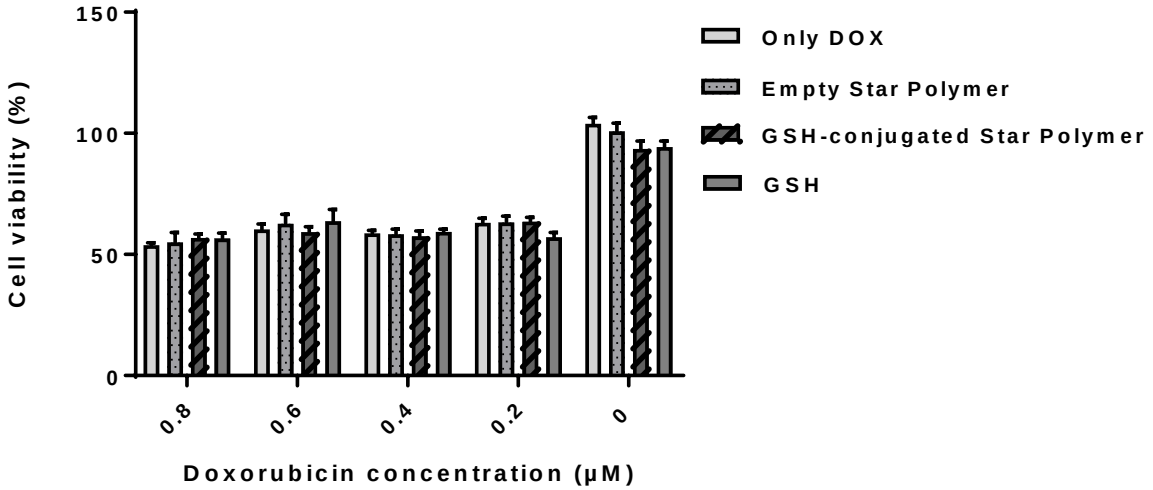

Figure 9. Cell viability (%) of MCF7/VP16 cells in the presence of empty star polymer (1.06 mg/mL), GSH-conjugated star polymer (1.38 mg/mL, inside [GSH] = 1 mM), and GSH (1 mM) with and without co-treatment of DOX (0 – 0.8 μM). Note: all toxicity studies have been repeated in 3 distinct experiments in triplicate. Error = SD, n = 3.

Following the cytotoxicity tests on MCF7/VP16 cells, the same experiments were performed using non-resistant MCF7 cells. In contrast to MCF7/VP16 cells, no enhancement of DOX cytotoxicity to MCF7 cells was observed with co-delivery of NO (Figure 10, 11).

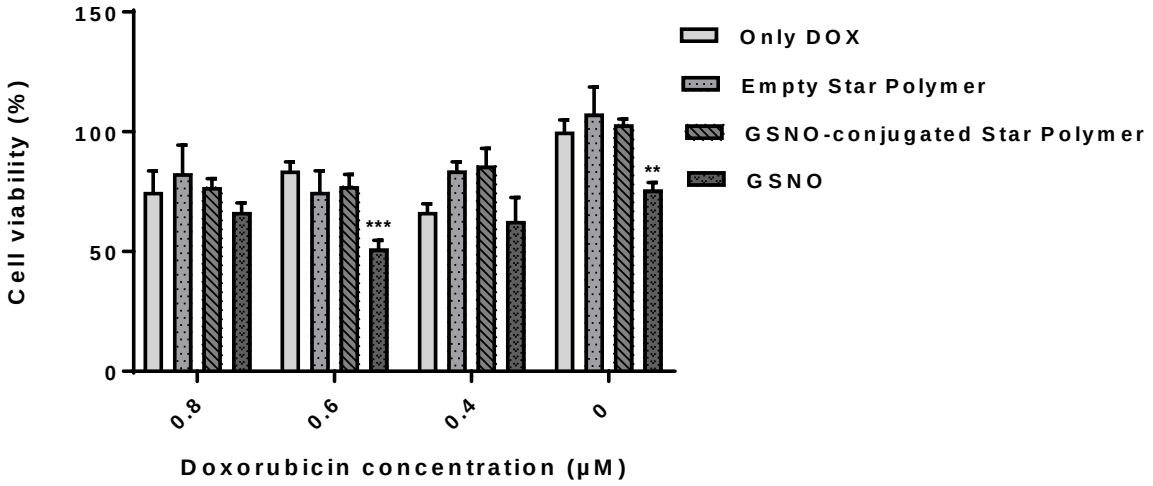

Figure 10. Cell viability (%) of MCF7 cells in the presence of empty star polymer (1.06 mg/mL), GSNO-conjugated star polymer (1.40 mg/mL, inside [GSNO] = 1 mM), and GSNO (1 mM) with and without co-treatment of DOX (0 – 0.8 μM). Note: all toxicity studies have been repeated in 3 distinct experiments in triplicate. *** $p < 0.001$, ** $p < 0.01$, error = SD, n = 3.

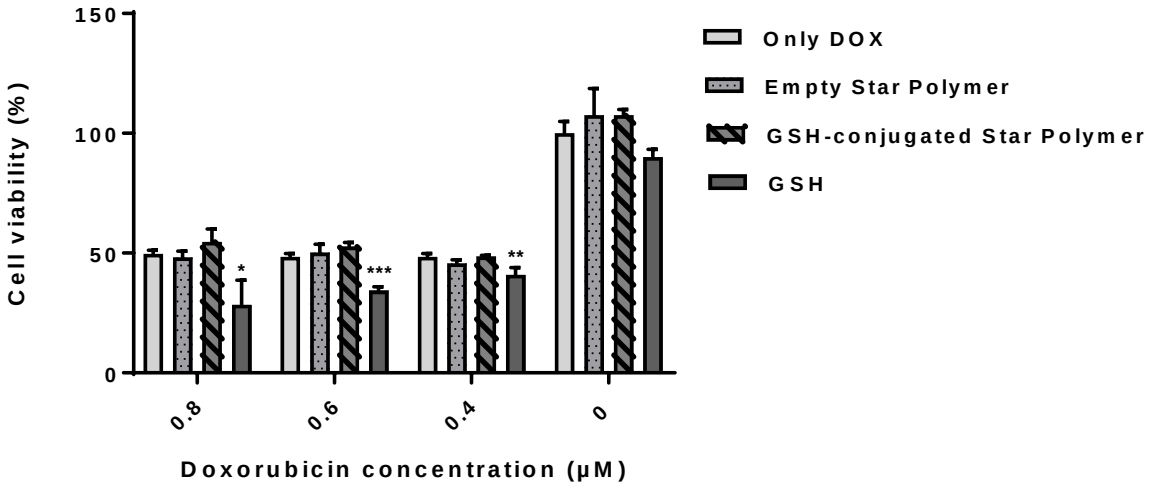

Figure 11. Cell viability (%) of MCF7 cells in the presence of empty star polymer (1.06 mg/mL), GSH-conjugated star polymer (1.38 mg/mL, inside [GSH] = 1 mM), and GSH (1 mM) with and without co-treatment of DOX (0 – 0.8 μM). Note: all toxicity studies have been repeated in 3 distinct experiments in triplicate. *** $p < 0.001$, ** $p < 0.01$, * $p < 0.05$, error = SD, n = 3.

While the co-delivery of GSNO and DOX appeared to exert a minor cytotoxic effect on MCF7 cells, co-treatment of GSH and DOX also decreased cell viability, indicating that the observed increase in toxicity in the case of non-resistant MCF cells could potentially be attributed to changes in GSH regulation (Figure 10, 11).

5.4 Conclusion

GSNO-conjugated star polymers were successfully synthesized, showing the slower NO releasing profile in comparison to GSNO itself. NO delivered from GSNO and GSNO-conjugated star polymers increased susceptibility of MCF7/VP16 cells to DOX cytotoxicity, which was not observed for non-resistant MCF7 cell lines. In future study, the GSNO-functionalised star polymer would be tested to show the improved the GSNO stability in aqueous conditions and even in the cellular environment. Western blot analysis would be useful to identify whether that the most likely mechanism might be through of the nitration of the tyrosine residues found in the MRP1 transporters over expressed in the MCF7/VP16 MDR cell line.

5.5 Reference

1 M. M. Gottesman, T. Fojo and S. E. Bates, Multidrug resistance in cancer: role of ATP-dependent transporters., *Nat. Rev. Cancer*, 2002, **2**, 48–58.

2 M. M. Gottesman, Mechanisms of Cancer Drug Resistance, *Annu. Rev. Med.*, 2002, **53**, 615–627.

3 S. M. Simon and M. Schindler, Cell biological mechanisms of multidrug resistance in tumors., *Proc. Natl. Acad. Sci. U. S. A.*, 1994, **91**, 3497–504.

4 G. Szakács, J. K. Paterson, J. A. Ludwig, C. Booth-Genthe and M. M. Gottesman, Targeting multidrug resistance in cancer, *Nat. Rev. Drug Discov.*, 2006, **5**, 219–234.

5 P. von Bossanyi, S. Diete, K. Dietzmann, M. Warich-Kirches and E. Kirches, Immunohistochemical expression of P-glycoprotein and glutathione S-transferases in cerebral gliomas and response to chemotherapy, *Acta Neuropathol.*, 1997, **94**, 605–611.

6 N. A. Colabufo, F. Berardi, M. Cantore, M. Contino, C. Inglese, M. Niso and R. Perrone, Perspectives of P-glycoprotein modulating agents in oncology and neurodegenerative diseases: pharmaceutical, biological, and diagnostic potentials., *J. Med. Chem.*, 2010, **53**, 1883–1897.

7 H. Thomas and H. M. Coley, Overcoming multidrug resistance in cancer: an update on the clinical strategy of inhibiting p-glycoprotein., *Cancer Control*, 2003, **10**, 159–165.

8 C. Ricciardelli, M. P. Ween, N. A. Lokman, I. A. Tan, C. E. Pyragius and M. K. Oehler, Chemotherapy-induced hyaluronan production: a novel chemoresistance mechanism in ovarian cancer, *BMC Cancer*, 2013, **13**, 476.

9 C. W. Kim, D. Asai, J.-H. Kang, A. Kishimura, T. Mori and Y. Katayama, Reversal of efflux of an anticancer drug in human drug-resistant breast cancer cells by inhibition of protein kinase Cα (PKCα) activity, *Tumor Biol.*, 2016, **37**, 1901–1908.

10 C. Riganti, S. Orecchia, G. Pescarmona, P. G. Betta, D. Ghigo and A. Bosia, Statins revert doxorubicin resistancevia nitric oxide in malignant mesothelioma, *Int. J. Cancer*, 2006, **119**, 17–27.

11 Q. Song, S. Tan, X. Zhuang, Y. Guo, Y. Zhao, T. Wu, Q. Ye, L. Si and Z. Zhang, Nitric Oxide Releasing <scp>d</scp> -α-Tocopheryl Polyethylene Glycol Succinate for Enhancing Antitumor Activity of Doxorubicin, *Mol. Pharm.*, 2014, **11**, 4118–4129.

12 S. Giri, R. Rattan, M. Deshpande, J. L. Maguire, Z. Johnson, R. P. Graham and V. Shridhar, Preclinical Therapeutic Potential of a Nitrosylating Agent in the Treatment of Ovarian Cancer, *PLoS One*, 2014, **9**, e97897.

13 A. de Luca, N. Moroni, A. Serafino, A. Primavera, A. Pastore, J. Z. Pedersen, R. Petruzzelli, M. G. Farrace, P. Pierimarchi, G. Moroni, G. Federici, P.

Sinibaldi Vallebona and M. Lo Bello, Treatment of doxorubicin-resistant MCF7/Dx cells with nitric oxide causes histone glutathionylation and reversal of drug resistance, *Biochem. J.*, 2011, **440**, 175–183.

14 N. E. Matthews, M. A. Adams, L. R. Maxwell, T. E. Gofton and C. H. Graham, Nitric Oxide-Mediated Regulation of Chemosensitivity in Cancer Cells, *JNCI J. Natl. Cancer Inst.*, 2001, **93**, 1879–1885.

15 L. J. FREDERIKSEN, D. R. SIEMENS, J. P. HEATON, L. R. MAXWELL, M. A. ADAMS and C. H. GRAHAM, Hypoxia Induced Resistance to Doxorubicin in Prostate Cancer Cells is Inhibited by Low Concentrations of Glyceryl Trinitrate, *J. Urol.*, 2003, **170**, 1003–1007.

16 S. De Boo, J. Kopecka, D. Brusa, E. Gazzano, L. Matera, D. Ghigo, A. Bosia and C. Riganti, iNOS activity is necessary for the cytotoxic and immunogenic effects of doxorubicin in human colon cancer cells, *Mol. Cancer*, 2009, **8**, 108.

17 C. Riganti, E. Miraglia, D. Viarisio, C. Costamagna, G. Pescarmona, D. Ghigo and A. Bosia, Nitric oxide reverts the resistance to doxorubicin in human colon cancer cells by inhibiting the drug efflux, *Cancer Res.*, 2005, **65**, 516–525.

18 R. Fruttero, M. Crosetti, K. Chegaev, S. Guglielmo, A. Gasco, F. Berardi, M. Niso, R. Perrone, M. A. Panaro and N. A. Colabufo, Phenylsulfonylfuroxans as modulators of multidrug-resistance-associated protein-1 and P-glycoprotein., *J. Med. Chem.*, 2010, **53**, 5467–75.

19 A. Bratasz, N. M. Weir, N. L. Parinandi, J. L. Zweier, R. Sridhar, L. J. Ignarro and P. Kuppusamy, Reversal to cisplatin sensitivity in recurrent human ovarian cancer cells by NCX-4016, a nitro derivative of aspirin, *Proc. Natl. Acad. Sci.*, 2006, **103**, 3914–3919.

20 K. Chegaev, C. Riganti, L. Lazzarato, B. Rolando, S. Guglielmo, I. Campia, R. Fruttero, A. Bosia and A. Gasco, Nitric oxide donor doxorubicins accumulate into Doxorubicin-resistant human colon cancer cells inducing cytotoxicity., *ACS Med. Chem. Lett.*, 2011, **2**, 494–497.

21 E. V. Stevens, A. W. Carpenter, J. H. Shin, J. Liu, C. J. Der and M. H. Schoenfisch, Nitric oxide-releasing silica nanoparticle inhibition of ovarian cancer cell growth., *Mol. Pharm.*, 2010, **7**, 775–85.

22 M.-F. Chung, H.-Y. Liu, K.-J. Lin, W.-T. Chia and H.-W. Sung, A pH-responsive carrier system that generates NO bubbles to trigger drug release and reverse P-glycoprotein-mediated multidrug resistance, *Angew. Chemie Int. Ed.*, 2015, **54**, 9890–9893.

23 H. T. T. Duong, Z. M. Kamarudin, R. B. Erlich, Y. Li, M. W. Jones, M. Kavallaris, C. Boyer and T. P. Davis, Intracellular nitric oxide delivery from stable NO-polymeric nanoparticle carriers, *Chem. Commun.*, 2013, **49**, 4190–4192.

24 M. H. Stenzel and T. P. Davis, Star polymer synthesis using trithiocarbonate functional β-cyclodextrin cores (reversible addition-fragmentation chain-transfer polymerization), *J. Polym. Sci. Part A Polym. Chem.*, 2002, **40**, 4498–

4512.

25 M. Eberhardt, R. Mruk, R. Zentel and P. Théato, Synthesis of pentafluorophenyl(meth)acrylate polymers: New precursor polymers for the synthesis of multifunctional materials, *Eur. Polym. J.*, 2005, **41**, 1569–1575.

26 Y. Li, H. T. T. Duong, M. W. Jones, J. S. Basuki, J. Hu, C. Boyer and T. P. Davis, Selective postmodification of copolymer backbones bearing different activated esters with disparate reactivities, *ACS Macro Lett.*, 2013, **2**, 912–917.

27 A. J. Friedman, G. Han, M. S. Navati, M. Chacko, L. Gunther, A. Alfieri and J. M. Friedman, Sustained release nitric oxide releasing nanoparticles: characterization of a novel delivery platform based on nitrite containing hydrogel/glass composites., *Nitric oxide Biol. Chem.*, 2008, **19**, 12–20.

28 E. Schneider, H. Yamazaki, B. Sinha and K. Cowan, Buthionine sulphoximine-mediated sensitisation of etoposide-resistant human breast cancer MCF7 cells overexpressing the multidrug resistance-associated protein involves increased drug accumulation, *Br. J. Cancer*, 1995, **71**, 738–743.

29 T. Y. E. Liaw, N. K. Salam, M. J. McKay, A. M. Cunningham, D. E. Hibbs and M. Kavallaris, Class I -tubulin mutations in 2-methoxyestradiol-resistant acute lymphoblastic leukemia cells: implications for drug-target interactions, *Mol. Cancer Ther.*, 2008, **7**, 3150–3159.

30 J. Ferreira, J. Syrett, M. Whittaker, D. Haddleton, T. P. Davis and C. Boyer, Optimizing the generation of narrow polydispersity ‘arm-first’ star polymers made using RAFT polymerization, *Polym. Chem.*, 2011, **2**, 1671–1677.

31 J. S. Basuki, H. T. T. Duong, A. Macmillan, R. Whan, C. Boyer and T. P. Davis, Polymer-Grafted, nonfouling, magnetic nanoparticles designed to selectively store and release molecules via ionic interactions, *Macromolecules*, 2013, **46**, 7043–7054.

32 J. A. Syrett, D. M. Haddleton, M. R. Whittaker, T. P. Davis and C. Boyer, Functional, star polymeric molecular carriers, built from biodegradable microgel/nanogel cores, *Chem. Commun.*, 2011, **47**, 1449–1451.

33 Y. Li, H. T. T. Duong, S. Laurent, A. MacMillan, R. M. Whan, L. Vander Elst, R. N. Muller, J. Hu, A. Lowe, C. Boyer and T. P. Davis, Nanoparticles based on star polymers as theranostic vectors: endosomal-triggered drug release combined with MRI sensitivity., *Adv. Healthc. Mater.*, 2015, **4**, 148–156.

34 J. Liu, H. Duong, M. R. Whittaker, T. P. Davis and C. Boyer, Synthesis of functional core, star polymers via RAFT polymerization for drug delivery applications., *Macromol. Rapid Commun.*, 2012, **33**, 760–766.

35 S. Y. Khor, J. Hu, V. M. McLeod, J. F. Quinn, C. J. H. Porter, M. R. Whittaker, L. M. Kaminskas and T. P. Davis, The pharmacokinetics and biodistribution of a 64 kDa polyPEG star polymer after subcutaneous and pulmonary administration to rats, *J. Pharm. Sci.*, 2016, **105**, 293–300.

36 S. Y. Khor, J. Hu, V. M. McLeod, J. F. Quinn, M. Williamson, C. J. H. Porter, M. R. Whittaker, L. M. Kaminskas and T. P. Davis, Molecular weight (hydrodynamic volume) dictates the systemic pharmacokinetics and tumour disposition of PolyPEG star polymers, *Nanomedicine Nanotechnology, Biol. Med.*, 2015, **11**, 2099–2108.

37 H. T. T. Duong, K. Jung, S. K. Kutty, S. Agustina, N. N. M. Adnan, J. S. Basuki, N. Kumar, T. P. Davis, N. Barraud and C. Boyer, Nanoparticle (Star Polymer) Delivery of Nitric Oxide Effectively Negates Pseudomonas aeruginosa Biofilm Formation, *Biomacromolecules*, 2014, **15**, 2583–2589.

38 P. G. Wang, M. Xian, X. Tang, X. Wu, Z. Wen, T. Cai and A. J. Janczuk, Nitric Oxide Donors: Chemical Activities and Biological Applications, *Chem. Rev.*, 2002, **102**, 1091–1134.

39 P. Cabrales, G. Han, C. Roche, P. Nacharaju, A. J. Friedman and J. M. Friedman, Sustained release nitric oxide from long-lived circulating nanoparticles, *Free Radic. Biol. Med.*, 2010, **49**, 530–538.

40 H. Kojima, N. Nakatsubo, K. Kikuchi, S. Kawahara, Y. Kirino, H. Nagoshi, Y. Hirata and T. Nagano, Detection and imaging of nitric oxide with novel fluorescent indicators: diaminofluoresceins., *Anal. Chem.*, 1998, **70**, 2446–2453.

41 S. H. Yu, J. Hu, F. Ercole, N. P. Truong, T. P. Davis, M. R. Whittaker and J. F. Quinn, Transformation of RAFT Polymer End Groups into Nitric Oxide Donor Moieties: En Route to Biochemically Active Nanostructures, *ACS Macro Lett.*, 2015, **4**, 1278–1282.

42 X. Zhang, W.-S. Kim, N. Hatcher, K. Potgieter, L. L. Moroz, R. Gillette and J. V. Sweedler, Interfering with Nitric Oxide Measurements, *J. Biol. Chem.*, 2002, **277**, 48472–48478.

43 F. Schreiber, L. Polerecky and D. de Beer, Nitric oxide microsensor for high spatial resolution measurements in biofilms and sediments., *Anal. Chem.*, 2008, **80**, 1152–1158.

44 Z. Benderra, A. Trussardi, H. Morjani, A. M. Villa, S. M. Doglia and M. Manfait, Regulation of cellular glutathione modulates nuclear accumulation of daunorubicin in human MCF7 cells overexpressing multidrug resistance associated protein, *Eur. J. Cancer*, 2000, **36**, 428–434.

45 R. N. Watts, C. Hawkins, P. Ponka and D. R. Richardson, Nitrogen monoxide (NO)-mediated iron release from cells is linked to NO-induced glutathione efflux via multidrug resistance-associated protein 1, *Proc. Natl. Acad. Sci.*, 2006, **103**, 7670–7675.

46 O. Tacar, P. Sriamornsak and C. R. Dass, Doxorubicin: an update on anticancer molecular action, toxicity and novel drug delivery systems, *J. Pharm. Pharmacol.*, 2013, **65**, 157–170.

47 E. Schneider, J. K. Horton, C. H. Yang, M. Nakagawa and K. H. Cowan, Multidrug resistance-associated protein gene overexpression and reduced

drug sensitivity of topoisomerase II in a human breast carcinoma MCF7 cell line selected for etoposide resistance., *Cancer Res.*, 1994, **54**, 152–158.

48 S. Chakravarthi, C. E. Jessop and N. J. Bulleid, The role of glutathione in disulphide bond formation and endoplasmic-reticulum-generated oxidative stress, *EMBO Rep.*, 2006, **7**, 271–275.

49 G. K. Balendiran, R. Dabur and D. Fraser, The role of glutathione in cancer, *Cell Biochem. Funct.*, 2004, **22**, 343–352.

Supporting Information

A.1 Amperometric NO Sensing

The NO-generating capability of polymers was examined via an amperometric approach using an NO-selective miniaturized Clark-type sensor manufactured by Unisense A/S. The working concept behind the sensor has been published by Schreiber and co-workers.[1]

Calibration of the sensor was performed after allowing the sensor signal to stabilize over a pre-polarization period (usually 2 hours or more). A stock solution of an NO donor was prepared anaerobically by dissolving a known quantity of S-nitrosoglutathione (0.0229 g, 6.81×10^{-5}) into degassed PBS 7.4 (1.4 mL) in a closed container. 10 mL of PBS buffer was transferred to a nitrogen-flushed bottle equipped with a stirrer and the bottle capped with a modified septum for facilitating insertion of the probe. The sensor was then immersed into the solution via a specialized opening on the septum which enabled the bottle to be capped after the sensor tip had been carefully passed through. Once the signal stabilized to a low, stable reading, the value was recorded and assumed to correspond to the zero [NO] value. Calibration points within the expected range of measurement were collected by injecting known amounts of GSNO stock solution using a micro-syringe into the stirred calibration buffer solution. The current increased upon addition of the first aliquot and reached a plateau after several seconds. Further calibration values were obtained as subsequent aliquots were added (seven in total, ranging from 0 – 5000 µL). The recorded data was used to generate a linear calibration curve for [NO] vs. current (amps). All measurements were conducted at 37 °C

GSNO and GSNO-conjugated star polymers were examined as follows. GSNO (0.085 mg) and GSNO-functionalised polymer (0.355 mg) in deoxygenated pH 7.4 PBS (5 mL) were prepared separately. The sensor was immersed into the polymer solution, using the septum to minimize exposure to air on immersing the sensor into the solution under the dark conditions at 37 °C. All measurement were started once the sensor was immersed and settled down. All conditions were measured at the same condition.

A.2 Post-modification of POEGA-block-P(MBAA-co-PFPA) with GSH

POEGA-block-P(MBAA-co-PFPA) prepared as above (0.01 g,) was dissolved in DMSO (500 µL). GSNO (8.2 mg, 2.68×10^{-5} mol) was added into the solution with

stirring and allowed to react at room temperature overnight. The resulting mixture was then dialysed overnight against water, using a dialysis membrane with molecular weight cut-off 12-14 kDa, to ensure removal of side products and the excess amount of GSH. The resulting polymer was dried under air and in vacuo, which were then analysed by ^{1}H NMR and ^{19}F NMR spectroscopy.

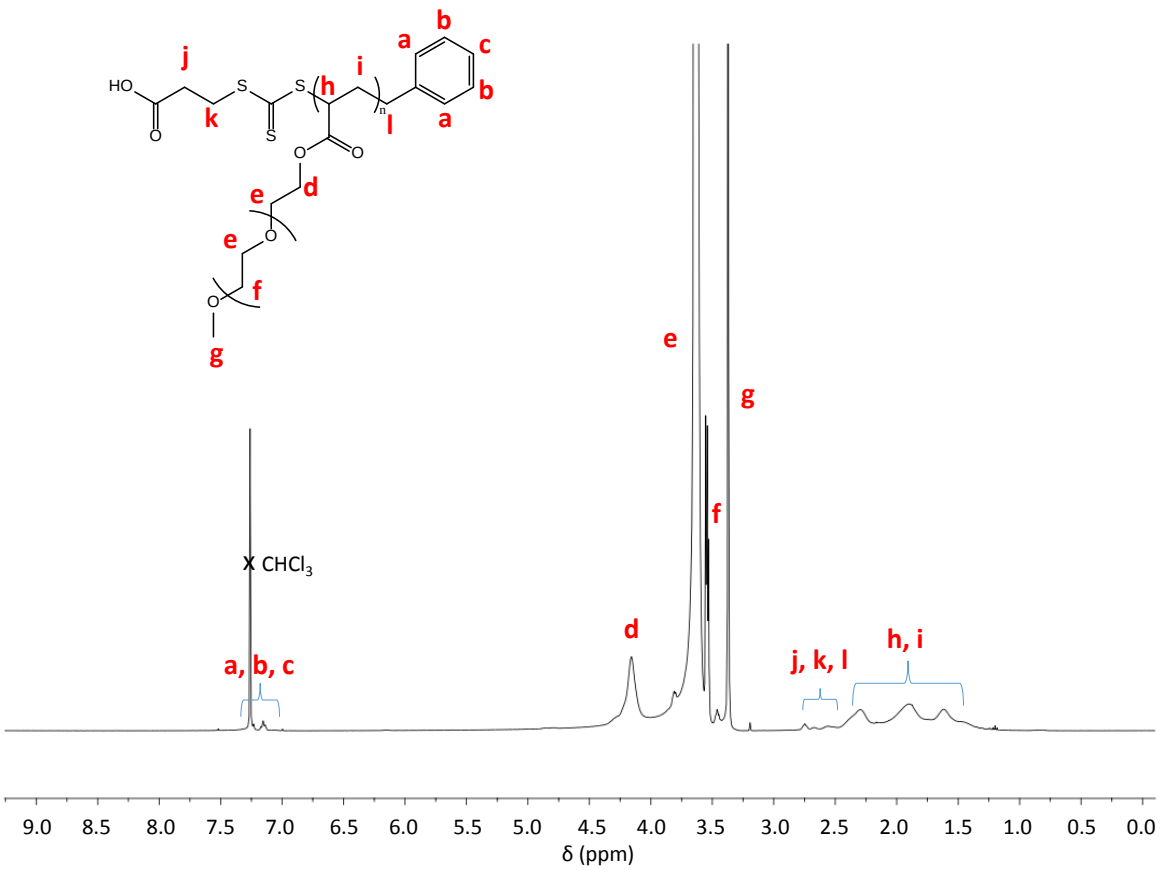

Figure S1. ^{1}H NMR spectrum of POEGA (M_n = 9551 g mol^{-1}, 19 units of OEGA), recorded in $CDCl_3$ (400 MHz). (Table 1, Entry 1)

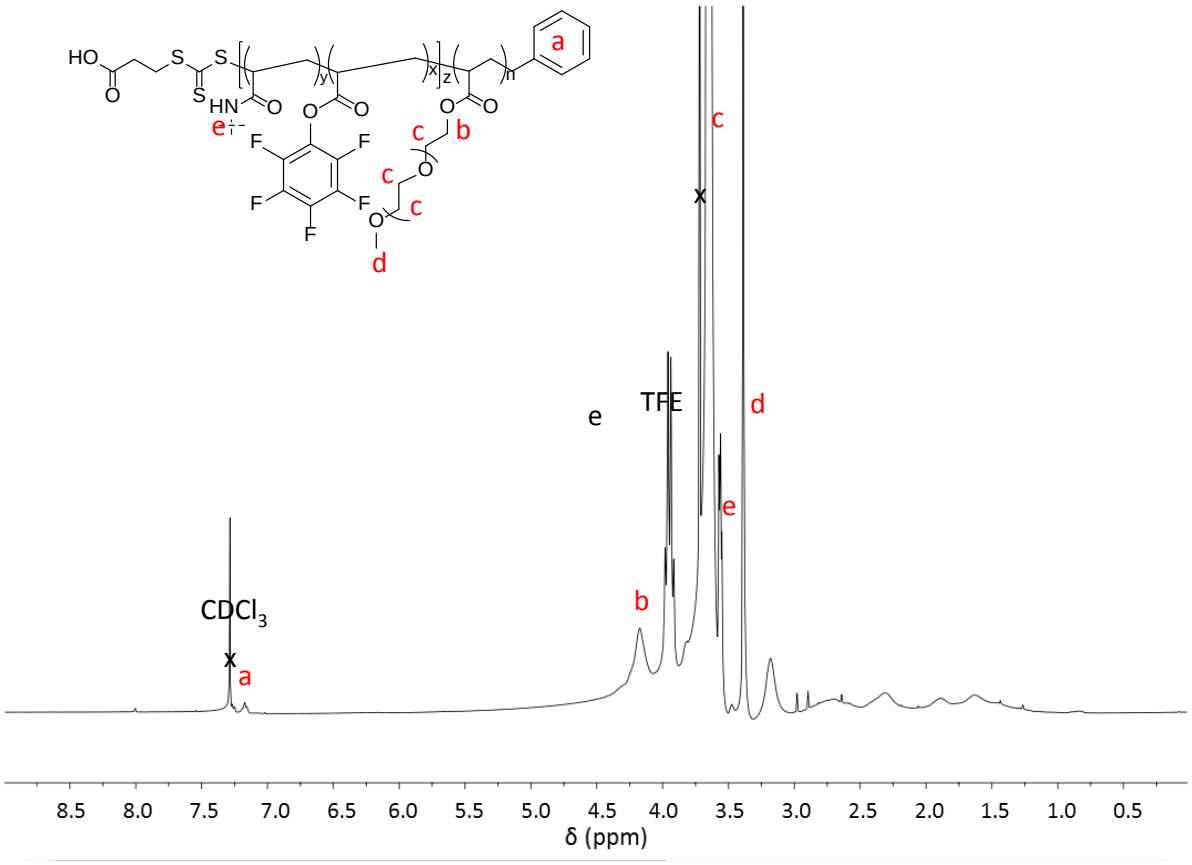

Figure S2. ^{1}H NMR spectrum of POEGA-*block*-P(MBAA-*co*-PFPA) containing PFPA in the core, recorded in $CDCl_3$ (400 MHz). (Table 1, Entry 2)

The final composition of the product determined by ^{1}H NMR and ^{19}F NMR is equal to 31.0/69.0 mol % in PFPA and OEGA using TFE as a reference peak.

F_{OEGA}:F_{TFE}= ($I^{3.3ppm}$/3):($I^{3.8\text{-}4.0ppm}$/2) in the ^{1}H NMR

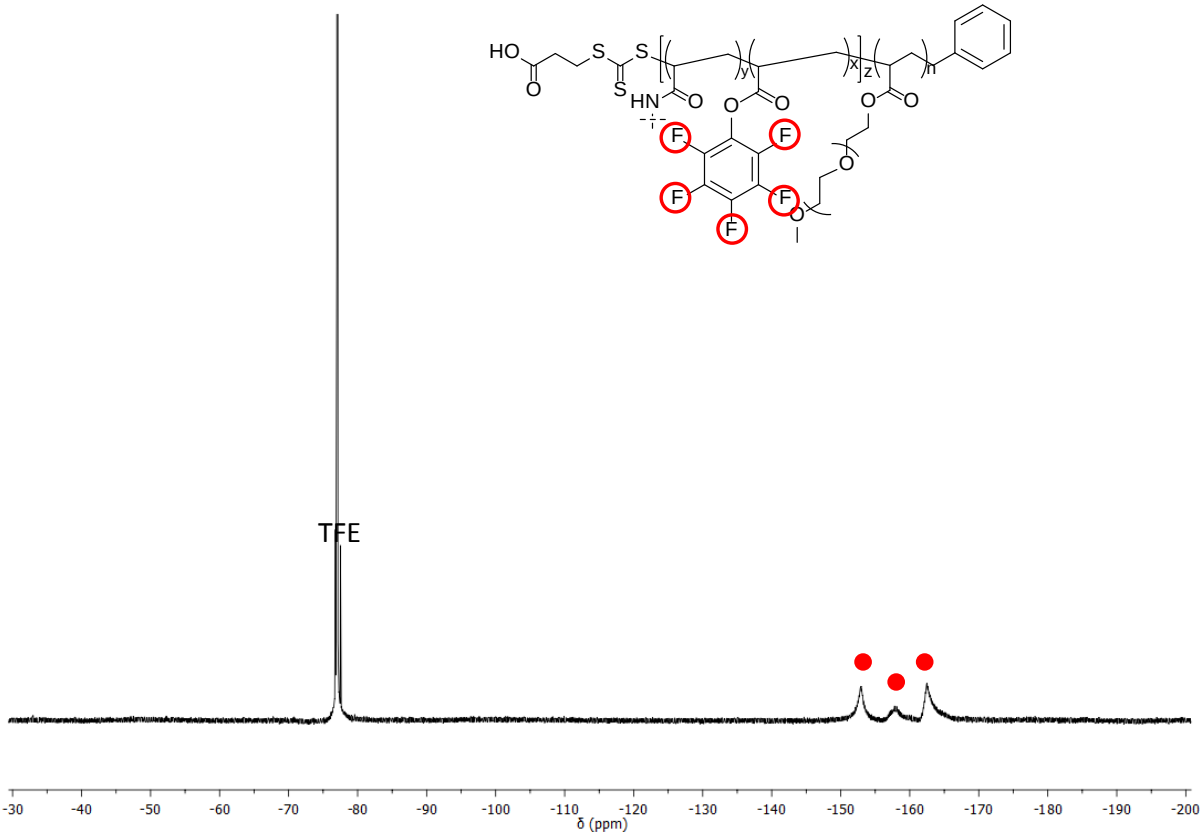

Figure S3. ^{19}F NMR spectrum of POEGA-*block*-P(MBAA-*co*-PFPA) containing PFPA in the core, recorded in $CDCl_3$ (400 MHz).

The final composition of the product determined by ^{1}H NMR and ^{19}F NMR is equal to 31.0/69.0 mol % in PFPA and OEGA using TFE as a reference peak, which calculation was reported in previous paper.[3]

$F_{OEGA}:F_{TFE} = (I^{3.3ppm}/3):(I^{3.8\text{-}4.0ppm}/2)$ in the ^{1}H NMR

$F_{PFPA}:F_{TFE} = [(I^{-152ppm} + I^{-158ppm} + I^{-163ppm})/5]:(I^{-78ppm}/3)$ in the ^{19}F NMR

By using this reference peak TFE, these two monomers, PFPA and OEGA can be compared. The molar composition can be calculated as follows;

$[F_{PFPA}:F_{TFE}/(F_{OEGA}:F_{TFE} + F_{OEGA}:F_{TFE})] : [F_{OEGA}:F_{TFE}/(F_{OEGA}:F_{TFE} + F_{OEGA}:F_{TFE})]$

= 31.0 : 69.0 mol % in PFPA and OEGA .

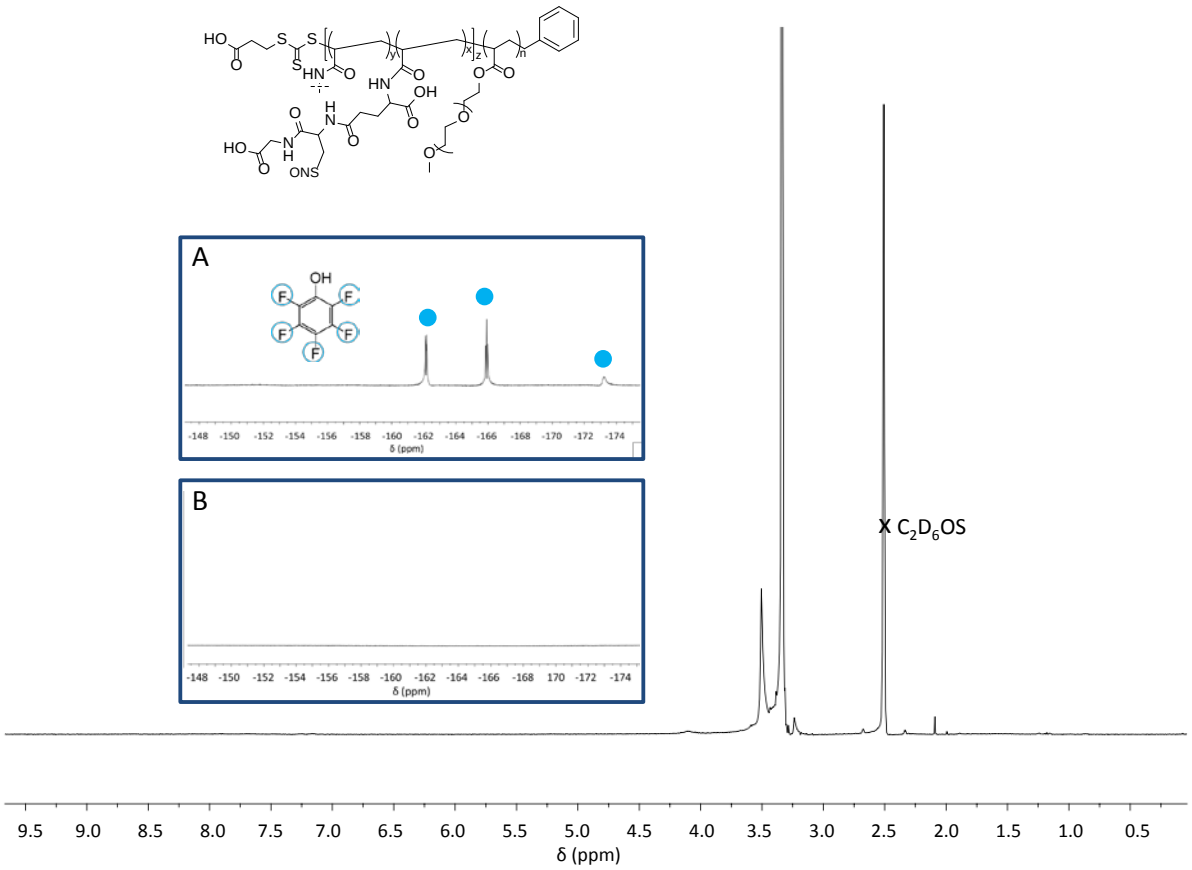

Figure S4. ^{1}H NMR spectrum after conjugation of GSNO onto POEGA-*block*-P(MBAA-*co*-PFPA) star polymer containing pentafluorophenyl-activated ester, recorded in C_2D_6OS and ^{19}F NMR spectra of A) POEGA-*block*-P(MBAA-*co*-PFPA) star polymer after attachment of GSNO and B) Purified POEGA-*block*-P(MBAA-*co*-PFPA conjugated GSNO) star polymer after the reaction, recorded in C_2D_6OS (400 MHz).

Note: ^{1}H NMR and ^{19}F NMR analysis confirmed that the reaction between GSNO and PFP group was selective and quantitative; Once the reaction was occurred, the side product, pentafluorophenol was released, which was confirmed by ^{19}F NMR. The three signals from PFPA in star polymer (Figure S3) were shifted to -162, -166 and -174 ppm, corresponding to pentafluorophenol (A). This also confirmed that all reaction was fully completed. After purification, no more side product pentafluorophenol was observed, which was also confirmed from ^{19}F NMR spectrum (no more peaks observed) (B).

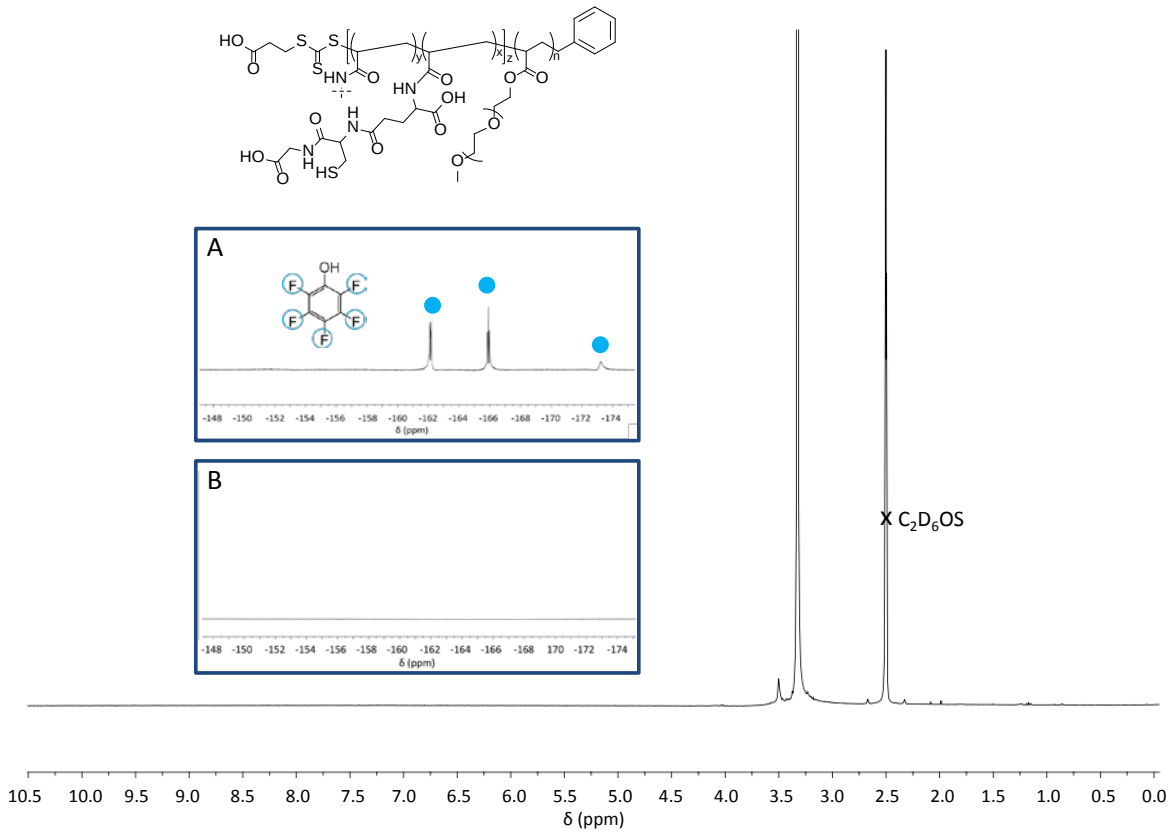

Figure S5. ^{1}H NMR spectrum after conjugation of GSH onto POEGA-*block*-P(MBAA-*co*-PFPA) star polymer containing pentafluorophenyl-activated ester, recorded in C_2D_6OS and ^{19}F NMR spectra of A) POEGA-*block*-P(MBAA-*co*-PFPA) star polymer after attachment of GSH and B) Purified POEGA-*block*-P(MBAA-*co*-PFPA conjugated GSH) star polymer after the reaction, recorded in C_2D_6OS (400 MHz).

Note: ^{1}H NMR and ^{19}F NMR analysis confirmed that the reaction between GSH and PFP group was selective and quantitative; Once the reaction was occurred, the side product, pentafluorophenol was released, which was confirmed by ^{19}F NMR. The three signals from PFPA in star polymer (Figure S3) were shifted to -162, -166 and -174 ppm, corresponding to pentafluorophenol (A). This also confirmed that all reaction was fully completed. After purification, no more side product pentafluorophenol was observed, which was also confirmed from ^{19}F NMR spectrum (no more peaks observed) (B).

Table S1. Molecular Weight of block polymers synthesized

Entry	M_n (g mol^{-1})[a]	M_n (g mol^{-1})[b]	PDI
1	9551	11095	1.10
2		76687	1.13

[a] Molecular weight determined by ^1H NMR spectroscopy.

[b] Molecular weight determined by gel permeation chromatography.

Note: POEGA (10K arm polymer) (Entry 1), POEGA-*block*-P(MBAA-*co*-PFPA) (Entry 2).

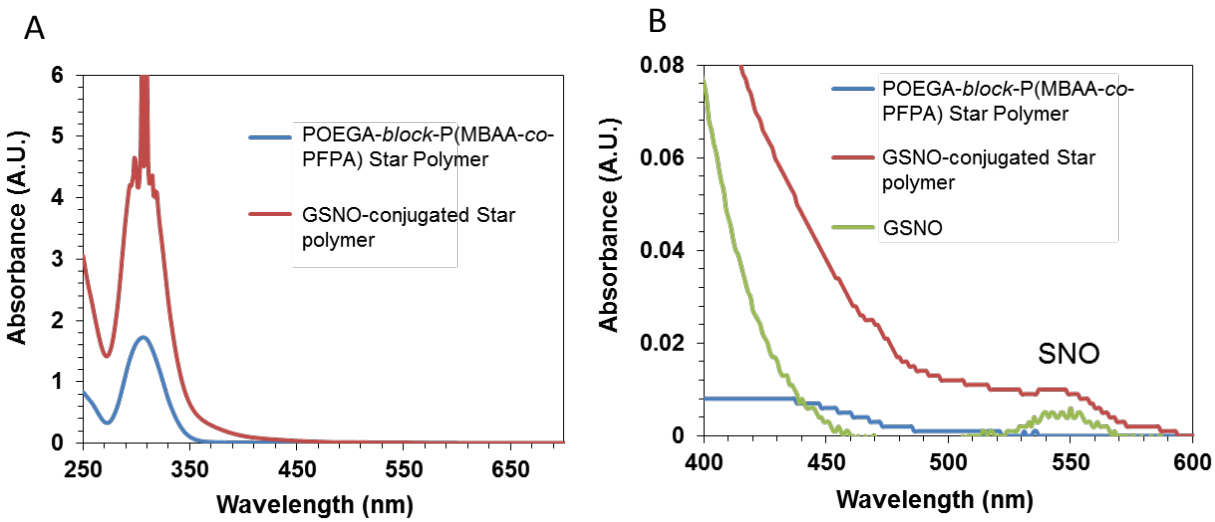

Figure S6. UV-visible spectra of POEGA-*block*-P(MBAA-*co*-PFPA) star polymer, GSNO conjugated star polymer and GSNO. (A) UV-vis spectra for POEGA-*block*-P(MBAA-*co*-PFPA) star polymer and GSNO conjugated star polymer (B) UV-vis spectra for POEGA-block-P(MBAA-co-PFPA) star polymer, GSNO conjugated star polymer and GSNO for the characteristic S-nitrosothiol band. (POEGA-*block*-P(MBAA-*co*-PFPA) star polymer = 1.9 mg/ml, GSNO conjugated star polymer = 15 mg/ml, GSNO = 2.0 mg/ml).

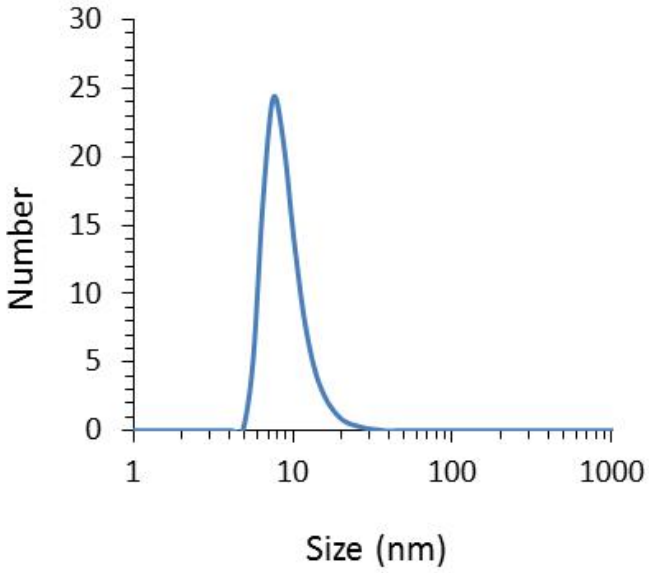

Figure S7. Size distribution (by number) for GSNO-functionalised star polymer in PBS pH 7.4, as determined by dynamic light scattering with number average diameter = 10.9 nm and PDI = 0.22.

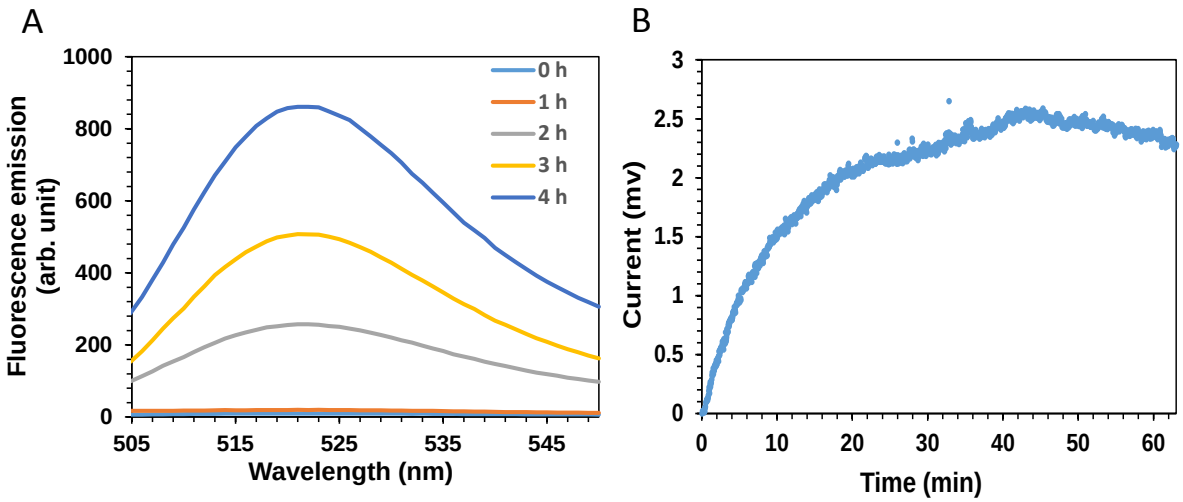

Figure S8. (A) Fluorescence spectra generated by the release of nitric oxide in the presence of 5,6-diaminofluorescein (DAF) (23 µM). Evolution of fluorescence emission spectra at 524 nm caused by NO release from GSNO (0.024 mg/mL) dissolved in PBS at pH 7.4. (B) Electrochemical response from GSNO (50 µM, 0.017 mg/mL) in PBS at pH 7.4 at 37 °C

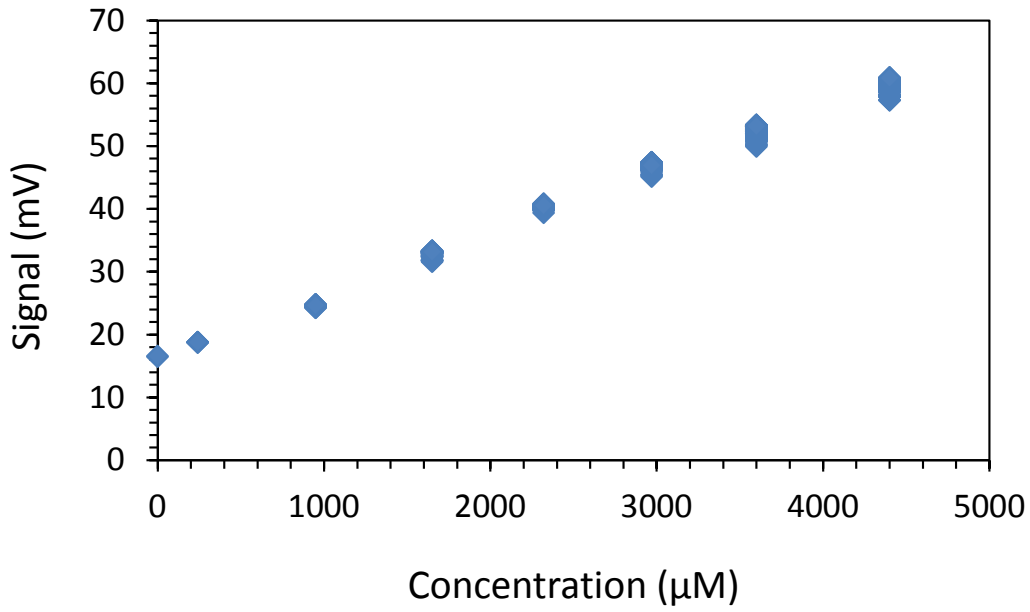

Figure S9. Calibration curve for the electrochemical sensing of nitric oxide from a known concentration of NO donor. S-nitrosoglutathione was used as the standard.

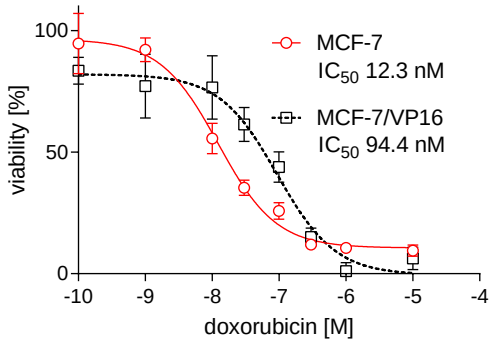

Figure S10. Cytotoxicity of doxorubicin in parental MCF-7 and drug-resistant MCF-7/VP16 cells. Data plotted relative to untreated cells and fitted in GraphPad Prism. Note: 7.7-fold difference in dox cytotoxicity observed; matches quite well with literature report of 9.1-fold difference.[2]

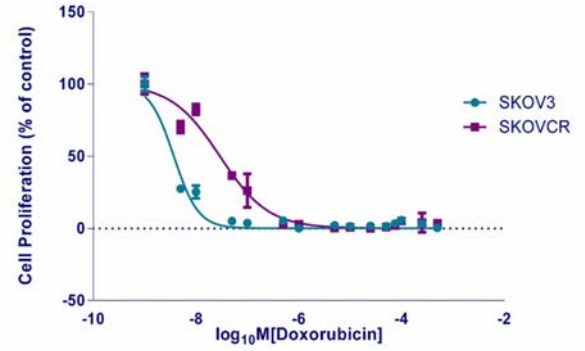

Figure S11. Cell proliferation of human ovarian carcinoma (SKOV3) and DOX-resistant ovarian carcinoma (SKOVCR) cells in the presence of different concentration of doxorubicin.

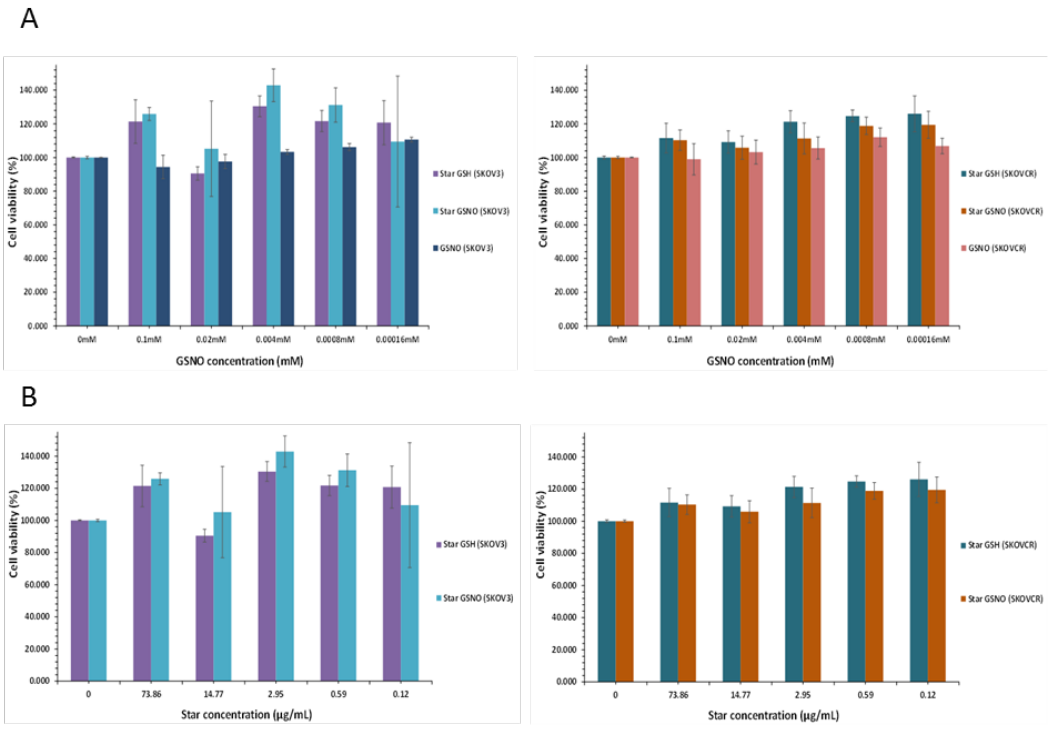

Figure S12. Cytotoxicity of GSNO/GSH-conjugated nanoparticles and GSNO on SKOV3 and SKOVCR cells. (A) X-axis scale was a range of GSNO concentration (mM). (B) X-axis was a range of star polymer concentration (µg/mL).

Figure S13. Western blot detection of Pgp, MRP1 and MRP3 in SKOV3 and SKOVCR cells

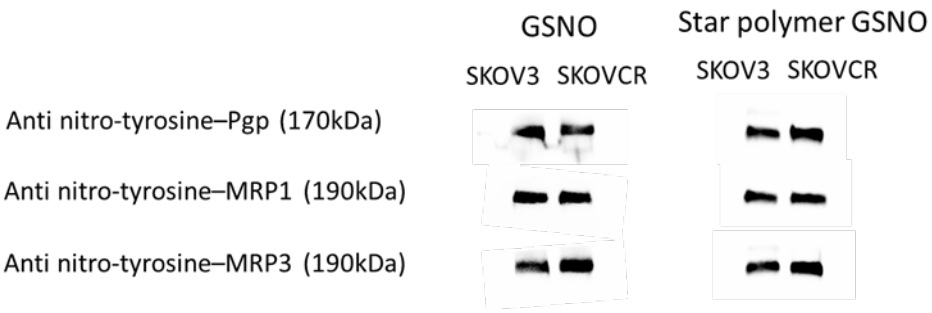

Figure S14. Western blot detection of nitrated drug efflux proteins, Pgp, MRP1 and MRP3 in SKOV3 and SKOVCR cells.

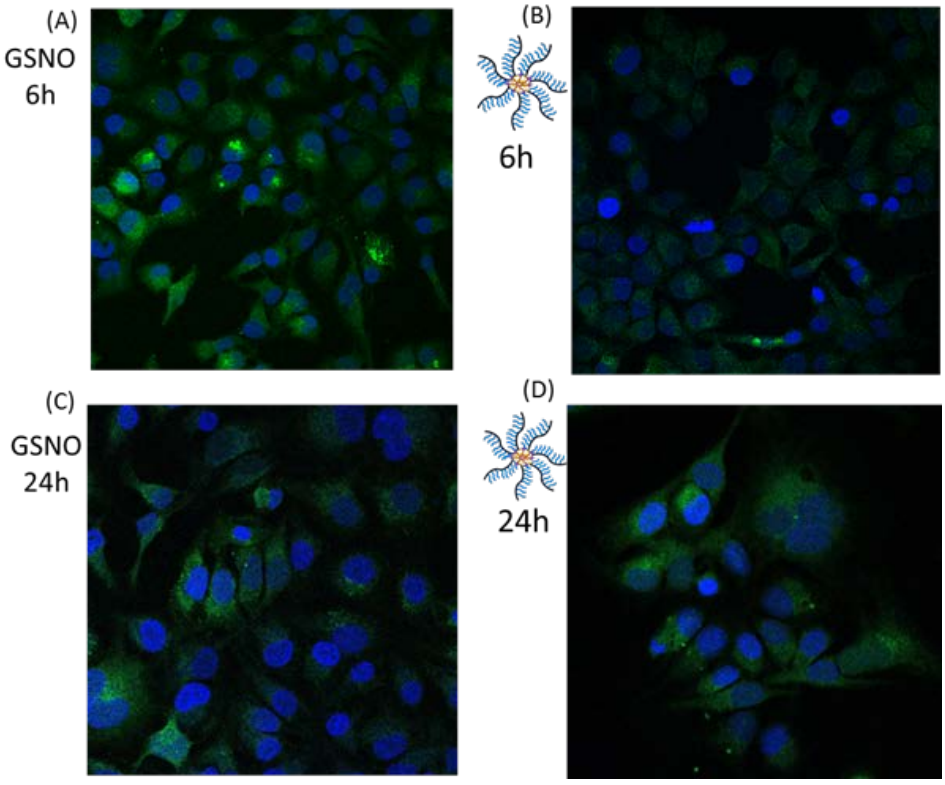

Figure S15. Confocal microscopy of SKOV3 cells: (A)/(C) treated cells with GSNO and DAF-FM DA, (B)/(D) treated cells with GSNO-conjugated star polymers and DAF-FM DA: (A)/(B)- incubation with GSNO/GSNO-conjugated star polymers for 6 h; (C)/(D)- incubation with GSNO/GSNO-conjugated star polymers for 24 h.

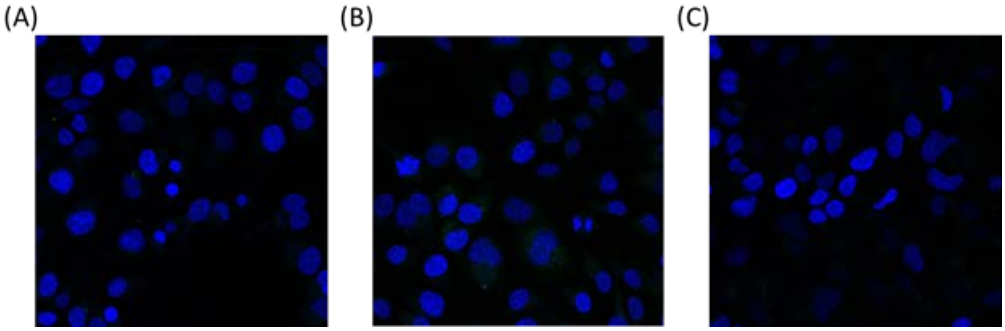

Figure S16. Confocal microscopy of SKOV-3 cells: (A) treated cells with empty star polymer and DAF-FM DA (B) treated cells with DAF-FM DA and (C) untreated cells.

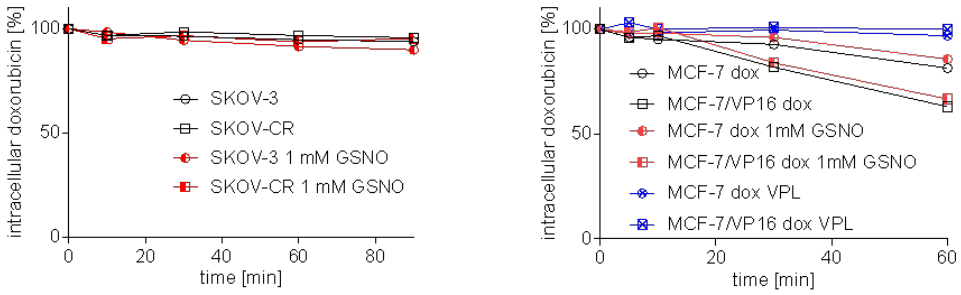

Figure S17. Efflux of DOX from different cell lines plotted as percent of intracellular doxorubicin relative to t=0 in four different cell lines. Cells were untreated or pre-treated (3 h) with 1 mM GSNO, or treated with 10 µM verapamil (n=1).

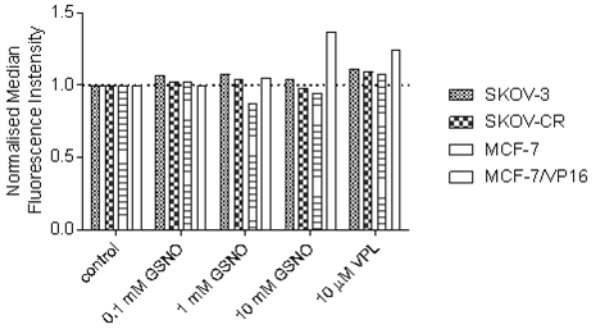

Figure S18. Normalised intracellular DOX content measured as median fluorescence intensity in four different cell lines after pre-treatment with NO donor S-nitrosoglutathione (GSNO) at different concentrations for 3 hours, and subsequent treatment with 4 µM DOX for 90 min, positive control also contained 10 µM verapamil. Data was normalised to cells incubated with 4 µM doxorubicin only (control) (n=1).

Reference

1 F. Schreiber, L. Polerecky and D. de Beer, Nitric oxide microsensor for high spatial resolution measurements in biofilms and sediments., *Anal. Chem.*, 2008, **80**, 1152–1158.

2 E. Schneider, J. K. Horton, C. H. Yang, M. Nakagawa and K. H. Cowan, Multidrug resistance-associated protein gene overexpression and reduced drug sensitivity of topoisomerase II in a human breast carcinoma MCF7 cell line selected for etoposide resistance., *Cancer Res.*, 1994, **54**, 152–158.

CHAPTER 6: Conclusion

6.1 Conclusion

The overall objective of this dissertation was to develop novel methods to synthesize gasotransmitter releasing (either NO or H_2S) polymeric nanoparticle systems that demonstrate enhanced stability and specificity of delivery for therapeutic clinical applications.

In **Chapter 2**, polymers with a terminal *S*-nitrosothiol NO donating moiety were prepared by the novel modification of the thiocarbonyl-thio end-group formed during reversible addition-fragmentation chain transfer polymerisation. The *S*-nitrosothiols are an important class of NO donor molecules and include substances such as *S*-nitrosoglutathione (GSNO) and *S*-nitroso-N-acetylpenicillamine (SNAP). A new synthetic method was developed for the effective *S*-nitrosation of a sulfhydryl group at the end of a polymer chain. Critically it was discovered that a stoichiometric amount of nitrous acid was needed for the formation of *S*-nitrosothiol-terminated polymers and this was achieved by maintaining the molar ratio of sulphuric acid (H_2SO_4) to sodium nitrite ($NaNO_2$) at 1:2. Excess nitrous acid was found to facilitate rapid destruction of the *S*-nitrosothiol on the polymer chain. Benzodithioate-terminated poly[oligo(ethylene glycol) methyl ether methacrylate] (POEGMA) was successfully converted into P[OEGMA]-SNO. Additionally, *S*-nitrosothiol was incorporated into a pH-responsive micelle system, P[OEGMA-co-DMAEMA-block-DIPMA]-SNO. Using the SNO-modified polymer systems, it was demonstrated that the reactivity of the *S*-nitrosothiol moiety is strongly affected by the local chemical environment. Furthermore, incorporating the *S*-nitrosothiol into a micelle could significantly reduce the thiol triggered degradation of *S*-nitrosothiol and therefore the release of NO when compared to a hydrophilic homopolymer under the same pH condition. Future studies of this convenient and versatile approach for preparing NO donor polymers might be applied in other polymeric NO donor systems and also potential therapeutic areas, including anticancer and antibacterial applications.

In **Chapter 3**, H_2S-releasing polymers with an acyl-protected perthiol chain terminus were prepared *for the first time* via the development of a simple, high yielding end-group modification approach. Poly(oligoethylene glycol methyl ether) methacrylate (P[OEGMA]-S(C=S)Ph) homopolymer was firstly prepared by RAFT polymerization in

the presence of 2-cyano-2-propyl benzodithioate. A one-pot reaction of P[OEGMA]-S(C=S)Ph with ethanolamine and Aldrithiol^{TM}-2 resulted in the formation of pyridy-2-dithiol terminated end-group polymer (P[OEGMA]-S-S-Py), which then underwent a thiol-disulfide exchange reaction with thiobenzoic acid to produce an acyl protected perthiol at the chain terminus. The same end-group post-modification approach was then applied to block polymer (P[OEGMA-block-BMA]-S(C=S)Ph) and a pH responsive block copolymer (P[OEGMA-co-DMAEMA-block-DIPMA]-S(C=S)Ph to create H_2S donating polymers. All polymers were shown to release H_2S when exposed to a thiol trigger (L-cysteine), with the release rate dependent on the polymer structure. In particular, translating the approach to pH-responsive H_2S-releasing micelles had a significant impact on thiol-triggered H_2S release kinetics by controlling the self-assembly of micelles at different pH conditions. Furthermore, confocal live cell imaging employing an H_2S specific fluorescent dye proved that these materials were clearly capable of releasing H_2S to live cells (HEK cells) upon exposure to endogenous sources of thiols at intracellular levels. In future studies, these novel H_2S donor polymers may be employed to deliver H_2S with subcellular precision, including targeted endosomal delivery, which could be used to better understand redox signalling in subcellular compartments.

In **Chapter 4**, a polymeric H_2S delivery system was developed which allowed access to both functional polymeric micelles and worms. Inspired by the previous work from **Chapter 3**, an alternative approach was developed to provide side-chain, acyl-protected perthiol functional polymers by using post-polymerization transformation of poly(glycidyl methacrylate) (PGMA) units. Simple block copolymer and self-assembled nanoparticles with different morphologies (spherical and worm-like micelles) containing PGMA units were initially prepared via RAFT PISA polymerization. This concept is based on the chain extension of a soluble polymeric macromer with a co-monomer that is soluble in the polymerization solution, but its polymer is not. This forms an AB amphiphilic block polymer which induces self-assembly. The thiol-reactive epoxide functional groups of the PGMA units in the corona were then chemically transformed into acyl-protected perthiol groups through a series of post-modification thiol based chemistries. This was the first example of a self-assembled nanoparticle H2S delivery system. Furthermore, the use of PISA has commonly led to nanoparticles with different shapes; a physical parameter that has been shown to

influence the biological behaviour of nanoparticles. In the case of self-assembled nanoparticle systems with different morphologies (spherical and worm-like micelles), the particle shape and size remained largely unaffected after each post-polymerization process. These functional linear, spherical and worm-like micelles were shown to successfully release H_2S in the presence of the model thiol, L-cysteine in a morphologically dependent manner. Moreover, these H_2S donor polymers were effective at releasing H_2S inside live cells (U2OS, osteosarcoma cells) upon exposure to endogenous thiols. This observation was confirmed using a fluorescent probe for H_2S detection. Finally, the co-administration of the morphologically controlled H_2S donor nanoparticles with doxorubicin (DOX) was examined on U2OS osteosarcoma cells. A systematic study of cellular toxicity revealed enhanced DOX cytotoxicity when delivered with the H_2S donor polymers compared to co-treatment of control polymers (non H_2S donor) with DOX, or native DOX treatment alone. This indicated that H_2S releasing nanoparticles strongly influenced DOX cytotoxicity in U2OS cell lines, decreasing the degree of DOX resistance. The results presented here demonstrate that H_2S-donating polymeric nanoparticles, combined with chemotherapeutics, may have potential for treatment of chemoresistant cells. Other H_2S donating polymeric systems could be designed by modifying the number of functional groups (PGMA), optimising the thiol chemistries or changing the polymeric chemical structure.

Finally, in **Chapter 5**, NO-delivery via core cross linked star polymers was developed. Pentafluorophenyl acrylate functional core cross linked star polymers were prepared using the ‘arm-first’ method, which was previously reported from our group.[1–5] GSNO was then covalently conjugated into the functional core of stars via displacement of the pentafluorophenyl groups. After successful conjugation, GSNO-functionalised star polymers were then examined for their capacity to release NO. Using 5,6-diaminofluorescein (DAF), a NO responsive fluorescent probe, the evolution of NO from GSNO-conjugated star polymers was detected via the increased fluorescence intensity over time. GSNO- star polymer nanoparticle showed a substantially slower NO release profile, compared to the small molecule GSNO. Additionally, the release kinetics of NO from the GSNO-conjugated star polymer nanoparticles was confirmed using an NO-specific electrochemical probe. The influence of co-delivering GSNO or GSNO-conjugated star polymer in combination with DOX was investigated on human breast cancer (MCF7) cells and MDR resistance cells (MCF7/VP16) cells. MCF7/VP16

cells are etoposide-resistant cancer cells, which are also 9-fold resistant towards doxorubicin and overexpress MRP1 transporters.[6–9] To confirm this, Western blot detection of the protein expression was performed in both cell lines, indicating that MCF7/VP16 cells did indeed highly express MRP1 transporters. In contrast, MCF7 cells expressed a negligible amount of MRP1 proteins. Thereafter, it was found that NO delivered from GSNO or GSNO-conjugated star polymers increased the susceptibility of MCF7/VP16 cells to DOX cytotoxicity. These results were also confirmed by other control experiments including co-treatment of empty star, GSH (glutathione) or GSH-conjugated star polymers with and without the same concentration range of DOX. However, in contrast to MCF7/VP16 cells, NO did not contribute to cytotoxic enhancement of DOX-sensitive MCF7 cells, indicating that GSH was mainly involved in cell cytotoxicity instead of NO. Importantly, these results were not transferrable to all resistant cell lines: star-polymer based co-delivery to doxorubicin resistant ovarian cancer cells (SKOVCR) did not improve the cell toxicity despite clear evidence of tyrosine nitration of the overexpressed MRP3 transporter. These results have implications for the pursuit of NO co-delivery as a broad spectrum approach for addressing MDR. In future work, star-shaped polymers with higher chain end fidelity and hence higher arm number could be developed using a variety of polymerization techniques including RAFT, Cu(0)-mediated living radical polymerization or ring-opening polymerization. Recent investigations in this area have shown that improved arm incorporation and higher molecular weight can be attained by employing specific synthesis methodologies.[10–13] Furthermore, other NO-donating small compounds, such as S-nitroso-N-acetylpenicillamine (SNAP), organic nitrates or *N*-diazeniumdolates, could be used for the incorporation into different polymeric systems by using appropriate and orthogonal conjugation chemistries. These potential macromolecular NO donors could then be applied to other cancer cell lines in combination with various anti-cancer agents to investigate effects of varying NO-flux from a nanoparticle platform on the chemotherapeutic effects.

6.2 Reference

1 J. Ferreira, J. Syrett, M. Whittaker, D. Haddleton, T. P. Davis and C. Boyer, Optimizing the generation of narrow polydispersity ‘arm-first’ star polymers made using RAFT polymerization, *Polym. Chem.*, 2011, **2**, 1671–1677.

2 J. S. Basuki, H. T. T. Duong, A. Macmillan, R. Whan, C. Boyer and T. P. Davis, Polymer-Grafted, nonfouling, magnetic nanoparticles designed to selectively store and release molecules via ionic interactions, *Macromolecules*, 2013, **46**, 7043–7054.

3 J. A. Syrett, D. M. Haddleton, M. R. Whittaker, T. P. Davis and C. Boyer, Functional, star polymeric molecular carriers, built from biodegradable microgel/nanogel cores, *Chem. Commun.*, 2011, **47**, 1449–1451.

4 Y. Li, H. T. T. Duong, S. Laurent, A. MacMillan, R. M. Whan, L. Vander Elst, R. N. Muller, J. Hu, A. Lowe, C. Boyer and T. P. Davis, Nanoparticles based on star polymers as theranostic vectors: endosomal-triggered drug release combined with MRI sensitivity., *Adv. Healthc. Mater.*, 2015, **4**, 148–156.

5 J. Liu, H. Duong, M. R. Whittaker, T. P. Davis and C. Boyer, Synthesis of functional core, star polymers via RAFT polymerization for drug delivery applications., *Macromol. Rapid Commun.*, 2012, **33**, 760–766.

6 Z. Benderra, A. Trussardi, H. Morjani, A. M. Villa, S. M. Doglia and M. Manfait, Regulation of cellular glutathione modulates nuclear accumulation of daunorubicin in human MCF7 cells overexpressing multidrug resistance associated protein, *Eur. J. Cancer*, 2000, **36**, 428–434.

7 R. N. Watts, C. Hawkins, P. Ponka and D. R. Richardson, Nitrogen monoxide (NO)-mediated iron release from cells is linked to NO-induced glutathione efflux via multidrug resistance-associated protein 1, *Proc. Natl. Acad. Sci.*, 2006, **103**, 7670–7675.

8 E. Schneider, H. Yamazaki, B. Sinha and K. Cowan, Buthionine sulphoximine-mediated sensitisation of etoposide-resistant human breast cancer MCF7 cells overexpressing the multidrug resistance-associated protein involves increased drug accumulation, *Br. J. Cancer*, 1995, **71**, 738–743.

9 E. Schneider, J. K. Horton, C. H. Yang, M. Nakagawa and K. H. Cowan, Multidrug resistance-associated protein gene overexpression and reduced drug sensitivity of topoisomerase II in a human breast carcinoma MCF7 cell line selected for etoposide resistance., *Cancer Res.*, 1994, **54**, 152–158.

10 J. M. Ren, T. G. McKenzie, Q. Fu, E. H. H. Wong, J. Xu, Z. An, S. Shanmugam, T. P. Davis, C. Boyer and G. G. Qiao, Star polymers, *Chem. Rev*., 2016, **116**, 6743–6836.

11 T. G. McKenzie, E. H. H. Wong, Q. Fu, A. Sulistio, D. E. Dunstan and G. G. Qiao, Controlled formation of star polymer nanoparticles via visible light photopolymerization, *ACS Macro Lett.*, 2015, **4**, 1012–1016.

12 S. Tan, J. Cui, Q. Fu, E. Nam, K. Ladewig, J. M. Ren, E. H. H. Wong, F. Caruso, A. Blencowe and G. G. Qiao, Photocontrolled cargo release from dual cross-linked polymer particles, *ACS Appl. Mater. Interfaces.*, 2016, **8**, 6219–6228.

13 S. J. Lam, N. M. O'Brien-Simpson, N. Pantarat, A. Sulistio, E. H. H. Wong, Y. Y. Chen, J. C. Lenzo, J. A. Holden, A. Blencowe, E. C. Reynolds and G. G. Qiao, Combating mulridrug-resistant gram-negative bacteria with structually nanoengineered antimicrobial pepetide polymers, Nature Microbiology, 2016, 1, 16162.